LIBRARY

JAN 23 1997

National Marine Fisheries Service
2570 Dole Street
Honolulu, Hawaii

14 JAN 1997

海洋開発及地球科学技術調査研究促進費

地球科学技術特定調査研究

アジアモンスーン機構に関する研究

JAPANESE EXPERIMENT ON ASIAN MONSOON (JEXAM)

（平成元年度～平成10年度）
（ＦＹ1989～ＦＹ1998）

平成７年度　成果報告書
ANNUAL REPORT
(APRIL 1995～MARCH 1996)

平成８年８月
August 1996

科学技術庁研究開発局
Research and Development Bureau
Science and Technology Agency
Japan

はじめに

大規模な季節変動として知られているアジアモンスーンは、インド洋・東南アジア周辺の海洋とチベット・ヒマラヤを始めとしたアジア大陸の地表面が、大気を媒体として熱・水蒸気等の交換により、相互に影響を及ぼし合っている現象です。その活動の年々変動は、東南アジア地域や、日本を始めとした周辺地域の気候のみならず、大気大循環を介して世界の気候に大きな影響を与えています。また、アジアモンスーンの活動が西部熱帯太平洋域の大気・海洋変動を引き起こし、太平洋規模で発生するエル・ニーニョ／南方振動の引き金になっている可能性があるという指摘もあり、この点からも注目されています。しかし、これらの地域・海域は広大であり、また観測環境が厳しいこと等から観測体制の整備が遅れており、気象・海象・陸象に関するデータの収集は必ずしも十分に行われていませんでした。

このため科学技術庁では、海洋開発及地球科学技術調査研究促進費により「アジアモンスーン機構に関する研究」を平成元年度より開始し、観測・解析を進めてきました。平成５年１月１１日には、「『アジアモンスーン機構に関する研究』プロジェクトに関する日本国科学技術庁と中華人民共和国国家気象局との間の実施取極」が結ばれ、日中の協力体制も整いました。

本研究の成果が、アジアモンスーン機構の解明に寄与し、さらには気候変動に対する理解を深めることを期待しています。

最後になりましたが、本研究に携わられた関係各位に対し感謝するとともに、今後とも御協力をお願いする次第です。

平成８年８月

科学技術庁研究開発局長
加藤　康宏

アジアモンスーン機構に関する研究

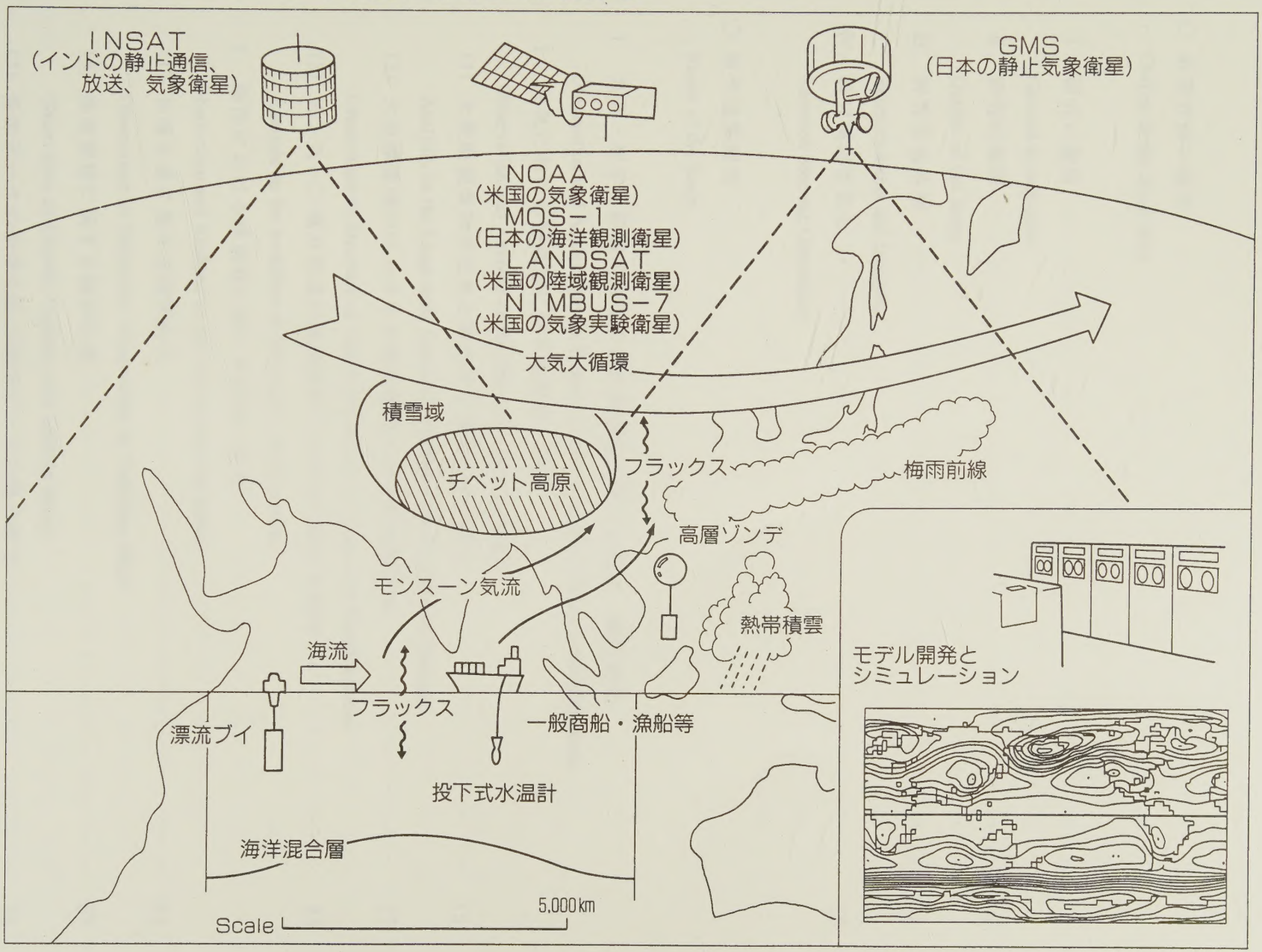

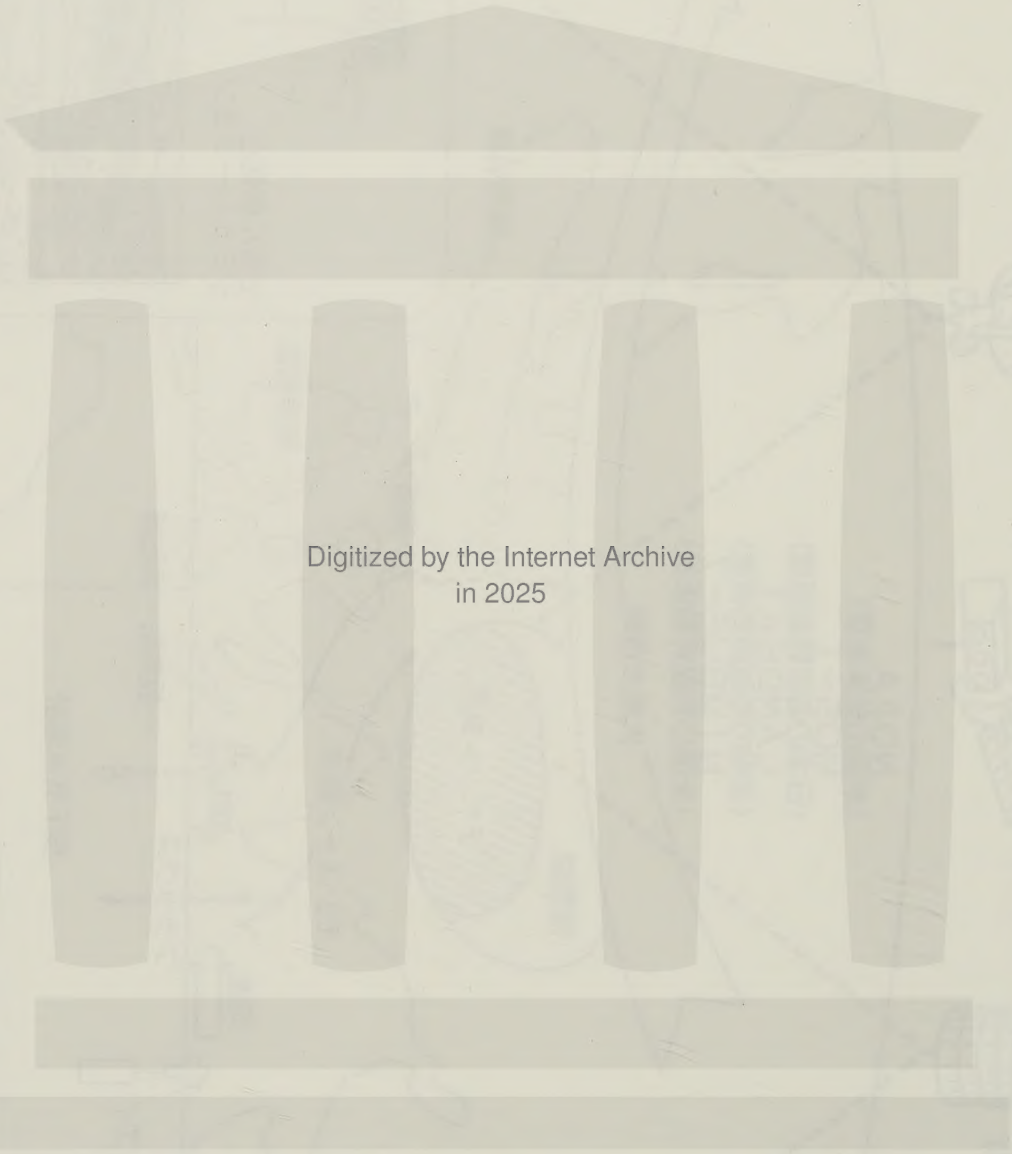

Digitized by the Internet Archive
in 2025

https://archive.org/details/annual-report-japanese-experiment-on-asian-monsoon-jexam_1996-08

目　次

Contents

○ 研究計画の概要

Outline of the Study Plan

Ⅰ. 研究の趣旨 …… 3

General Introduction

Ⅱ. 研究の概要 …… 5

Outline of the Study

Ⅲ. 研究実施体制 …… 8

Research Items and Institutes

Ⅳ. 研究検討委員会 …… 10

Research Steering Committee

○ 研究成果報告

Result of the Study

Ⅰ. 大気・海洋・陸域間相互作用の諸過程に関する観測・解析研究

Observation and Analysis on the Process of the Atmosphere-Ocean-Land Interactions

1. 大気における諸過程に関する観測・研究

Observation and Analysis on the Process in the Atmosphere

(1) 大規模積雲対流活動と降水系に関する解析研究 …… 15

Analysis on the Large scale Convective Activity and Precipitation Systems

(2) 大規模雲域内における対流雲構造に関する観測研究 …… 27

Observation of Structure of Convective Clouds in Large-scale Cloud Systems

(3) モンスーン域対流雲の維持過程と水収支に関する研究 …… 35

Analysis on the evolution of Convective cloud systems

2. 海洋における諸過程に関する観測・研究

Observation and Analysis on the Process over the Ocean

(1) 表層水温に関する観測研究 …… 45

Observation on Subsurface Temperature by Voluntary Ships

(2) 海流循環に関する観測研究 …… 67

Observation on Oceanic Currents with Drifting Buoys

(3) 海洋データの標準化及び海洋データ交換の推進 …… 75

Standardization of Oceanic Data and Promotion of Exchange of Oceanic Data and Information

3．陸域における諸過程に関する観測・研究
Observation and Analysis on the Process over the Land
(1) チベット・ヒマラヤにおける水文変動に関する観測研究 …… 79
Observation on Hydrology over the Tibetan Plateau and Himalayas
(2) 地表面熱収支に関する観測研究 …… 91
Observation on Regional Surface Heat Budget Observational Study of the Ground Surface Heat Budgets
(3) モンスーン循環広域条件及び雪氷変動状況に関する解析研究 …… 113
Analysis on Environmental Condition and Snow-Ice Cover Changes Affecting Monsoon Cycle in Asia
(4) 地域水収支に関する解析研究 …… 117
Analytical study of water balance on representative river basins

Ⅱ．数値モデルによる大気・海洋・陸域間相互作用の実験研究
Experiment of the Atmosphere-Ocean-Land Interactions by the Use of Numerical Models
1．数値モデルによる４次元資料同化システムの開発に関する研究 …… 123
Development of the Four Dimensional Data Assimilation System by the Use of Numerical Model
2．広域水収支モデルの開発に関する研究 …… 131
Development of the Water Balance Model over the Wide Area

Ⅲ．大気・海洋・陸面間の相互作用に関する総合研究
Synthetic Study on the Atmosphere-Ocean-Land Interactions
1．大規模モデルによる大気・海洋・陸面間の相互作用に関する実験研究 …… 143
Experiment of the Atmosphere-Ocean-Land Interactions by the Use of General Circulation Models
2．モンスーンのエネルギー収支に関する解析研究 …… 153
Analysis of the Energy Balance of Monsoon
3．モンスーン循環系の総合解析 …… 163
Synthetic Study of the Monsoon Circulations

○ 観測・解析研究ディレクトリー …… 169
Directory of Observation/Analysis Data Set

研究計画の概要

Outline of the Study

Ⅰ．研究の趣旨

アジアモンスーンは、インド洋・東南アジア周辺の海洋とチベット・ヒマラヤを始めとしたアジア大陸の地表面が、その熱的特性の相違により大気を媒体とした熱・水蒸気等の交換を通じて、それぞれ相互に影響を及ぼし合う結果、東南アジア・東アジア地域における季節的な現象として発現している。その活動の年次の変動は、東南アジア地域や、日本を始めとした周辺地域の気候の変動に大きな影響を及ぼすばかりでなく、大気大循環変動を介して世界の気候にも大きな影響を与えている。また最近、アジアモンスーンの活動の異常は西部熱帯太平洋域の大気・海洋変動を引き起こし、これが太平洋規模で発生するエル・ニーニョ／南方振動の引き金となっている可能性があるという研究報告もあり、この点からも注目する必要がある。しかしながら、これらの地域・海域は、対象域の広大さや観測環境の厳しさ等から観測体制が整備されておらず、気象・海象・陸象の基本的な要素に係るデータの収集が必ずしも十分に行なわれているとは言えない。

従って、アジアの一員であり、アジアモンスーンの直接的影響を受け、大気・海洋観測の十分なポテンシャルを有する我が国が、世界の気候を形成する複雑なシステムの一つであるアジアモンスーンの機構を解明するため長期的・総合的な研究を実施することが緊要となっている。本研究を実施することにより、我が国を含むアジア地域における旱ばつや長雨といった異常気象発現の予測技術のみならず、世界的規模の気候変動を予測する技術の発展に寄与することが期待される。

以上のような状況を踏まえて、本研究は１９８９年度から１０年間の計画で行っている。

I . General Introduction

Asian Monsoon is caused by the thermal contrast between the Indian Ocean and surrounding oceans, and the land surface of Asian Continent. These two land and ocean areas interact with each other through the exchange of the heat and moisture. Its consequence is observed as a seasonal phenomenon in the regions of Southeast Asia and East Asia, including Japan.

The year-to-year variation of the Asian Monsoon has a significant influence not only on the climate of Southeast Asia and the surrounding area including Japan, but also on the worldwide climate through the global atmospheric circulations. Furthermore, it is recently reported that the anomalous activities of the Asian Monsoon causes the atmospheric/oceanic variations over the tropical western Pacific which, in turn, trigger the El Nino/Southern Oscillation events over the whole Pacific Ocean.

Though it is recognized that Asian Monsoon plays an important role in the global climate system, its mechanism has not yet been made clear. This is mainly attributable to the fact that the atmospheric and oceanographic data are sparse over those regions due to the technical difficulties in the observations and the insufficiencies of conventional observation network.

Japan, as a member of the Asian countries, is situated under the direct influence of the Asian monsoon and has a capability to conduct the atmospheric and oceanographic observations. Therefore, it is an important role of Japan to carry out the research projects for the study on Asian Monsoon in cooperation with the countries such as China and India.

This project is expected to make a contribution for the improvement of the long-range forecast of the global climate change as well as the forecasting technique of the unusual weather, such as drought and long spell of rain.

Based on the understandings as mentioned above, Science and Technology Agency (STA) of Japan has launched this ten-year research project since April 1989.

Ⅱ. 研究の概要

1. 大気・海洋・陸域間相互作用の諸過程に関する観測・解析研究

(1) 大気における諸過程に関する観測・解析研究

・ 静止気象衛星資料をデータベース化し、モンスーン活動の年々変動、降水システム、エルニーニョとの関連についての解析を行う。

・ 前期に観測した対流雲のデータを解析し、対流雲の構造、対流雲による熱、水、運動量の輸送過程を明らかにする。

(2) 海洋における諸過程に関する観測・解析研究

・ 東南アジア周辺海域及びインド洋を航行する公庁船、商船及び漁船により海洋表層水温の通年観測を行う。

・ インド洋に漂流ブイを放流し、大規模海流循環の通年観測を行う。

・ 上記で取得した海洋データの標準化、データベース化を促進する。また、インド洋及び東南アジア周辺海域の海洋観測情報交換システムを構築し、取得データを交換する。

(3) 陸域における諸過程に関する観測・解析研究

・ チベット地域における気象及び陸面の観測を行い、大気陸面間のエネルギー収支を見積もる。

・ 商船委託により、インド洋から東南アジア周辺に至る海域での海上気象・高層気象観測、及びウィンドプロファイラーにより下層大気の観測を行い、大気海洋間、大気陸面間のエネルギー収支を見積もる。

・ 極軌道地球観測衛星資料から、積雪、雲分布、土壌水分量を算出し、解析する。

・ 中国の代表流域の水文資料、水文・気象データを収集し、水収支解析及び蒸発発散解析を行う。

2. 数値モデルによる大気・海洋・陸域間相互作用の実験研究

(1) 数値モデルによる４次元資料同化システムの開発に関する研究

・ 現在の４次元資料同化システムに、現在使用されていない衛星データ等を組み込めるように高度化を図り、得られた物理量からモンスーン機構を考察する。

(2) 広域水収支モデルの開発に関する研究

・ 前期に開発した流出量モデル、蒸発散量モデルへの検証・改良を行うと共に、積雪・流出量サブモデルを開発し、積雪地域への広域水収支モデルの適用を図る。

3. 大気・海洋・陸面間の相互作用に関する総合研究

(1) 大規模モデルによる大気・海洋・陸面間の相互作用に関する実験研究

・ 前期に用いたモデルの改良を行う。また、大気海洋結合モデルを導入し、アジアモンスーンの機構に対する海洋や陸面の役割を評価する。さらに高分解能の大気大循環モデルを開発し、地表面状態や対流活動の影響を評価する。

(2) モンスーンのエネルギー収支に関する解析研究

・ モデルのシミュレーション結果を衛星観測データの解析結果によって検証し、モンスーン機構のエネルギー収支解析を行う。

(3) モンスーン循環系の総合解析

・ 海洋や雪氷分布の変動と、モンスーン循環を含む大気大循環や日本の天候の関連を調査する。また、高層・地上・海洋・陸面観測データを用いて総合的に解析することによって、モンスーン循環系を解明する。

Ⅱ . Outline of the Study

1 . Observation and Analysis on the Process of the Atmosphere-Ocean-Land Interactions

(1) Observation and Analysis on the Process in the Atmosphere

-To construct a database of the Japanese and Indian satellites and make an analysis of the large scale cloudiness changes.

-To observe and three dimensional structures of the tropical convective clouds related to the heat budget of the atmosphere-ocean interaction by wind Doppler radar.

(2) Observation and Analysis on the Process over the Ocean

-To observe sub-surface temperature throughout the year by voluntary, official, commercial and fishing ships over the Southeast Asia and the Indian Ocean.

-To observe larg-scale oceanic current throughout the year by drifting buoys over the Indian Ocean.

-To standardize and construct a database of the oceanic data and promote a data exchange. To construct an information exchange systemconcerning to the observation in the Indian Ocean.

(3) Observation and Analysis on the Process over the Land

-To observe weather and land surface conditions over the Tibetan area and estimate an energy budget of the atmosphere-land interaction.

-To observe three dimensional structures of low level air flow related to the heat budget of the atmosphere-land interaction by wind profiler.

-To promote a maritime meteorological observation by voluntary commercial ships and estimate an energy budget of the atmosphere-ocean interaction.

-To construct a database of the polar orbiting earth observation satellites and make an analysis of the atmosphere-ocean-land situations related to the large scale hydrological variations.

-To collect daily hydro-meteorological data over the Yangtze River basin and make an analysis of the long-term variations.

2 . Experiment of the Atmosphere-Ocean-Land Interactions by the Use of Numerical Models

(1) Development of the Four Dimensional Data Assimilation System by the Use of Numerical Model

-To develop the four dimensional data assimilation system by the use of numerical models for the analysis on the process of the atmosphere-ocean-land interactions.

(2) Development of the Water Balance Model over the Wide Area

-To develop numerical models for the investigation of the large scale hydrological budget over the Tibet,India and Southeast Asia related to the heat transport.

3 . Synthetic Study on the Atmosphere-Ocean-Land Interactions

(1) Experiment of the Atmosphere-Ocean-Land Interactions by the Use of General Circulation Models

-To perform numerical experiments of the effect of intraseasonal 30-60 day variation on Asian monsoon.

-To perform numerical experiments by the atmosphere-ocean coupled model for the investigation of the effects of oceanic conditions on the long-term variation of the atmosphere-land condition.

(2) Analysis of the Energy Balance of Monsoon

-To construct a database of Earth radiation budget through the polar orbiting meteorological satellites and make an analysis of an effect of the monsoon variation.

(3) Synthetic Study of the Monsoon Circulations

-To make a comprehensive analysis of the monsoon circulation by the use of the standardized data.

Ⅲ. 研究実施体制
Research Items and Institutes

研究項目 Research Items	担当機関 Research Institutes
Ⅰ. 大気・海洋・陸域間相互作用の諸過程に関する観測・解析研究 Observation and Analysis on the Process of the Atmosphere-Ocean-Land Interactions	
1. 大気における諸過程に関する観測・解析研究 Observation and Analysis on the Process in the Atmosphere	
(1) 大規模積雲対流活動と降水系に関する解析研究 Analysis on the Large scale Convective Activity and Precipitation Systems	気象庁 気象研究所 Meteorological Research Institute (MRI), Japan Meteorological Agency (JMA)
(2) 大規模雲域内における対流雲構造に関する研究 Observation of Structure of Convective Clouds in Large-scale Cloud Systems	気象庁 気象研究所 MRI/JMA
(3) モンスーン域対流雲の維持過程と水収支に関する研究 Analysis on the evolution of Convective cloud systems	科学技術庁 防災科学技術研究所 National Research Institute for Earth Science and Disaster Prevention (NIED), Science and Technology Agency (STA)
2. 海洋における諸過程に関する観測・解析研究 Observation and Analysis on the Process over the Ocean	
(1) 表層水温に関する観測研究 Observation on Subsurface Temperature by Voluntary Ships	水産庁 遠洋水産研究所 Far seas Fisheries Research Laboratory, Fisheries Agency 気象庁 海洋気象部 Marine Department, JMA
(2) 海流循環に関する観測研究 Observation on Oceanic Currents with Drifting Buoys	海上保安庁 水路部 Hydrographic Department (HD), Maritime Safety Agency (MSA)
(3) 海洋データの標準化及び海洋データ交換の推進 Standardization of Oceanic Data and Promotion of Exchange of Oceanic Data and Information	海上保安庁 水路部 HD/MSA
3. 陸域における諸過程に関する観測・解析研究 Observation and Analysis on the Process over the Land	
(1) チベット・ヒマラヤにおける水文変動に関する観測研究 Observation on Hydrology over the Tibetan Plateau and Himalayas	科学技術庁 防災科学技術研究所 NIED/STA

研究項目 Research Items	担当機関 Research Institutes
(2) 地表面熱収支に関する観測研究 Observation on Regional Surface Heat Budget Observational Study of the Ground Surface Heat Budgets	気象庁 気象研究所 MRI/JMA 郵政省 通信総合研究所 Communications Research Laboratory, Ministry of Posts and Telecommunications
(3) モンスーン循環広域条件及び雪氷変動状況に関する解析研究 Analysis on Environmental Condition and Snow-Ice Cover Changes Affecting Monsoon Cycle in Asia	科学技術庁 防災科学技術研究所 NIED/STA
(4) 地域水収支に関する解析研究 Analytical study of water balance on representative river basins	科学技術庁 防災科学技術研究所 NIED/STA
Ⅱ. 数値モデルによる大気・海洋・陸域間相互作用の実験研究 Experiment of the Atmosphere-Ocean-Land Interactions by the Use of Numerical Models	
1. 数値モデルによる4次元資料同化システムの開発に関する研究 Development of the Four Dimensional Data Assimilation System by the Use of Numerical Model	気象庁 予報部 Forecasting Department (FD), JMA
2. 広域水収支モデルの開発に関する研究 Development of the Water Balance Model over the Wide Area	科学技術庁 防災科学技術研究所 NIED/STA
Ⅲ. 大気・海洋・陸面間の相互作用に関する総合研究 Synthetic Study on the Atmosphere-Ocean-Land Interactions	
1. 大規模モデルによる大気・海洋・陸面間の相互作用に関する実験研究 Experiment of the Atmosphere-Ocean-Land Interactions by the Use of General Circulation Models	気象庁 気象研究所 MRI/JMA
2. モンスーンのエネルギー収支に関する解析研究 Analysis of the Energy Balance of Monsoon	気象庁 気象研究所 MRI/JMA
3. モンスーン循環系の総合解析 Synthetic Study of the Monsoon Circulations	気象庁 予報部 FD/JMA
Ⅳ. 検討委員会の開催等 Research Steering Committee	気象庁 気象研究所 MRI/JMA 科学技術庁 研究開発局 Research and Development Bureau, STA

Ⅳ. 研究検討委員会

Research Steering Committee

委員名 Membership	所属 Affiliation
委員長　浅井　冨雄 Chairman: Prof. Tomio Asai	広島大学総合科学部自然環境研究コース教授 Faculty of Integrated of Arts and Sciences, University of Hiroshima
委員　岩崎　俊樹 Member: Dr. Toshiki Iwasaki	気象庁予報部数値予報課予報官 FD/JMA
大塚　伸 Mr. Shin Ohtsuka	気象庁気象研究所台風研究部長 MRI/JMA
大畑　哲夫 Dr. Tetsuo Oh'hata	滋賀県立大学環境科学部助教授 School of Environmental Science, University of Shiga Prefecture
幾志　新吉 Dr. Shinkichi Kishi	科学技術庁防災科学技術研究所先端解析技術研究部長 NIED/STA
久保田　雅久 Prof. Masahisa Kubota	東海大学海洋学部教授 School of Marine Science and Technology, Tokai University
住　明正 Prof. Akimasa Sumi	東京大学気候システム研究センター長 Center for Climate System Research, University of Tokyo
辰野　忠夫 Mr. Tadao Tatsuno	海上保安庁水路部海洋情報課長 HD/MSA
西田　英男 Mr. Hideo Nishida	海上保安庁水路部企画課海洋研究室長 HD/MSA

委員名 Membership	所属 Affiliation
新田　勉 Prof. Tsuyoshi Nitta	東京大学気候システム研究センター教授 Center for Climate System Research, University of Tokyo
萩野谷　成徳 Dr. Shigenori Haginoya	気象庁気象研究所物理気象研究部主任研究官 MRI/JMA
増田　悦久 Dr. Yoshihisa Masuda	郵政省通信総合研究所 Communications Research Laboratory, Ministry of Posts and Telecommunications
三河　哲也 Mr. Tetsuya Mikawa	気象庁海洋気象部海洋課エルニーニョ監視センター調査官 MD/JMA
水野　恵介 Dr. Keisuke Mizuno	水産庁遠洋水産研究所海洋・南大洋部低緯度域海洋研究室長 Far Seas Fisheries Research Laboratory, Fisheries Agency
安成　哲三 Prof. Tetsuzoh Yasunari	筑波大学地球科学系教授 Institute of Geosciences, University of Tsukuba
山形　俊男 Prof. Toshio Yamagata	東京大学大学院理学系研究科教授 Graduate School of Science, University of Tokyo
中村　英俊 Mr. Hidetoshi Nakamura	科学技術庁研究開発局地球科学技術推進室長 Office of Earth Science and Technology, Research and Development Bureau, STA

研究成果報告

Result of the Study

I. Observation and analysis on the process of the atmosphere-ocean-land interactions

大気・海洋・陸域間相互作用の諸過程に関する解析・観測研究

1. Observation and analysis on the process in the atmosphere

大気における諸過程に関する解析・観測研究

(1) Analysis on the Large scale Convective Activity and Precipitation Systems

大規模積雲対流活動と降水系に関する解析研究

Japan Meteorological Agency
Meteorological Research Institute,
Masato Murakami, Toshiro Inoue,
Nobuo Yamazaki, Tetsuo Nakazawa,
Kiyotoshi Takahashi, Minoru Tanaka
Meteorological Satellite Center
Kazuo Itoh, Tomoo Ohno
気象庁
気象研究所
村上勝人、井上豊志郎、
山崎信雄、中沢哲夫、
高橋清利、田中実
気象衛星センター
伊藤和男、大野智生

(Abstract)

The influence of the intraseasonal variations(ISV) to the diurnal variation is investigated using 3 hourly mean GMS infrared data. At the inactive phase of the ISV the phase of the diurnal variation tends to be delayed over the sea and advanced over the land. This pattern of the phase change is found especially over the Indian subcontinent and Indochina Peninsula.

The daily rainfall variations over the Tibetan Plateau are found to be well correlated with the variations of the Outgoing Longwave Radiation (OLR) and water budget data prepared by the Numerical Forecast Division of the Japan Meteorological Agency.

The ISV is studied over the Asian summer monsoon period in 1991, using the split window data aboard NOAA polar orbiting satellite. The ISVs of SST, water vapor and convection are seen clearly over the west off the Philippine Islands during May to July. Two peaks of this variation appear during the period with

the SST peak followed by the convection peak. The 20 days difference between the two peaks are consistent with the previous studies. However, the third peak of convection in August does not correspond to the SST variation. Mt. Pinatubo erupted in July. It seems the SST retrieval is affected by aerosol due to the eruption.

The South China Sea (SCS) monsoon influences the convective activities and synoptic-scale cyclone activities in the East Asia as well as in the Southeast Asia. Variations of the synoptic-scale cyclone activities well correspond to those of the convective activities.

The analysis of the precipitation systems using 5-day mean sea level pressure data from 1978 to 1992 shows that the onset of the summer monsoon over the western north Pacific near 15N are early in the La Nina years and late in the El Nino years. This confirms the similar delay of 20-25 days in the phase-lock of the intraseasonal oscillations obtained using the GMS high-cloud-amount data.

1. Objectives

This study aims at revealing the large scale features of the Asian Monsoon by using satellite data and the objective analysis data. The diurnal and intraseasonal variations(ISVs) are known as principle variations in the tropical convective activity. Efforts were made to reduce the influence of surface temperature variation and to understand the effect in the monsoon activities.

Split window data is effective to classify convective clouds and non-precipitating cold cirrus clouds. Convective activity can be assessed more reliably by split window than single infrared data. Split window is also effective in retrieving SST and water vapor amount over the cloud free ocean area. We can study ISV of convective activity in relation to these oceanic parameters.

The influence of the South China Sea(SCS) monsoon is large in the Southeast Asia. The effect of the SCS monsoon, however, has not been well studied. To this aim we examine how the SCS monsoon affects convective activities and synoptic-scale disturbances in the East Asia.

2. Methods

One degree square mesh 3 hourly mean equivalent black body temperature (TBB) data were used in the analysis of diurnal variation. Analysis area is from 80E to 180W in longitude and from 15S to 35N in latitude. Analysis period is summer season (May - September) for 14 years (1980-1994, excluding 1984).

To avoid the influence of temperature variation of the ground and sea surface, we defined the index (hereafter referred as IC255) as follows.

$$IC255 = |255-TBB| \quad \text{if } TBB < 255K$$
$$0 \quad \text{if } TBB > 255K$$

Firstly we decided the active and inactive periods of ISV on each mesh based on 30-60 day filtered anomaly of daily mean IC255. We defined the period as active (inactive) when the filtered anomaly is larger (less) than 1K(-1K). We computed diurnal components using Fourier analysis for both periods.

By using the station data over the Tibetan Plateau and the neighbor region during the summer period from May to September in 1994, we analyzed the daily rainfall and compared it with the Outgoing Longwave Radiation (OLR) data and water budget dataset prepared by the Numerical Forecasting Division of Japan Meteorological Agency.

Convection index was estimated using the brightness temperature optically thick cumulus clouds classified by the split window method. Non-precipitating cirrus clouds classified by the split window were discarded in estimating this convection index. SSTs were retrieved using the NOAA multi-channel SST algorithm for day time. Cloud free ocean areas were classified by the spatial coherence method.

In order to examine how the South China Sea monsoon affects convective activities and synoptic-scale disturbances, composite analysis is employed by reference to low-level zonal wind averaged over the South China Sea. Data used are wind at 850 hPa provided by NMC and TBB derived from GMS. Activities of synoptic-scale disturbances, which are defined as frequency of positive vorticity centers, are also composited.

The analysis of the precipitation systems using 5-day mean sea-level pressure data was carried out with emphasis on the interannual variations of the intraseasonal oscillations and its relationship to El Nino and La Nina.

3. Results

The computed phase change of the diurnal variation due to the intraseasonal variation (ISV) is shown in Fig. 1. The phase of the diurnal variation tends to be delayed over the sea and advanced over the land at the inactive phase of the ISV. This pattern of the phase change is seen over the Indian subcontinent, the Bay of Bengal, the Indochina Peninsula and the South China Sea.

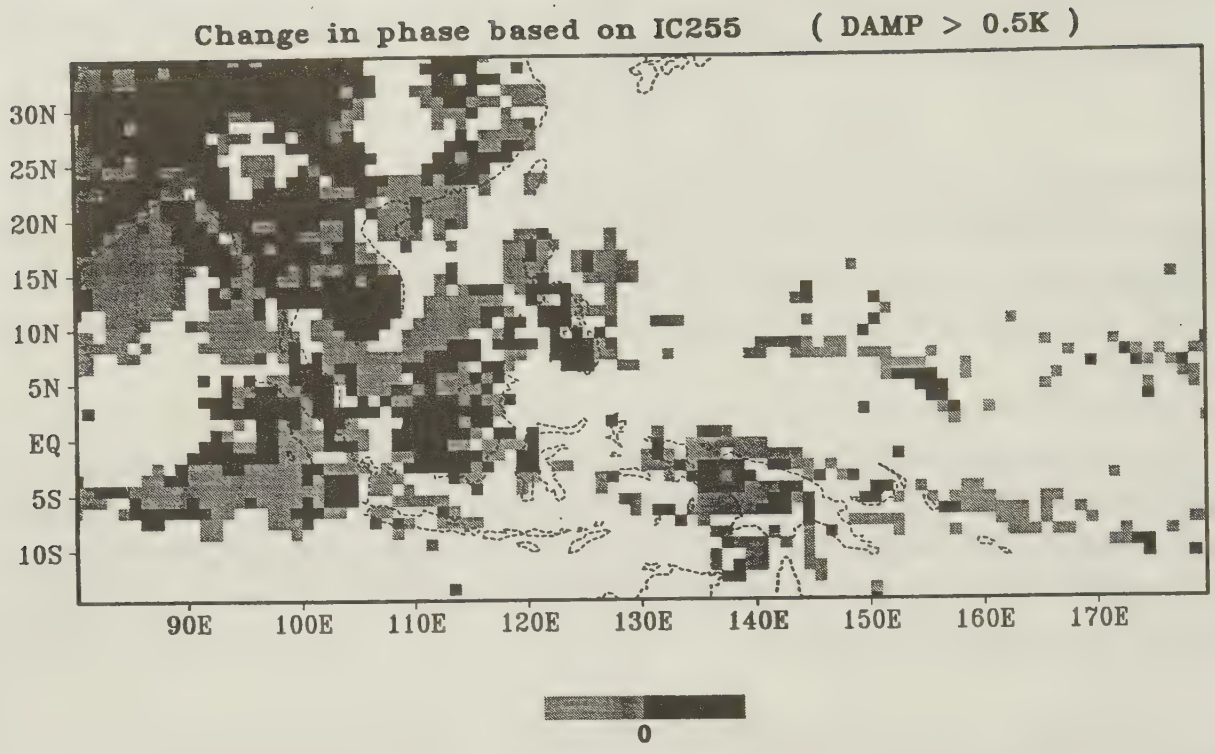

Fig. 1 The distribution of the difference of diurnal phase between active and inactive phases of the ISV (30-60 day mode). Dense(Light) shaded region is the one where diurnal phase is advanced(delayed) at the inactive phase of the ISV. The meshes with larger than 0.3K diurnal amplitude are plotted.

For the analysis of the rainfall variations over the Tibetan Plateau we divided the Tibetan area into two regions, one in the western part (80-90E, 30-37.5N), another in the eastern part (90-100E,30-37.5N). Table 1 shows monthly mean rainfall in these regions. Figure 2 is the OLR data (upper) in both regions from June to August, Total Precipitable Water (TPW) (middle) and the subtraction of the precipitation minus evaporation (lower). Figure 3 is the regionally averaged rainfall data from the water budget dataset. The rainfall is rich over the eastern Tibet in May and June, and that is rich over the western Tibet in July and August. From these data it is found that the OLR and the water budget dataset is well correlated each other.

Table 1 Monthly mean rainfall (mm/day) over the Tibetan Plateau in the summer of 1994

	5/94	6/94	7/94	8/94	9/94
Eastern Tibet	1.87	2.38	1.29	1.30	1.26
Western Tibet	0.84	1.27	2.03	1.84	0.93
Whole Tibet	1.36	1.82	1.66	1.57	1.09

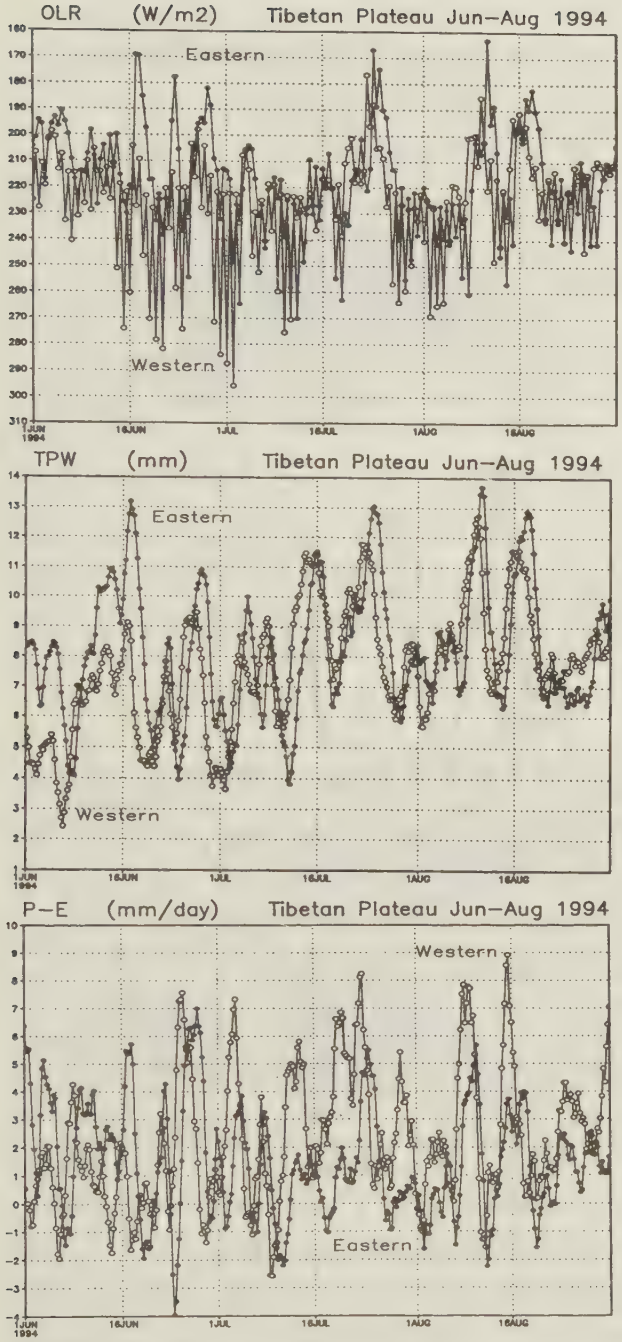

Fig. 2 OLR data (upper) in both regions from June to August, Total Precipitable Water (TPW) (middle) and the subtraction of the precipitation minus evaporation (bottom).

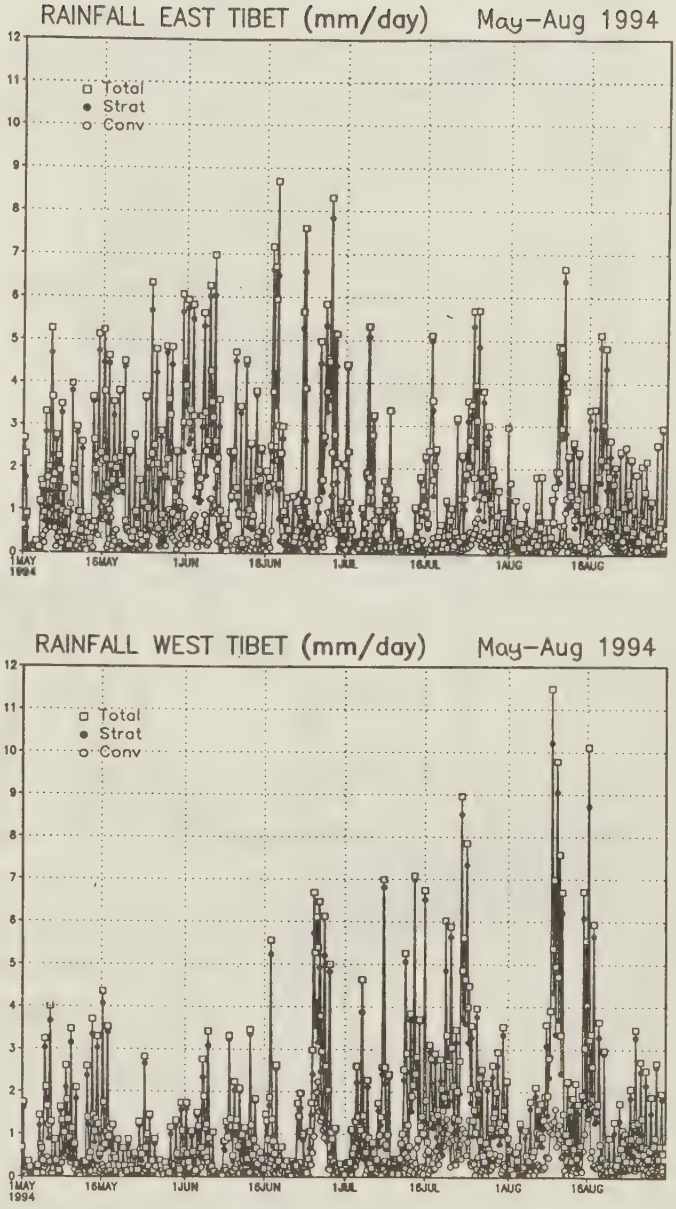

Fig. 3 Regionally averaged rainfall data from the water budget dataset.

Figure 4 shows the plots and smoothed curve of convection index and SST over the west off the Philippine islands where the intraseasonal variation (ISV) signal is very large. The convection index and SST were computed as 5-days mean over the area of 15N-20N and 115E-120E. The convection peaks appeared three times during this period (1 May - 31 August, 1991) in the time scale of the ISV. The SST indicated two significant peaks during the period. The SST peaks were followed by the convection peaks with 20 days time lag. This feature was consistent with our previous results and Kawamura (1983).

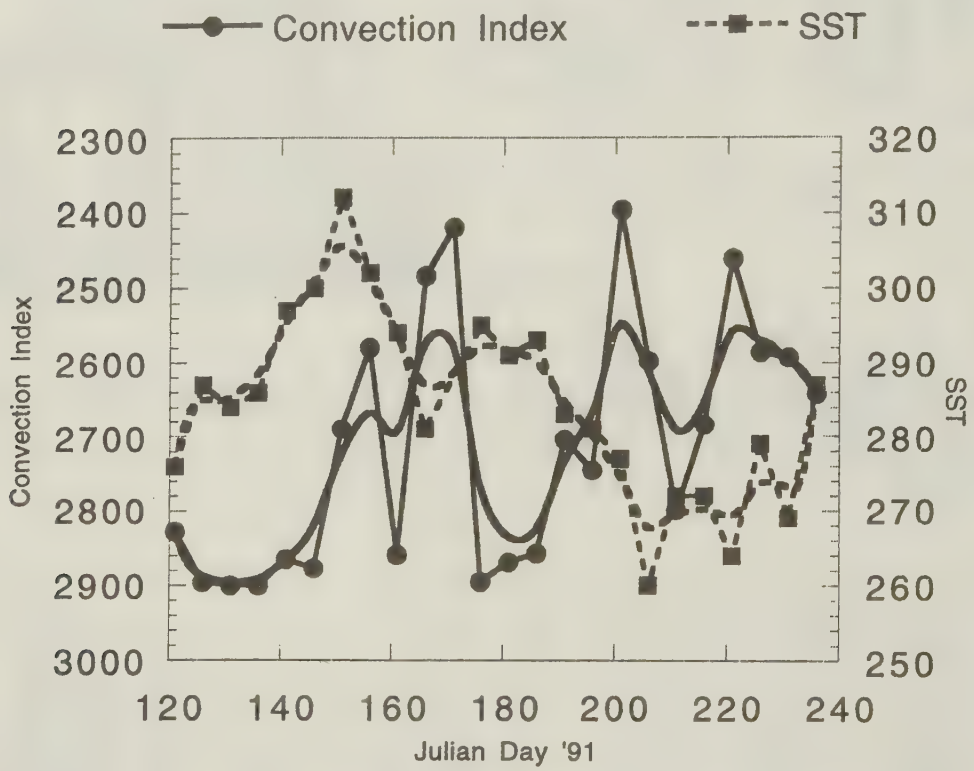

Fig. 4 Plots of five-day mean of convection index and SST over the area (15N-20N, 115E-120E).).

Figs. 5a and 5b show anomalies of the composites of 850 hPa wind and TBB at the active monsoon and break monsoon in the South China Sea (SCS), respectively, while Figs. 6a and 6b are anomalous plus time-mean fields of 850 hPa wind and the cyclone frequency distributions. At the active phase of the SCS monsoon enhanced cyclonic circulation over the SCS, enhancement of convection and cyclonic activities from Indochina to the western Pacific are seen. Easterly anomaly and intensified ridge from mid China to the East China Sea are observed. On the other hand at the break phase of the SCS monsoon the opposite anomalies are seen such as enhanced south westerly, intensification

of convective activities and more cyclone occurrences over the Yangtze Valley. From these figures the cyclone occurences well correspond to the convective activities.

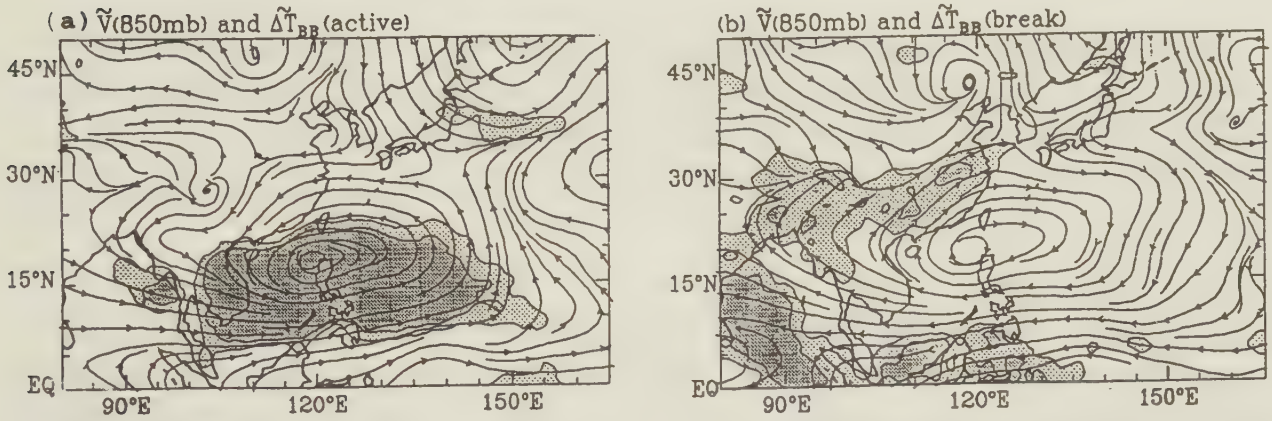

Fig. 5 15 years composite anomalies of 850 hPa stream functions (solid lines) and those of TBB (a) for the active South China Sea (SCS) monsoon and (b) for the break SCS monsoon. Light and dark shading denote regions where TBB anomalies are less than -0.5 and -1.5, respectively.

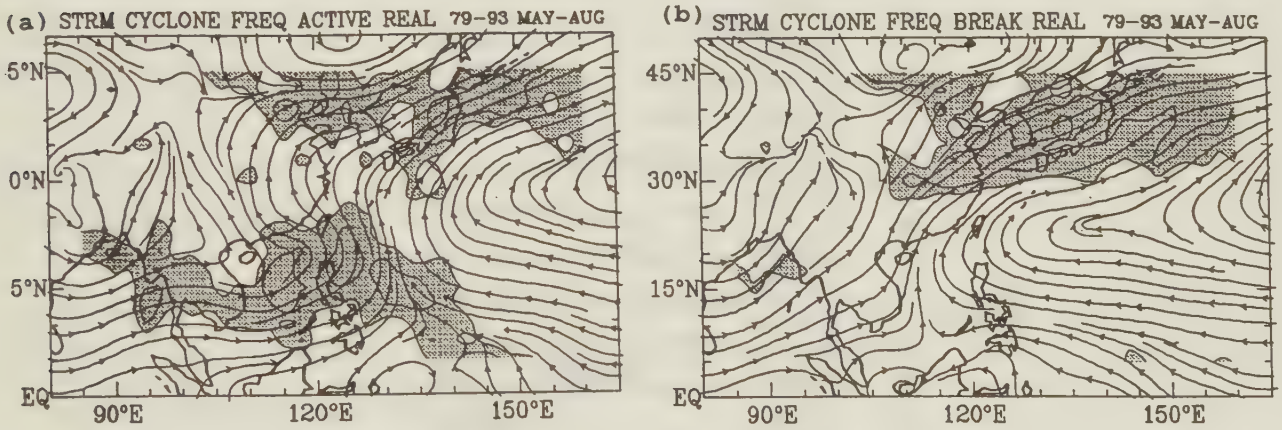

Fig. 6 15 year composites of 850 hPa stream functions and those of objectively analyzed cyclone frequency distribution (a) for the active SCS monsoon and (b) for the break SCS monsoon. Seasonal-mean fields are added. Light and dark shading denote regions where cyclone occurrences are larger than 12 days and 15 days for 15 years, respectively.

Time sequences of the composite fields from the active to the break phase (figures not shown) show that low-level cyclonic circulation moves smoothly

northward and dissipates while enhanced convection and cyclone frequencies move northward but weaken around 27N and strengthen again over the Yangtze Valley as shown in Fig. 5b and Fig. 6b. These suggest that the SCS monsoon deeply influences the convective activities and cyclone activities with about 5 day period in the East Asia.

The analysis of the precipitation systems using the 5-day mean sea-level pressure data from 1978 to 1992 confirmed that the onset of the western north Pacific summer monsoon defined by the sea-level pressure difference (10N minus 20N) at 140E (Fig. 7) are delayed by about 20-25 days in the El Nino years (1982, 83, 87, 91, 92) compared to the La Nina years (1978, 84, 85, 88).

4. Discussions

The result that the phase of the diurnal variation is delayed (advanced) at the active phase of the intraseasonal variation (ISV) is consistent with a hypothesis that diurnal variation is caused by solar heating over the land and by nocturnal cooling over the sea. Around the East China Sea it's known that biweekly mode is also prominent as the ISV, so ISV with periods other than 30-60 day is needed to be taken into consideration. To investigate more detailed structure of the diurnal variations, it'll effective to utilize histogram data of GMS infrared data.

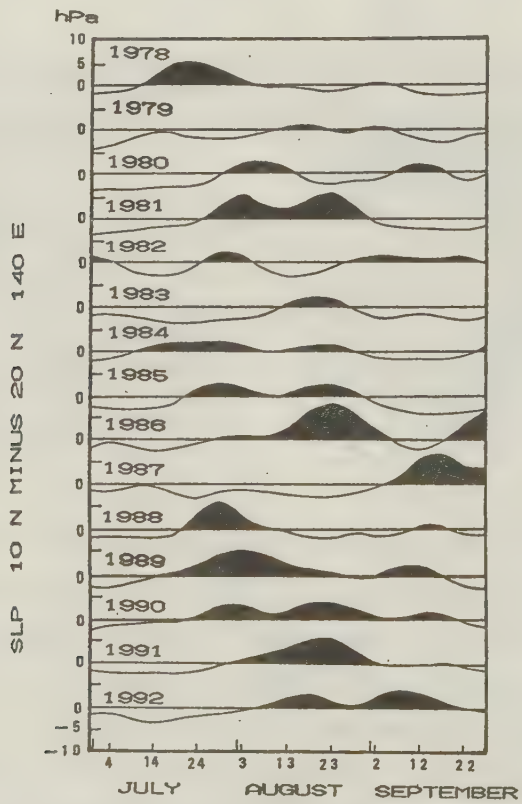

Fig. 7 Year-to-year change in the 1-2-1 filtered 5-day mean sea level pressure difference (10N minus 20N) at 140E from 1978 to 1992. Shaded areas show the period of westerly geostrophic winds at 15N.

The previous work on the rainfall pattern over the Tibetan Plateau shows that there exists much rainfall over the eastern Tibet compared with the western Tibet. The rainfall in 1994 summer does not agree with the simple expectations. Further analysis is needed to examine weather system responsible to these rainfall events.

In Fig. 4 the third peak of convection does not correspond to the SST peak. Mt. Pinatubo erupted middle of July. The SST retrieval by the satellite data seems less accurate due to aerosol by the eruption. This seems one reason for absence of the third peak of the convection.

In the analysis of the convective activities over the East Asia TBB might not be a good indicator for the convection in the mid latitude. Daily precipitation data in China are used to check the TBB data. Preliminary composite analysis suggests that precipitation data give the similar pattern as the TBB.

To clarify further the relationship between the Asian monsoon and the ENSO, currently we are also conducting the analysis of the relationship between the western north Pacific summer monsoon, Baiu cloud and rain in the East Asia and the SST in the eastern Equatorial Pacific.

5. References

R. Kawamura ;J. Meteor. Soc. Japan, 6, pp1007-1012, 1988.

6. Publications

(Oral presentation)

M. Tanaka: Interannual variations of the summer monsoon over East Asia and western north Pacific. Its relationship to the El Ninos.
1995 Spring meeting of MSJ, May 1995

T. Inoue and K. Mori: Comparison of Keifu-Maru radar data with MIT radar data.
1995 Autumn meeting of MSJ, October 1995.

T. Inoue and T. Kurino: Cloud classification by NOAA polar orbiting satellite and GMS-5, 1995 Autumn meeting of MSJ, October 1995.

K. Takahashi and M. Murakami: Analysis of the influence of the intraseasonal variation on the diurnal variation using the geosynchronous satellite data Part 3.
1995 Autumn meeting of MSJ, October 1995.

M. Tanaka: Effects of the eastern equatorial Pacific SST on the seasonal change in locations of the typhoons in the western north Pacific.
Technical Conference on Spectrum, November 1995

T. Inoue: Current status of precipitation estimate by split window method.
6th TRMM workshop in Japan, March 1996.

N. Yamazaki: Influence of the South China Sea monsoon on the short-term disturbances in the East Asia. 6th TRMM workshop in Japan, March 1996.

K. Takahashi and M. Murakami: Analysis of diurnal variation of cumulative activity and influence by intraseasonal variation using GMS TBB data.
6th TRMM workshop in Japan, March 1996.

7. International Cooperation

The cooperation with China has been carried out based on the agreement signed in 1993 between Japan Science and Technology Agency and China Meteorological Administration. During FY 1995, three Chinese experts were invited to M.R.I. and performed the joint study on the interannual aspects of Asian monsoon by using the GMS satellite data. From Japanese side, one research official visited China during FY 1995 and performed the joint study on the analysis of monsoon related rainfall activity.

要旨

ＧＭＳ衛星資料による１度格子平均赤外データを用いて南シナ海及びベンガル湾周辺における季節内変動が積雲対流活動の日変化に及ぼす影響を調査し、日変化の位相は海上では季節内変動不活発期に遅れ、陸上では早まることを見出した。

１９９４年夏季のチベット付近の日降水量を解析し、外向き長波放射及び気象庁数値予報課作成の水収支データと整合性ある変動を示すことが分かった。

スプリットウィンドウにより海面水温、水蒸気量、対流活動の季節内変動を１９９１年５月から８月まで調べた。これらの季節内変動はフィリピンの西海上で明瞭に見られた。５月から７月では以前の研究と同じく海面水温のピークの２０日後に対流活動のピークが見られたが、８月の対流活動のピークは海面水温の変動と対応していなかった。７月のピナツボ火山の噴火によるエアロゾルが衛星による海面水温の評価に影響したと考えられる。

南シナ海モンスーンの変動が中国を含む東アジア域における対流活動、降水及び総観規模擾乱の活動度に与える影響を調べ、東アジア域に大きな影響を与えるとともに総観規模の擾乱の活動度は対流活動と密接に関連することが分かった。

５日平均の海面気圧を１９７８年から１９９２年の期間について調べ、西太平洋上の１５Ｎ付近の夏のモンスーンの開始はラニーニヤ年にはエルニーニヨ年にくらべて２０－２５日ほど早いことが見出された。これはＧＭＳ上層雲量で見られた季節内変動の位相の進みが海面気圧でも見られることを示す。

I. Observation and analysis on the process of the atmosphere–ocean–land interactions

大気・海洋・陸域間相互作用の諸過程に関する観測・解析研究

1. Observation and analysis on the process in the atmosphere

大気における諸過程に関する観測・解析研究

(2) Observation of structure of convective clouds in large-scale cloud systems

大規模雲域内における対流雲構造に関する観測研究

Meteorological Research Institute,
Japan Meteorological Agency
気象庁気象研究所
H.Sakakibara, H.Okamura, K.Akaeda,
K.Mori, Y.Shimazu
榊原均、岡村博文、赤枝健治、
森一正、島津好男

(ABSTRACT)

In order to reveal the structure of convective clouds in cloud clusters, convective clouds in typhoons and cloud clusters associated with the Baiu front which is a stationary front extending from China to Japan in early summer months were observed by using X-band Doppler radars and omega-sondes in the island of Miyako (24.8N,125.4E) from 1990 to 1992.

Structure of convective clouds in meso-α-scale cloud systems in Severe Tropical Storm 9219 (Ted) and in the Baiu-frontal zone was analyzed. Two meso-α-scale cloud clusters which developed 500km northeast of the STS center brought heavy rain more than 150mm during their passage over the island. They contained a few meso-β-scale precipitation systems. The precipitation systems consisted of several convective systems. Some of them were associated with a mesocyclone. One of the mesocyclones is supposed to have produced a wind-spout.

Cloud clusters which occurred near the Baiu front from 8 June to 11 June 1992 were classified into moving type on 8 and 9 June and quasi-stationary type on 10 and 11 June. Upper-air soundings at the island of Ishigaki 110km west-southwest of the island of Miyako indicate that relative humidity at middle levels increased after 21JST 9 June and that wind at low levels weakened after 12JST 10 June. These upper-air features may relate to the type of cloud clusters.

1. OBJECTIVES

Cloud clusters which form and develop over the warm sea transport upward heat and water

vapor added through the sea surface. Water vapor condenses during the upward transportation. Some fraction of condensed water falls and reaches the sea surface as rain. Latent heat released by condensation of water vapor to form raindrops remains in the atmosphere and heats the air in the cloud cluster. This heating is not only the energy source of the cloud cluster but one of the energy sources of monsoon.

In this study we aimed to reveal the structure of convective clouds in cloud clusters and the interaction between convective clouds and cloud clusters and to discuss the processes of precipitation and vertical transport of heat and water substances.

2. METHODS

Convective clouds in typhoons and cloud clusters associated with the Baiu front which is a stationary front extending from China to Japan in early summer months were observed by using X-band Doppler radars of MRI and NIED and omega-sondes in the island of Miyako (24.8N, 125.4E) from 1990 to 1992. Structure of convective clouds in meso-α-scale cloud systems in Severe Tropical Storm 9219 (Ted) and in the Baiu-frontal zone were analyzed. In the analysis we used the specially observed data in the island of Miyako and operationally obtained data of conventional radar, GMS, upper-air and surface observations.

3. RESULTS

(1) Mesoscale precipitation system northeast of Severe Tropical Storm 9219

Severe Tropical Storm (STS) 9219 was located south-southwest of the island of Miyako and was moving westward on 21 September 1992. Its central pressure was 985 hPa. After 06JST on 21 September mesoscale cloud systems tended to line up from southwest to northeast to the north of the STS center.

Two mesoscale cloud systems (MCSs) which brought heavy rain (20-40mm/2-3h) on the island of Miyako started to develop northeast of STS 9219 about 0130JST and 1530JST on 21 September. The first one (MCS1) was extensive from 04JST to 21JST on 21 September. It dissipated after its passage over the island. The second MCS (MCS2) developed, as the first one dissipated. Both MCSs moved northeastward. Most of the total rainfall of 181mm on the island of Miyako was brought by the MCSs.

Figure 1 shows the distribution of T_{BB} at 0040JST on 22 September. The MCS2 was nearly stationary and was extending. There were two meso-β-scale precipitation systems in the MCS2, that is, MPS21 and MPS22 (Fig.2). They moved north-northwestward at a speed of 55-65 km/h, and the MPS22 was passing over the island of Miyako. The MPS12 in the MCS1 which had passed over the island of Miyako on the previous day remained 200km north of the island and were dissipating.

The MPS12 had horizontal scale of 300km and consisted of a strong precipitation band on the southwestern portion and a stratiform precipitation area on the northeastern portion. The MPS12 passed over the island of Miyako north-northwestward at a speed of 20-40 km/h from 09 JST to 21 JST on 21 September. Convective systems in the MPS consisted of convective cells being in line from north-northeast to south-southwest. Some of the convective systems were associated with a pair of maximum and minimum of Doppler velocity, which suggests the existence of a cyclonic circulation (D~10km, vorticity~$10^{-3}s^{-1}$) in the lowest layer on its rear side (Fig.3). Some of these convective systems passed over the MRI site. Heavy rain, wind shift, and pressure dip of 1.4 hPa were observed during the passage of the convective system A (Fig.4).

The MPS22 passed over the island of Miyako from 21JST on 21 September to 02 JST on 22 September. It contained a band of strong precipitation oriented from northwest to southeast whose horizontal scale was about 200km. The MPS moved north-northwestward at a speed of 65km/h. Most of convective systems in this MPS were composed of convective cells, which lined up from north-northeast to south-southwest, and had a low-level cyclonic circulation (D~10km, vorticity~$10^{-3}s^{-1}$) near its southwestern edge. The convective systems lined up from north-northwest to south-southeast at intervals of 20km and moved north-northwestward at the speed of 55km/h.

The convective system B in the MPS22 is supposed to have contained a wind-spout based on damage of houses and trees. Figure 5 shows its structure observed by the Doppler radar. In the lower layer, it shows a line structure of 30km long containing three convective cells. The convective cell at the southwestern end had the highest reflectivity and coincided with the center of a low-level cyclonic circulation. In the middle layer the cells sloped toward the northeast. The precipitation area extended rear-rightward in the upper layer. The convective system B passed over the MRI site at 0005JST on 22 September and the time changes of pressure, wind and temperature similar to those with the convective system A were observed.

Environment of the MCSs was largely affected by the STS 9219. Middle and lower tropospheric winds over the island of Miyako were easterly on 20 September. Southerly winds appeared after 09JST on 21 September between the 800 hPa and 500 hPa levels, as the STS moved from south to west of the island and made the vertical wind shear strong in the lowest layer until 03JST 22 September. The MPS12 and MPS22 were formed under the condition of latent instability and strong veering shear (Fig.6). The occurrence of vortices in MPSs may relate to the strong vertical shear.

(2) Mesoscale cloud systems in the Baiu-frontal zone

Features of mesoscale cloud systems (MCSs) around the island of Miyako during 8 June and 11 June 1992 were studied.

MCSs are classified into two types, moving type and quasi-stationary type, based on their motion. Moving MCSs occurred on 8 June to 9 June, while quasi-stationary ones on 10 June to 11 June. On 10 June, several MCSs occurred successively, merged each other and formed a larger MCS. Upper-air soundings at the island of Ishigaki (110 km west-southwest of the island of Miyako) show weakening of winds below the 5-km level after 12 JST on 10 June and increase of relative humidity at middle levels after 21JST on 9 June (Fig.7). The change of types of MCSs may relate to these changes of upper-air conditions.

Features of the MCSs on 10 June in comparison with those on 8-9 June are:

(1) Larger cold domes produced by MCSs.

(2) Stronger convergence at the front edge of the cold dome.

(3) Smaller temperature difference between the cold air and environment at the surface.

In addition, a wide stratiform precipitation area was associated with the MCSs on 10 June, while it was not associated with the MCSs on 8-9 June.

Divergence of wind normal to convective cloud lines was calculated from VAD data of NIED and MRI Doppler observations and vertical velocity was also calculated. In the area containing the convective cloud line on 9 June, large convergence existed at low levels and weak convergence was at middle levels. Divergence at high levels was not clear. On the other hand, the convective cloud line at 1541 JST on 10 June was associated with low-level deep convergence layer and upper divergence layer.

4. DISCUSSIONS

Heavy rain fell on the island of Miyako 500km northeast of the STS 9219. Two MCSs brought rain of more than 150mm. Although the island was far from the STS center, synoptic situations seems to be favorable for the occurrence of MCSs. The STS circulation transported warm and moist air from the south at low levels. Low-level convergence (high-level divergence) would be caused by the STS circulation and low-level easterly (high-level westerly) north of the island.

Types of MCSs in the Baiu-frontal zone may relate to the upper-air conditions and structural features mentioned above. The structural features would result largely from the upper-air conditions.

The relation between the synoptic situations and mesoscale phenomena including MCSs and MPSs needs to be studied more extensively. Furthermore, structure of convective systems in MPSs needs to be studied in relation to upper-air conditions. For convective systems in typhoons structure should be studied in relation to parameters of typhoon such as central pressure, maximum wind and so on.

5. REFERENCES

None

6. PUBLICATIONS

Akaeda,K. and S.Nakai, Two types of organized convective system observed in subtropical cloud cluster. American Meteorological Society. Preprints of 27th Conf. on Radar Meteor., 383–385, 1995

Mori,K., Y.Shimazu, H.Okamura, H.Sakakibara and S.Nakai, Mesoscale precipitation systems with severe phenomena in a typhoon area –Preliminary report–. Meteorological Society of Japan. Preprints of the presentation, May 1995.

Mori,K., Y.Shimazu, H.Okamura, H.Sakakibara and S.Nakai, Mesoscale precipitation systems with severe phenomena in a typhoon area –Fine structure–. Meteorological Society of Japan. Preprints of the presentation, October 1995.

7. INTERNATIONAL COOPERATION

None

（要旨）

アジアモンスーン域の暖かい海洋上に発生する大規模雲域内の対流雲は暖かい海面から熱、水蒸気を上空に輸送する。水蒸気の凝結（及びその後の降水）による潜熱の放出は大規模雲域のエネルギー源であると同時にモンスーンのエネルギー源でもある。熱、水の輸送過程に関連する対流雲の構造と対流雲と大規模雲域の相互作用を調べる目的で、１９９０年から９２年まで宮古島（北緯２５度、東経１２５度）でドップラーレーダーとオメガゾンデによる大規模雲域（台風と梅雨期クラウドクラスター）内の対流雲の３次元構造の観測を行った。

今年度は台風９２１９号に伴い発生したクラウドクラスター内の対流雲構造と梅雨期クラウドクラスターのメソαスケール、メソβスケール、メソγスケールの特徴を調べた。

台風９２１９号の北東側５００ｋｍで台風固有の雲域から離れ発生した二つのメソαスケールクラウドクラスターは宮古島通過時に１５０ｍｍ以上の降雨をもたらした。その中には数本の北西から南東に伸びるメソβスケール降雨帯が含まれていた。この降雨帯は南西部に約２０ｋｍ間隔で北西から南東に並ぶ対流系から成っていた。対流系の中にはその南西端にメソγスケールの渦度集中域を伴う活発な対流系がいくつかあった。このうちの一つは竜巻を伴っていたと考えられる。これら対流系が観測地点を通過したとき、強い雨、風の急変、気圧の急な低下が観測された。

梅雨期クラウドクラスターについては、期間を１９９２年６月８日から１１日までと広げて解析した。クラウドクラスターは移動型と停滞型に分けられた。８日と９日には移動型が１０日と１１日には停滞型が現れた。１０日には停滞型が続けて発生して融合したため、大きなクラウドクラスターとなった。西南西１１０ｋｍの石垣島における高層観測では９日２１時以降中層の湿度が高くなり、１０日１２時以降下層の風が弱くなった。これらがクラウドクラスターの型の変化と関連しているかもしれない。１０日のクラウドクラスターを８－９日のクラウドクラスターと比較すると寒気ドームはより大きく、その先端での収束もより強いが、寒気とその周囲の気温差はより小さかった。

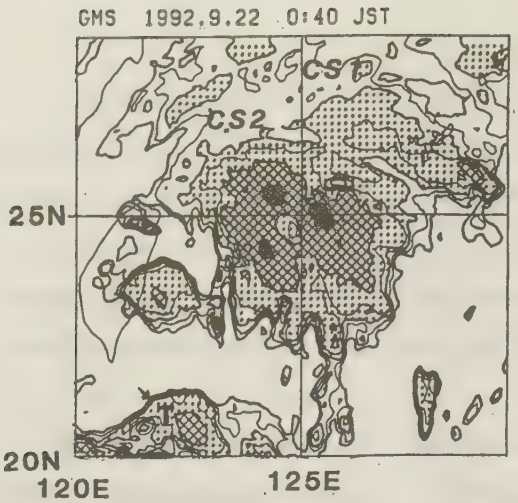

Fig.1 Equivalent blackbody temperature (T_{BB}) observed by GMS at 0040JST 22 September 1992. Contours are at intervals of 10C starting from −20C. The STS center is shown by "T".

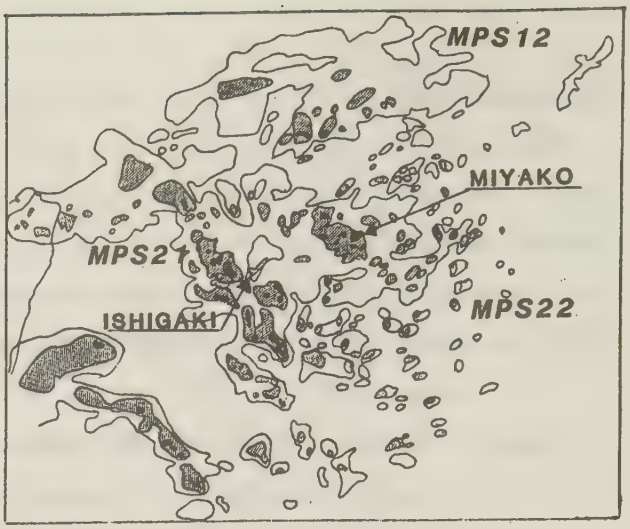

Fig.2 Composite radar echo observed by the Miyako and Ishigaki radars at 0000JST 22 September 1992.

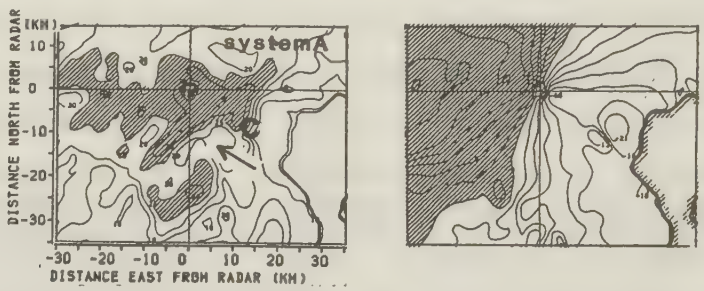

Fig.3 Reflectivity (left) and Doppler velocity (right) at the 1−km level observed by the MRI Doppler radar at 1609JST 21 September 1992. Contours of reflectivity are at intervals of 5dB starting from 0dBZ. Contours of Doppler velocity are at 3m/s intervals. Hatched shading represents receding velocities. The center of cyclonic circulation is shown by "C".

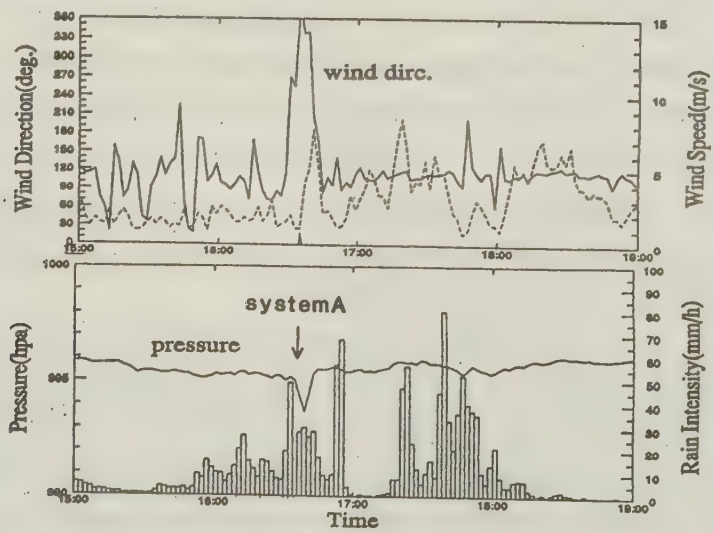

Fig.4 Surface wind direction, wind speed, pressure and rainfall intensity observed at the MRI Doppler radar site from 1500JST to 1900JST 21 September 1992.

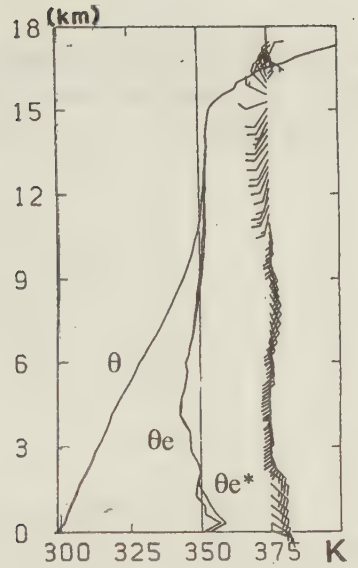

Fig.6 Upper-air sounding at the island of Miyako at 1745JST 21 September 1992. A full barb indicates 5m/s.

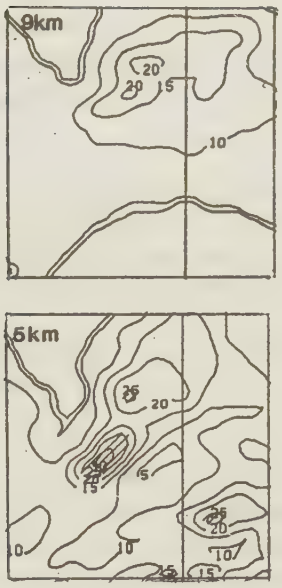

Fig.5 Reflectivity at the 1-km, 5-km, and 9-km levels observed by the MRI Doppler radar at 0035JST 22 September 1992. Contours are at intervals of 5dB starting from 0dBZ. The center of cyclonic circulation is shown by "C".

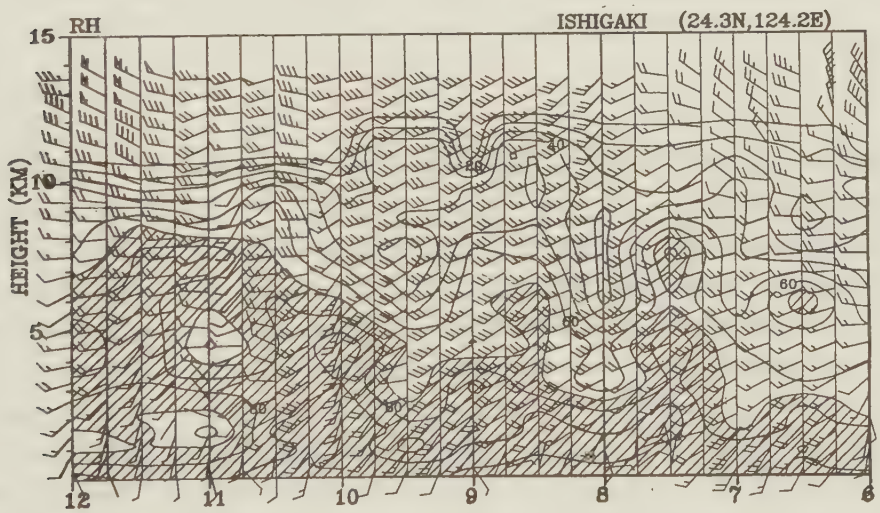

Fig.7 Time-height section of horizontal wind and relative humidity observed at the island of Ishigaki from 6 June to 12 June 1992.

I. Observation and analysis on the process of the atmosphere-ocean-land interactions
1. Observation and analysis on the process in the atmosphere
(3) Analysis on the evolution of convective cloud systems

Advanced Measurement and Analysis Technology Division
National Research Institute for Earth Science and Disaster Prevention (NIED)
Science and Technology Agency
S. Nakai

Abstract

Baiu frontal zone over the East China sea and the northwestern Pacific is one of the regions that generate many convective cloud systems. They play an important role on the water cycle of Baiu front. The activity of Baiu front is closely related to the global Monsoon circulation. So, it is important to clarify the water cycle of the Baiu frontal zone focusing on the evolution of convective cloud systems.

In FY1995, the attenuation of X-band radar beam by rain was estimated using the equivalent reflectivity factor (Ze) data. The attenuation rate was assumed to be the form of $K=a\ Ze^{0.755}$ (dB km^{-1}) following the formulation by Kozu (1991) based on Marshall-Palmer raindrop size distribution (hereafter referred to as K-MP). First, the attenuation rate was obtained using the beams of two radars in the opposite directions. Seventy pairs of beams were selected along the base line of the dual observation from the data on June 10, 1992. The 'real' equivalent reflectivity factor was calculated assuming that the difference of reflectivity between the two radars was attributed to the attenuation by rain. The attenuation of the beams was corrected successfully, though, the derived attenuation rate $K_1=5.67\times10^{-4}\ Ze^{0.755}$ was too large. Next, the equivalent reflectivity factor values of the two radars were compared and the difference was examined on a common horizontal section. The attenuation rate which made the difference to be smallest was $K_2\sim2.3\times10^{-4}Z^{0.755}$. This is 1.3 times larger than K-MP value, and is considered to represent the average attenuation rate on the horizontal section. It is inferred that K_1 was biased by the inhomogeneous distribution of raindrops within the sampling volumes, though K_1 may suffer from the contamination of ground clutter.

1. Objectives

The characteristics of the convective clouds vary from place to place in the world. Baiu frontal zone over the East China sea and the northwestern Pacific is one of the regions that generate many convective clouds. Especially, mesoscale convective systems (MCSs) play an important role on the water cycle of Baiu front. The activity of Baiu front closely related to the global Monsoon circulation (*e.g.*, Kato, 1993). It is important to clarify the evolution and the water cycle in MCSs observed in the Baiu frontal zone.

Cooperative observations on the structure of convective clouds were made in June 1992 by Meteorological Research Institute (MRI) and National Research Institute for Earth Science and Disaster Prevention (NIED). The investigation of the observed precipitating clouds has been carried out mainly using the observation data and the satellite data. The primary interest is on 1) the process that MCSs vertically transport water, 2) redistribution of water as precipitation, upper level cloud and water vapor, and 3) the mesoscale circulation and its role in the maintenance of MCSs.

In FY1995, the attenuation of X-band radar beam by rain was estimated using the equivalent reflectivity factor data. We can take the attenuation into account subjectively, and usually, it is tolerable for the analysis of the structure of precipitating convective clouds. However, for the comparison of the X-band radar data with satellite data, it is necessary to correct the attenuation by rain numerically. This is the problem practically of X-band radars, which have the advantage of high-resolution and high-sensitivity, and which we used in the observation of this project. We usually do not have to consider about the attenuation at C-band or at longer wavelengths, for example, operational radars of Japan Meteorological Agency.

The attenuation of electromagnetic wave by rain has been investigated from 1940s. The attenuation rate

Table 1. K-Ze relations for a X-band radar derived by combining K-R and Ze-R relations based on the common raindrop size distribution (DSD). The units are K(dB km^{-1}), T(°C), Ze(mm^6m^{-3}) and R(mm $hour^{-1}$).

K-Ze relation	K-R relation Wavelength , T Reference	Ze-R relation Wavelength , T Reference	DSD(Phenomena) Location Reference
$K=5.99\times10^{-5}Ze^{0.840}$	$K=0.0074R^{1.31}$ 3.2cm , 18°C Gunn and East, 1954	$Ze=310R^{1.56}$ 3.2cm , 18°C Gunn and East, 1954	storms Washington, D. C., USA Laws and Parsons, 1943
$K=2.68\times10^{-5}Ze^{0.929}$	$K=0.007R^{1.3}$ 3.2cm , 20°C Imai, 1957	$Ze=400R^{1.4}$ Doviak and Zrnić, 1984	storms Washington, D. C., USA Laws and Parsons, 1943
$K=5.64\times10^{-5}Ze^{0.864}$	$K=0.01R^{1.21}$ 3.2cm , 18°C Doviak and Zrnić, 1984	$Ze=400R^{1.4}$ Doviak and Zrnić, 1984	storms Washington, D. C., USA Laws and Parsons, 1943
$K=1.70\times10^{-4}Ze^{0.742}$	$K=0.011R^{1.15}$ 3.21cm , 0°C Wexler and Atlas, 1963	$Ze=275R^{1.55}$ 3.21cm , 0°C Wexler and Atlas, 1963	stratiform rain Ottawa, Canada Marshall and Palmer, 1948
$K=2.02\times10^{-5}Ze$	$K=0.018R$ 3.21cm , 0°C Wexler and Atlas, 1963	$Ze=890R$ 3.21cm , 0°C Wexler and Atlas, 1963	showers Florida, USA Mueller and Jones, 1960
$K=1.75\times10^{-4}Ze^{0.744}$ Kabèche and Testud, 1995	$K=0.0114R^{1.154}$ 9.22GHz(3.25cm) , 0°C Olsen et al., 1978	$Ze=275R^{1.55}$ 3.21cm , 0°C Wexler and Atlas, 1963	stratiform rain Ottawa, Canada Marshall and Palmer, 1948
$K=2.82\times10^{-4}Ze^{0.742}$	$K=0.00952R^{1.12}$ (0.5-80mm/h) 10.0GHz(3.00cm) , 10°C Kozu , 1991	$Ze=115R^{1.51}$ (0.5-80mm/h) 10.0GHz(3.00cm) , 10°C Kozu , 1991	drizzle Locarno, Switzerland Joss et al., 1968
$K=1.78\times10^{-4}Ze^{0.755}$	$K=0.0101R^{1.20}$ (0.5-80mm/h) 10.0GHz(3.00cm) , 10°C Kozu , 1991	$Ze=211R^{1.59}$ (0.5-80mm/h) 10.0GHz(3.00cm) , 10°C Kozu , 1991	stratiform rain Ottawa, Canada Marshall and Palmer, 1948
$K=1.12\times10^{-4}Ze^{0.759}$	$K=0.0136R^{1.23}$ (0.5-80mm/h) 10.0GHz(3.00cm) , 10°C Kozu , 1991	$Ze=557R^{1.62}$ (0.5-80mm/h) 10.0GHz(3.00cm) , 10°C Kozu , 1991	thunderstorm Locarno, Switzerland Joss et al., 1968
$K=1.24\times10^{-4}Ze^{0.819}$	$K=0.00988R^{1.13}$ (1-100mm/h) 10.0GHz(3.00cm) , 10°C Kozu , 1991	$Ze=209R^{1.38}$ (1-100mm/h) 10.0GHz(3.00cm) , 10°C Kozu , 1991	two-year disdrometer data Kashima, Japan Kozu, 1991

(K) was deduced by theoretical calculation of Mie scattering based on various raindrop-size distributions (DSDs). K was defined for one-way attenuation and expressed by dB km^{-1} or dB km^{-1} (mm h^{-1})$^{-1}$ as a function of rainfall rate (R). Ze-R relations are necessary to use these attenuation rate for the analysis of radar observation data. K-Ze relations, compiled and appropriately combined by the author, are listed in Table 1.

The correction of attenuation by rain can be made in a certain degree of approximation using observed equivalent reflectivity factor data only. Such method is applicable to a lot of dual-Doppler observation data which do not have polarization information so that methods using 'specific differential phase' (*e.g.*, Ryzhkov and Zrnić, 1995) is not available. This approach is similar to that of 'stereoradar analysis (Kabèche and Testud, 1995; Testud and Amayenc, 1989)'. Their method, using dual-beam airborne Doppler radar data, successively retrieved the 'real' equivalent reflectivity factor field where the data of both radars were available. However, in case of ground-based radars, the required 'boundary condition' will be less frequently satisfied. We derived average attenuation rate of 1-day observation data of NIED Doppler radar (NIED-BD) and MRI 3cm wavelength Doppler radar (MRI-3CD) using two different methods, and compared the results with each other and with Ks in Table 1.

2. Methods

(a) Attenuation rate obtained by the beam pairs along the base line

The basic idea of this method is shown in Fig. 1. The x-axis is the line passing through the two radars. It is assumed that equivalent reflectivity factors in decibel units, I_1 (dBZ=dB[mm^{6}m^{-3}], by radar 1 located at x=0) and I_2 (dBZ, by radar 2 located at x=d), are observed simultaneously at the same sampling volumes. I_1 and I_2 are expected to suffer from the attenuation by rain and to be systematically smaller than the 'real' equivalent reflectivity factor I_0 (dBZ).

The relation between I_1 and I_0 is expressed using attenuation rate K (>0, dB km^{-1}) as

$$I_1(x) = I_0(x) - 2\int_{x_{m1}}^{x_{m2}} K(I_0(\xi))\, d\xi \quad , \tag{1}$$

where x_{m1} and x_{m2} are used instead of 0 and d, respectively, to avoid the contamination of main bank of the radars. This formulation is the same as that of 'stereoradar analysis'. It is assumed that no attenuation occurred at $0 \leqq x < x_{m1}$ and $x_{m2} < x \leqq d$. Differentiating this equation with respect to x, and similarly formulating with I_2, leads to

$$\frac{dI_1}{dx} = \frac{dI_0}{dx} - 2K(I_0) \quad , \qquad \frac{dI_2}{dx} = \frac{dI_0}{dx} + 2K(I_0) \quad .$$

Then, dI_0/dx and K are expressed as

$$\frac{dI_0}{dx} = \left(\frac{dI_1}{dx} + \frac{dI_2}{dx} \right) \Big/ 2 \tag{2}$$

$$K(I_0) = \left(\frac{dI_2}{dx} - \frac{dI_1}{dx} \right) \Big/ 4 \quad . \tag{3}$$

Applying (2) and (1) to the observation data I_1 and I_2 yields I_0 at $x_{m1} \leqq x \leqq x_{m2}$. Using $I_2(x_{m2})$ instead of $I_1(x_{m1})$ in (1) yields another I_0. We adopted the average of two I_0s as the result. Figure 2 is an example of the attenuation correction. Two curves for the observed values, I_1 and I_2, are crossed with each other as shown in Fig. 1. The attenuation was 10 dB at about 20km from either radar. The corrected equivalent

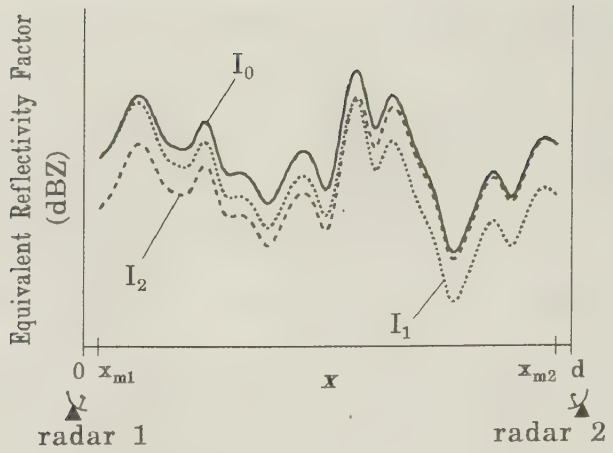

Fig. 1. The basic idea of the method to obtain attenuation rate using a pair of beams in opposite directions along the base line of the dual observation. See text.

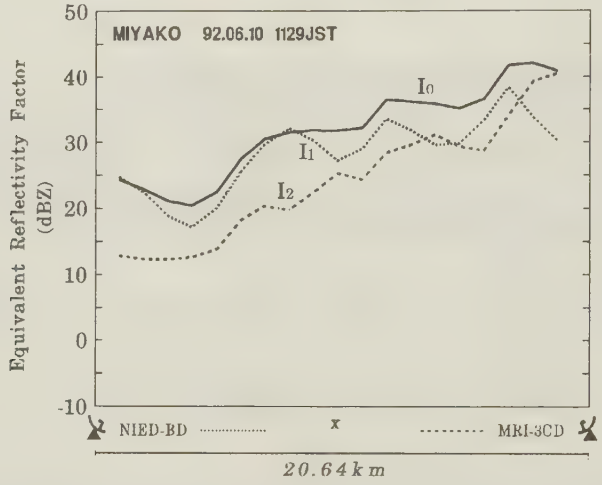

Fig. 2. Attenuation correction using a pair of beams. I_1, I_2 and I_0 are the same as shown in Fig. 1. NIED-BD (NIED Doppler radar) and MRI-3CD (MRI 3cm wavelength Doppler radar) correspond to radar 1 and 2 in Fig. 1, respectively. Noises and small-scale fluctuations have been removed from I_1 and I_2.

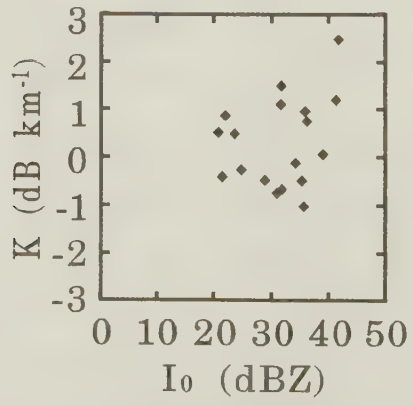

Fig. 3. A set of K calculated by (3) from the data shown in Fig. 2.

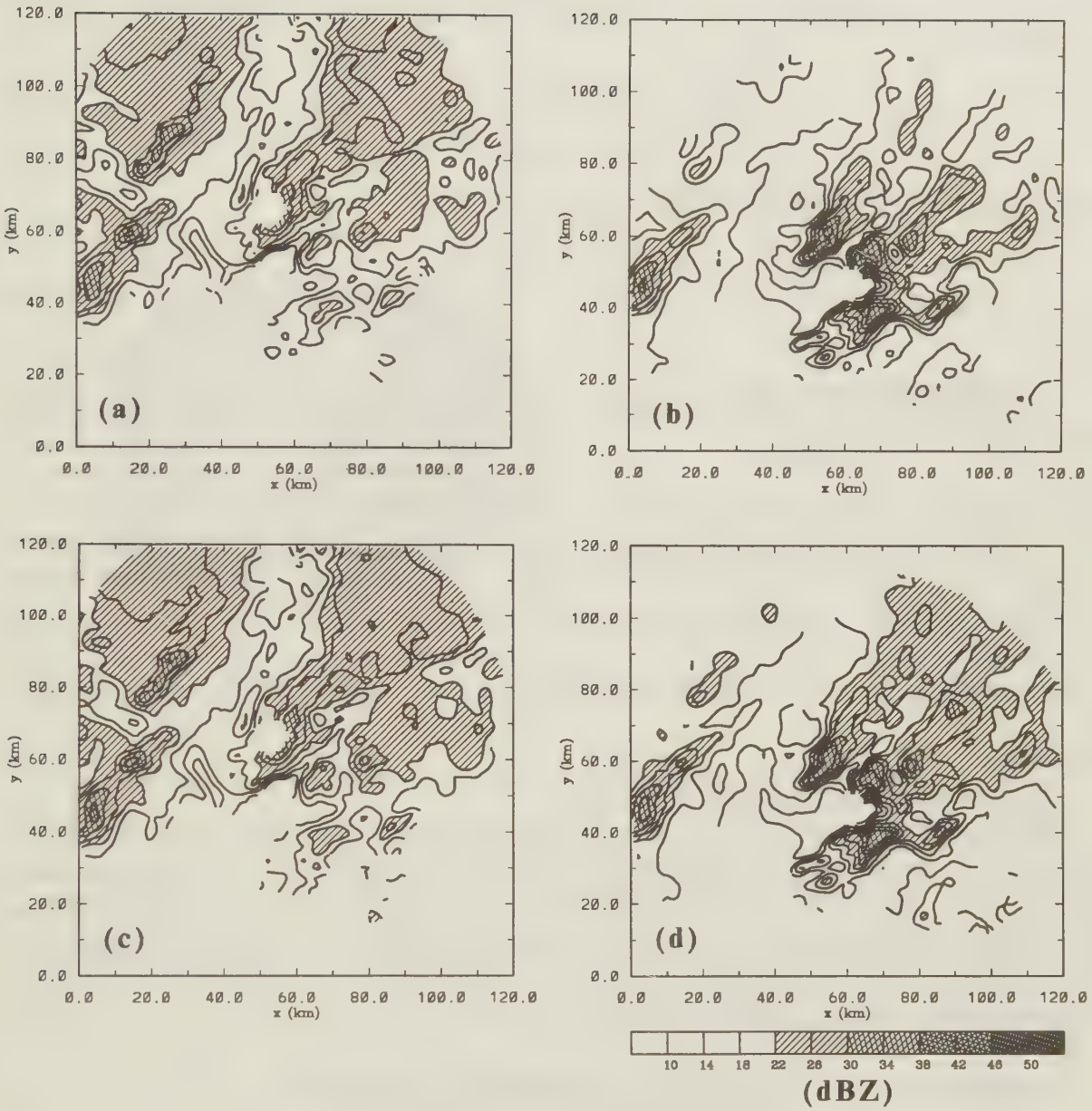

Fig. 4. Equivalent reflectivity factor distribution in dBZ on the horizontal section at a height of 3km at 1256JST on June 10, 1992. (a) NIED-BD, no attenuation correction. (b) MRI-3CD, no attenuation correction. (c) NIED-BD, attenuation correction by K-MP. (d) MRI-3CD, attenuation correction by K-MP.

reflectivity factor ,I_0, indicated the successful result of the calculation.

Direct calculation of K by (3) often results in $K<0$ as shown in Fig. 3, which contradict the definition of K. This may be because of the small-scale fluctuation of the reflectivity, and/or the slight distance between corresponding sampling volumes of the two radars. However, integration of (3) can avoid the difficulty. Assuming that the attenuation rate is the form of $K\,(\mathrm{dB\ km^{-1}}) = a\,Ze^{b}$ following the existing ones, (3) is expressed as

$$a\,Ze_0^{\,b} = \left(\frac{dI_2}{dx} - \frac{dI_1}{dx}\right) \Big/ 4 \quad . \tag{3}'$$

where $10\log_{10}Ze_0=I_0$. Integrating (3)' from x_{m1} to x_{m2}, we obtain

$$a\,\overline{Ze_0^{\,b}} = \frac{1}{4}\left[\overline{\left(\frac{dI_2}{dx}\right)} - \overline{\left(\frac{dI_1}{dx}\right)}\right] = \frac{\{I_2(x_{m2})-I_2(x_{m1})\}-\{I_1(x_{m2})-I_1(x_{m1})\}}{4(x_{m2}-x_{m1})} \quad . \tag{4}$$

b must be chosen appropriately, then a is obtained by plotting the right-side value of (4) versus $\overline{Ze_0^{\,b}}$ and fitting a line to the scattergram.

(b) Attenuation rate minimizing the Ze difference on a horizontal section

This is the method using the data on a common horizontal section. First, Ze of the two radars are derived with given attenuation correction on a common horizontal section by usual coordinate conversion for the volume data processing. Then, the root mean square (RMS) of the Ze difference in decibel is calculated using all of the derived pairs of Ze. $K\,(\mathrm{dB\ km^{-1}}) = a\,Ze^{b}$ is again assumed and b is chosen appropriately. The RMS is calculated for a variety of a, and a that gives the minimum RMS is considered as the best value for K.

3. Results

(a) Attenuation correction by existing K-Ze relations

Attenuation correction using K in Table 1 was made for comparison. Among them, $K=1.78\times10^{-4}Ze^{0.755}$ was selected. This formula, hereafter referred to as K-MP, was deduced by Kozu(1991) using the famous Marshall-Palmer DSD. K-MP gives medium attenuation rate at wide range of Ze. Figure 4(a) and (b) shows an example of the Ze patterns of the two radars without attenuation correction in decibel units. The correction using K-MP yields fairly reasonable result, however, the comparison of corrected Ze patterns of the two radars suggests that the correction is a little insufficient (Fig. 4(c)(d)).

(b) Attenuation correction by K obtained by the beam pairs along the base line

Seventy data along the base line of the dual observation were used to get the attenuation rate (K_1) by the method described in subsection 2(a). The data were extracted from the radar observation data acquisited in June 10, 1992 at Miyako Islands in this project. There was a shadow area of NIED Doppler radar near the base line. Using the data slightly deviated from the base line resulted in a horizontal distance up to about 900m between a pair of data. The lowest elevations of the two radars were 0.8° and 0.9° and the vertical distance between a pair of data was up to about 400m. The difference of acquisition time was 33 seconds in average. These differences may cause a slight change in equivalent reflectivity factor from the data at ideal time and locations, however, it is small and was considered to be negligible. Ground clutter and other errors in I_1 and I_2 were carefully checked.

b was chosen the same as that of K-MP, that is , 0.755. a was derived by plotting the right-hand side of (4) versus $\overline{Ze^{0.755}}$ (Fig. 5, left panel). The result is $K_1=5.67\times10^{-4}Ze^{0.755}$. K_1 is three times larger than K-MP

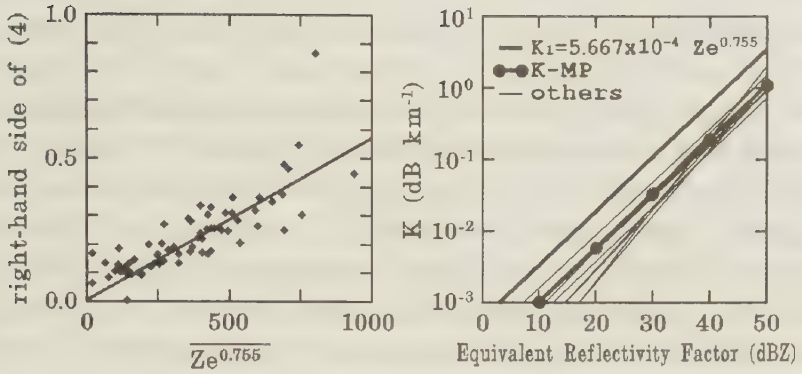

Fig. 5. Derivation of K_2 from 70 pairs of beams along the base line.

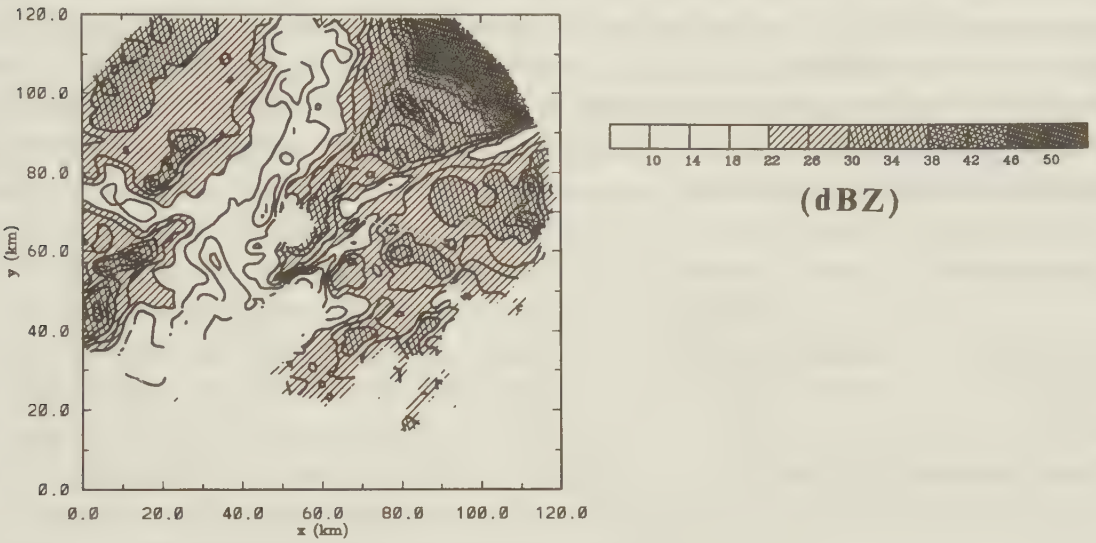

Fig. 6. As in Fig. 4, except the data are from NIED-BD, attenuation correction by K_1.

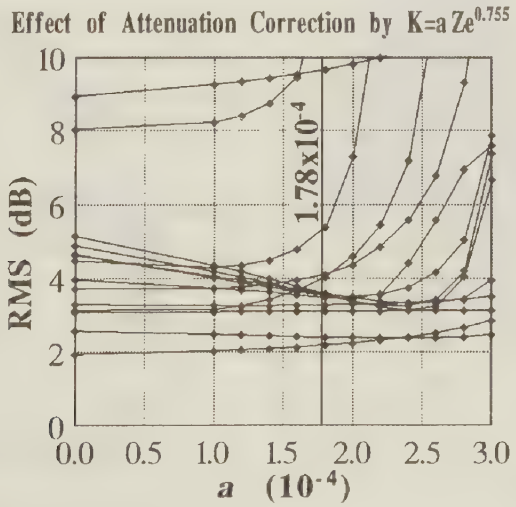

Fig. 7. The RMS of Ze difference in decibel for 15 horizontal sections (one of which is out of the vertical scale) at a height of 3km. Each line corresponds to the RMS of each horizontal section calculated varying *a*. The thin vertical line indicates *a* of K-MP.

value and other attenuation rates listed in Table 1 (Fig. 5, right panel). Applying K_1 to the observation data resulted in the excess attenuation correction (Fig. 6, around (x,y)=(100km,100km)).

(c) Attenuation correction by K that minimize the Ze difference on a horizontal section

Attenuation rate (K_2) by the method described in subsection 2(b) was derived using 15 pairs of volume-scan data. The data were selected by about 1-hour intervals from the same data as used in the previous subsection. The height of the horizontal section was 3.0km. The contamination of ground clutter and effect of the melting layer was not recognized in the corrected Ze patterns. Again, K-MP's value, 0.755, was used as *b*. Ze on the 3.0km horizontal section were calculated varying *a* around 1.78×10^{-4}, K-MP's value.

The RMS of the Ze difference in decibel took a minimum at an *a* value larger than 1.78×10^{-4} in 7 of 15 data (Fig. 7). Three of other 8 data yielded large RMSs clearly inadequate for the deduction of *a*. The large RMSs were because of the strong attenuation close to at least one of the radars. The other 5 data showed the continuous increase of RMS as *a* increased and had no minimum RMS around 1.78×10^{-4}. The average of *a* that led to the minimum RMS was 2.3×10^{-4}. So, it is inferred that $K_2 \sim 2.3 \times 10^{-4} Ze^{0.755}$. This is 1.3 times larger than K-MP value, and is considered to represent the average attenuation rate on the horizontal section. Applying K_2 to the observed data gave slightly better result than that is given by applying K-MP value (Fig. 8), though the Ze difference still remained.

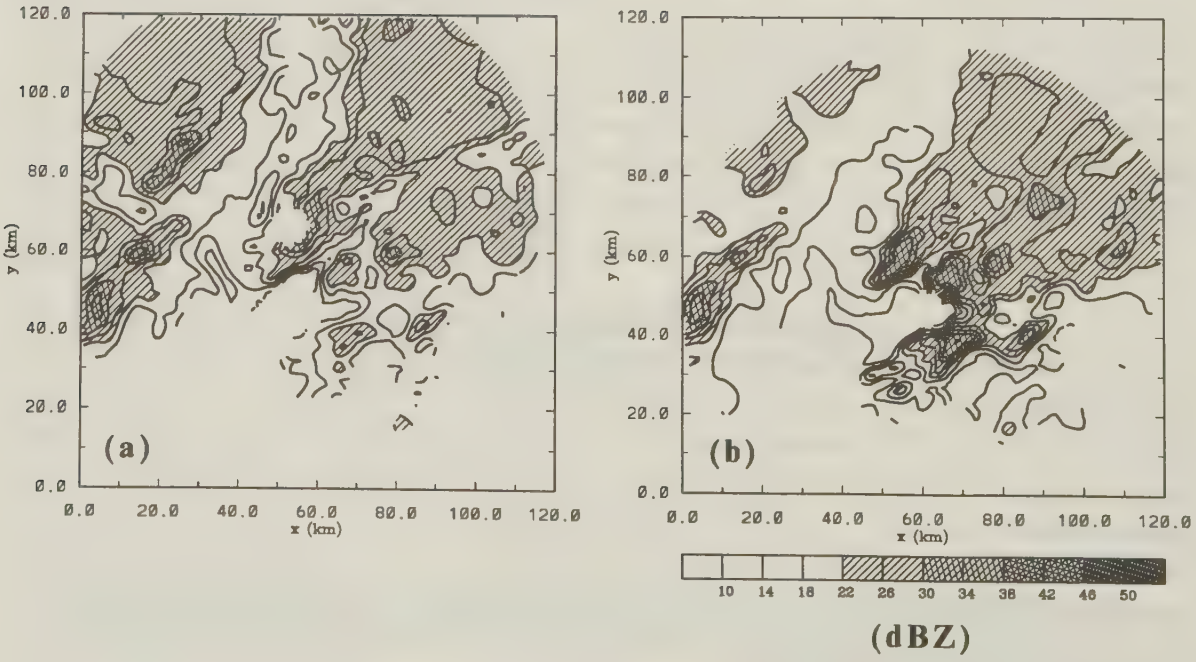

Fig. 8. As for Fig. 4, except the data are from (a) NIED-BD, attenuation correction by K_2, and (b) MRI-3CD, attenuation correction by K_2.

4. Discussions

In subsection 3(a), one of the existing K was examined, and considered that it was a little insufficient. The most appropriate value for the *average* attenuation rate was K_2 derived in subsection 3(c). Comparing with the other attenuation rates in Table 1, K_2 gave large values, and was almost identical to the attenuation rate of Kozu (1991) using 'drizzle' DSD of Joss et al. (1968) (Table 1, hereafter referred to as K-JD). However, the phenomena expressed in the original data of K_2 and K-JD are completely different. These high attenuation rates are attributed to the different reasons with each other.

Although K_2 gives the appropriate correction in average, there are significant variation in the attenuation. Sometimes applying K_2 to the observation data gives excessively corrected Ze, and sometimes the reverse occurs. For example, the RMS continuously increased as *a* increased in 8 data in Fig. 7. This may be attributed to the insufficient correction by K_2 where the widespread stratiform rain with rather large Ze. Overestimation of attenuation sometimes happened at strong convective bands.

K_1 is too large and the reason can be related to the method, because K_2, derived using the same data, is appropriate as an average value. In subsection 2(a), it is assumed that equivalent reflectivity factors, I_1 and I_2 are observed simultaneously at the same sampling volumes. The actual beam spread by a certain beam width, and the sampling volumes of the two radars were different. Especially, a large sampling volume allow the inhomogeneous distribution of raindrops, which contradict the assumption that is the basis of the radar equation. Moreover, in this method, all the unresolved attenuation is attributed to the rain expressed in Ze. So, it is inferred that K_1 was biased by the inhomogeneous distribution of raindrops within the sampling volumes, though K_1 might suffer from the contamination of ground clutter.

X-band research radar data is of the highest quality for the validation of satellite microwave radiometer data. The analysis of satellite microwave data is hopeful to clarify the distribution of water in Baiu frontal zone including MCSs. The result described in this report will contribute to the quantitative analyses of convective cloud systems using satellite microwave radiometer data. The correction of attenuation make both radar and satellite data analyses more quantitative; leads to more accurate convective system structures and to the deduction of the inhomogeneity of precipitation within the footprint.

Considering the wide variety of the convective systems, it is important to analyze as many cases as possible. So far, the analysis was limited to the data in June 1992. In FY1996, it is planned to analyze satellite microwave data of June-July 1996 as well as the data in 1992. Continuing analysis of the radar observation data is also necessary as the basis of satellite data analysis.

5. References

Doviak, R. J. and D. S. Zrnić, 1984: Doppler radar and weather observations. Academic Press. 458pp.

Gunn, K. L. S. and T. W. R. East, 1954: The microwave properties of precipitation particles. Quart. J. Roy. Meteor. Soc., 80, 522-545.

Imai, I., 1957: Attenuation of microwaves through rain for various drop-size distributions. J. Meteor. Soc. Japan, 75th Ann. Vol., 65-71.

Joss, J., J. C. Thams and A. Waldvogel, 1968: The variation of raindrop size distribution at Locarono. Proc. Int. Conf. Cloud Physics, 369-373.

Kabèche, A. and J. Testud, 1995: Stereoradar meteorology: A new unified approach to process data from airborne or ground-based meteorological radars. J. Atmos. Oceanic Technol., 12, 783-799.

Kato, K, 1993: The processes of the seasonal transition of Baiu front in East Asia: The effect of Indian Monsoon and the semiarid region around China (Japanese). Kaiyo Monthly, extra issue No.5, 96-101.

Kodaira, N., 1963: The radar wave attenuation caused by precipitation particles. Papers Meteor. Geophys., 14, 181-189.

Kozu, T., 1991: Estimation of raindrop size distribution from space-borne radar measurements. Ph. D. dissertation, Kyoto University, 196pp.

Laws, J. O. and Parsons, D. A., 1943: The relation of raindrop-size to intensity. Trans. Am. Geophys. Union, 24, 452-460.

Marshall, J. S. and W. M. K. Palmer, 1948: The distribution of raindrops with size. J. Meteor., 5, 165-166.

Mueller, E. A. and D. M. A. Jones, 1960: Drop-size distributions in Florida. Proc. Eighth Weather Radar Conf., Boston, Amer. Meteor. Soc., 299-305.

Olsen, R. L., D. V. Rogers and D. B. Hodge, 1978: The aR^b relation and the calculation of attenuation. IEEE Trans. Antennas Propag., 26(2), 318-329.

Ryzhkov, A. and D. S. Zrnić, 1995: Precipitation and attenuation measurements at a 10-cm wavelength. J. Appl. Meteor., 34, 2121-2134.

Testud, J. and P. Amayenc, 1989: Stereoradar meteorology: A promising technique for observation of precipitation from a mobile platform. J. Atmos. Oceanic Technol., 6, 89-108.

Wexler, R. and D. Atlas, 1963: Radar reflectivity and attenuation of rain. J. Appl. Meteor., 2, 276-280.

6. Publications

①oral presentations

Nakai, S., K. Akaeda and H. Sakakibara, 1995: The modification of wind field by organized MCSs observed at Miyako Islands in Baiu season (Japanese). Preprints of the 1995 Spring Semi-annual Meeting of the Meteorological Society of Japan, 15-17 May 1995, Tokyo, C367.

Nakai, S, 1996: The analysis of MCSs using radar observation data and satellite data (Japanese). Proceedings of the Workshop on the Formation Mechanism of the Heavy Rainfall System, IHAS/NU, February, 1996, 47-53.

和文アブストラクト

本研究では、4年度に取得したデュアルドップラー観測データの解析によって対流雲内の雨水量、気流の分布を明らかにすること、およびその結果を基にした衛星データ（主にマイクロ波センサ）の解析によって、対流雲による水蒸気消費量および鉛直輸送量を調査し、対流雲の維持過程、モンスーン雲域の水収支、およびこれらの関係を解明することを目的としている。

平成７年度は、デュアル観測による２台のレーダーの観測データの反射強度値から降雨減衰を見積もった。減衰係数は古津(1991)のMarshall-Palmer分布による式(以後K-MPという)に基づいて$K=a\ Ze^{0.755}$ (dB km^{-1})と仮定した。まず、２台のレーダーの基線上で互いに向き合うビームのデータを用いた減衰補正を試みた。1992年6月10日の観測から70組のビームのデータを用い、２台のレーダーの反射強度値の差が全て降雨減衰によるものとして'真の'反射強度値と減衰係数K_1を求めた。その結果$K_1=5.67\times10^{-4}Ze^{0.755}$となったが、これは明らかに過大であった。次に、高度3kmの水平面上で２台のレーダーの反射強度差が最小となる減衰係数K_2を求めたところ、$K_2\sim2.3\times10^{-4}Z^{0.755}$となった。これはK-MPの約1.3倍の値であり、この水平面上のデータに対する平均的な減衰係数であると考えられる。K_1が過大となった理由は、クラッターの混入だけではなく、目標体積内の不均一な降水分布によってバイアスされたためでもあると考えられる。

I. Observation and analysis on the process of atmosphere-ocean-land interactions

I. 大気・海洋・陸域間相互の諸過程に関する観測・解析研究

2. Observation and analysis on the process over the ocean

2. 海洋における諸過程に関する観測・解析研究

(1) Observation on Sub-Surface Temperature by Voluntary Ships

(1) 表層水温に関する観測研究

Keisuke Mizuno* , Tomowo Watanabe*
水野 恵介*, 渡邊 朝生*

National Research Institite of Far Seas Fisheries
遠洋水産研究所

1. Objectives

In the Indian Ocean, westerly wind prevails on the equatorial band at sea surface in the intermonsoon period (around May and November). Ekman transport induced by that wind system tends to accumulate water on to the equator. The generated pressure field constructs equatorial Kelvin wave which propagates eastward. So, the currents on the equator flows eastward in considerably high speed. Wyrtki(1973) first described the equatorial jet in the Indian Ocean. O'brien(1974) showed that this flow is the same as Yoshida Jet dynamically. Modelers reproduced this jet in numerical models. However, the intensive observation to detect entire spatial structure of the jet has not been done. We planed hydrographic observation along the equator by using a research ship in fall 1995. The observation includes releasing drifting buoy experiment (Hydrographic Office) and AWS installation on deck (Meteorological Research Institute). These are discribed by the organizations.

2. Methods

We conducted hydrographic observation in the tropical Indian Ocean by using Shoyo Maru (Fisheries Agency Research Ship ; 1362 gloss ton, during October 10 through January 8). Cruise track in the Indian Ocean sector is shown in Figure 1. At each CTD station (open/solid circles in the figure), CTD (Sea Bird Instrument Co. model 910 plus) with Rosset sampler (12 Niskin bottle array) was lowered down to 3000m. Measured salinity and dissolved oxygen (hereafter D.O.) by CTD were corrected by comparing with the laboratory measurements of sampled sea water.

Currents were measured by Acoustic Doppler Current Profiler (ADCP; RD instrument Co.) during all steaming time. The pinging interval is about 1 sec. and the data set was constructed by each 5 minutes ensemble mean and 16m depth bin from surface to about 500m. Although several kinds of

biological parameters were observed, these topics will not be mentioned here.

3. Results

3-1. Sea surface wind and current

Sea surface wind vectors along the ship route is shown in Figure 2 (upper panel). Westerlies were predominant especially in the eastern part with the speed of over 10m/sec which is much larger than COADS clomatologies for November. In Arabian Sea and 6N, most of the data were taken in December. So, winter monsoon started and north east winds were dominant.

Surface currents on the equator reveals strong eastward flow greater than 2-3 knots. The jet is strong in the central part but is small in both ends. In the eastern part, directions of the current vector fluctuated, indicating eddies on the equator. On the other hand the current is rather uniform in the west.

3-2. Surface layer structure along the equator

The thermal field shows (Figure 3 upper panel) surface thermostad is deeper in the eastern part than the west. Thermocline is also deeper in the east. But it in the central part, downstream of Maldive(73E) islands, the thermocline clearly undulated. It shows the current structure is well affected by bottom bathymetory.

The salinity field shows (Figure 3 upper panel) different feature form thermal field. In the eastern part (east of 90E), less saline water has strong front. The surface water in Arabian Sea has higher salinity because of strong evaporation and less fresh water supply. Also high salinity interleaved to the west near the bottom of upper layer. East of Maldive, halocline is also undulated similar to that of thermal field.

The D.O. field is similar to the thermal field in the upper layer. However, it is generally lower in Bengal Bay sector beneath the oxiocline. And D.O. minimum layer appears about at the depth of 150-200m.

Isobaric height is estimated by density field measured by CTD (Figure 4 upper panel), assuming isobaric surface of 2500db is horizontal. Sea surface (0db) shows zonal gradient higher in the east. This slope will be balanced by wind stress at the equilibrium state eventually . The zonal slope can be traced down to 100m, but is not clear deeper than that.

Vertical section of zonal component of the current(Figure 4 lower panel) shows the current structure of the equatorial jet clearly. The current is confined to the surface layer, and its depth is about 100m which is consistent with isobaric height. In the eastern part, the current is rather deeper. The strong current appears in the central part near the Maldives. Disturbances in the current can be seen at the lee of the Maldives.

3-3. Surface layer structure across the equator

Vertical sections across the equator (64E) are shown in Figure 5. Near the equator, thermostad (28℃) is deeper (Figure 5;upper panel) in the vicinity of the equator. Thermal and salinity structure on the equator is isolated. Blow the surface layer, D.O. structure shows meridional

contrast, and nearly vertical front can be seen around 7N. D.O. is lower in the north (Arabian Sea).

Isobaric height is also estimated (Figure 6 upper panel) in the same manner as the previous one. Sea surface (0db) shows small peak at the equator. The down slopes to both sides of the equator generate meridional pressure gradient which balances the equatorial jet as eastward geostrophic flow. This small pressure gradient can generate fast current(the equatorial jet) because of small Colioli's parameter near the equator.

The vertical section (Figure 6; lower panel) shows the cross stream structure of the jet clearly. This flow is confined to upper 100m or less. Northern limit of the jet is 2N, but the southern one is not clear because it is joined to the equatorial counter current. Judging from high speed core of the jet, the southern limit of the jet is 2-3S. Mass transport of this jet is calculated to be 20Sv.

4. Discussion

The structure of the equatorial jet can be clearly obtained. The jet is confined to shallow depths, and its width is estimated to be approximately 400km (2S-2N). Eastward mass transport is large (comparable to the Kuroshio). On the other hand, the zonal temperature difference is so faint, that the zonal heat transport may be small. However, the jet is a duct which transport warm water to the east twice a year (May-June, October-November). It generates thick warm pool off Sumatera. The warm water has also dynamical impacts to wide areas (Yamagata et al. 1996). The results obtained here will be useful to verify ocean models which reproduces the equatorial jet.

5. References

O'Brien,J.J. and H.E.Hurlburt (1974) An equatorial jet in the Indian Ocean: Theory. Science, 184, 1075-1077.

Wyrtki, K. (1973b) An equatorial jet in the Indian Ocean. Science 181, 262-264.

Yamagata T, K.Mizuno and Y.Masumoto (1996): Seasonal Variations in the equatorial Indian Ocean with their Impacts on the Lombok throughflow. J.G.R, 101,(C5),12456-12473..

6. Publications

Yamagata T, K.Mizuno and Y.Masumoto (1996): Seasonal Variations in the equatorial Indian Ocean with their Impacts on the Lombok throughflow. J.G.R, 101,(C5),12456-12473..

Mizuno K. (1996): Annual and Interannual variation in the subsurface temperature in the Indian Ocean. Annual Meet.ing of Fisheries Oceanography.

7. International Cooperation

None

和文要旨

春と秋のモンスーン休止期にインド洋赤道上において発生する赤道ジェットの構造を調べるため，１９９５年１１月に調査船によりスマトラ沖からセーシェル付近までの赤道上の海洋観測を実施した．この時期海上風は西風が卓越し，赤道ジェットの構造が詳細にとらえられた．

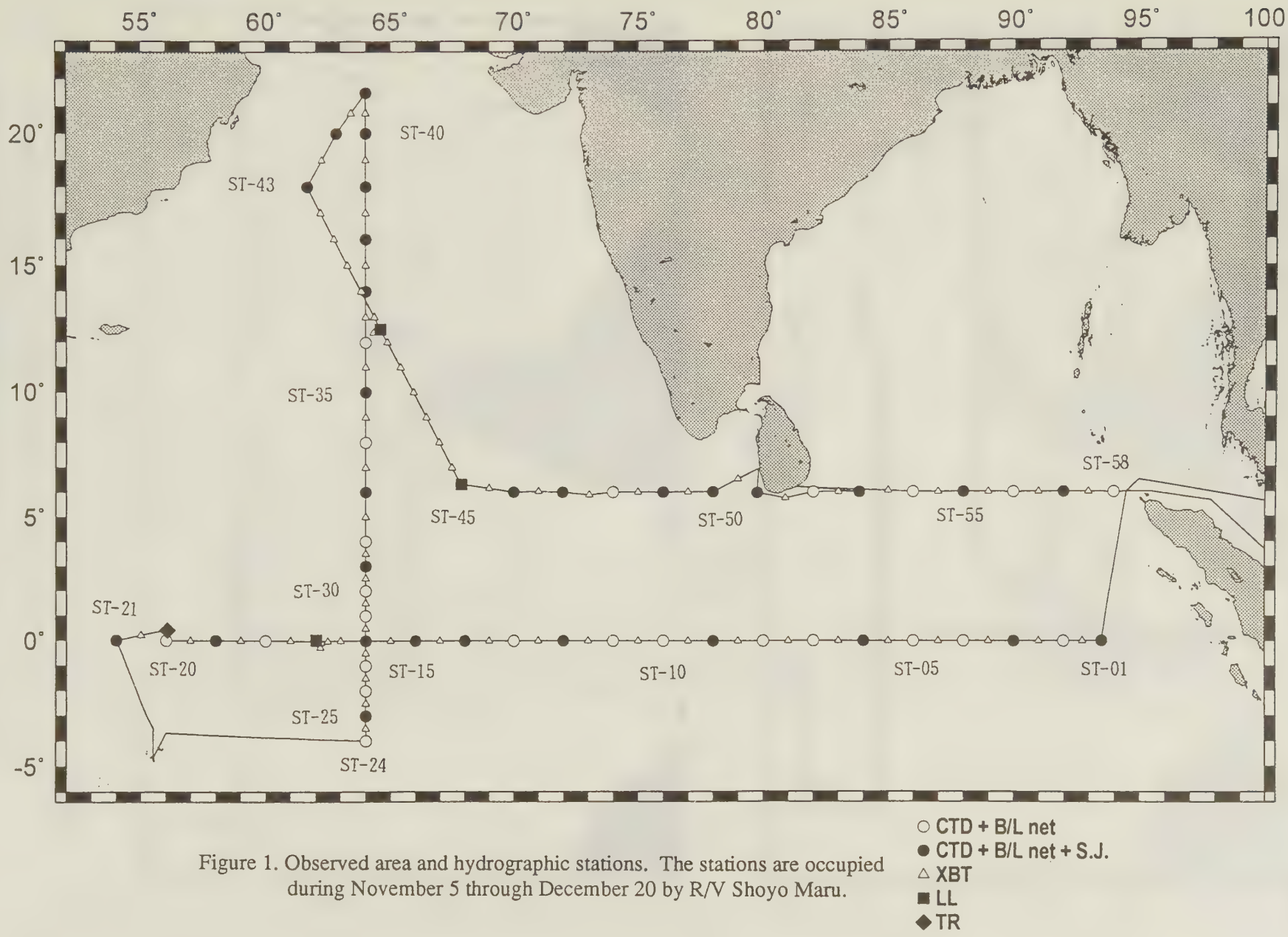

Figure 1. Observed area and hydrographic stations. The stations are occupied during November 5 through December 20 by R/V Shoyo Maru.

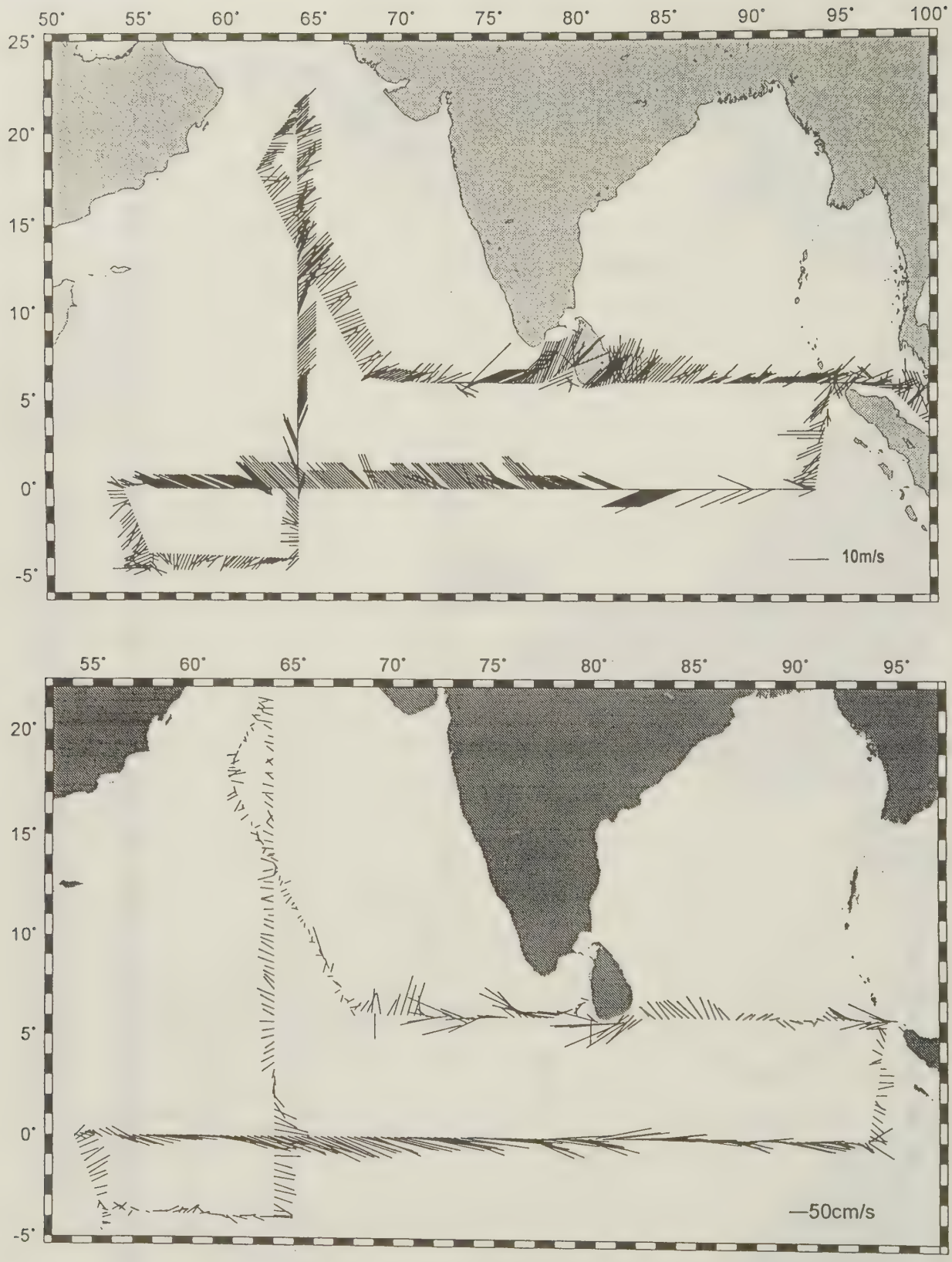

Figure 2. upper panel : Sea surface wind vector along the ship rane. Sampling interva l is hour, and the vector direction is classified 16 directions.

lower panel : Surface layer current vector measured by ADCP. Actual depth is 20-36m which is the first bin of ADCP measurement.

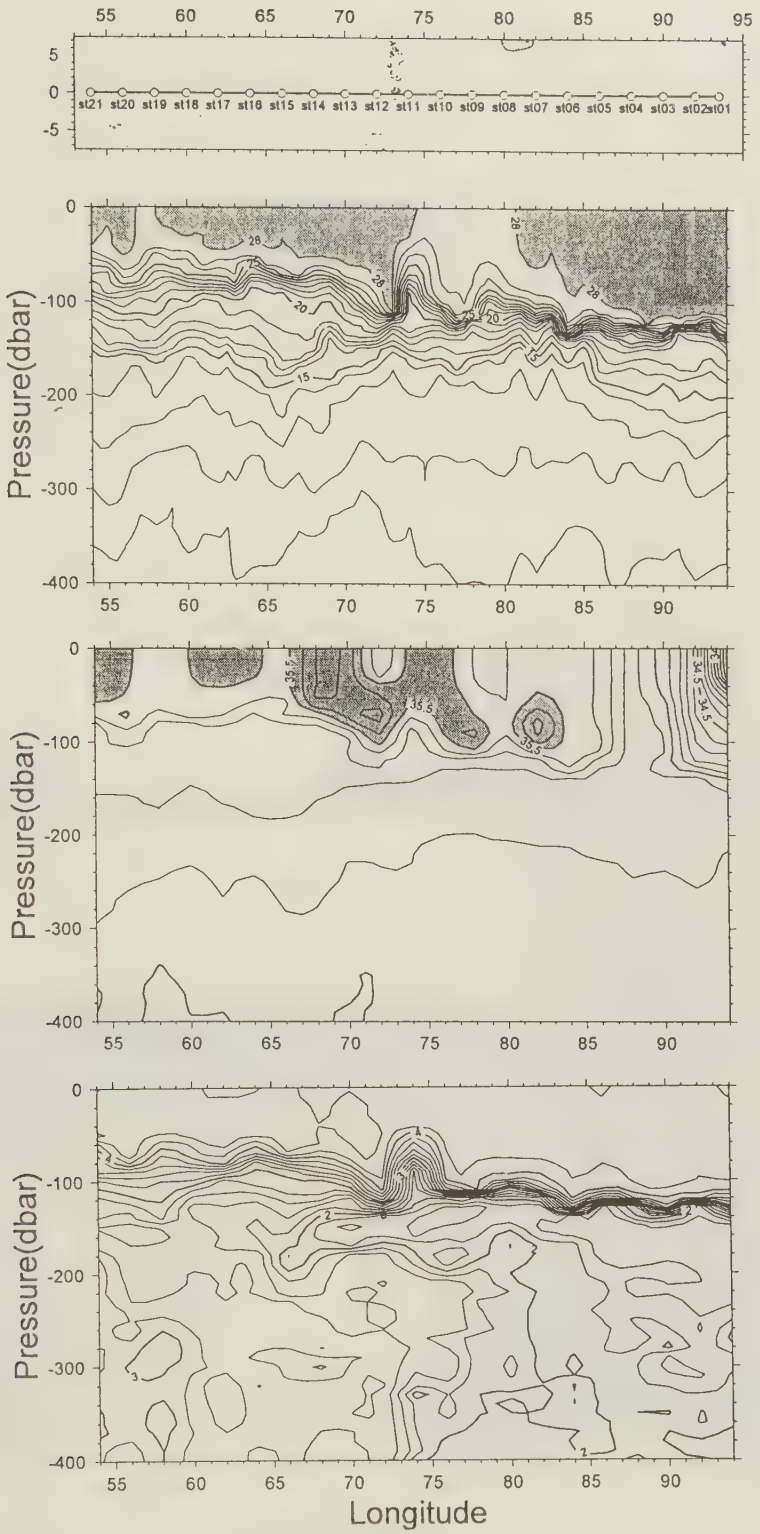

Figure 3. upper panel : Vertical temperature section along the equator. Warm water higher than 28℃ is shaded. Contour interval is 1℃.

middle panel : The same section as the upper panel but for salinity. Salinities higher than 35.5psu is shaded. Contour interval is 0.1psu.

lower panel : The same section as the upper panel but for dissolved oxigen. Contour interval is 0.2ml/l.

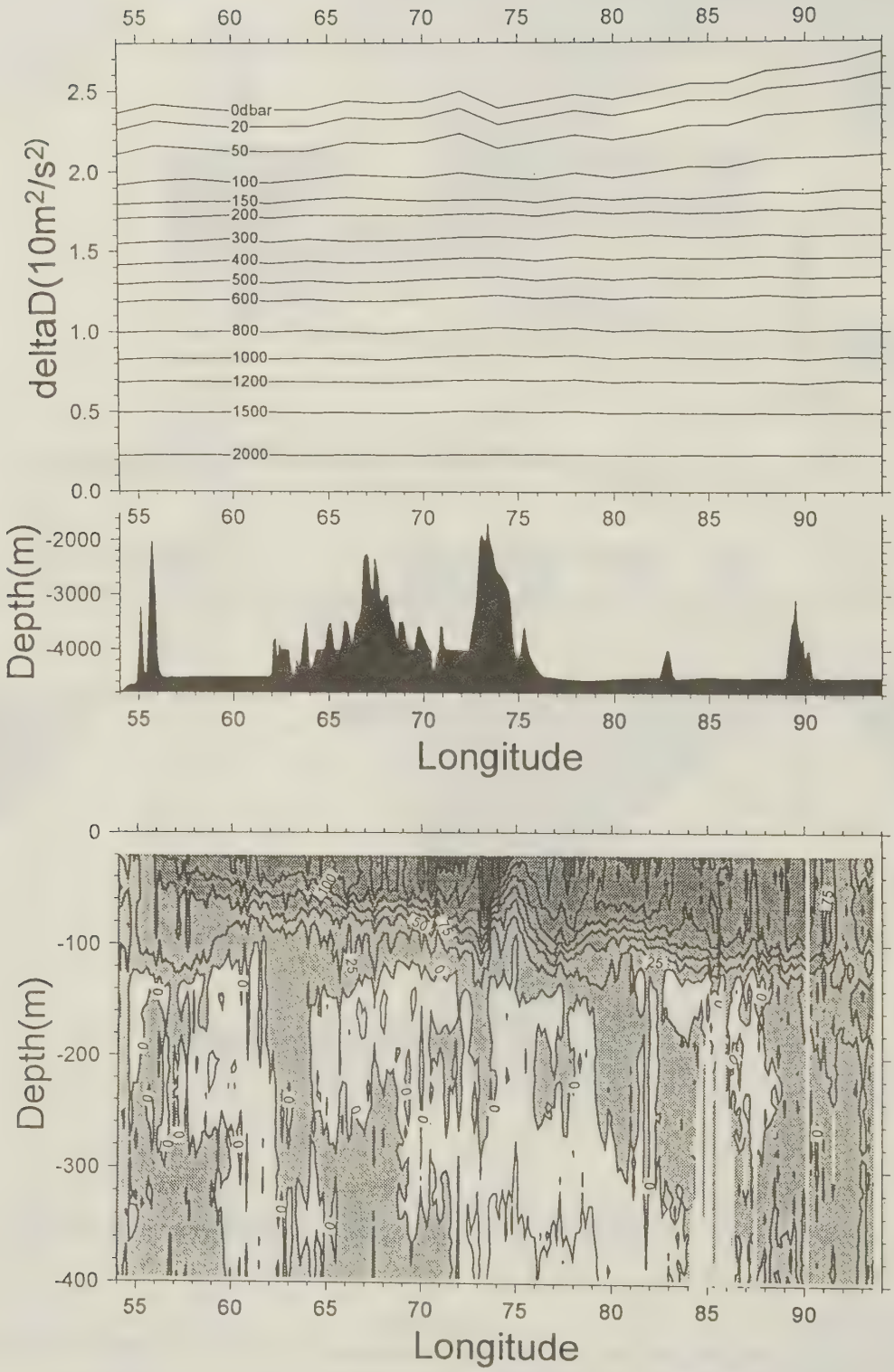

Figure 4. upper panel : Anomaly of dynamic depth of isobaric surfaces (referrence level is 2500db).

lower panel : Vertical section of zonal component of ocean current. Positive (eastward) values are shaded, and the contour interval is 25cm/s.

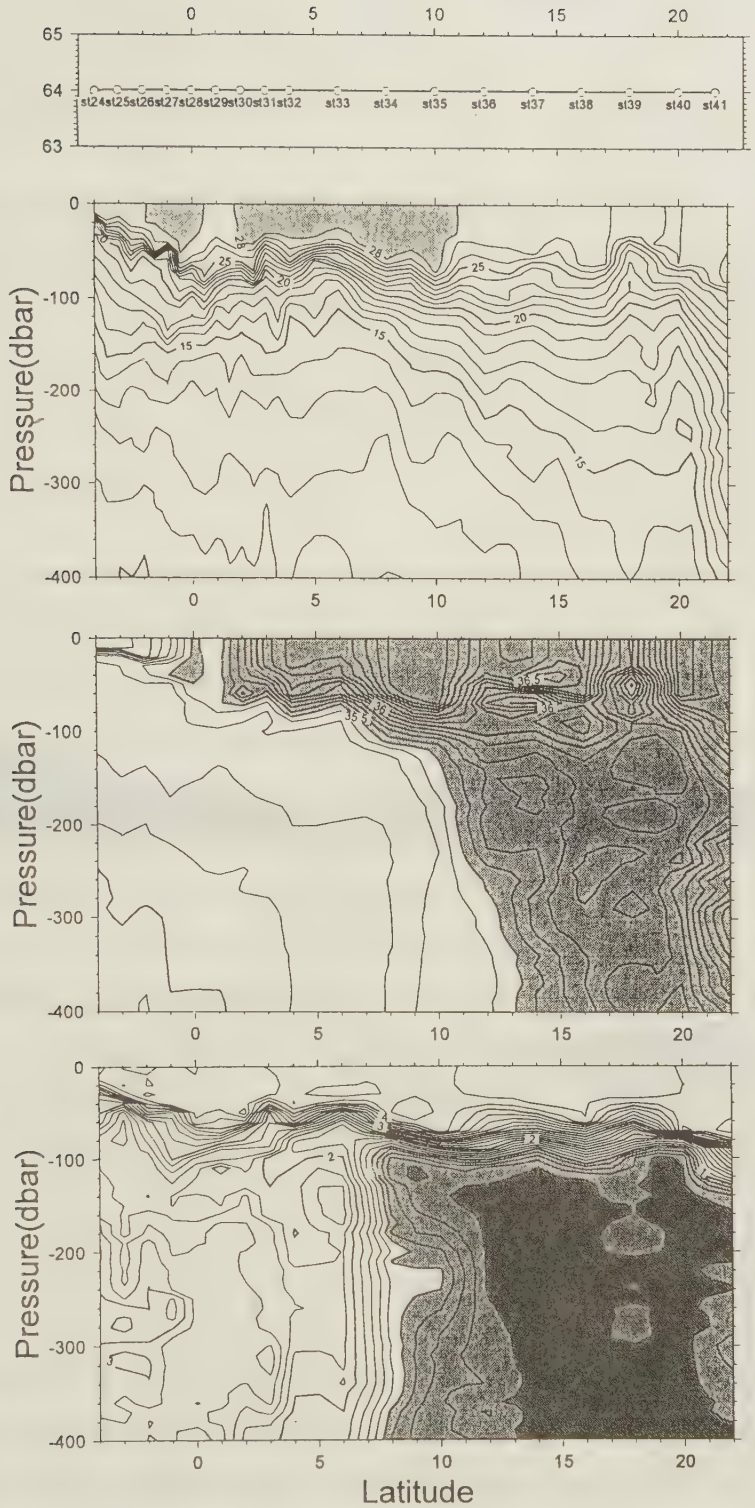

Figure 5. upper panel : Vertical temperature section along 64' E. Warm water higher than 28℃ is shaded. Contour interval is 1℃.

middle panel : The same section as the upper panel for salinity. Salinities higher than 35.5psu is shaded. Contour interval is 0.1psu.

lower panel : The same section as the upper panel but for dissolved oxigen. Values less than 1ml/l are shaded.

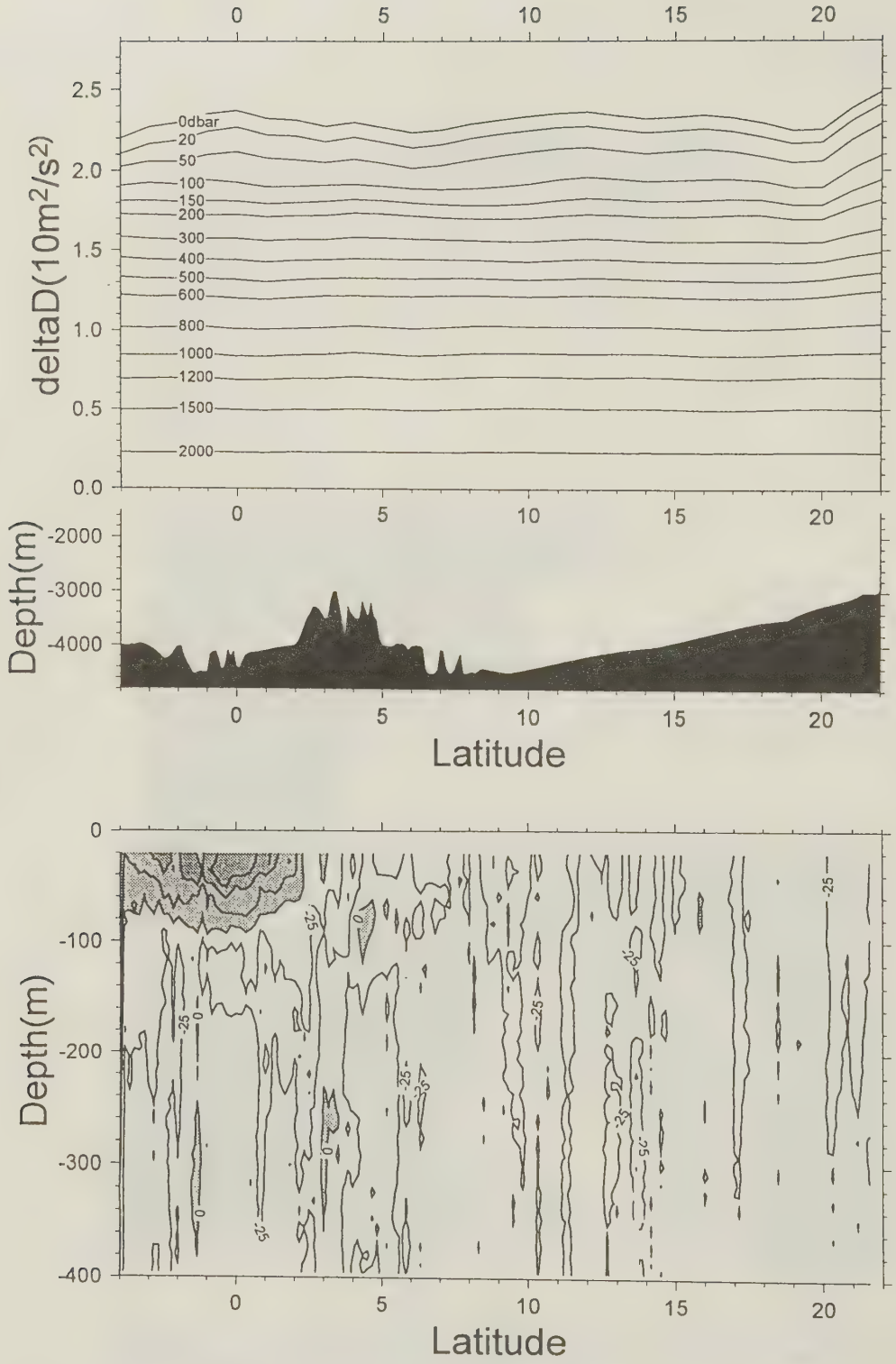

Figure 6. upper panel : Anomaly of dynamic depth of isobaric surfaces(referrence level is 2500db).

lower panel : Vertical section of zonal component of ocean current. Positive (eastward) values are shaded, and the contour interval is 25cm/s.

Ⅰ．大気・海洋・陸域間相互作用の諸過程に関する観測・解析研究

Observation and analysis on the process of the atmosphere-ocean-land interactions

２．海洋における諸過程に関する観測・解析研究

Observation and analysis on the process over the ocean

(１)表層水温に関する観測研究

Observation on Subsurface Temperature by Voluntary Ships

気象庁海洋気象部　三河哲也、水野孝則

Tetsuya Mikawa and Takanori Mizuno

Marine Department, Japan Meteorological Agency (JMA)

(Abstract)

Subsurface temperature observations with XBT probes have been made by a voluntary observing ship, "Kashimasan-Maru" in the Indian Ocean since 1990. XBT data collected from the above observations as well as other subsurface temperature data obtained through the Global Telecommunication System (GTS) were analyzed to investigate the variations in the thermal structure of the Indian Ocean under the Ocean Data Assimilation System (ODAS) developed by the JMA.

The output derived from the ODAS shows a clear picture of the seasonal variations in the thermal structure in the Indian Ocean. In the eastern Indian Ocean, subsurface warm water masses are piled up by the westerly wind in the central equatorial Indian Ocean and move east up to the western coast of Southeast Asia during both transition periods between the two monsoons. And then the coastal Kelvin waves start propagating southward and northward along the coast. Accompanied by a transition from the southwest monsoon to the northeast monsoon, the Rossby wave propagates westward in the northern hemisphere.

1. Objectives

The Asian Monsoon over the Indian Ocean and the seas around Southeast Asia is considered to be related to El Niño events which affect the global climate, through the interaction between the ocean and the atmosphere in the Indonesian region (Barnett 1983[1)], Nicholls 1984[2)]). Recently, a better understanding of the physical structure of the ocean in these regions, and a clearer elucidations of the relation between the Asian Monsoon and El Niño events have been required. However, in these regions, amount of oceanographic data are too sparse to fully understand the physical structure of the ocean. The subsurface temperature data observed with XBT probes and reported by a crude oil tanker cruising between Japan and the Persian Gulf have been distributed to national meteorological/oceanographical services throughout the world via the Global Telecommunication

System (GTS) of the World Meteorological Organization (WMO) since October 1990. XBT data collected via GTS including those from the crude oil tanker are analyzed to investigate annual variation of subsurface waters in this region.

2. Methods

Subsurface temperature in the Indian Ocean and the South China Sea is observed four times a day by a crude oil tanker, "Kashimasan-Maru" which makes a fifty-day round trip between Japan and the Persian Gulf via the Strait of Malacca. Fig. 1 shows the route of the ship.

JMA has developed the Ocean Data Assimilation System (ODAS) and commenced its operational use at the beginning of 1995. The ODAS consists of a dynamical ocean general circulation model and an analysis system of sea surface and subsurface temperature. The output derived under the ODAS from XBT data observed by the ship mentioned above as well as from those collected via GTS is used to investigate the thermodynamical structure of subsurface waters and its variation in the Indian Ocean.

Although subsurface temperature is observed with a rather high spacial density along regular ship routes, it is observed very sparsely elsewhere both in time and space. Thus, it is difficult to understand the time-serial three-dimensional structure of the ocean only from the observed data. However, this difficulty is solved by the ODAS. The ODAS demonstrates various information on ocean phenomenon. The ODAS has been operated every 5 days from May 1986. Climatology was computed by the ODAS from the data observed during the 1987-1995 base period. In the Annual Report of JEXAM 1994, climatic feature in the equatorial Indian Ocean analyzed by the ODAS was reported (Mikawa et al. 1995)[3]. In the present study seasonal and annual variations of the subsurface not only in the equatorial region but also in other regions in the Indian Ocean are investigated.

3. Results

(1) Observation of subsurface temperature by voluntary observing ships

As many as 2,245 subsurface temperature data were obtained by "Kashimasan-Maru" in the South China Sea, the Bay of Bengal and the Arabian Sea for the period from October 1990 to April 1996. Those subsurface temperatures were usually observed four times a day. From 10th to 13th November 1995, high density observation (eight times a day) was performed. Almost every data including high density observation were applied for analysis under the ODAS.

(2) Analysis using results derived from the ODAS

i) Seasonal variation of the depth of 20℃ isotherm (D20)

As the external forcing to drive the oceanic model in the ODAS, surface wind stress derived from

the JMA Global Data Assimilation System (GDAS) is applied (Yoshikawa et al. 1995)[4]. Motion of the ocean driven by surface wind stress affects the thermal structure of the ocean. Fig. 2 and 3 show normals of monthly mean of surface wind stress and D20 derived from the ODAS, respectively. Rao et al. (1989)[5] and Mizuno et al. (1992)[6] presented similar maps made only from observed data. D20 is roughly corresponding to the thickness of the warm surface layer. A large high value of D20 means a thick pile of subsurface warm water.

As shown in Fig. 2 and 3, seasonal variation signal is weak in the southern part of the Indian Ocean. The region that D20 is more than 150m extends from Madagascar to Australia between 15S and 25S, while D20 less than 100m are extended zonally between 5S and 10S throughout the year. The reason why seasonal variation in the southern Indian Ocean is weak, is because circulation of atmosphere does not change so much compared to that in the northern Indian Ocean where the winds turn over twice a year.

On the other hand, in the equatorial region and the northern hemisphere, strong seasonal variation is found all over the place as follows:

1) In the Equatorial region

In the eastern equatorial Indian Ocean, subsurface warm water is piled up during a period from May to December including the southwest monsoon season. In particular, during both transition periods between two monsoons the maximum value of D20 is found in this region. Thermocline along the equator is shallower than that to the north of or that to the south of the equator during the northeast monsoon (From January to March), because of upwelling in the equator.

2) In the Arabian Sea

Very strong coastal upwelling in the western part of the Arabian Sea occurs during the southwest monsoon in consequence with strong southwest wind blowing along the eastern coast of Africa and Arabian Peninsula. Thus, the region where D20 is less than 100m extends along the coast to the Arabian Peninsula. East of the region, D20 is more than 150m, because of the removing of subsurface warm water by the Ekman transport. D20 during the northeast monsoon is deep in the northwestern part of the Arabian Sea and shallow in the southeast part.

3) Off the south of Indian Peninsula

During the southwest monsoon, a part of southwest winds blowing in the Arabian Sea makes a detour and passes south of the India Peninsula (Fig.2). Therefore, strong westerly wind blows mainly between the south edge of the India Peninsula and the equator. Because the winds move the subsurface warm water southward through Ekman transport, D20 is very shallow in the south of the India Peninsula. Fig. 4 shows depth-longitude section along 6N in August. Cold water mass can be found near the surface around 80E. In contrast, D20 becomes deep in the same region during the northeast monsoon.

4) In the Bay of Bengal

Southwest monsoon blows northeastward from the southern region of the India Peninsula to the central part of the Bay of Bengal. Subsurface warm water in the southeastern part of the Bay of Bengal is piled up by this wind. In August-October, the warm water reaches the northern part of the bay. Shallow D20 appears in the eastern coast of the India Peninsula in the same periods. In January-March, the opposite feature is found.

The distribution of subsurface warm water in the Indian Ocean is formed mainly by Ekman transport. Seasonal characteristics found in the output of ODAS is in good agreement with those by Rao et al. (1989) and Mizuno et al. (1992).

ii) Pile of subsurface warm water in the eastern Indian Ocean and propagation of wave

In the eastern Indian Ocean, subsurface warm water masses are piled up by strong eastward jet flow along the equator caused by westerly wind in the central Indian Ocean during both transition periods between the two monsoons (Wyrtki, 1973[7]), namely May/June and October/November. The relation of westerly wind with the pile of subsurface warm water along the equator has already been reported on Annual Report of JEXAM 1994. In the present study, annual variation of surface wind stress and the pile of subsurface warm water in the eastern Indian Ocean are investigated in detail. Fig. 5a and 5b show time-longitude sections of zonal surface wind stress and its anomalies along the equator in the Indian Ocean during May 1986 and December 1995, respectively. Surface wind stress derived from GDAS whose grid intervals are 1.875 degrees X 1.875 degrees is interpolated to the grid of ODAS, and then is averaged between 5N and 5S. Some characteristics found in these figures are as follows:

- Strong westerly wind appears during both transition periods between the two monsoons. Wind is strong in 1987, 1988, 1989, 1991 and 1995, and weak in 1986 and 1994, especially in 1994.
- Intraseasonal variation of westerly wind with the period of one or two months observed.
- Southwest monsoons blow from the central Indian Ocean to 90E. Winds are weak east of 90E throughout the year.

Fig. 5c shows time-longitude sections of D20 derived from ODAS. D20 becomes deep whenever strong westerly wind anomalies occur. The deepest position of D20 is seen to move eastward quickly. But, it is difficult to estimate the moving speed of warm water from this figure, because the range of propagation is too short. Thus we cannot conclude whether or not the movement of subsurface warm water is caused by the propagation of the Kelvin wave. Assuming that the depth of upper layer is 150m in the Indian Ocean, the theoretical phase speed of the Kelvin wave in the two layer model is about 1.7m/s. In the central equatorial Pacific, the Kelvin waves caused by westerly wind anomalies propagate eastward at a speed of about 2m/s, and this value agrees with theoretical speed.

Fig. 6 shows D20 every 5 days from 12th July to 6th August 1992. The warm water reached to the eastern part of the Indian Ocean propagates both northward and southward along the coast. Such phenomenon often occurs (about twice a year on average), when the warm water is piled up in large volume. Some of them propagate a long way to the northernmost part of the Bay of Bengal or to the east of Java Island. Since the speed of propagation corresponds with one of the Kelvin wave, it is considered that the propagation of deep D20 along the coast are caused by the coastal Kelvin wave.

As can be seen in Fig. 7a, 7b (time-longitude sections of D20 along 6N and 6S in the Indian Ocean), a part of the warm water reached to the western coast of Sumatra stays in the eastern part of the Indian Ocean during the southwest monsoons. But this water began to move westward at the end of southwest monsoon. The speed of propagation estimated by the figure is approximately 0.5m/s that agrees with the speed of the Rossby wave. The propagation along 6S is found during southwest monsoons.

4. Discussions

The output derived from the ODAS shows the seasonal variation of the thermal structure, the coastal Kelvin wave and the Rossby wave in the Indian Ocean. It is necessary to validate these phenomenon by other data which are not used in the assimilation of ODAS.

It is difficult to investigate the physical structure of the Indian Ocean, because of less observed data there than in the Pacific and the Atlantic. More in situ data such as the XBT data by "Kashimasan-Maru" are needed for understanding the thermal structure of the Indian Ocean. We intend to investigate interannual variation of the physical structure of the Indian Ocean and its relation to El Niño.

5. References

1) Barnett, T. P., 1983: Interaction of the Monsoon and Pacific Trade Wind System at Interannual Time Scales. Part I: The Equatorial Zone, Mon. Wea. Rev., 111, 756-773.

2) Nicholls, N., 1984: The Southern Oscillation and Indonesian Sea Surface Temperature, Mon. Weather Rev., 112, 424-432.

3) Mikawa, T. and K. Ishikawa, 1995: Annual Report of JEXAM 1994, 61-71.

4) Yoshikawa, I., M. Kimoto and M. Ishii, 1995: Ocean Data Assimilation System for Climate Monitoring at JMA, WMO/TD-No. 651, volume II, 561-564.

5) Rao, R. R., R.L.Molinari and J.Festa 1989: Evolution of the Climatological Near-Surface Thermal Structure of the Tropical Indian Ocean. Part I: Description of Mean Monthly Mixed Layer Depth, and Sea Surface Temperature, Surface Current, and Surface Meteorological Fields, J. Geophys. ., 94, 10801-10815.

6) Mizuno, K., M. Yukinawa and T. Watanabe, 1992: Annual report of JEXAM 1991, 15-28 (in

Japanese).

7) Wyrtki, K., 1973: An Equatorial Jet in the Indian Ocean. Science,181, 262-264.

6. Publications

None

7. International Cooperation

None

(和文アブストラクト)

本研究では、1990年よりインド洋を航行するタンカー「鹿島山丸」によって表層水温を観測してきた。これらの観測データと世界気象機関(WMO)の全球気象通信網(GTS)を通じて取得した他の商船などによる観測データを併せ、気象庁で開発した「海洋データ同化システム(ODAS)」を用いてインド洋の赤道上の海洋構造の変化を解析した。その結果、ODASはモンスーンに現われるインド洋の表層における海洋構造の季節変化をうまく表現していた。また、インド洋東部ではインド洋中部赤道上の西風により蓄積された暖水の東進が見られるが、東岸に到達した後、沿岸ケルビン波として南北に伝播する現象が見られた。また、西進するロスビー波は北緯6度と南緯6度の東西断面図に見られるが、南西モンスーンの期間は暖水はベンガル湾に留まり、北東モンスーンへの移行とともに西に伝播している。

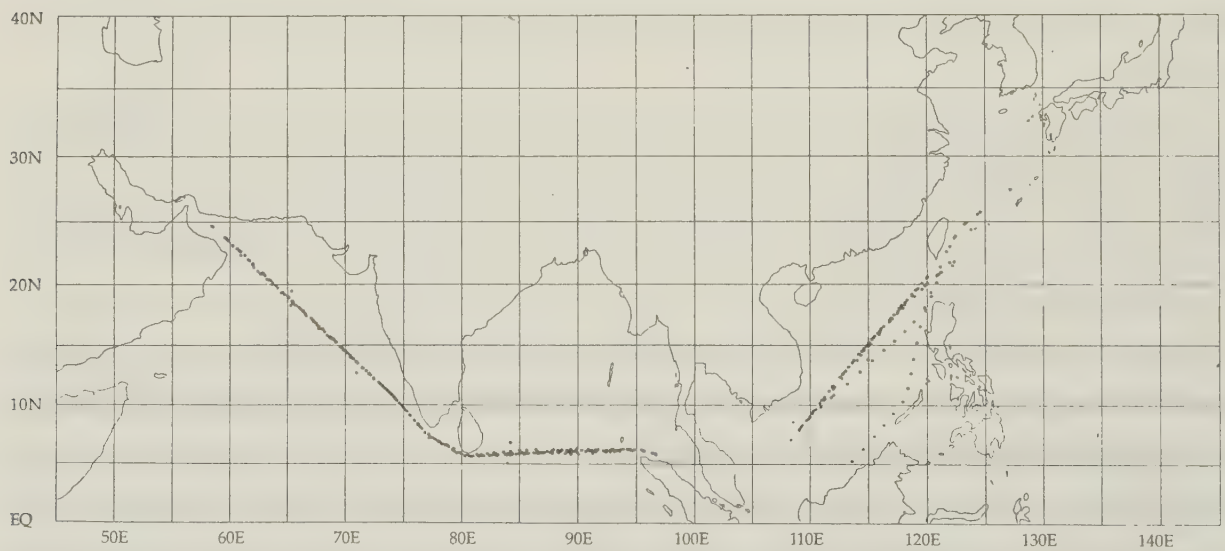

図1　委託商船「鹿島山丸」が航路上で1995年に観測した測点分布。

Fig. 1 Distribution of XBT's observation along the cruise tracks of "Kashimasan-Maru" for 1995.

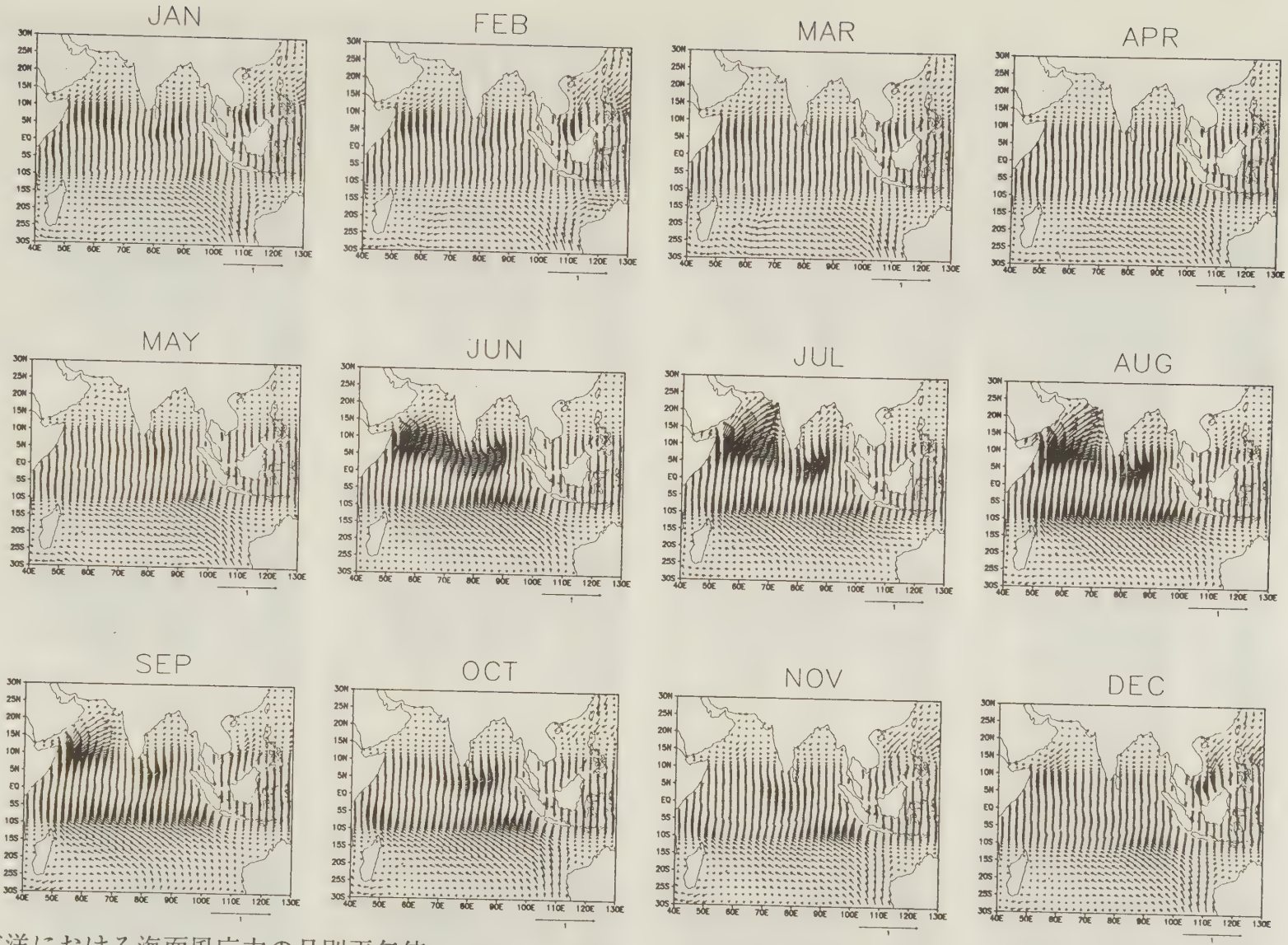

図2　インド洋における海面風応力の月別平年値

Fig. 2 Normals of monthly mean surface wind stress in the Indian Ocean. Data is derived from the Atmospheric Global Data Assimilation System of JMA. Normals are computed from 1987-1995 base period means.

図3　インド洋における20度等温線深度の月別平年値

Fig. 3 Normals of monthly mean depth of the 20℃ isotherm in the Indian Ocean. Data is derived from the Ocean Data Assimilation System of JMA. Contour interval is 10m. Normals are computed from 1987-1995 base period means.

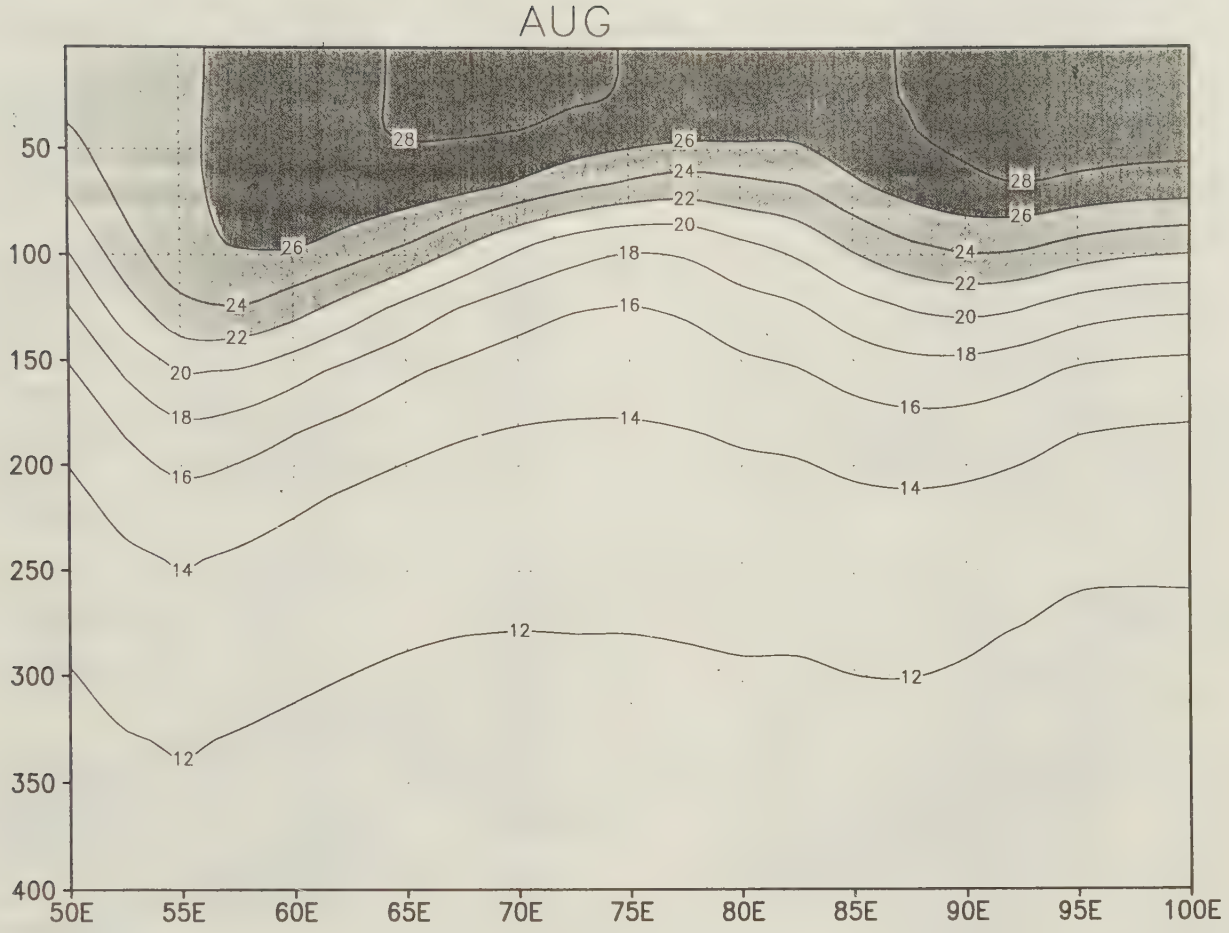

図４　インド洋の８月の北緯６度に沿った表層水温の経度－深度断面図

Fig. 4 Normals of monthly mean depth-longitude section of temperature along 6N in the Indian Ocean. Data are derived from the Ocean Data Assimilation System of JMA. Contour interval is 2℃. Normals are computed from 1987-1995 base period means.

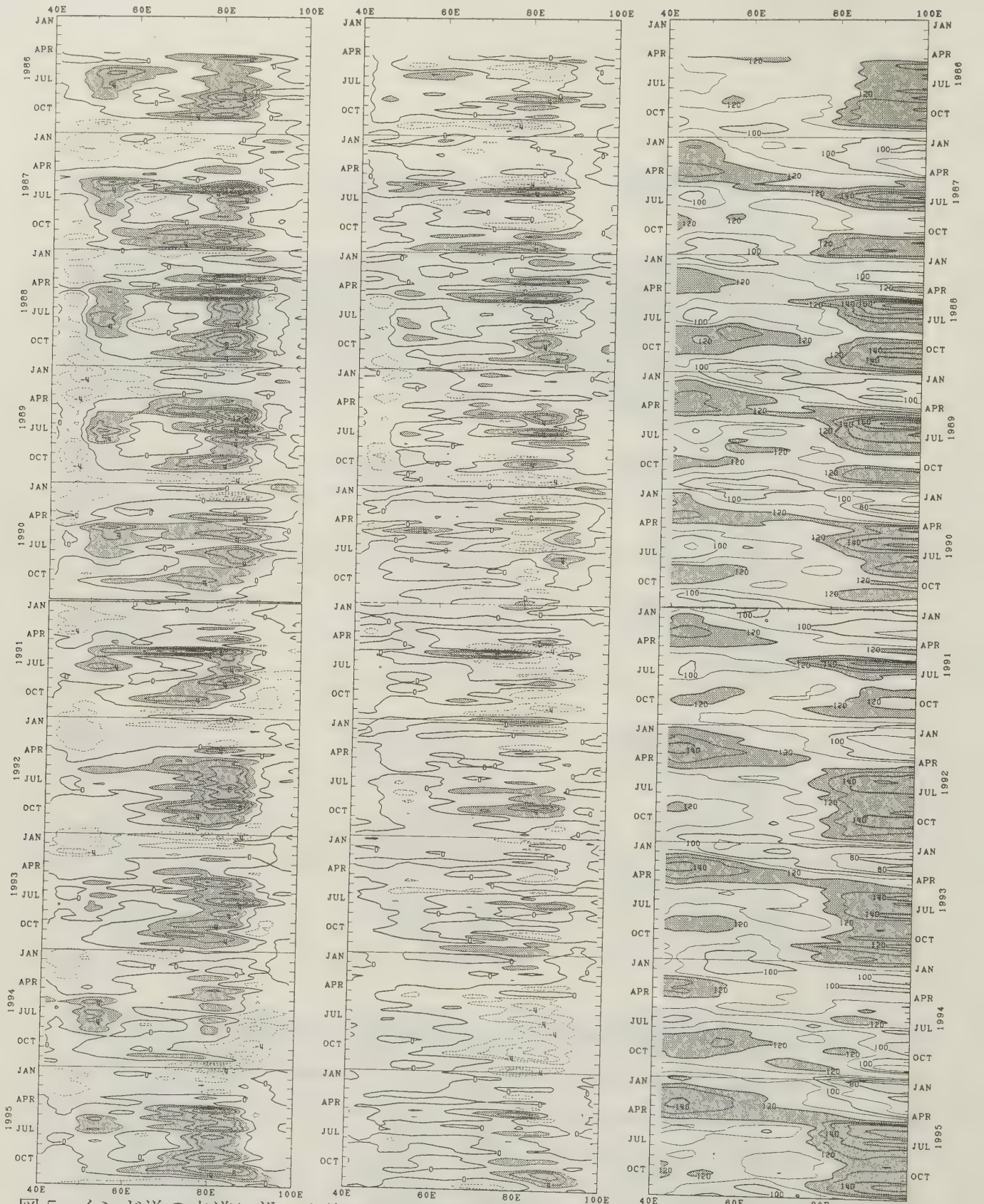

図5 インド洋の赤道に沿った海面風応力の東西成分(a)、平年偏差(b)及び20度等温線深度(c)の時間－経度断面図

Fig. 5 Time-longitude sections of zonal surface wind stress(a), anomalies(b) and depth of the 20℃ isotherm(c) along the equator in the Indian Ocean. Data are derived from the Ocean Data Assimilation System of JMA. Contour interval is 0.02N/m^2. Normals are computed from 1987-1995 base period means.

図6　1988年5～6月のインド洋で見られた20度等温線深度の平年偏差分布の時間変化

Fig. 6 Depth of the 20℃ isotherm anomalies from 20 May to 24 June 1988 in the Indian Ocean. Data are derived from the Ocean Data Assimilation System of JMA. Contour interval is 10m. Normals are computed from 1987-1995 base period means.

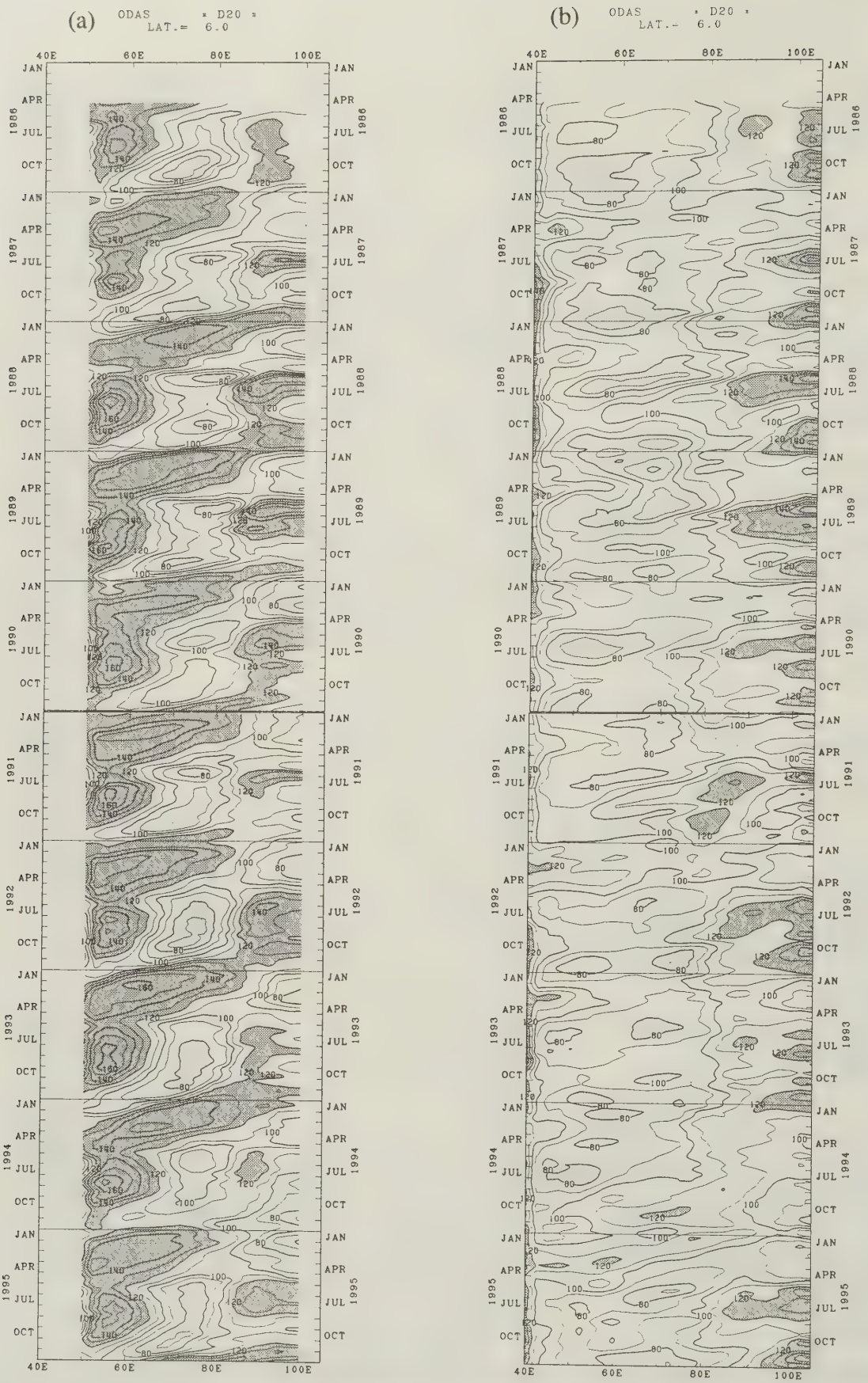

図7 インド洋の北緯6度(a)と南緯6度(b)に沿った20度等温線深度の時間－経度断面図

Fig. 7 Time-longitude sections of depth of the 20℃ isotherm along 6N (a) and 6S (b) in the Indian Ocean. Data are derived from the Ocean Data Assimilation System of JMA. Contour interval is 10m.

I. Observation and analysis on the process of the atmosphere-ocean-land interactions

2 Observation and analysis on the process over the ocean

(2) Observation on Oceanic Currents with Drifting Buoys

Hydrographic Department
Maritime Safety Agency
Yutaka Michida and Hideki Kinoshita

(Abstract)

Six drifters were deployed in the western tropical Indian Ocean and in the Arabian Sea in November and December 1994, to cover the area where very few buoys have been tracked in JEXAM programme. They were all released from a research vessel '*Shoyo-maru*' of National Institute for Far Seas Fisheries, Fisheries Agency. Their tracks are described together with those of the previous drifters in this paper as the results of investiogation for fiscal 1995. One drifter sampled a data set of surface currents near the equator and traced zonal currents including Wyrtki's jet along the equator in April 1996 whose maximum eastward velocity was smaller than that estimated with JEXAM drifters deployed in 1990 and 1992. It also tracked westward flow along 2° S in January 1996, eastward flows 2 -3° S in December 1995 and February 1996.

1. Objectives

Interannual variation of the Asian Monsoon, which has big influence upon the climatical variabilities in the region of south east Asia, may play an important role in the global climate change through the atmospheric general circulation. Some of previous studies have suggested that the Aisan Monsoon would cause changes in the oceanographic condition in the western tropical Pacific and should have close relationship with ENSO events. As a successful example of oceanographic research related to climate change, TOGA (Tropical Ocean and Global Atmosphere), whose major field was the tropical Pacific, provided so much knowledge on ENSO mechanism. In the Indian Ocean, on the other hand, there have been very few oceanographic data available in comparison with other oceans.

Fourty-three surface drifters were deployed by the end of 1995 in the Indian Ocean and tracked with ARGOS system within this research programme, Japanese EXperiment on Asian Monsoon (JEXAM) to illustrate the surface current system of the tropical Indian Ocean and the Seas adjacent to Indonesia, which is very interesting issue for oceanographers from the view points of, for examples, mass/heat/salt exchange between the Pacific Ocean and the Indian Ocean, or air-sea interactions there.

A schematic representation of the Indian Ocean currents and their seasonal changes has been proposed by *Molinari et al.*[1990], who have presented a monthly climatology of surface currents by analysing historical drifter data. To investigate thier results and to complement

thier study, trajectories of the drifters which are uniformly designed according to the recommendation of WOCE/TOGA SVP (Surface Velocity Programme) have been analysed in this study. The results of analysis for the drifters deployed in 1995 are mainly described in this paper.

2. Methods

Six to ten drifters have been deployed in the Indian Ocean every year since 1990, the commencement of JEXAM programme. The drifters are designed according to the WOCE/TOGA SVP standard. A holey sock drogue of 8.6m in length whose drag center is at 15m below the sea surface is attached to the surface float that contains a processing unit for sensor data (sea surface temperature, on/off of the drogue and battery voltage) and a transmitter for ARGOS system. There is also a small subsurface float, which would reduce the tension of the tether between the surface float and the drogue (cf. *Michida and Ishii*, 1993; *Michida and Yoritaka*, 1995).

Six drifters were deployed in the western tropical Indian Ocean and in the Arabian Sea in November and December 1994, to cover the area where very few buoys have been tracked in JEXAM programme. All the above drifters were released from a research vessel '*Shoyo-maru*' of National Institute for Far Seas Fisheries, Fisheries Agency.

3. Results

All trajectories of the drifters deployed by the fiscal year 1995 within JEXAM are shown in Figure 1 as a 'spaghetti' diagram. The coverage of them extends mostly tropical Indian Ocean, north of 20S, Arabian Sea and the area of Indo-Pacific throughflow. Seasonal mean current fields were discussed by *Michida and Yoritaka* [1996] by analysing the data set shown in Figure 1 except for the Arabian Sea where drifters were just released in 1995.

The tracks of six drifters deployed in the western equatorial Indian Ocean and Arabian Sea in 1995 are shown in Figure 2. They were released along a meridional line across the Arabian Sea and on the equator east of Somalian coast during an expedition in the Indioan Ocean on board the research vessel 'Shoyo-maru' of Fisheries Agency.

One drifter released on the equator, 54° E, on November 20, 1995, drifted eastward until mid-December probably in the equatorial jet, showing its maximum drifting velocity at 80cm/sec. It turned northwestward on December 20 and sustained its drifting direction until January 28, 1996, when the transmission stopped at 8° 28'N, 55° 59'E. On December 11, before the direction turning, the drouge presence sensor indicated undrogued, and the tracks after the drogue loss might contain significant down-wind slip components.

One drifter(23914) released at 3° S, 64° E on November 26, 1995, drifted eastward until the end of December, getting slightly closer to the equator. It turned westward on December 29 and kept drifting west along approximately 2° S for about one month. Then it turned east again on January 25, 1996, and kept drifting east along 3° -4° S until mid-March. It drifted north slowly(~30cm/sec), tracing an anticlockwise trajectory and reached at the equator on March 30. It turned for the third time to drift eastward on the strong equatorial jet. The drogue presence sensor confirmed that the drogue of this drifter

was attached all the time.

One drifter released at 2° 47'N, 64° E on November 30, 1995, drifted generally northeast, showing a meandering trajectory. It seemed to get ashore around Laccadive Is. on March 13 or 14, 1996.

One drifter released at 12° N, 64° E in the central area of Arabian Sea on December 1, 1995, drifted generally westward. It seemed to get into a cold eddy at the end of January and drifted west to southwest showing anticlockwise circular tracks according to the movement of the eddy.

One drifter released at 21° 30'N, 64° E, south of the coast of Pakistan in the northern part of Arabian Sea on December 5, 1995, traced a clockwise gyre whose center was located at 22° 20'N, 63° 50'E for about 20 days. It drifted northeast toward the coast of Pakistan from January to March 1996. It seemed to be picked up south of the coast of Pakistan in early March and transported to the port of Karachi.

The last one released at 18° N, 61° 40'E, southeast of Arabian Peninsula on December 7, 1995, drifted east for about one month, then turned west on January 3. It sustained a westward flow until the end of February when it got ashore on the coast of Oman.

4. Discussions

Wyrtki[1973] pointed out that an equatorial jet, a strong eastward current along the equator, is observed during the transition periods of the monsoon; twice a year, April to May and November to December. Three of our drifters have also tracked the equatorial jet; in 1990, 1993 and in the experiment of the fiscal 1995 as mentioned in the section 3.

The trajectory of drifter 11216 deployed in February 1990, which survived until March 1991, is displayed in Figure 3(a). It turned eastward in April 4, 1990 after westward drift for about one month, suggesting that a strong eastward jet appeared in boreal spring (*Michida and Yoritaka*, 1996). Daily drifting velocity of drifter 11216 calculated from the first fix points of the day is shown in Figure 3(b) . The east component of the drifting velocity exceeded 100cm/s on April 11, seven days after the onset of the jet. The maximum eastward velocity was 185cm/s observed on April 18. Eastward flow lasted until May 7.

The trajectory of drifter 17260 deployed southwest of Smatra in November 1992 is shown in Figure 4(a). A clockwise gyre extending almost entire tropical Indian Ocean was tracked with the drifter south of the equator. As a part of the gyre, an equatorial jet was again observed from December 1993 to January 1994, in boreal autumn during another transition period of the monsoon, with its trajectory which displayed that it reached north of Madagascar and turned east in November 1993 then drifted east along the equator for about two months(*Michida and Yoritaka*, 1996). The east component of the daily drifting velocity shown in Figure 4(b) exceeded 100cm/s on November 29. It kept drifting east until January 7, 1994, with a maximum eastward velocity component over 170cm/s observed on December 10.

Drifter 23914 tracked an equatorial jet in April 1996, in boreal spring, as described in section 3, which was the third time that the equatorial jet was traced with drifters in

JEXAM programme. The daily drifting velocity shown in Figure 5, however, was much smaller than the previous drifters which tracked the equatorial jet. The maximum eastward component of drifter 23914 was only 102cm/s observed on December 2, 1995, while those of the previous ones were both over 170cm/s. The drifter reversed its drifting direction four times for five month since deployment, basically tracking zonal flows; east or west. In the first two months it was gradually turning from eastward flow to westward along 2° S, as shown in the time series of east-west component of the velocity given in Figure 5. The maximum westward velocity was 150cm/s which was observed on January 20. The zonal velocity quickly reversed to the east within 5 days and sustained eastward current along 3° S until mid-March. It looks like an equatorial jet described by *Wyrtki*[1973], though it was observed about 300km away from the equator with smaller zonal velocity, two months earlier than the onset of the jet in the period of monsoon transition. The data set described in this paper is too limited to make detailed discussion on this 'weak jet' observed as a eastward flow along 3° S from February to March 1996, whether it was a part of Wyrtki's jet, substructure of it or a current driven by different dynamics from it. It would be needed to combine this data set with the data set provided from WOCE/TOGA SVP for further analysis.

5. References

Michida, Y. and H. Ishii, Observation of ocean circulation with surface drifters, *Kaiyo monthly*, **extra 4** ,115-122,1993 (in Japanese).

Michida, Y. and H. Yoritaka, Survivability of the surface drifters deployed by Hydrographic Department of Japan for the period from 1988 to 1993, *J. Japan Soc. Mar. Surv. Tech.* **7(2)**, 21-28, 1995.

Michida, Y. and H. Yoritaka, Surface currents in the area of the Indo-Pacific throughflow and in the tropical Indian Ocean observed with surface drifters, *J. Geophys. Res.* **101**, 12475-12482,1996.

Molinari, R. L., D. Olson and G. Reverdin, Surface current distributions in the tropical Indian Ocean derived from compilations of surface buoy trajectories, *J. Geophys. Res.* **95**, 7217-7238, 1990.

Wyrtki, K., An equatorial jet in the Indian Ocean, *Science*, **181**, 262-264, 1973.

6. Publications

①Scientific Journals

Y. Michida and H. Yoritaka, Surface currents in the areas of Indo-Pacific throughflow and tropical Indian Ocean observed with surface drifters, *J. Geophys. Res..*, 101, 12475-12482, 1996.

Y. Michida and M. Yoritaka, A Comparison between the Tracks of Surface Drifters and Sea Levels Derived from Satellite Altimetry in the Seas Adjacent to Indonesia, Proceedings of International Workshop on the Throughflow Studies in and around Indonesian Waters, 177-183, 1996.

②Oral Presentations

Y. Michida and M. Yoritaka, A Comparison between the Tracks of Surface Drifters and Sea Levels Derived from Satellite Altimetry in the Seas Adjacent to Indonesia, Jakarta, Oct. 9-11, 1995.

7. International Cooperation

The United States has been deploying many drifters in the Indian Ocean within WOCE/TOGA Surface Velocity Programme in 1995 and 1996. It is strongly required for us to provide our experiences and knowledge acquired in JEXAM Programme to the international scientific communities and to keep close contact and relationship with the drifter groups in US in exchanging information on the plan of deployments or cooperative deployment.

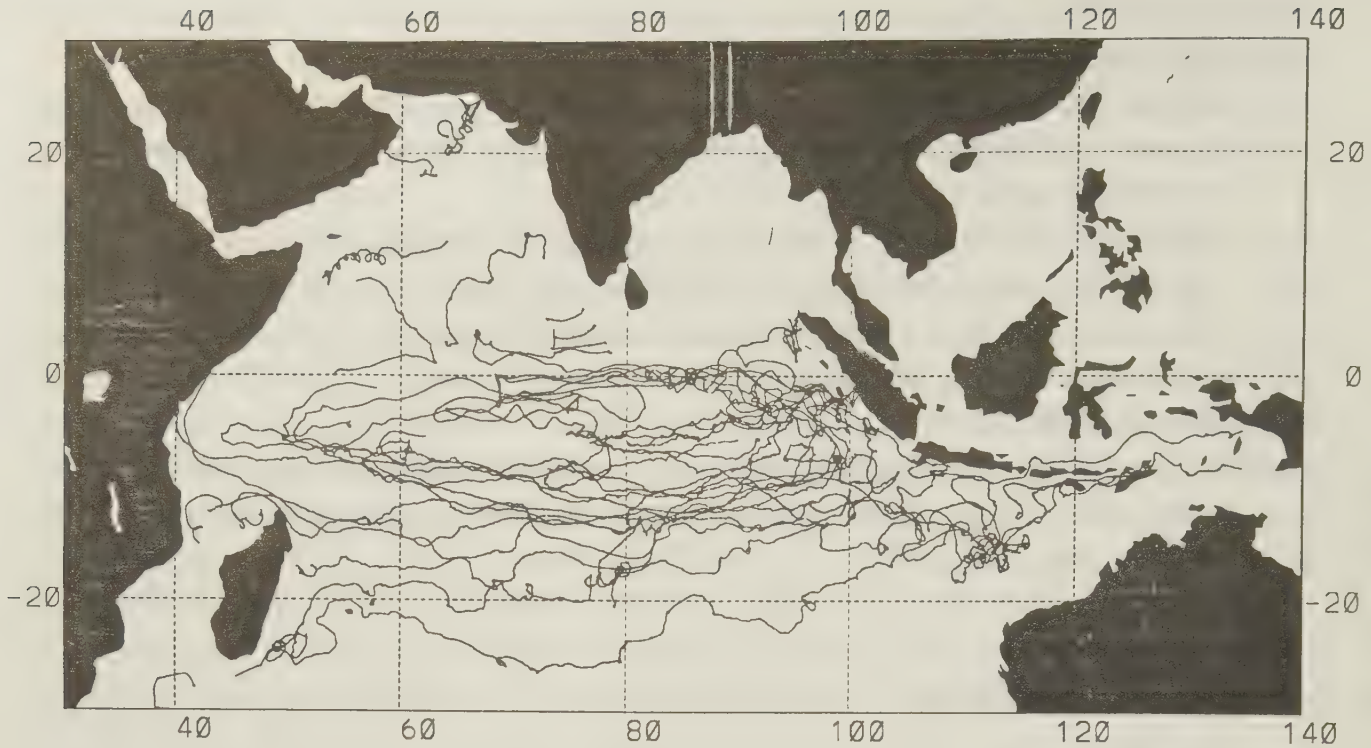

Figure 1. All trajectories of the drifters deployed in JEXAM since 1990.

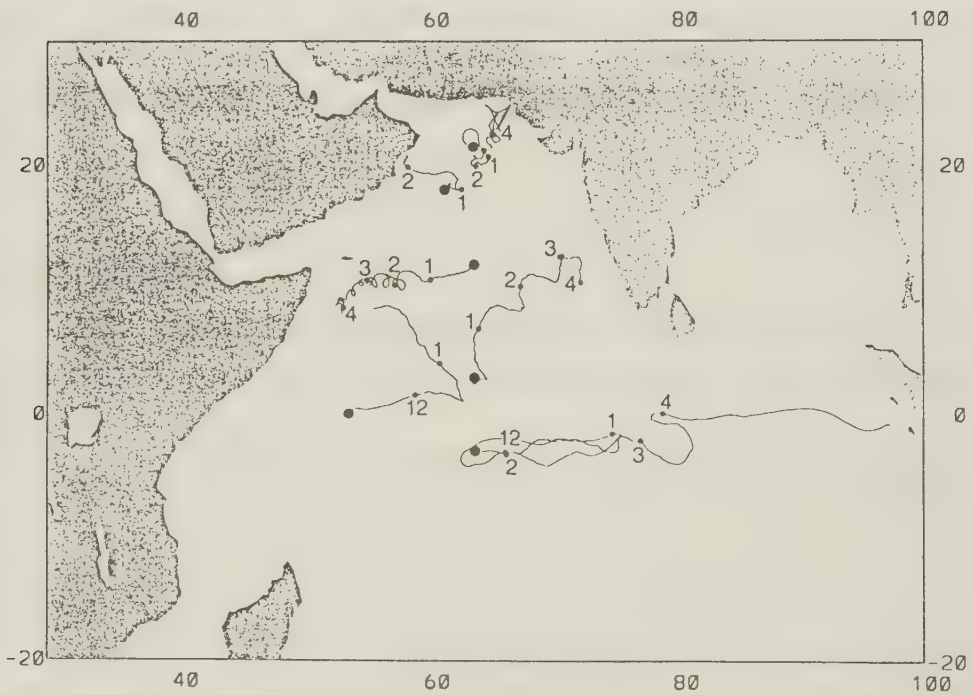

Figure 2. Trajectories of the drifters deployed in the western tropical Indian Ocean and Arabian Sea in November-December 1995. Large solid circles mark the deployment location, while small ones mark the locations on the first day of every month, with the month number (January is 1, February is 2,..).

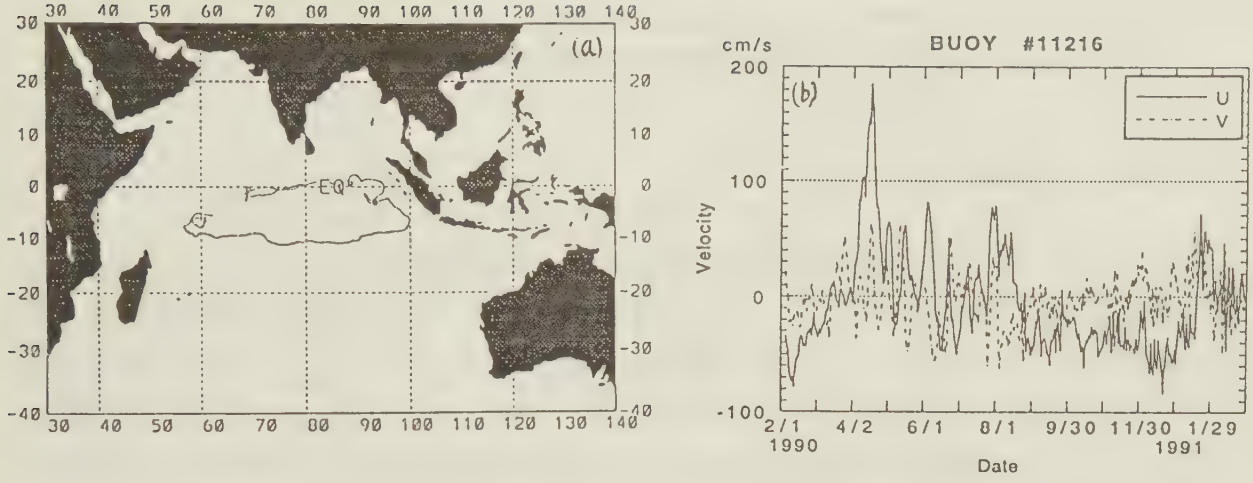

Figure 3. (a) Trajectory and (b) time series of daily drifting velocity for drifter 11216, which was released in February 1990.

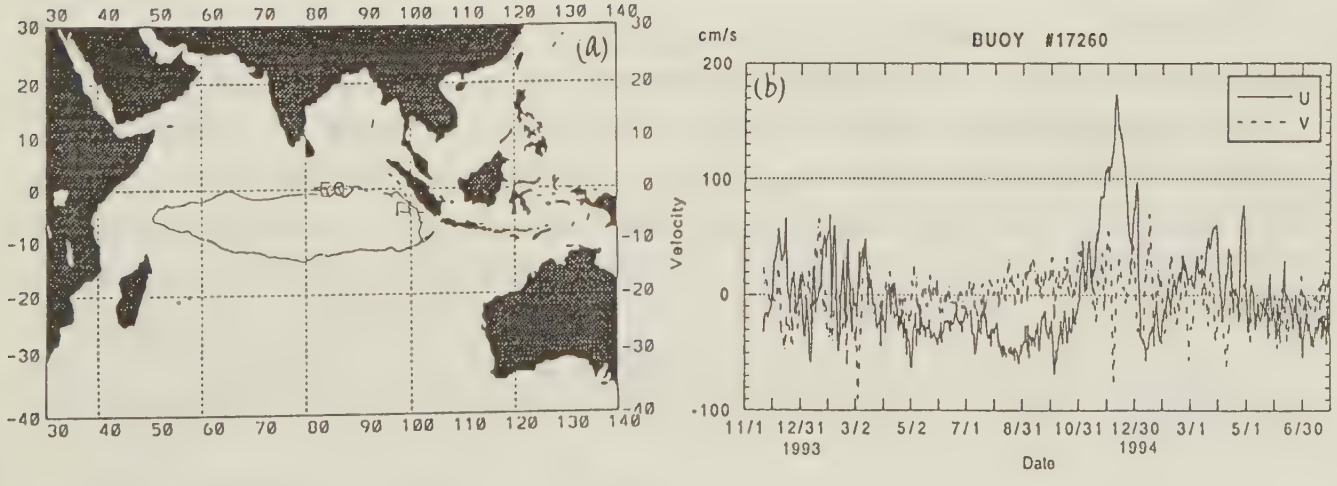

Figure 4. Same as Figure 3, except for drifter 17260, which was released in November 1992.

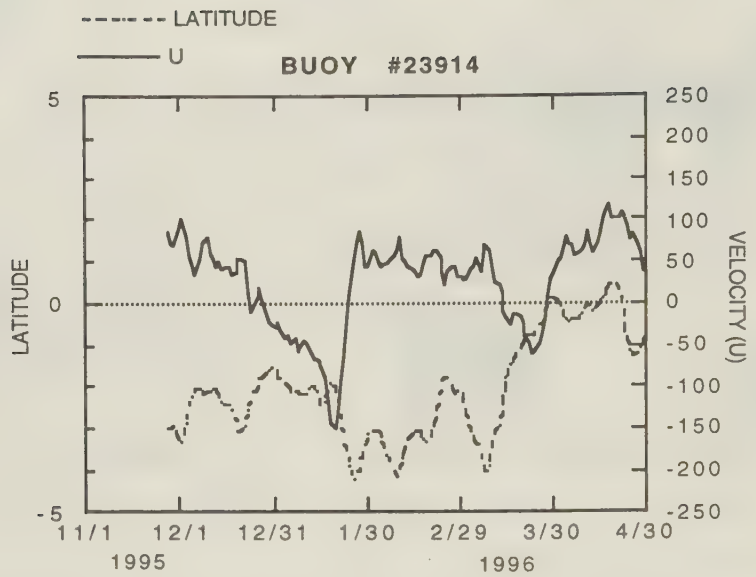

Figure 5. Time series of daily drifting velocity for drifter 23914, which was released in November 1995. Solid line shows eastward component of the velocity and dashed one does the latitude of the location.

(要旨)

「アジアモンスーン機構に関する研究（JEXAM）」の一環として、1989年以来実施してきた表面漂流ブイによる海流観測の空白域を埋めるため、1994年11月から12月にかけて水産庁遠洋水産研究所の調査船「照洋丸」の協力を得て、西部熱帯インド洋及びアラビア海に計６個の漂流ブイを投入した。ここでは、平成７年度の研究成果としてそれらの軌跡及び過去のブイの軌跡を記述する。平成７年度の投入したブイのうち１個によって赤道付近の海流データが得られ、Wyrtkiジェット等赤道付近の東西流が測定された。観測されたWyrtkiジェットの東向き最大流速はJEXAMにおいて以前放流されたブイによる見積もりよりも小さくなっていた。またこのブイは南緯２度付近に沿った西向きの流れを1996年１月に観測し、南緯２～３度付近に沿った東向きの流れを1995年12月及び1996年２月にそれぞれ観測した。

I. Study on Air-Sea-Land Interactions and their Long Term Variations

2. Observation and Analysis on the Process over the Ocean

(3) Standardization of Oceanic Data and Promotion of Exchange of Oceanic Data and Information

Japan Oceanographic Data Center
Hydrographic Department
Maritime Safety Agency
Taiji Imoto, Yoshio Shimizu

(Abstract) The purpose of study is to provide a sufficient data set and timely information for promoting the JEXAM study. In order to suffice this goal, sub-themes have been established; data standardization and quality control of JEXAM data; collection of existing data from other nations; establishment of international on-line network system for data and information exchange.

The JODC Online Information and Data Exchange Service (JOIDES) was added with information exchange system for NODCs, and JODC collected the information of oceanographic data resources for JEXAM in 1995.

1. Purpose of study

The purpose of this study is to provide researchers engaged in the "Japanese Experiment on Asian Monsoon" (hereinafter referred to as JEXAM) and research study on the Indian Ocean with the best available data set as well as information on research in order to be carried out those studies smoothly and effectively.

To achieve this purpose, oceanic data such as water temperature obtained through the "Observation in the Indian Ocean", one of the research subjects of JEXAM, will be standardized so that researchers can share their data with each other smoothly. In addition, existing oceanic data and information will be collected in order to provide full basic data for each study of JEXAM. Efforts will be also made to improve the accuracy of quality control of data by enhancing the reliability of statistics based on the obtained data.

In addition to such data management activity, a data base will be built, which permits on-line input/output or retrieval of information to check the state of data management or marine research programs with the view of speeding up distribution of information. Furthermore, a data information network system will be established between national oceanographic centers of various countries and JODC to allow it to easily obtain cooperation from various countries for acquisition of data

and information while another system will be established to allow Japan and other countries to share consistent oceanic data and information.

Those systems will contribute to easy, fast and smooth use of oceanic data for JEXAM and to effective use of such data for various projects related to global environment.

2. Methods for study

(1) Support the system for fast and smooth distribution of data in this project through on-line computer network system, JOIDES.

(2) Standardize obtained data (water temperatures, ocean currents, drifting buoys), and building a data base of such data.

(3) Collect information and data on the marine research in the Indian Ocean.

3. Results of study

(1) On-line computer network system JOIDES

The system for fast and smooth distribution of information for this project is supported by the on-line computer network system JOIDES.

(2) Building a data base of observation data on the Japanese Experiment on Asian Monsoon

JODC received surface water temperature data (XBT) observed by voluntary ships at 400 points from February 1994 to January 1995 through "Observation and Analytical Study on Various Processes in the Indian Ocean" of JEXAM from Meteorological Agency.

Observation points for the received data are shown in Fig. 1.

Fig. 1 Observation points for data received from JMA

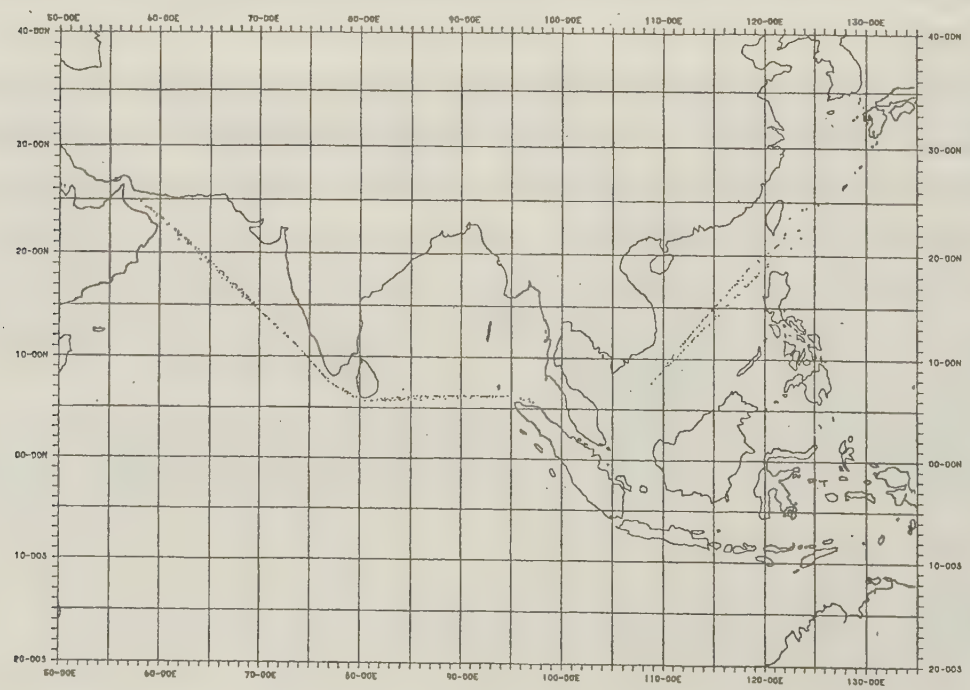

(3) Data related to the sea area covered by the project

JODC received "Sea Level Data ", one CD-ROM, from the NOAA National Oceanographic Data Center (NODC) . The CD-ROM, created by the NODC, is composed two main directories. One of directories of the CD-ROM contains Tropical Ocean Global Atmosphere (TOGA) sea level data, the file formats, and associated documentation. The other directory contains the Permanent Service for Mean Sea Level (PSMSL) data, documentation, and a few related data sets.

The TOGA sea level data is managed by the TOGA Sea Level Center at the University of Hawaii in cooperation with the NODC through the Joint Archive for Sea Level. It is a well documented archive of hourly, daily, and monthly sea level values in standardized formats from 289 sea level stations in the Pacific, Atlantic, and Indian Oceans. These data are collected in support of the TOGA project and are primarily in the tropical ocean areas of TOGA interest (30 deg. N - 30 deg. S latitude). The CD-ROM contains the TOGA sea level holdings as of July 1994.

The PSMSL is based at the Proudman Oceanographic Laboratory, Bidston Observatory, United Kingdom and contains monthly and annual mean values of sea level from approximately 1500 tide gauge stations around the world. Other related data sets are also included. The CD-ROM contains the PSMSL data holdings as of August 1994.

4. Summary

Recently, there has been a sharp increase in use of Internet among researchers in Japan. Thus, it is necessary to be able to down load the data using FTP server, in order to distribute the data rapidly.

（要　約）

本研究は、「アジアモンスーン機構に関する研究」（以降 JEXAM）及びインド洋に関する調査研究の円滑かつ効果的な実施を図るため、当該研究に携わる研究者に対し、利用可能な最良のデータセット及び調査に係る情報を提供するためのものである。この目的を達成するために、JEXAM の一研究項目である「海洋に関する観測研究」において取得される水温等の海洋データの標準化を行い、研究者間のデータ相互利用の円滑化を図った。また、JEXAM の各研究における基礎資料の充実を図るため、インド洋及び周辺海域における既存の海洋データ及び関連情報の収集を行い、さらに得られたデータにより統計値の信頼度を増すことによってデータ品質管理の精度向上を図った。

一方、これらのデータ管理活動のほかに、情報流通の迅速化を図るため、データの管理状況及び海洋調査計画等に関する情報のオンライン入出力・検索が可能なデータ

ベースを構築した。さらに、データ・情報提供に関する各国の協力を得やすくするため、各国国立海洋データセンター等とJODCとの間に海洋データ・情報交換のためのデータ情報ネットワークシステムを構築し、国内から国外まで一貫した海洋データ・情報交換のためのシステムを確立し、JEXAMにおける海洋データの迅速・容易かつ円滑な利用、さらに、その他の地球環境関係の各種プロジェクトでの有効利用に寄与している。

Ⅰ. Observation and analysis on the process of the atmosphere-ocean-land interactions
大気・海洋・陸域間相互作用の諸過程に関する観測・解析研究

3. Observation and analysis on the process over the land
陸域における諸過程に関する観測研究

(1) Observation on Hydrology over the Tibetan Plateau and Himalayas
チベット・ヒマラヤにおける水文変動に関する観測研究

Shinjo Branch of Snow and Ice Studies,
National Research Institute for Earth Science
and Disaster Prevention,
Science and Technology Agency
Takeshi Sato
防災科学技術研究所
新庄雪氷防災研究支所
科学技術庁
佐藤　威

(Abstract)

In this study, automatic observation sites of snow weight (water equivalent of snow), ground temperature, and frozen ground depth were established at Lhasa, Rikeze and Nagqu in the Tibetan Plateau. Based on their long term records, variations of snow cover and frozen ground together with their relation to the Asian Monsoon will be analyzed.

In July, 1993, the instruments were set and continuous observations started. These works were done in cooperation with Chinese scientists. At the same time, Meteorological Research Institute (MRI) started micrometeorological observations at the same sites. The data collection has been carried out once a year since July, 1994.

Analyzing the records from July, 1993 to July, 1995, following results were obtained : The maximum frozen ground depth at Nagqu was 158cm in 93/94 winter and 134cm in 94/95 winter, which are smaller than the routinely measured values by about 40cm. The seasonal variations of the frozen ground depth show that the observation agrees well with the routine data before the midwinter but does not after the midwinter. Especially, the decay of the frozen ground layer was faster in the observed data than in the routine data. It was found that the routine soil temperatures at the depths of 80cm and 160cm were from +0.4 to +0.6℃ when the soil melted at the corresponding depths. This can be a reason why the routinely measured maximum frozen ground depth was greater than the observation and the frozen ground layer was recorded for longer period in the routine data. At Lhasa and Rikeze where the frozen ground layer was thinner than at Nagqu, the observed frozen ground depths were smaller than the routine data.

At Nagqu, the maximum frozen ground depth was greater in 93/94 winter than in 94/95 winter. The amount of the soil moisture might affect the development of the frozen ground layer through the soil thermal conductivity. The precipitation in the preceding summer (July to September) was 348mm in 1993 and 115mm in 1994, and the soil was considered to be wetter in 93/94 winter than in 94/95 winter.

By improving the correction of the snow weight data, its accuracy attained $\pm 3 kg/m^2$. During the snow accumulating periods from January to February, 1995 at Nagqu, the snow density calculated from snow weight and routine snow depth data did not change largely and was about

$0.1 g/cm^3$. This small snow density indicates that the densification of snow was not remarkable due to the thin snow cover.

1. Objectives

Snow cover and frozen ground in the Tibetan Plateau have great influence not only on the Asian Monsoon activity but also on the global climate system. In order to understand the mechanism of the Asian Monsoon, seasonal and annual variations of snow cover and frozen ground should be clarified and the relationship between them and the Asian Monsoon activity should be studied. Though areal and quantitative investigation of snow cover and frozen ground is required, present remote sensing technology has not yet made such measurements possible. In this study, automatic observation of snow cover and frozen ground are continued for several years at three sites (Lhasa, Rikeze and Nagqu) in the Tibetan Plateau. The data will be analyzed to clarify the relationship between the snow cover and frozen ground conditions and the Asian Monsoon.

2. Methods

The structure of the snow weight meter and its principle of measurement have already been described in the literature.[1),2),6)] In case of the Tibetan Plateau except for high mountain, snow cover is not thick and diurnal temperature variation is very large. So, temperature dependence of the snow weight meter should be considered to obtain a true snow weight value. After examining the diurnal variations of apparent snow weight, corresponding to the output voltage of the snow weight meter, and ground temperature, which is actually the temperature beneath the metal wafer unit, it was found that apparent snow weight has thermal hysteresis. It is impossible to correct the snow weight values taking fully the hysteresis into account. In this study, a regressive relation between the apparent snow weight and the ground temperature was obtained from the data when the ground temperature variation was small in the nighttime. By using this regressive relation, the snow weight values were corrected and the accuracy of the snow weight attained $\pm 3 kg/m^2$.

The structure of the frozen ground depth meter (FDM2) and its principle of measurement have also been shown in the literature.[3)] The sensor unit is a FRP cylinder, 225cm long and 1.6cm in diameter, in a Silicon rubber tube and deaired water is filled between the sensor unit and the tube. There are 104 electric terminals, separated 2cm from each other, on the sensor unit to detect the state of deaired water around the terminals by measuring the resistance between the detection terminals and the one common terminal. The scanning is made by eight paired detection terminals. The observed frozen ground depth sometimes changed stepwise. This may be due to the scanning method shown above. In July, 1995, the frozen ground depth meter was changed from FDM2 to FDM3, whose scanning method is improved. The structure of the FDM3 sensor unit is shown in Fig.1. A soft PVC tube is attached to the board, in which deaired water is filled. One sensor unit has 16 detection terminals in the deaired water at an interval of 2cm. And seven units are connected to obtain a record from the ground surface to the depth of 2m. The state of the deaired water (water/ice) is detected by scanning every detection terminal.

In 95/96 winter, performance tests of FDM2 and FDM3 together with the soil temperature profile observation were carried out in Kitami, Japan, where the maximum frozen ground depth is several tens of centimeters every winter. Although the analysis has not been completed yet, the results will be useful for the validation of the frozen ground depth values observed in the Tibetan Plateau.

3. Results

3.1. Observation in 94/95 winter

The second data collection was carried out in June to July, 1995. Summary of the observations are shown in Table 1 together with those in 93/94 winter. Since there was ambiguity in the frozen ground depth record at Nagqu, the data was partly missed and the daily active layer[6] could not be distinguished. No significant snow weight was recorded at Lhasa and Rikeze in 94/95 winter.

3.2. Frozen ground depth

The meteorological observatories at Lhasa, Rikeze and Nagqu routinely measure the frozen ground depth. Their instrument is a rubber tube of about 1cm diameter, in which water is filled, and they measure the length of frozen part every morning (00Z). The rubber tube is installed in a steel protect tube whose inner diameter is 2.6cm. The routine data in 93/94 and 94/95 winters are now available.

An observed frozen ground depth at Nagqu in 93/94 winter is shown in Fig.2(a) where the white bar indicates a daily active layer[6] near the ground surface and the black bar indicates a frozen ground layer. The bottom of the daily active layer corresponds to the daily maximum depth of the melted layer during the period from 04Z to 02Z of the next day. The bottom of the frozen ground layer corresponds to its daily maximum depth during the period from 04Z of the previous day to 02Z. The corresponding routine data is shown in Fig.2(b). Since the routine data is obtained once a day in the morning when the frozen ground depth becomes maximum in the diurnal variation, the routine data cannot give the information about the daily active layer.

At the beginning of winter, the daily active layer often formed and the daily maximum frozen ground depth did not increase. At this stage, a thin frozen ground layer was sometimes not observed by FDM2. From the middle of November to the end of December, frozen ground layer grew and the observed data coincided with the routine data. After that, the observation indicates that the frozen ground layer was getting deep until the beginning of March and it attained maximum (158cm). However, the routine data shows that the development continued until the beginning of April and the maximum depth was 200cm. In spring, the frozen soil melted rapidly both from the surface and from below. The decay of the frozen ground layer was faster in the observed data than in the routine data. This comparison shows that the observation agrees well with the routine data before the midwinter but does not after the midwinter.

The data in 94/95 winter are shown in Fig.3 and have a similar tendency as in 93/94 winter. The maximum frozen ground depths at Lhasa, Rikeze and Nagqu are summarized in Table 2. At Lhasa, maximum frozen ground depth was 15cm from the routine measurement, but the frozen ground layer was not detected by FDM2 in 94/95 winter. At Rikeze, the observed values are smaller than the routine data in both winters. Since the frozen ground layer at these two sites is thin and confined to near the ground surface, the soil temperature distribution around the FDM2 sensor might be different from that around the instrument used in the routine measurement.

The discrepancy between the observed and routine data in the decay stage will be discussed in the following. The soil temperatures at the depths of 80cm and 160cm were analyzed, which are measured routinely near the routine frozen ground depth meter. When the frozen soil melted at the depths of 80cm and 160cm, the routine soil temperatures at the corresponding depths were from +0.4 to +0.6°C. This means that the temperature in the steel protect tube for the routine frozen ground depth meter was lower than the soil temperature. This may be a reason why the routinely measured maximum frozen ground depth was greater than the observation and the routinely measured frozen ground layer remained longer than the observation by FDM2.

The profile of the soil temperature is shown in Fig.4 which was routinely measured at Nagqu meteorological observatory. On the 1st of April, 1994, the soil temperature between the depths of 40cm and 160cm was close to 0℃ and its vertical gradient was very small. In this situation, small disturbance of the soil temperature distribution would affect the decay of frozen ground layer.

3.3. Snow Weight

The snow weight at Nagqu is shown in Fig.5(a) for 93/94 winter and in Fig.5(b) for 94/95 winter. In Fig.5, the routinely measured snow depth is also shown in the lower part. The snow weight in 93/94 winter were corrected by using the air temperature[6] since the ground temperature was not observed. Thus the correction may not be sufficient. Maximum snow weight of 6kg/m^2 was found even if the snow depth was zero. On the other hand, the snow weight in 94/95 winter was corrected by using the ground temperature and the effect of the thermal hysteresis was removed. The correction was improved and the error in the snow weight values is considered to be within $\pm$3kg/m^2.

The snow density was calculated from the observed snow weight and the routine data of snow depth at Nagqu in 94/95 winter (Fig.6). During the snow accumulating periods from January to February, 1995, the snow density did not change largely and was about 0.1g/cm^3. This value corresponds to the that for the new snow observed in Japan. Small snow density indicates that the densification of snow was not remarkable due to the thin snow cover.

The snow density is sometimes measured by the Nagqu meteorological observatory when the accumulated snow exists. The routine snow density is also plotted in Fig.6, and is close to the observation.

4. Discussion

The frozen ground depth D (cm) can roughly be expressed by the following equation[4] :

$$D = \alpha \sqrt{I}, \tag{1}$$

where I (℃·day) is an accumulated freezing index defined by

$$I = \Sigma T. \tag{2}$$

Here, T (℃) is a daily mean ground surface temperature, and the summation is made for only negative values of T. The value of α depends on the physical property of the soil, especially on the thermal conductivity. The accumulated freezing index of Nagqu was calculated from the routine data of the ground surface temperature, measured at an interval of 6hours (00Z, 06Z, 12Z, and 18Z). The routinely measured frozen ground depths are plotted against the accumulated freezing index for 93/94 and 94/95 winters in Fig.7. The frozen ground depth in 93/94 winter was greater than in 94/95 winter except for the early stage of freezing ($I \leqq 100$℃·day). Although D is not proportional to the square root of I throughout the winter, Eq.(1) was fitted to the obtained D-I relation except for the early stage of freezing. The values of α were 4.0 for 93/94 winter and 3.2 for 94/95 winter.

The difference in the frozen ground development between the two winters might be ascribed to the soil moisture difference. As the precipitation in the preceding summer (July to September) was 348mm in 1993 and 115mm in 1994, the soil moisture was considered to be wetter in 93/94

winter than in 94/95 winter, which might result in larger soil thermal conductivity in 93/94 winter. This may be a one reason why the frozen ground layer was deeper in 93/94 winter than in 94/95 winter.

After July, 1995, the soil moisture has been observed by MRI at the same sites, and the thermodynamic constants of the soil will be determined. So, quantitative discussion on the annual variation of frozen ground depth will be possible in the near future, which will be based on the heat budget of the soil layer.

5. References

1) Sato, T. and T. Kimura, 1994 : Observation on hydrology over the Tibetan Plateau and Himalayas., *Annual Report of Japanese Experiment on Asian Monsoon*, Research and Development Bureau, STA, 69-76. (in Japanese with English abstract)

2) Kimura, T., 1983 : Observation of water equivalent of snow cover by metal wafer., Report of the National Research Center for Disaster Prevention, 31, 203-217. (in Japanese with English abstract)

3) Kimura, T., 1992 : Observation on hydrologic variations in Tibet-Himalaya area., Annual Report of Japanese Experiment on Asian Monsoon, Research and Development Bureau, STA, 80-83. (in Japanese)

4) Kinosita, S. (ed.), 1982 : Physics of frozen ground., Morikita Shuppan, 227pp. (in Japanese)

5) Kinosita, S., K. Horiguchi, K. Tanuma, and T. Ohno, 1968 : Frost heave in Kitami (1967-1968)., Low Temperature Science, Ser.A, 26, 363-381. (in Japanese with English summary)

6) Sato, T., 1995 : Observation on hydrology over the Tibetan Plateau and Himalayas., *Annual Report of Japanese Experiment on Asian Monsoon*, Research and Development Bureau, STA, 85-95. (in English with Japanese abstract)

6. Publications

Author	Title	Name of Publications	Notes
(oral)			
T. Sato *et al.*	Continuous measurements of snow weight and frozen ground depth in the Tibetan Plateau (2)	Japanese Society of Snow and Ice. Preprints of the presentation, Sept., 1994.	

7. International cooperation

The observations of the snow weight and frozen ground have been carried out as the cooperative study with China Meteorological Administration. National Research Institute for Earth Science and Disaster Prevention invited Prof. Li Yuehong (Chinese Academy of Meteorological Sciences) for 19 days in 1995. At the same time, Meteorological Research Institute invited Mr. Jia La (Tibet Meteorological Bureau). During their stay in Japan, we discussed the cooperative study, for example, results of the action items in 1995 F.Y., working

plan in 1996 F.Y., research themes and so on. They were summarized in the memorandum and approved in the 4th Working Group Meeting held from 4 to 5 March, 1996 in Yamanashi, Japan.

（要旨）

本研究ではチベット高原に３ヶ所（ラサ、シガセ、ナチュ）の積雪重量（相当水量），地温，凍結深度の自動観測点を設置し、長期間のデータを蓄積するとともに、積雪、凍土の変動ならびにそれらとアジアモンスーンの関係を解析する。

1993年７月に中国側研究者の協力を得て、積雪重量計及び凍結深度計を設置し連続観測を開始した。また、同時期に気象研究所は同じ観測点で接地気象の観測を開始した。データ回収は1994年７月以降年１回の割合で行っている。

1993年７月から1995年７月のデータを解析し、以下の結果を得た。ナチュにおける最大凍結深度は158cm（93/94冬期）及び134cm（94/95冬期）で、いずれもルーチン観測より約40cm小さい値であった。凍結深度の季節変化をみると、厳冬期以前は観測値とルーチンデータは一致するが、厳冬期以降は一致しなかった。ルーチンの地温データを調べたところ、深さ80cmと160cmにおいて、ルーチン観測から凍土が融解したと判断されたときの地温は＋0.4～＋0.6℃であった。即ち、ルーチン観測で使用しているゴム管式凍結深度計の保護管内の温度が地温より低いことがわかった。このため、ルーチンデータの凍結深度が大きめとなり、かつ凍結層が遅くまで残ったものと考えられる。ラサ及びシガセでは凍結層は薄く、観測された凍結深度はルーチンデータより小さかった。

ナチュにおける最大凍結深度は、93/94冬期のほうが94/95冬期より大きかった。その前の夏（７月～９月）の降水量は1993年のほうが多かったため、93/94冬期の土壌水分がより多く、また土壌の熱伝導率も大きかったことがこの原因として考えられる。

積雪重量の補正方法を改良することにより、測定精度は±３kg/m^{2}まで向上することができた。ナチュにおいて、1995年１月～２月の間の積雪があるときの積雪密度は、変化が小さく0.1g/cm^{3}程度であった。これは積雪が少ないために圧密があまり起こらなかったことを意味する。

Table 1 Summary of observations in 93/94 winter and in 94/95 winter.
○: no trouble, △:see captions , ×: sensor broke.

Site	Frozen Ground Depth		Snow Weight		Ground Temperature	
	93/94	94/95	93/94	94/95	93/94	94/95
Lhasa	×	△*1	○	○	○	○
Rikeze	△*1	○	△*2	△*4	○	○
Nagqu	○*1	△*3	○	○	×	△*4

*1 : Total number of data disagrees with snow weight data
*2 : Large drift
*3 : Some ambiguity in data
*4 : Partly bad

Table 2 Summary of maximum frozen ground depth (cm).

Site	93/94		94/95	
	Obs.	Routine	Obs.	Routine
Lhasa	-	13	0	15
Rikeze	12	35	12	42
Nagqu	158	200	134	177

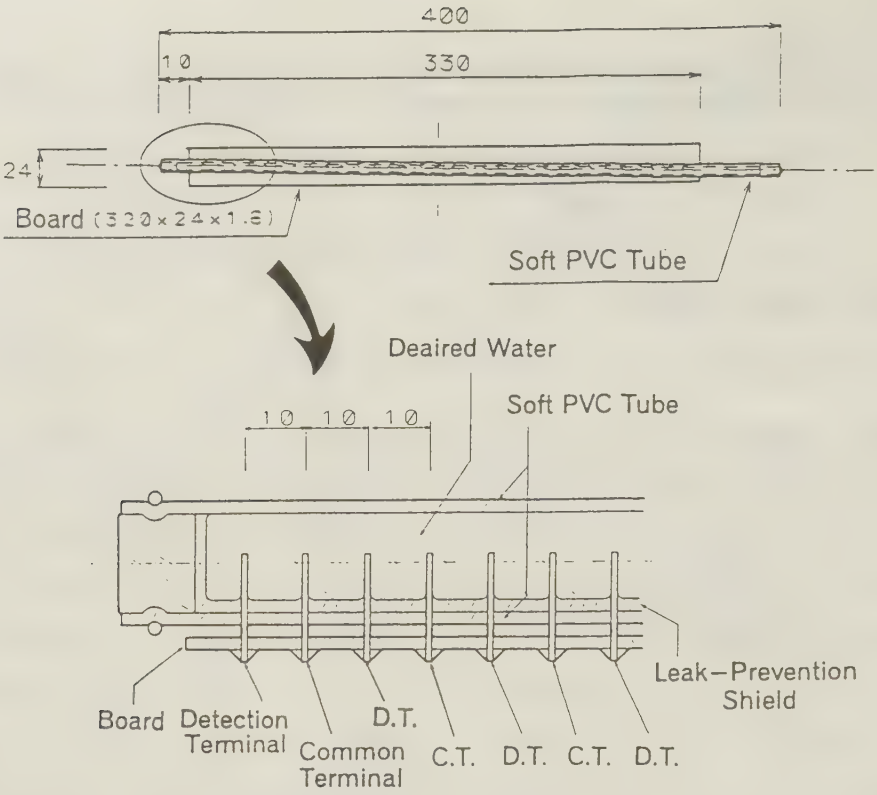

Figure 1　FDM3 sensor unit.
図1　ＦＤＭ３センサーユニットの構造。

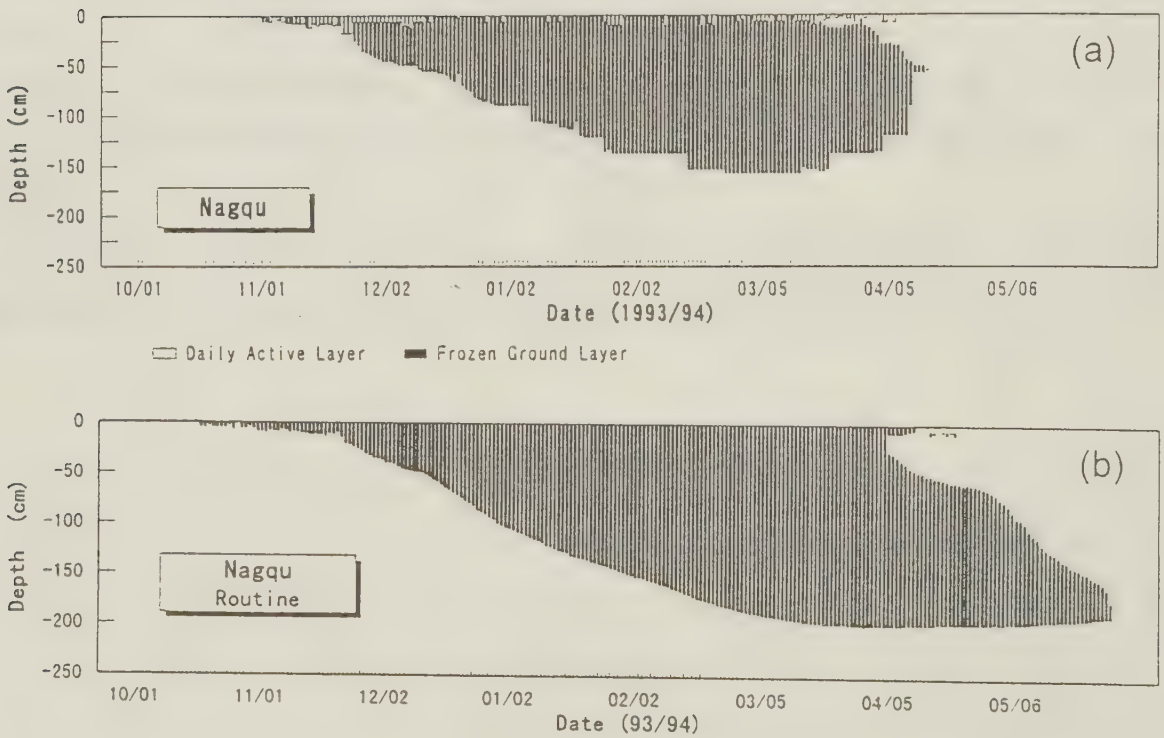

Figure 2　Seasonal variation of the frozen ground depth at Nagqu (93/94 winter).
(a) : Observed by FDM2.　White bar indicates a daily active layer near the ground surface and the black bar indicates a frozen ground layer.
(b) : Routine measurement.

図２　ナチュにおける凍結深度の季節変化（93/94冬期）。
(a)：ＦＤＭ２による観測値。白棒は地表面付近の日活動層、黒棒は凍結層を表す。(b)：ルーチン観測値。

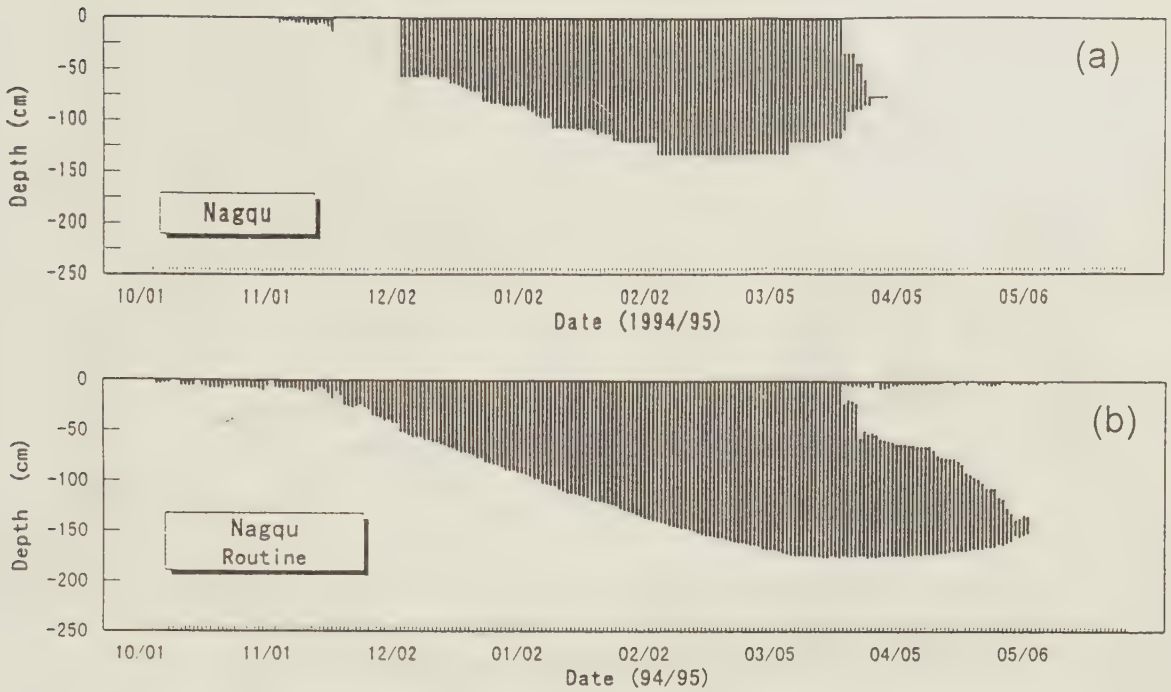

Figure 3　Seasonal variation of the frozen ground depth at Nagqu (94/95 winter).
(a) : Observed by FDM2,　(b) : Routine measurement.

図３　ナチュにおける凍結深度の季節変化（94/95冬期）。
(a)：ＦＤＭ２による観測値。(b)：ルーチン観測値。

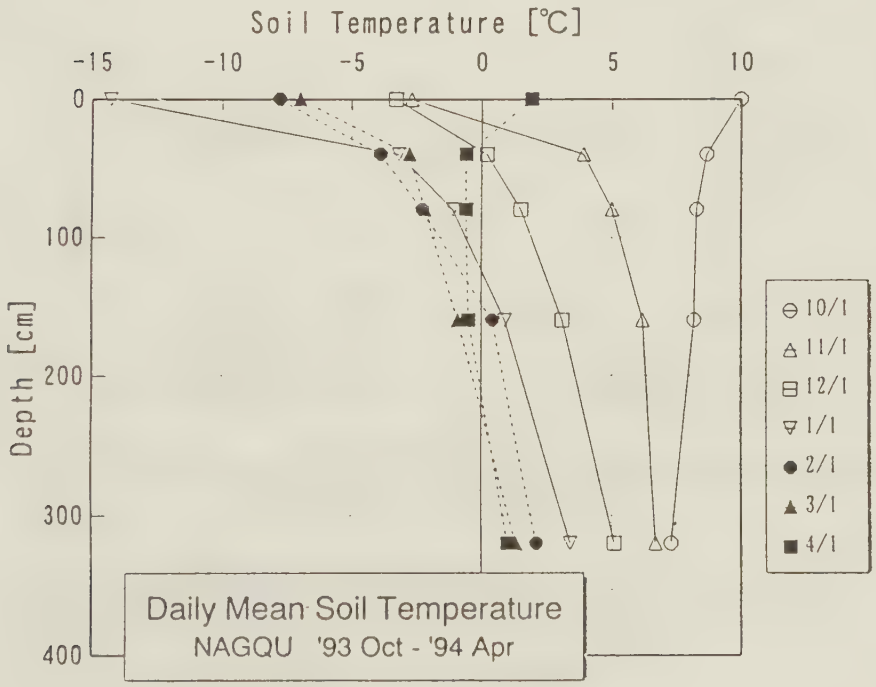

Figure 4　Profile of daily mean soil temperature at Nagqu (93/94 winter).

図４　ナチュにおける日平均地温の鉛直分布（93/94冬期）。

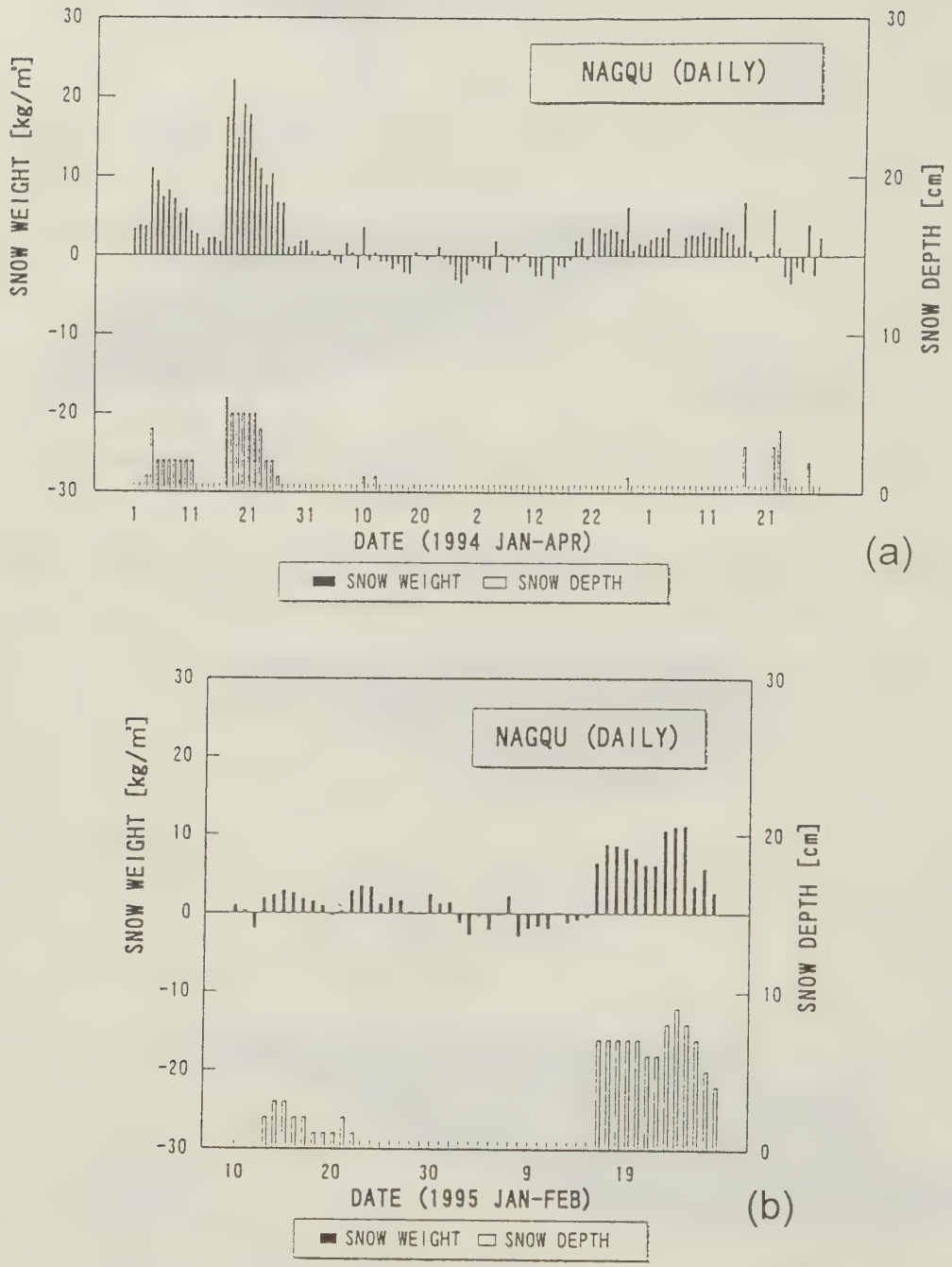

Figure 5 Time series of observed snow weight (upper) and routinely measured snow depth (lower) at Nagqu.
(a) : 93/94 winter, (b) : 94/95 winter.

図5 ナチュにおける積雪重量の観測値（上）と積雪深のルーチン観測値（下）。
(a)：93/94冬期、(b)：94/95冬期。

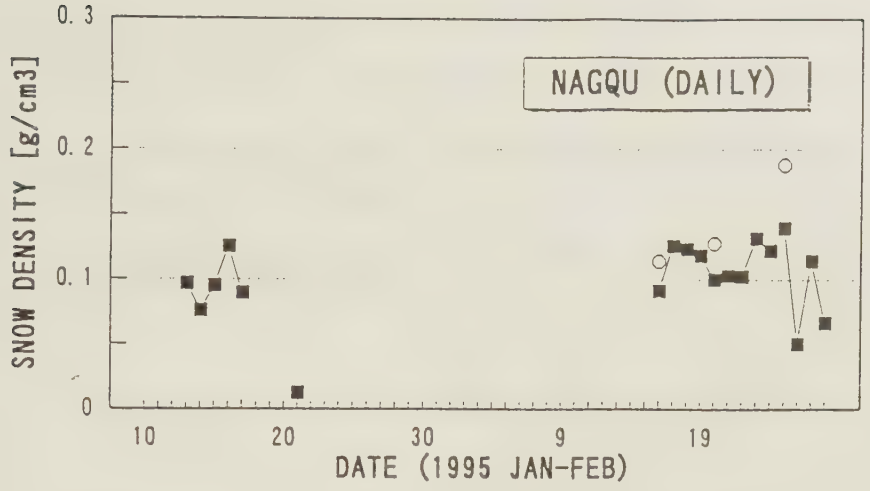

Figure 6 Time series of snow density at Nagqu in 94/95 winter.
■: Calculated from snow weight and routinely measured snow depth, ○ : Routinely measured.

図6 ナチュにおける積雪密度の時系列（94/95冬期）。
■：積雪重量とルーチン積雪深からの計算値、
○：ルーチン観測値。

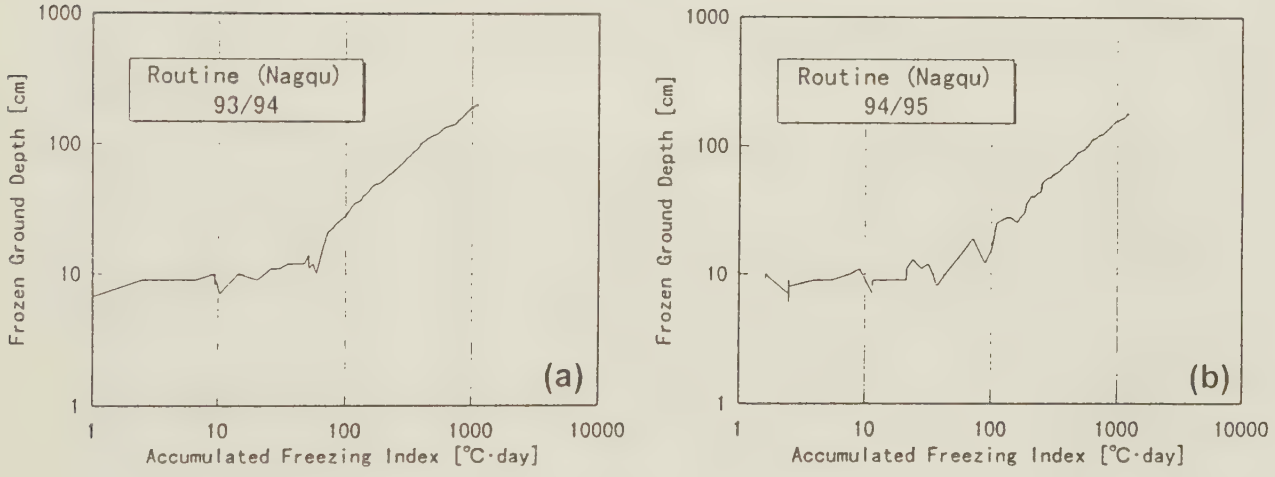

Figure 7 Relation between the frozen ground depth and the accumulated freezing index at Nagqu. (a) : 93/94 winter, (b) : 94/95 winter.

図7 ナチュにおける凍結深度と積算寒度の関係。
(a)：93/94冬期、(b)：94/95冬期。

Ⅰ. Observation and analysis on the process of the atmosphere-ocean-land interactions
大気・海洋・陸域間相互作用の諸過程に関する観測・解析研究

3. Observation and analysis on the process over the land
陸域における諸過程に関する観測研究

(2) Observation on Regional Surface Heat Budget
地表面熱収支に関する観測研究

Meteorological Research Institute,
Japan Meteorological Agency
S. Haginoya, H. Naoe,
N. Kinosita, M. Kato.
気象庁気象研究所
萩野谷 成徳、直江 寛明、
木下 宣幸、加藤真規子

(Abstract)

In order to clarify the mechanism of the Asian Monsoon caused through Air-Sea-Land interactions, the large-scale heat budgets over two different areas should be estimated: Tibetan-Himalaya Mountains Area and the Indian Ocean-South China Sea Area. This study aims to collect the basic meteorological data and to estimate large-scale heat budgets over the two areas.

Field observations were carried out in the Tibetan Plateau and Indian Ocean in 1995 FY. This paper describes the following results through the observations.

(1) Tibetan Plateau

The four sets of Automatic Weather Station (AWS) were installed in the Tibetan area in summer 1993. Japanese scientist visited four AWS sites (Lhasa, Rikeze, Nagqu and Lingzi) in June to July 1995. He investigated the observation sites and around topography. Wind profile were measured at 5 levels at Lhasa and Nagqu. Aerodynamic roughness length z_0 at Lhasa is estimated 4cm in the south to south-west direction in January 1995. That at Nagqu is 5cm in the north-east direction and 2cm in the south-west direction in July 1995. The simple Ekman layer model simulated the diurnal variation of wind at Nagqu site. Angstrom's turbidity coefficient was estimated. Its value is from 0 to 0.02. The atmosphere over Tibetan Plateau is very clear. Global solar radiation data were checked by theoretical value. To estimate daily accumulated global solar radiation from routine sunshine duration, the empirical formula was made. Global solar radiation at 9 routine meteorological stations in the Tibetan Plateau were estimated from the empirical formula. Soil heat physical constants were estimated from the amplitude of daily and yearly soil temperature variation. Soil water content and dry soil density were measured directly.

(2) Indian Ocean

Atmospheric boundary layer was observed by Chofu-Maru's Omega sonde in the East China Sea and the Pacific Ocean. Mixed layer height were estimated by potential temperature profile. Average height of mixed layer is below 1000m. AWS observations were made on the two ships. One is Osaka-Maru, which made

three times round trips between Japan and Republic of South Africa through the South China Sea, the Strait of Malacca and the Indian Ocean in this fiscal year continued from last fiscal year. Another AWS observation is made on Shoyo-Maru from October 1995 to January 1996 in the equator of Indian Ocean and Arabian sea.

1. Objectives

In order to clarify the mechanism of the Asian Monsoon caused through Air-Sea-Land interactions, the large-scale heat budgets over two different areas should be estimated: Tibetan-Himalaya Mountains Area and the Indian Ocean-South China Sea Area. Because of the vastness of the areas and of their unsuitable conditions for observations, observatories or ships in these areas are very sparsely distributed. Therefore the basic meteorological data to clarify the mechanism of the Asian Monsoon has been lacking. This study aims to collect these basic data and estimate large-scale heat budgets over the two areas.

2. Methods

Since the heat budgets in two areas are studied by different methods, they are described separately.

(1) Tibet

The four sets of Automatic Weather Station (AWS) were installed in the Tibetan area in summer 1993. Observation sites are Lhasa, Rikeze, Nagqu and Lingzi (see Table 1 and Figure 1). The observation were carried out continued from last fiscal year. Japanese scientist visited Lhasa, Rikeze, Nagqu and Lingzi in June to July 1995. He investigated the observation sites and around topography. He also supported data collection and AWS maintenance. Chinese side checked AWS every month and collected data twice a year. Chinese side finished the first data collection in July 1995, the second data collection from December 1995 to January 1996. Collected data were sent to Japan by mail. Routine surface meteorological data of 20 stations in Tibetan area from May to September 1994 were collected. Routine aerological data of 2 stations in Tibetan area from January to December 1994 were collected.

(2) Indian Ocean

Omega sonde observation (aerological observation) was carried out on the Meteorological Observation Ship, Chofu-Maru (430GT) of JMA in October 1995 in the East China Sea and the Pacific Ocean. AWS observations were made on the two ships. One is Osaka-Maru (31,382GT) of Mitsui O.S.K. Lines, which made three times round trips between Japan and Republic of South Africa through the South China Sea, the Strait of Malacca and the Indian Ocean in this fiscal year continued from last fiscal year. When the Osaka-Maru came back to Yokohama, the data were collected. AWS are exchanged some times for maintenance. Osaka Maru observation were finished in October 1995. Its observation were continued for four years science October 1991. Observation data from April to October 1995 were analyzed. Another AWS observation is made on Shoyo-Maru (1,363GT) of Fisheries agency from October 1995 to January 1996 in the equator of Indian Ocean and Arabian sea.

3. Results

(1) Tibet

Japanese scientist visited 4 AWS sites in summer 1995. We summarized the observation sites. Lhasa site is located at the bottom of valley. The length of valley is 40km in the east and west direction. Its width is 7km-8km at the bottom and is 25km at the ridge lines of mountains. Average height difference between the bottom and the ridge line is 1500-2000m. Nagqu is located over a plateau, about 220km north-east of Lhasa. This site is representative place in Tibet which is located in the rural area on the opened plateau. Rikeze is located in a basin bottom, about 230km west of Lhasa. The horizontal scale of basin bottom is 20km. Lingzi is located in a bottom of valley, 320km east of Lhasa. The length of valley is 30km in the north-west and south-east direction. Its width is 5km at the bottom. Average height difference between the bottom and the around mountain peak is 1500-2000m. This valley is narrower than that of Lhasa.

(1.1) To estimate the aerodynamic roughness length z_0 to a certain accuracy, we measured wind profile between 2.5 m and the ground surface and picked up the relatively strong wind data. AWS at Lhasa observed temperature profile (10m, 5m, 2.5m) and wind profile (10m, 5m, 2.5m, 1.25m and 0.5m) in January 1995. That at Nagqu did the same level profile observation in July 1995. z_0 at Lhasa is 4cm in the south to south-west direction. In this observation, the average wind speed at 10m height is 5m/s. z_0 at Nagqu is 5cm in the north-east direction and 2cm in the south-west direction. In this observation, the average wind speed at 10m height is 7m/s. These results are a little bit smaller than the previous results[1].

(1.2) The simple Ekman layer model simulated the diurnal variation of wind at Nagqu site. The wind characteristics on daily cycle are as follows. Surface wind velocity increases and reaches maximum (some times above 10m/s) in the daytime (from 04Z to 09Z). It decreases from 10Z to 14Z and becomes below 2m/s in the nighttime and early morning (from 14Z to 03Z). The hodograph changes the clockwise. Diurnal strong wind is westerly. It is conceivable that diurnal convective mixing transports the upper layer momentum to the ground surface level[1]. The mechanism of daily cycle of wind is as follows. After sunrise, solar radiation heats up ground surface. Then surface boundary layer is heating and mixed layer is developed in the daytime. This accompanies the daily pressure variation. Surface pressure variation is the measure of the heating or cooling amount of air column. So that the pressure variation indicates the development of atmospheric boundary layer[2]. Surface pressure decreases from 03Z to 09Z at Nagqu site in November 1993. It shows that the mixed layer at Nagqu develops from 03Z to 09Z. Momentum of westerly wind is transported downward. Then, the ground surface wind velocity increases. In the nighttime, radiational cooling stabilizes the atmospheric boundary layer. The momentum transfer from the upper layer is stopped, then wind is weakened. Figure 2 shows the hodographs of observation and one layer simulation model[3]. Model simulates quantitative feature.

(1.3) To check the data quality of global solar radiation, Angstrom's turbidity coefficient (β_{dust}) was estimated by QXPMEX-79 data[4] and the AWS data. Figure 3 shows the relation between the ratio of sky solar radiation (D) to direct solar radiation on horizontal level ($I\cos\theta$) and inverse of air mass ($1/\cos\theta$). θ is the zenith angle. The line shows β_{dust}=0, 0.02, 0.04, 0.06, 0.08 and 0.1[5]. The data

are scattered between β_{dust}=0 and 0.02. The atmosphere over Tibetan Plateau is very clear. Figure 4 shows the time series of daily accumulated global solar radiation. In the figure, several lines show the global solar radiation on a fine day. Parameters are β_{dust}. The maximum value of observational data are scattered near β_{dust}=0.02. This fact shows that the observation data are not inconsistent.

(1.4) To estimate daily average of global solar radiation (S) from routine sunshine duration (N_J), we made the following empirical formula. $S/S_0=a+b^*(N_J/N_0)$, where S_0 is daily average of global solar radiation at the top of atmosphere, N_J is daily sunshine duration measured by Jordan's sunshine recorder, N_0 is daily possible sunshine duration, a and b are empirical constants. We use S_0 instead of S_{0f} which is daily average of global solar radiation at the surface on a fine day. Because the relation between S/S_{0f} and N_J/N_0 is scattered as same as S/S_0. Table 2 shows the summary of a and b at the four AWS sites. Daily global solar radiation at 9 routine meteorological stations in the Tibetan Plateau were estimated by the empirical formula. Figure 5 shows the results. Solar radiation and precipitation have good correlation. Solar radiation in western Tibet is larger than eastern Tibet. On the other hand, amount of rainfall in western Tibet is smaller than eastern Tibet. Solar radiation of central and eastern Tibet in 1993 is smaller than that in 1994. Amount of rainfall has reverse relation. The remarkable difference between 1993 and 1994 is not found at western station "1".

(1.5) Thermal diffusivity for soil $a=\lambda_g/(C_g\rho_g)$ were estimated from the amplitude of soil temperature variation. Where λ_g is heat conductivity for soil, C_g is spesific heat for soil and ρ_g is soil density. Figure 6 shows the sample of yearly variation of soil temperature. The smooth line in the figure which is approximate to the observation shows the following periodical formula[6].

$$T_{soil}(z,t)=A_0+\Sigma A_n \exp(-z\sqrt{(n\omega/2a)})\cos(n\omega t-b_n-z\sqrt{(n\omega/2a)})$$

where $\omega=2\pi/T$, T is the period of one year, t is time, n is the number from 1 to 4. This formula is obtained from the solution of heat conduction equation. We can estimate $a=\lambda_g/(C_g\rho_g)$ from the ratio of different level amplitude that is $\exp(-z\sqrt{(n\omega/2a)})$ or the difference of phase that is $z\sqrt{(n\omega/2a)}$. Deep soil has generally large value of $a=\lambda_g/(C_g\rho_g)$, because deep soil has large water content. Its value is from 1×10^{-7} to 8×10^{-7} m^2/s (from surface to 320cm in depth).

(1.6) Soil water content (w) and dry soil density (ρ_g) were measured directly at Lhasa, Rikeze and Nagqu. Table 3 summarized the results.

(2)Indian Ocean

Atmospheric boundary layer was observed by Chofu-Maru's Omega sonde in the East China Sea and the Pacific Ocean. Figure 7 shows the course of Chofu-Maru's cruise. Observation was made in October 1995. Figure 8 shows samples of potential temperature profile. Height of atmospheric mixed layer were defined by the kink of profile (refer to the arrows in the figure). Mixed layer height was summarized in Figure 9. In this cruise, disturbance with rainfall destroyed the mixed layer from run 1 to 5. After that, the mixed layer developed up to 1800m. Average height of mixed layer is below 1000m.

AWS observation were made on Shoyo-Maru and Osaka-Maru in 1995. Figure 10 shows the cruise course of each ship. Figure 11 shows the preliminary results of daily net radiation of Shoyo-Maru cruise.

4. Discussions

We could obtained a certain accurate roughness length at Lhasa and at Nagqu from the wind profile near the ground surface. Solar radiation is the important element of heat balance equation. To maintain the data accuracy, sensors must be calibrated periodically and the observation data should be checked by other available data or theoretical method. ($C_g \rho_g \lambda_g$) can be estimated by the surface radiative cooling. Heat physical constants for soil (C_g, ρ_g, λ_g) must be obtained separately. AWS observation sites are located in the eastern part of Tibetan Plateau. To estimate an energy balance over the Plateau, it is necessary to install AWS in the western part of Tibet.

Atmospheric boundary layer over the Ocean developed up to 1800m. This height is roughly twice as large as that in tropical ocean. Osaka-Maru observation accumulated the basic data for estimating heat balance over the Indian Ocean for four years. The yearly variation of heat balance should be clarified.

5. References

1) Haginoya, S. et al.: Observation on Regional Surface Heat Budget. Annual Report of Japanese Experiment on Asian Monsoon, Research and Development Bureau, STA, 97-107. (1995)

2) Kuwagata T., M. Sumioka, N. Masuko and J. Kondo: The Daytime PBL Heating over Complex Terrain in Central Japan under Fair and Calm Weather Conditions. Part I : Meso-scale Circulation and the PBL Heating Rate. *J. Meteor. Soc. Japan*, 68, 625-638. (1990)

3) Alan J. Thorpe and Trevor H. Guymer: The nocturnal jet. *Quart. J. R. Met. Soc.*, 103, 633-653 (1977)

4) Zhang Jijia, Zhu Baozhen, Zhu Fukang, Weng Duming, Sun Guowu, Lu Junning, Peng Yongqing and Wang Yuanzhong: Advances in the Qinghai-Xizang Plateau Meteorology. The Qinghai-Xizang Plateau Meteorological Experiment (1979) and Research. pp.268. (1988)

5) Kondo J. and A. Miura: Empirical formula of the solar radiation at the ground level and a simple method to examine an inaccurate pyranometer. *Tenki*, 30, 284-290. (1983)

6) Kondo J.(ed.): Meteorology on water environment. -ground surface water balance/heat balance-, pp.350. (1994)

7) Kondo J., T. Nakamura and T. Yamazaki: Estimation of solar and downward atmospheric radiation. *Tenki*, 38, 41-48. (1991)

6. Publications

(report)

S. Haginoya et al., Observation on Regional Surface Heat Budget. Research and Development Bureau, Science and Technology Agency, Japan. Annual Report of Japanese Experiment on Asian Monsoon, 1994JFY, pp97-107, 1995.

(oral)

S. Haginoya et al. Automatic Meteorological Observation over Tibetan Plateau (3). Meteorological Society of Japan. Preprints of the presentation, 67, pp9, 1995.

S. Haginoya, Automatic Meteorological Observation over Tibetan Plateau (4).

Meteorological Society of Japan. Preprints of the presentation, 68, pp160, 1995.
S. Haginoya, Automatic Meteorological Observation over Tibetan Plateau (5). Meteorological Society of Japan. Preprints of the presentation, 69, pp47, 1996.
H. Naoe and S. Haginoya, Wind characteristic over Tibetan Plateau. Meteorological Society of Japan. Preprints of the presentation, 69, pp323, 1996.

7. International cooperation

Meteorological observation over the Tibetan Plateau is carried out the cooperative study with China Meteorological Administration. Meteorological Research Institute invited one Chinese scientist named Mr. Jia La (Tibet Meteorological Bureau) for 19 days. In the same time, National Research Institute for Earth Science and Disaster Prevention, Science and Technology Agency invited another scientist named Prof. Li Yuehong (Chinese Academy of Meteorological Sciences). Japanese side discussed the Tibet observation with them. Japanese and Chinese sides examined the results of 1995 F.Y. and the plan of 1996 F.Y. They summarized the results of discussion as "Working Plan". Japanese side and Chinese side agreed the "Working Plan" in the 4th Working Group Meeting held from 4 to 5 March, 1996 in Yamanashi, Japan. Details concerning the "Working Plan" are summarized in the Appendix 1 of "SUMMARY REPORT ON THE 4TH WGM OF PRC-JAPAN COOPERATIVE PROGRAM ON ASIAN MONSOON".

要旨

本研究は，大気を媒体とした海洋と陸面間の相互作用として発現しているアジアモンスーンの機構を解明するため２つの異なる地域における広域のエネルギー収支を評価するものである。そのうちの１つはチベット・ヒマラヤの山岳地帯の地表面フラックス，もう１つはインド洋・東南アジア地域の海面フラックスである。これらの地域において、熱収支解析に必要な気象要素を現地観測により収集し，それに基づいて広域熱収支解析を行うことを目的としている。

チベット関連：拉薩（ラサ）、日喀則（シガセ）、那曲（ナチュ）および林芝（ニンチ）の4ヶ所の観測地点に山岳用自動気象観測装置(AWS)を設置し，1993年夏から観測を継続して実施している。今年度は4ヶ所の現地を視察し，周辺の状況を調査した。気象関連の全てのセンサを回収し、日本において再検定をした。チベット地域のルーチン観測所のデータ（地上及び高層）を入手した。1995年12月までの観測データを回収・解析した。中国人研究者を日本に招聘した。

データ解析の結果以下の成果が得られた。

ラサとナチュにおいてAWSで常時測っている10m、5mおよび2.5m高度の風速のほかに、1.25mと0.5mの風速を短期間測定した。それらのデータを用いて地表面の空気力学的粗度を推定し、ラサは4cm、ナチュは2～5cmの結果を得た。この値はAWSで常時測っているデータから求めた値よりも小さい。

ナチュの風速日変化の様子を簡単なエクマン層モデルでシミュレートし。その結果、日中強風、夜間弱風という定性的な性質が再現され、境界層高度の日変化が風速の日変化に影響を与えていることが示された。

チベット高原上のオングストロームの大気混濁係数を求めた。係数は0から0.02と

なり、チベット高原上の大気が大変清澄であることがわかった。この係数から理論的に計算される快晴時の日射量と快晴時の観測データとを比較し、日射量データが矛盾のないことが示された。次に、日射量の観測データとルーチンの日照時間から日射量を求める実験式を作成した。本実験式を用いてチベット域内のルーチンの日照データから全天日射量を求め、降水量との関係を調べた。その結果、日射量と降水量の間に強い負の相関が見られた。また、チベット高原上は西側の日射量が強く、雨量の少ない地域から東側の日射量が弱く雨量の多い地域まで、気候の変化が大きいことがわかった。

土壌の熱拡散係数を地温データから求め、$\lambda_g/(C_g \rho_g)=1\times10^{-7}\sim8\times10^{-7}m^2/s$が得られた。ラサ、シガセおよびナチュにおいて土壌の含水率と乾燥密度を直接測定した。土壌の含水率は8～24%、密度は1.0～1.4g/cm^{3}であった。

インド洋関連：大阪商船三井船舶株式会社の定期コンテナ船「大阪丸(31,382GT)」に船舶用AWSを搭載し，インド洋航路の観測を継続して実施した。本船の観測は1995年10月で終了した。「照洋丸(1,363GT)」に船舶用AWSを搭載し，インド洋の海上気象観測を実施した。両船舶のデータから航路に沿った海面熱収支解析を行った。「長風丸(430GT)」を用いて東シナ海～太平洋上（（東経124度、北緯24度）と（東経131度、北緯33度）を対角線とする矩形の領域）でオメガゾンデによる高層観測を実施し，大気境界層の構造と大気混合層高度の水平分布を調べた。

Table 1 Summary of the AWS sites.

site name	Lhasa	Nagqu	Rikeze	Lingzi
latitude	29° 40'N	31° 29'N	29° 15'N	29° 34'N
longitude	91° 08'E	92° 04'E	88° 53'E	94° 28'E
altitude(m)	3649	4507	3836	3000
around the topography	bottom of valley	flat hill	bottom of basin	bottom of valley
conditions around the site	city	rural town	rural town	rural
ground surface conditions	bare soil short grass	bare soil	irrigated vegetable field	short grass

Table 2 Empirical formula of solar radiation: $S/S_0=a+b*(N_J/N_0)$, where, S:daily average of global solar radiation, S_0: daily average of global solar radiation at the top of atmosphere, N_J: daily sunshine duration, N_0: daily possible sunshine duration, a and b: empirical coefficient, σ : standard error of estimate, $\sigma(b)$: standard error of b.

site name		a	b	σ	$\sigma(b)$	correlation coefficient	observation period
Lhasa		0.313	0.519	0.0494	0.011	0.962	1993/7-1994/12
	Q	0.314	0.527			0.939	
Nagqu		0.287	0.569	0.0488	0.008	0.947	1993/7-1994/12
	Q	0.277	0.588			0.860	
Rikeze		0.263	0.576	0.0468	0.011	0.911	1993/7-1994/12
Lingzi		0.243	0.574	0.0413	0.007	0.909	1993/7-1994/12
	Q	0.314	0.527			0.939	
Japan		0.179	0.550	0.0482			1979/8-1980/10

"Q" indicates the results of QXPMEX-79. Observation period is May to August 1979. Lhasa and Lingzi value are the average value around the station. Japan is referred to Kondo et al.[7].

Table 3 Soil water content and density measured by soil sampling.

volumetric water content(%)

date	94/07/05, 06	95/06/28	94/07/09	95/07/07
depth(cm)	Lhasa	Lhasa	Rikeze	Nagqu
0-5	7.55	17.35	8.70	24.07
10-15	16.32	19.33	12.48	16.98
20-25	13.37	19.21	14.60	14.85
30-35	13.42	14.31	12.68	16.79

dry soil density(g/cm^3)

date & time	94/07/05, 06	95/06/28	94/07/09	95/07/07
depth(cm)	Lhasa	Lhasa	Rikeze	Nagqu
0-5	1.126	1.104	1.159	1.029
10-15	1.116	1.230	1.123	1.200
20-25	1.169	1.079	1.247	1.261
30-35	1.044	1.135	1.404	1.292

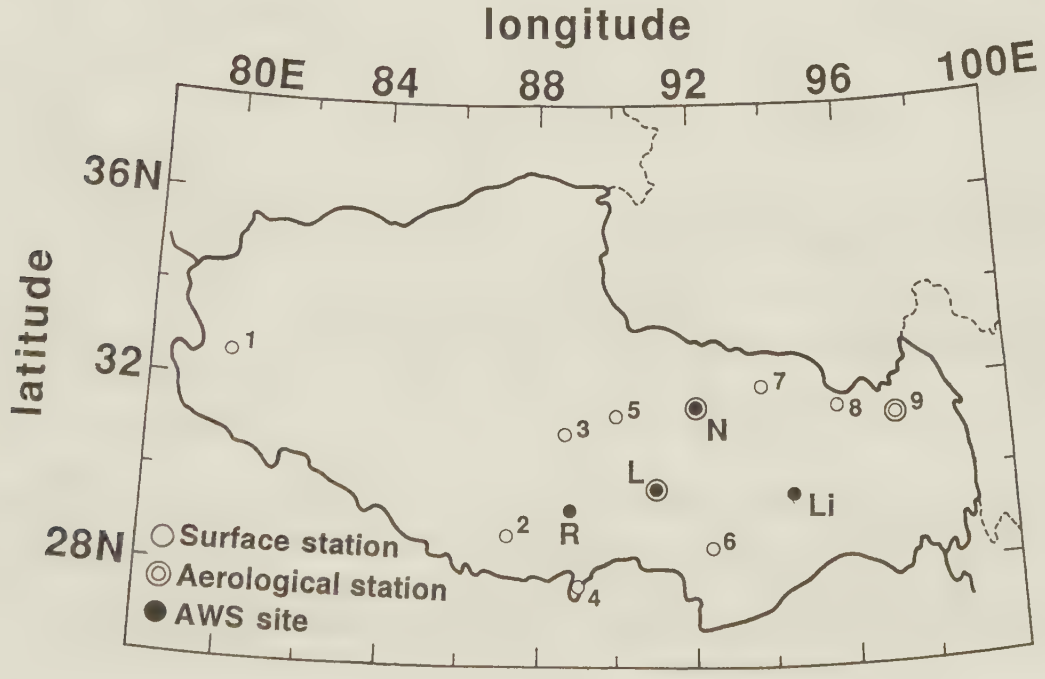

Figure 1 AWS sites and routine meteorological station inside the Tibet Autonomous Region.

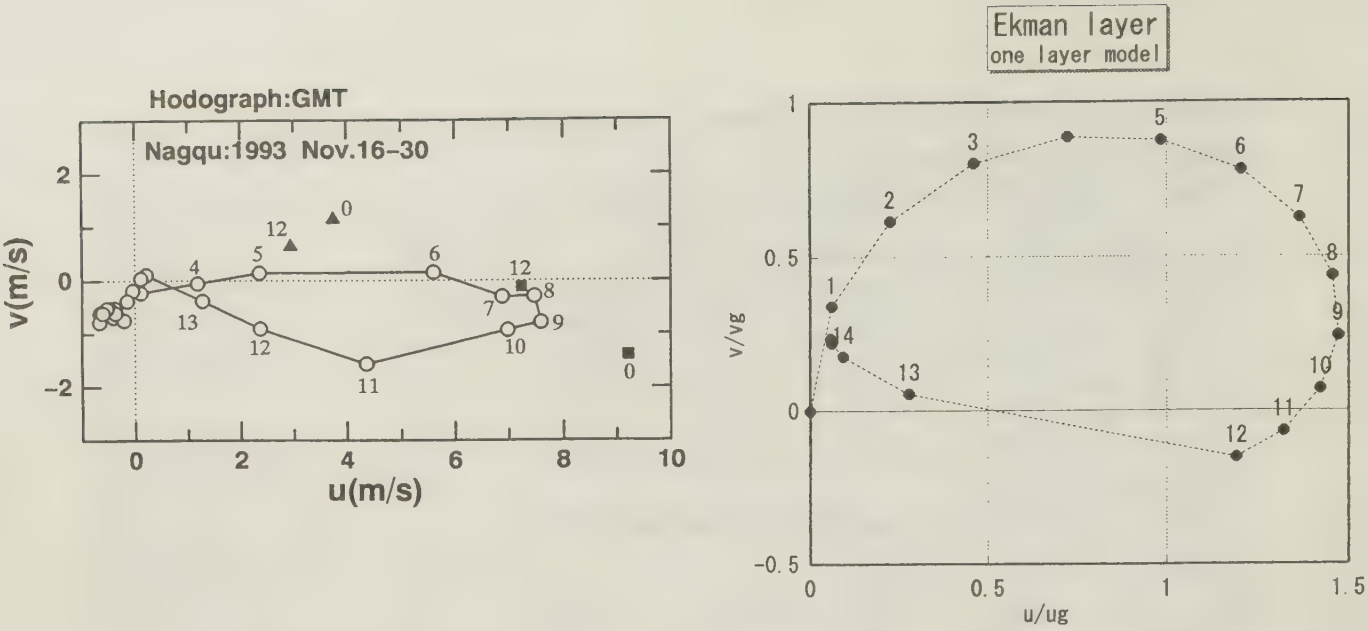

Figure 2 The hodograph of observation at Nagqu and one layer simulation model. Number indicates GMT. Local time is GMT+6.

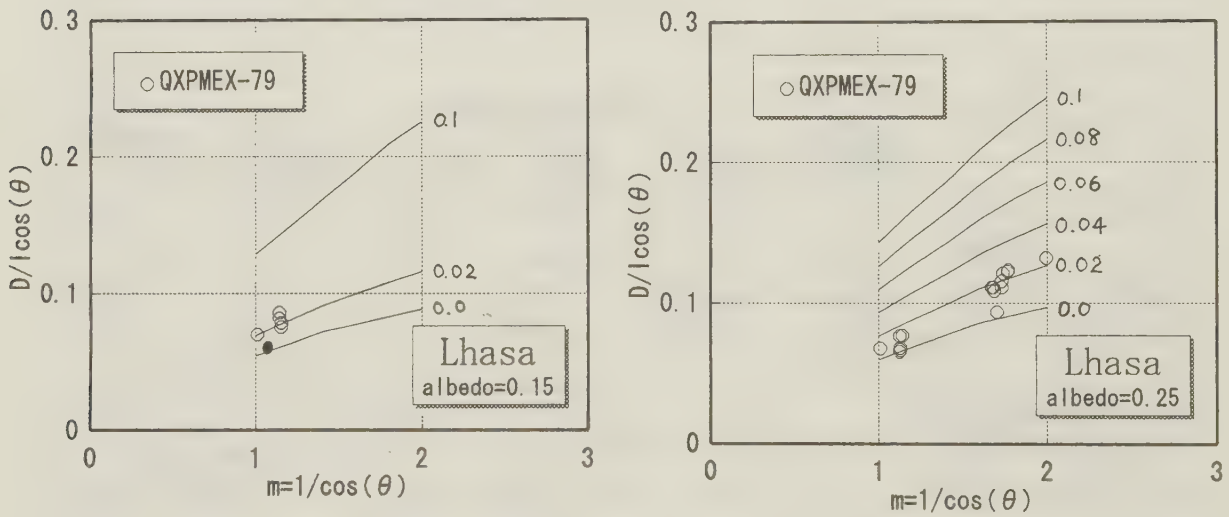

Figure 3 The relation between the ratio of sky solar radiation (D) to direct solar radiation on horizontal level (Icos θ) and inverse of air mass (1/cos θ). θ is the zenith angle. The lines show β_{dust}=0, 0.02, 0.04, 0.06, 0.08 and 0.1 in ascending order. The mark "●" is estimated from AWS data.

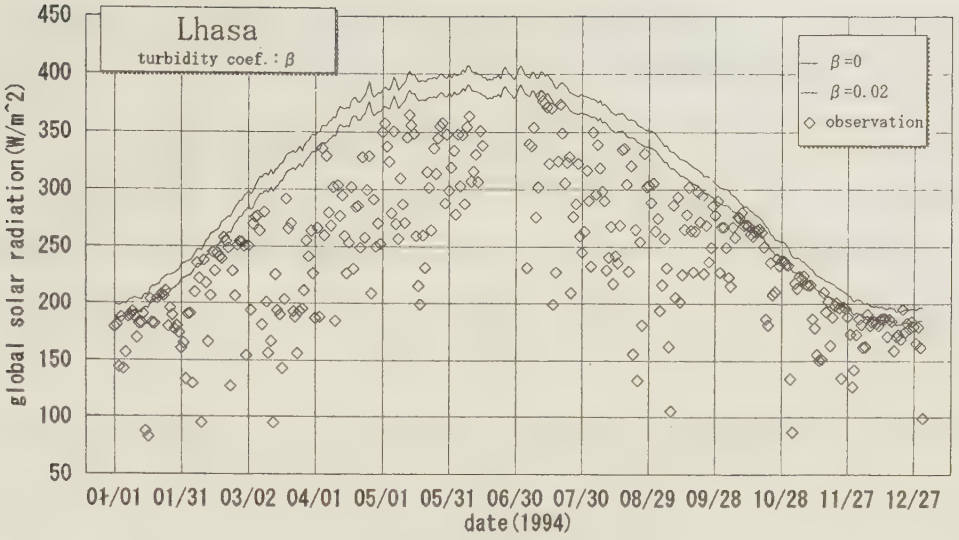

Figure 4 Variation of daily mean global solar radiation. Mark "◇" indicates observation data. Lines indicate empirical value at fine day. Parameters are β_{dust}.

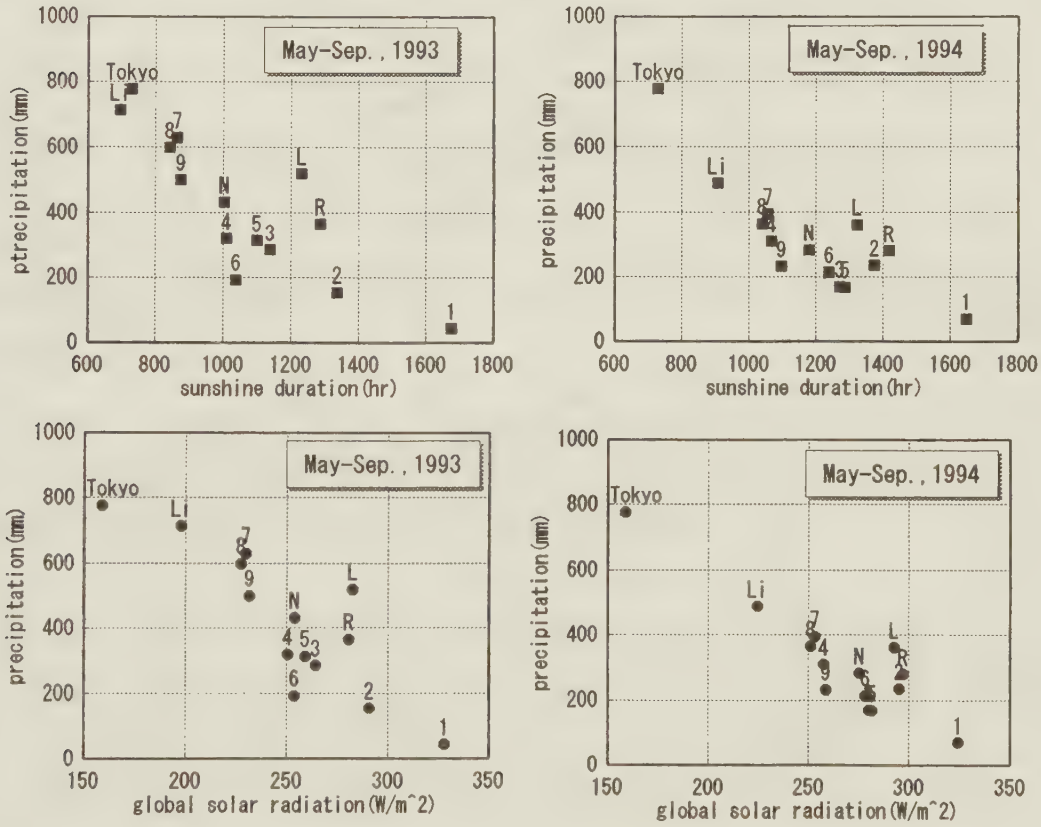

Figure 5 (a) The relation between sunshine duration and precipitation. The data are routine observatories inside the Tibet Autonomous Region. The number is the same station as in Figure 1. Tokyo is average for 30 years from 1961 to 1990.
(b) The relation between global solar radiation and precipitation. Global solar radiation is calculated by empirical formula with sunshine duration.

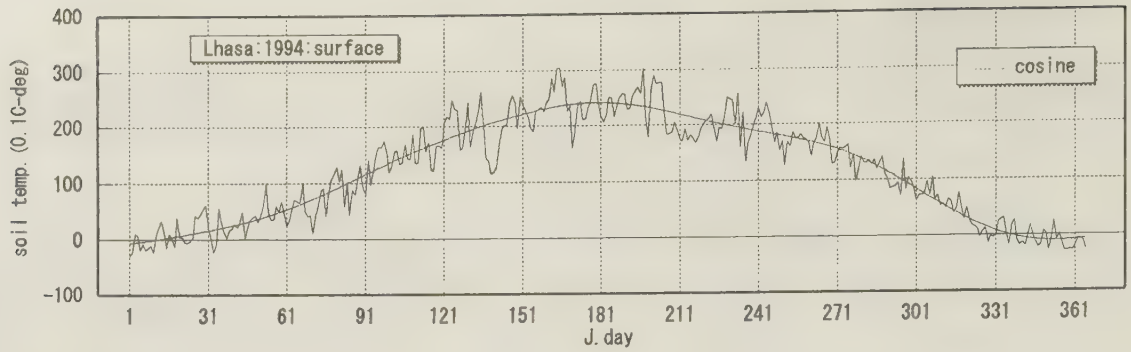

Figure 6 The sample of yearly soil temperature variation at Lhasa.

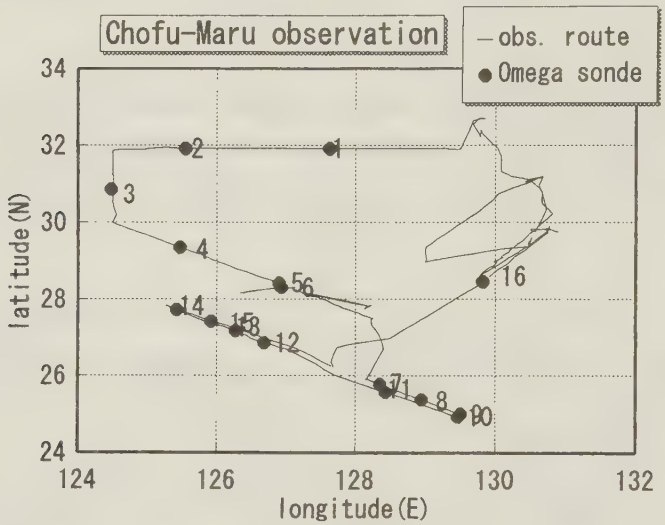

Figure 7 Chofu-Maru cruise course. Number indicates observation run number.

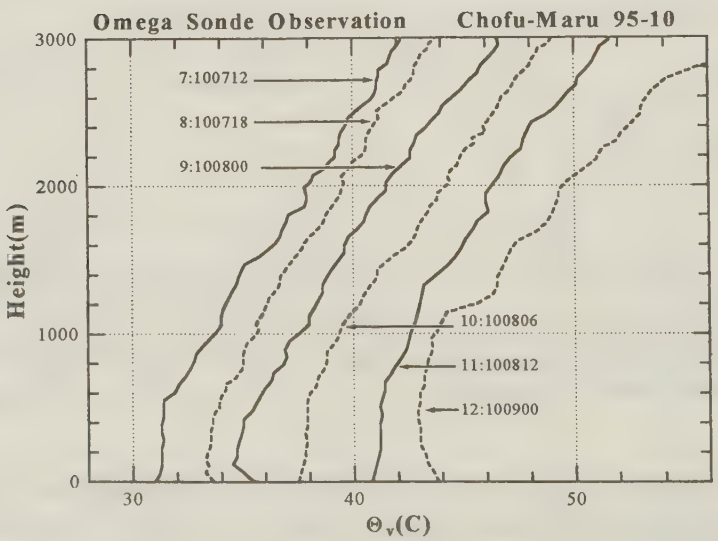

Figure 8 Sample of potential temperature profile. "7:100712" means "run 7: October 7th 12Z".

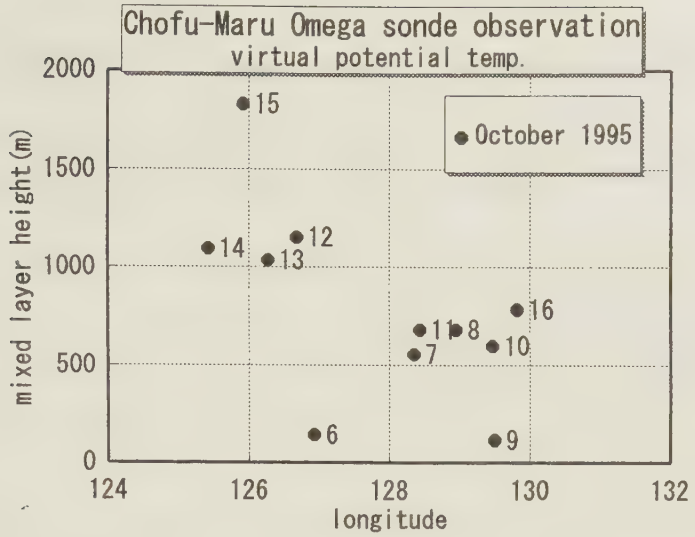

Figure 9 Atmospheric mixed layer height observed by Chofu-Maru. The run number is referred to Figure 7.

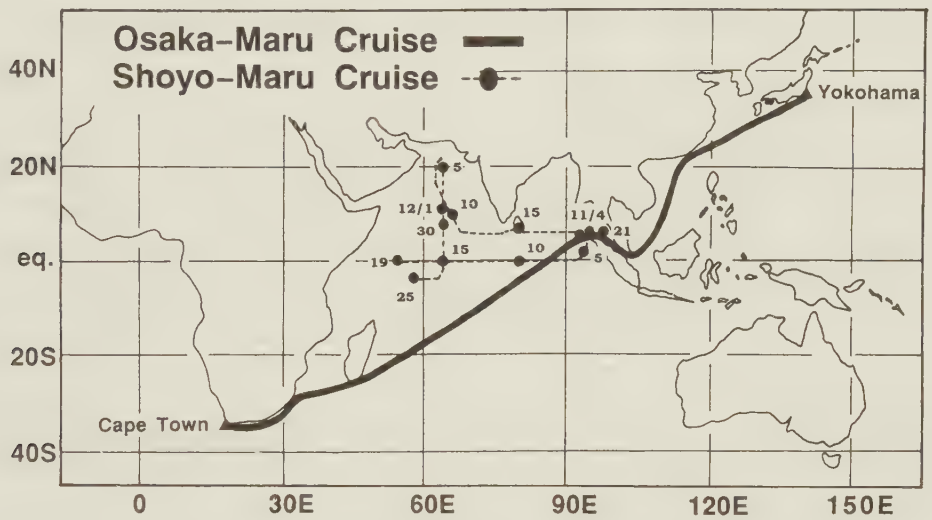

Figure 10 Cruise course of Shoyo-Maru and Osaka-Maru. Note that Shoyo-Maru course is shown only in the Indian Ocean.

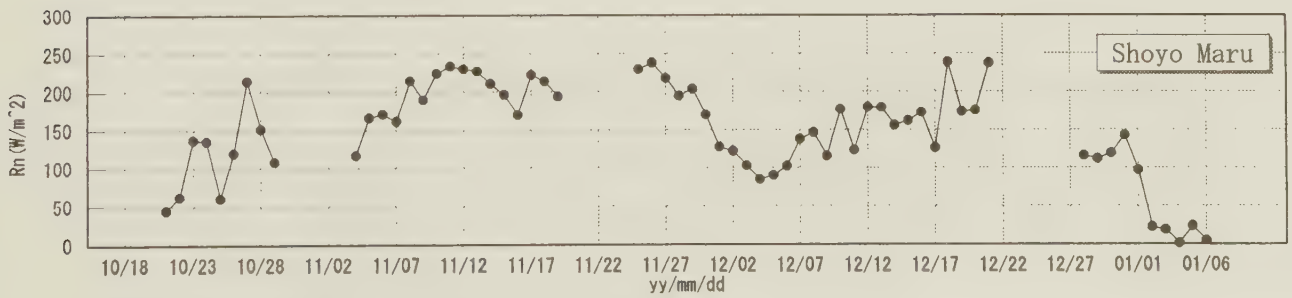

Figure 11 Variation of net radiation observed on Shoyo-Maru.

I. Observation and analysis on the process of atmosphere-ocean-land interactions

3. Observation and analysis of over the land

(2) Observational study of ground surface heat budgets

Communications Research Laboratory
Ministry of Posts and Telecommunications
Yoshihisa Masuda and Yuji Ohsaki

(Abstract)

The Communications Research Laboratory (CRL) developed the first L-band wind profiler in 1991. This boundary layer radar (BLR) is now operating at the Okinawa Radio Observatory. Two other BLRs have since been developed, one has been operating at the CRL in Tokyo since 1992, and one has been operating at the King Monkut's Institute of Technology Ladkrabang (KMITL) in Thailand since 1993.

These radars are used to measure the altitude profiles of the wind and temperature, and the fluctuation intensity of the atmospheric refractive index. They are thus powerful tools for meteorological research.

This paper describes the results of wind measurement at CRL in Japan and at KMITL in Thailand, and several methods for clutter rejection.

1.Objectives

Since developing our original windprofiler in 1991, we have been studying its possible uses as tool for the meteolorogical research. Our developed windprofiler can automatically measure the vertical profile of three-dimensional wind vectors with high time and range resolutions[1]. It can also measure the vertical wind velocity immediately above its antenna, where a conventional radiosonde is unable to measure.

A windprofiler/RASS, combined with a windprofiler and an acoustic source is the most effective system for measuring temperature profiles under all weather conditions. We previously determined the effect of wind and temperature profiles on the measurable height coverage for RASS[2], and showed how to design a useful acoustic waveform for accurately measuring temperature[3]. The validity of the windprofiler/RASS was confirmed by the MU (Middle and Upper atmosphere) Radar/RASS experiment [4].

Our BLRs have been used to measure the dynamic structures in the lower atmosphere, such as Asia monsoon, and land and sea breeze circulation[5][6]. An open question is the effect of ground clutter contamination on BLR. This contamination is the principle problem in estimating winds from Doppler spectra.

There are two methods for reducing the clutter; one uses sofware, the other uses hardware techniques. Our objective in the study reported here was to analyze the clutter characteristics in the developed BLR and to develop a method to reduce their influence.

2. Methods

2-1 Principle of atmospheric dynamics measument

Figure 1 shows an antenna of our first developed BLR; the BLR specifications are shown in Table 1.

Table 1: Specifications of our developed BLRs

Frequency	1357.5 MHz
Transmit peak power	1 kW
Pulse width	1.0 μ s (variable)
Data sampling rate	0.5 μ s (variable)
Time resolution	5 min.
Antenna type	parabolic
Antenna bean width	3.9 degrees
Beam directions (azimuth, zenith)	Vertical(0,0), East (90,15), North(0,15)

In the atmospheric refractive index, fluctuation whose wavelength along the radar line-of-sight is half the radio wavelength causes Bragg scattering in the BLR. This is primarily caused by microscopic motion of the air parcels.

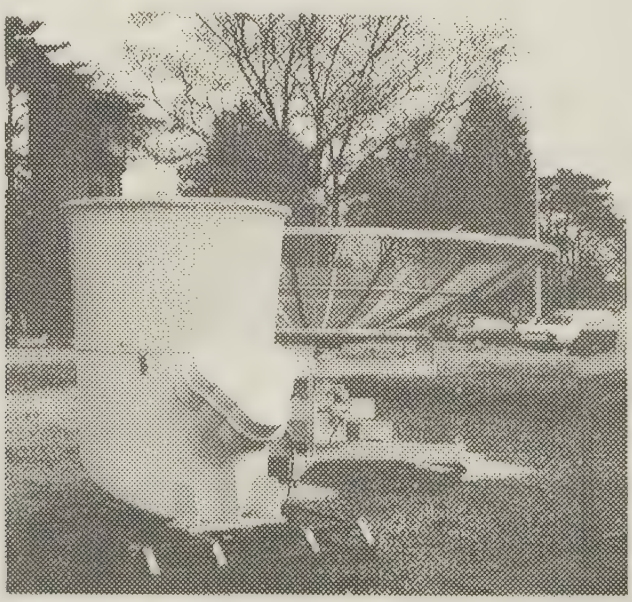

Figure 1: The acoustic- and radio-wave antennas for the BLR/RASS.

The fluctuations are transported by the atmospheric wind, so they always move at the local velocity. The BLR transmits radiowaves in three radial directions immediately above its antenna and receives the echoes scattered by the moving fluctuations from three directions.

The power of the received echoes is proportional to the square of both the number density and the fluctuation-amplitude of the refractive index. The frequency of the received echoes is Doppler shifted to be proportional to the wind velocity. The velocity of the targets measured by the BLR with the Doppler technique is a line-of-sight velocity, which is the projection of a velocity vector in the radial direction. That is, the BLR uses the Doppler-beam-swing method to determine the three components of the velocity vector.

The maximum coverage height of the BLR depends on the intensity of the fluctuations and the system specifications, such as the average transmitting power and the effective antenna area. It is about 3 km. This paper shows the results of dynamic structures observed with the BLR of above specifications at the KMITL in the tropical area since 1993.

2-2 Clutter rejection

We studied a software technique for processing BLR spectra and proposed two alternative methods for identifying the BLR echoes in the spectra. The first method is based on spatial information resident in the range-gated spectra of each observation; the other uses temporal continuity information in a sequence of local power density maxima of temporally contiguous spectra[7]. We are now examining a hardware technique.

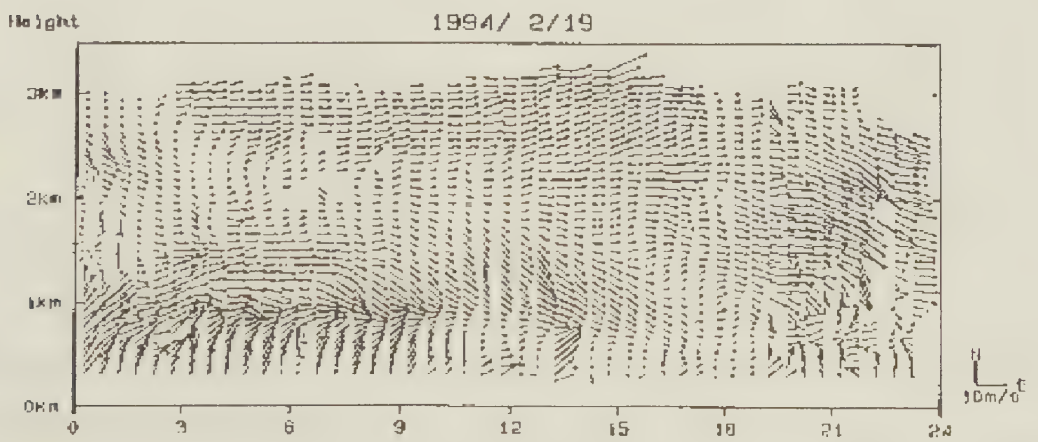

Figure 2. Time-height section of horizontal wind vectors on 19 February 1994 in Bangkok.

3. Results

We are now conducting the Asia Monsoon research using data gathered by the BLRs since 1993.

Figure 2 shows an example of the measured wind profiles, averaged over 30 minutes. The upward and rightward arrows indicate northward and eastward winds, respectively. Continuous variations in wind direction and strength over both time and height are evident.

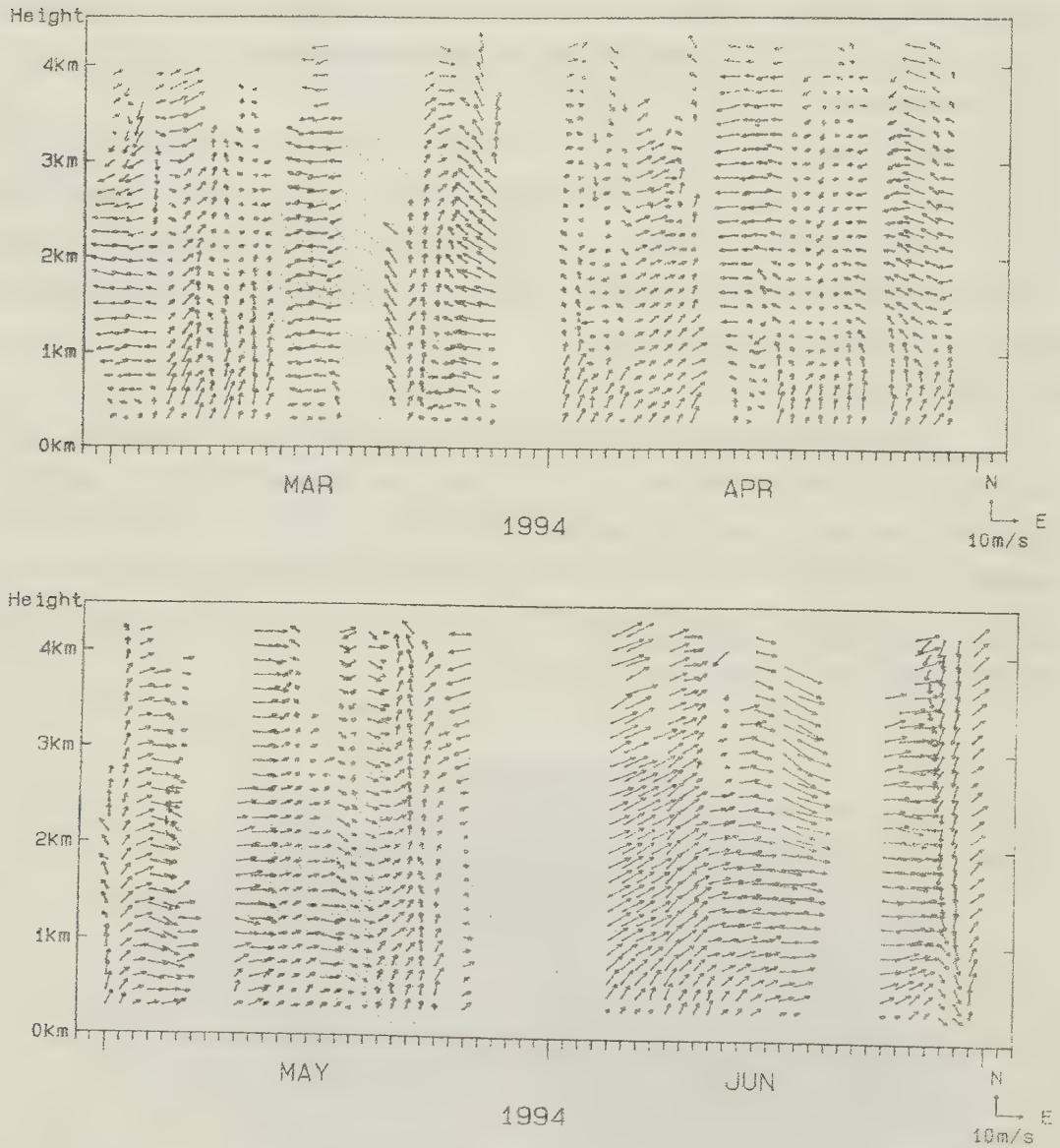

Figure 3: Horizontal wind time-height for March, April, May. June 1994

The seasonal variation of the wind in Bangkok is evident in the daily mean horizontal wind change data for April and May and September and October 1994 (Figs. 3 and 4). Even though data for same days is missing due to radar trouble, an outline of the wind change can be seen in these figures.

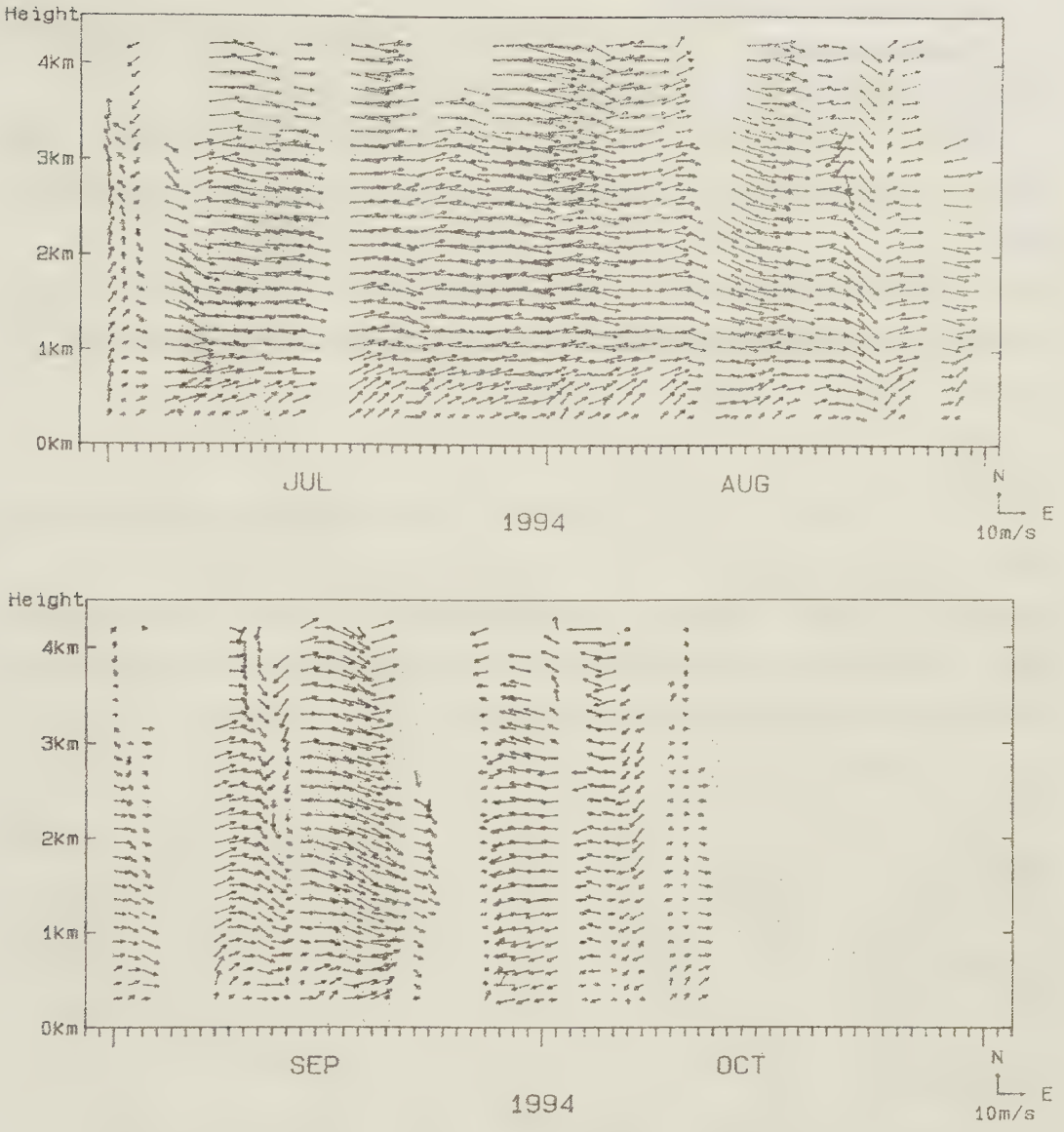

Figure 4: Horizontal wind time-height for July, August, September, October 1994

As shown in Fig. 3, the dominant wind directions are easterly in April and westerly in May, indicating the seasonal change from northeast monsoon to southwest monsoon. The reverse change is seen at the end of September in Fig. 4. In tropical Asia monsoon areas, therefore, the wind direction changes abruptly. From May to September, the wind is mainly southwest; this period corresponds to the rainy season in Bangkok.

One of the two algorithms we studied for clutter rejection determines the spacial continuity between range gates in a group of wind spectra data obtained in real time. The local power density maxima are linked across the spectra corresponding to these range gates, creating a set of local maxima lying in contiguous range gates. The other algorithm determines the temporal

continuity across the time scale instead of across the range gates by using the same process as in the first algorithm.

These methods select, in cases of two or more points to be selected for both the continuities, the local maxima belonging to the longest chain.

We have also developed a clutter rejection method that uses hardware and tested it using the Okinawa BLR. It uses the diffraction effect of radiowaves to reduce the

clutter received from ground and sea targets around the BLR antenna. We constructed a a columnar metal net 4 m high around a parabola antenna. The clutter level was reduced almost one hundredth fold.

4. Discussions

Our BLRs provide accurate data on the atmospheric dynamic structures with

high time and height resolutions. The BLR located in Thailand has been shown to be a useful tool for continuously observing dynamic structures, such as Asia monsoons and land and sea breeze circulation[9].

However, we have not yet clarified the constituent of fluctuation contrbuting to BLR scatterer and the causes of short- and long-term changes in wind direction. We are thus planing to conduct a comparative study using BLR and convensional radiosonde to answer these questions. We are also planing to compare the results of our clutter rejection methods by using BLR and radiosonde data.

5. References

1) Y. Masuda, K. Okamoto, K. Nakamura, T. Ihara, and T. Onishi: J. Remote Sensing Soc. Japan, 12, 1, pp.43-56, 1992.

2) Y. Masuda; Radio Sci., 23, 4, pp.647-654, 1988.

3) Y. Masuda, J. Awaka, K. Nakanura, T. Adachi, and T. Tsuda: Radio Sci., 27, 5, pp.681-691, 1992.

4) T. Tsuda, T. Adachi, Y. Masuda, S. Fukao, and S. Kato; J. Atmos., Ocean Tech., 11.

1, pp.50-62.

5) Y. Ohno, A. Manyano, N. Leelaruji, N. Hemmakon, and Y. Masuda: Proc. Second International Study Conference on GEWEX in Asia and GAME., p. 121, 1995.

6) Y. Ohno, Y. Masuda, and K. Nakamura; Extended Abstract of Third International Synposium on Troposheric Profiling, pp. 310-312, 1994.

7) Y. Rangsanseri and Y. Ohno; Research & Development Report on the Co-operative Environment Observation by MPT and KMITL, pp. 9-14, 1995.

6. Publications

1) Y. Ohno, A. Manyano, N. Leelaruji, N. Hemmakon, and Y. Masuda; Proc. Second International Study Conference on GEWEX in Asia and GAME., p. 121. 1995.

2) Y. Ohno, Y. Masuda, and K. Nakamura; Extended Abstract of Third International Synposium on Troposheric Profiling, pp. 310-312, 1994.

3) Y. Rangsanseri and Y. Ohno; Research & Development Report on the Co-operative Environment Observation by MPT and KMITL, pp. 9-14, 1995.

7. International Cooperation

The BLR with RASS operating in Thailand to study the dynamic structure of the tropical atmosphere is a joint project between the CRL and the KMITL and is sponsored by the Japanese Ministry of Posts and Telecommunications.

(要約)

郵政省通信総合研究所は、１９９１にＬバンド境界層観測用レーダ１号機の観測を開始している　この境界層観測用レーダは、「モンスーン」観測を目的として１９９４年に沖縄電波観測所へ移設した　このレーダの開発後、更に２台の境界層観測用レーダを開発し、１台目は、１９９２年から東京国分寺の通信総合研究所構内に、２台目は、１９９３年末から熱帯域のタイ国キングモンクット工科大学構内に設置した

これらのレーダは、境界層の風向風速及び気温高度分布の観測が可能であり、大気擾乱に伴う電波屈折率の乱れをターゲットとしており、乱れ強度の観測も可能である　即ち、同レーダは、大気運動及び大気の熱的構造の観測に有用な装置である。

この報告では、境界層観測用レーダを国分寺及びモンスーン域のタイ国に設置し観測した大気運動解析の結果を紹介する。タイの観測は、偏東風（乾期）から偏西風（雨期）のモンスーン変化を連続観測する事に成功している

Ⅰ．大気・海洋・陸域間の諸過程に関する観測・解析研究

I. Observation and Analysis on the Process of the Atmosphere-Ocean-Land Interactions

３．陸域の諸過程に関する観測・解析研究

3. Observation and Analysis on the Process over the Land

（３）モンスーン循環広域条件及び雪氷変動状況に関する解析研究

(3) Analysis on Environmental Conditions and Snow-Ice Cover Changes Affecting Monsoon Cycle in Asia

科学技術庁防災科学技術研究所
矢崎　忍、中根 和郎、諸星 敏一、幾志 新吉
National Research Institute for Earth Science and Disaster Prevention, Science and Technology Agency
S.Yazaki, K.Nakane, T.Morohosi, S.Kishi

(Abstract) The mode of Asian monsoon activities is said storongly affected by environmental conditions of the area especially SST of Indian ocian and snow-ice cover over the continent. The purpose of this study is to make clear the relation between them mainly by analyzing satellite data.

Our method is

(1) To make regional satellite image date base covering whole Asian area with NOAA/AVHRR data in a regular period(one in 7 days).

(2) To establish algorithms to detect various air, sea and land conditions with the satellite image data.

(3) For snow-ice cover in Tibetan-Himalayan area, sea ice in the Sea of Okhotsk or air water content over ocians, another adequate satellite data will be adopted for precise analysis.

This year's results are as following.

(1) The algolithm to detect snow covered area with the regional satellite image data is improved and applied to whole area of the image. To distinguish snow from cloud both spectral information and temporal change are used. As a result almost cloud free image of snow cover is obtained.

(2) Detectability of soil moisture with NOAA/AVHRR data and JERS-1/SAR data is verified for Shangdong area. The result was examined with ground observation data.

(3) The method of estimation of ground temperature with the regional satellite data is improved continuously.

１．研究目的

アジアモンスーンの変動はインド洋、西太平洋の海水温、ユーラシア大陸の積雪面積と深く関わっていることが指摘されており、またモンスーン活動によってもたらされる降水は災害、水資源、植生活性度に大きく関係する．本研究ではアジアモンスーン地域を対象として、モンスーン循環活動に関わる各種環境条件（海面水温、地表面温度、積雪、海氷、植生指標、雲頂温度、大気水分量等）の分布状況を各種の地球観測衛星データを用いて検出し、時系列的なデータベースとして整備するとともに、それらを用いて環境条件とモンスーン循環変動との関係を明らかにする．

２．研究方法

（１）アジアモンスーンの変動に大きく影響すると考えられるインド洋、西太平洋、ユーラシア大陸を含む東経３０°～１６０°、南緯２０°～北緯６０°の範囲を解析対象領域として、この領域をカバーするＮＯＡＡ／ＡＶＨＲＲ画像を幾何補正、モザイク合成して広域衛星画像データベースを一定期間（７日）毎に作成する．
（２）（１）で作成する広域衛星画像データベースを用いて、前記の各種環境条件を検出する手法を開発し、その手法を用いて環境条件画像を時系列に作成する．
（３）アジアモンスーンの変動に影響が大きいチベット・ヒマラヤ地域の雪氷分布を分解能の高いＬＡＮＤＳＡＴ／ＴＭ，ＭＯＳ－１／ＭＥＳＳＲを用いて詳細に解析する．
（４）以上のような各種環境条件画像を長期間にわたって整備し、その季節変動、経年変動を解析する．さらにこれらの環境条件とモンスーン循環の変動、特に降水量との関係を明らかにする．

３．研究成果

（１）広域積雪分布の検出

アジア大陸の広域的な積雪分布はモンスーン循環の変動との関連において、また、水収支との関連においても重要である．上記の広域衛星画像を用いて、主として中国地域を対象に広域の積雪分布を検出する手法の開発を引き続き行った．雲と積雪を区別するために特徴空間におけるそれぞれの分布パターンを調べた．その結果、スペクトル情報だけからは積雪と雲は完全には識別できないことが分かった．そこで時期のわずかに異なる複数のデータを用い、スペクトル情報と時間変動情報を併用することにより検出精度の向上をはかった．

（２）土壌水分の検出

ＪＥＲＳ－１／ＳＡＲとＮＯＡＡデータを用いた土壌水分の検出手法の開発を引き続き行った．また、中国山東省で土壌水分計による土壌水分の連続観測を行い、本手法の検証を行った．

（３）地表温度の推定

広域衛星画像を用いた地表温度の推定手法の開発を引き続き行った．

4．考察

特になし

5．引用文献

なし

6．成果の発表

なし

7．関係国との協力

中国国家気象局衛星気象センターとの協力を行っている．本年度は同センターより2名の研究者が来訪し、当研究所との共同研究を行った．また、本研究項目の研究分担者が1名同センターを訪問し、同センターと共同で行う中国山東省における土壌水分の自動観測について協議し、また現地視察を行った．

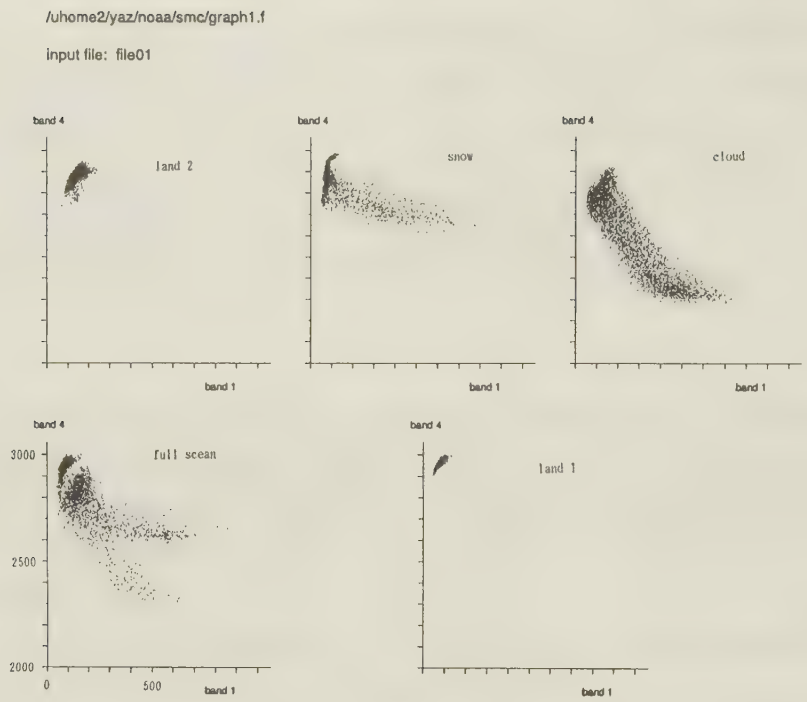

図1　特徴空間における積雪、雲、地表の識別

Fig.1　Distinction between snow, clowd and bear land in feature space

図2　検出された積雪分布（ヒマラヤ地域）

Fig.2　Detected snow cover area in Himarayan area

Ⅰ．大気・海洋・陸域間相互作用の諸過程に関する観測・研究

Observation and analysis on the process of the atmosphere-ocean-land interactions

3. 陸域における諸過程に関する観測・解析研究

Observation and analysis on the process over the land

(4)地域水収支に関する解析研究

Analytical Study of Water Balance on Representative River Basins

科学技術庁防災科学技術研究所
岸井徳雄、葛葉泰久、矢崎　忍
杉田　文

National Research Institute for Earth
Science and Disaster Prevention,
Science and Technology Agency
T.Kishii, Y. Kuzuha, S.Yazaki & F.Sugita

(Abstract) The activity of Asia monsoon is influenced by water cycle and change of water cycle affects Asia monsoon. This study aims to clarify water balance of the regional scale in China. For the purpose hydrological data base, the element are precipitation, runoff, evapotransipiration, temperature, humidity, wind velocity and radiation, has been made. Using this database the monthly rainfall , runoff and evapotranspiration are analyzed.

The results are following. The rainfall - runoff analysis by the Tank model in the Huai He river show that the calculated runoff coincide with the observed one in the flood season. But is not good coincide in the dry season. The reason is considered as the use of artificial drainage.

Further more, evapotranspiration is analyses in the Huai He river basin. Annual potential evapotranspiration is estimated to 830 mm.

1. Objectives

This study aims to clarify water balance of the regional scale in China. For this purpose Hydrological data base, the elements, that is precipitation, runoff, evaporation, temperature, humidity and wind speed etc. have been collected.

This report shows the daily rainfall runoff analysis by Tank model and the change of the monthly potential evapotranspiration in the Huai He river basin.

2. Method

The daily runoff data (1983) for rainfall runoff analysis were collected by the "Remote Sensing Technology Application Center, Department of Water Resources of China. The discharge station used here is the "Bengbu" (basin area 121,330 km^2). The Tank model is used for this analysis.

Further more "Thornthwaite method" is employed for the estimation of potential evapotranspiration using the monthly data (1987) of temperature in the five hydrological stations (Fig.1).

3. Results

The daily rainfall runoff analysis by the Tank model show that

a. The parameters of the model are considerably small comparison with that of the Japan river.

b. The calculated runoff show good agreements with the period of flood season from June to October. But not good agreement with the period from November to May (Fig. 2).

The reason will be following. This basin mainly used for the cultivated land, that is , paddy field and other farm land. So discharge of the river used for irrigation. The effect is more large in dry season. This bring to be difference in the dry season.

The result of the analysis of evapotranspiration in the Huai He river basin are showed from Fig. 3 to Fig. 7. Maximam evapotranspiration occurred in July to August and the values from 150 to 160 mm and annual amounts rises 806 to 864 mm. The average values of the year of the five hydrological station amounts 832 mm.

4. Discussions

The daily rainfall - runoff analysis by the Tank model shows good coincide with the observed one. The Annual rainfall of the year 1,129 mm and 301 mm as the annual runoff . So the annual rainfall loss becomes 828 mm. Monthly change of rainfall loss by water balance method is shown in Fig. 8.

Otherwise the average potential evapotranspiration shows the amounts of 832 mm above mentioned.

Both results shows that the evapotranspiration of the Huai He river basin is about 830 mm per year.

5. References

1) I. Kayane (1973) : Water Cycle (in Japanese). Kyoritu Shuppan co Ltd. pp. 86-99.

2) S. Shin and M. Sawamoto (1995) : Analysis of spatial characteristics for hydrologic quantities in the Han Gang Basin. Jounal of Japan Society of Hydrology & Water Resources, Vol. 8, No. 6, pp. 560-567.
3) N. Takase (1978) : River Hydrology (in Japanese). Morokita Shuppan co. Ltd. pp.67-101.

6. Publications

①Publication on Society

1) Journal etc. in Japan

T. Kishii, Y. Kuzuhá and S. Cao(1966) : Comparison of Yearly Water Balance between Huai He River in China and Experimental Basin in Japan(in Japanese). Proceedings of Hydraulic Engineering, No. 40, pp.87-92.

②Publication beside Society

2) Publication in foreign country

T. Kishii, Y. Kuzuha and C.X. Yan (1996) : Evapotranspiration in the Huai He River Basin. Proceedings of the International Workshop on Macro-scale Hydrological Modeling.

③ Presentation by oral

T. Kishii and S. Cao (1994) : Water balance in Huai He river(in Japanese). Conference of Japan Society of Hydrology and Water Resources.

7. International Cooperation

One researcher was invited to our institute from "Remote Sensing Technology Application Center", Department of Water Resources of China and exchanged informatrions of water balance.

（要旨）

アジアモンスーンの変動は、アジア地域の水循環に大きな影響を及ぼし、その変動は、地表面の水文過程、特に水収支の特性を変えることが推定される。

本研究は、中国を対象とし、この地域の水収支の特性を明らかにすることを主目的とする。この目的のため、水文要素、すなわち、降雨、流出、蒸発、気温、湿度、風速および日射等のデータベースが作成される。 このデータベースを利用して、水収支の主要な要素である降雨、流出および蒸発散の解析を行った。

その結果、タンクモデルを利用した淮河の流出解析により、洪水期（雨期）および乾期の流出特性が明らかとなった。

さらに、実験式を用いた蒸発散の解析と合わせ、淮河流域の降雨損失および蒸発散を推定できた。

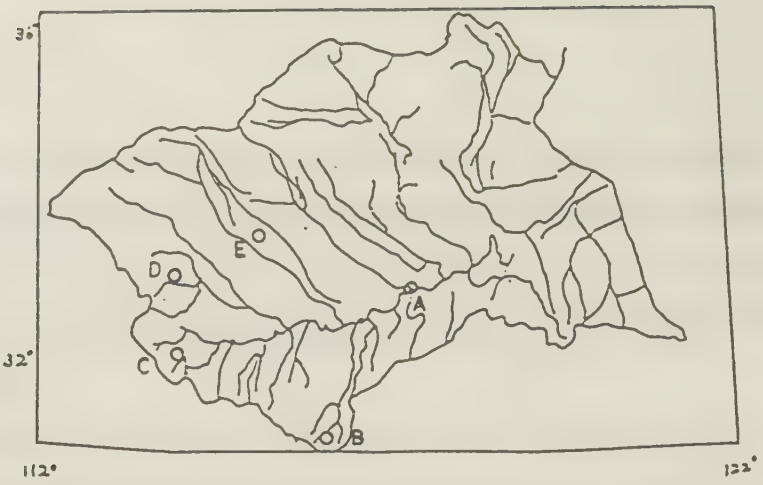

Fig. 1 Location of hydrological stations

(A: Bengbu, B: Huoshan, C: Xinyang, D: Zhumadian, E: Boxiang)

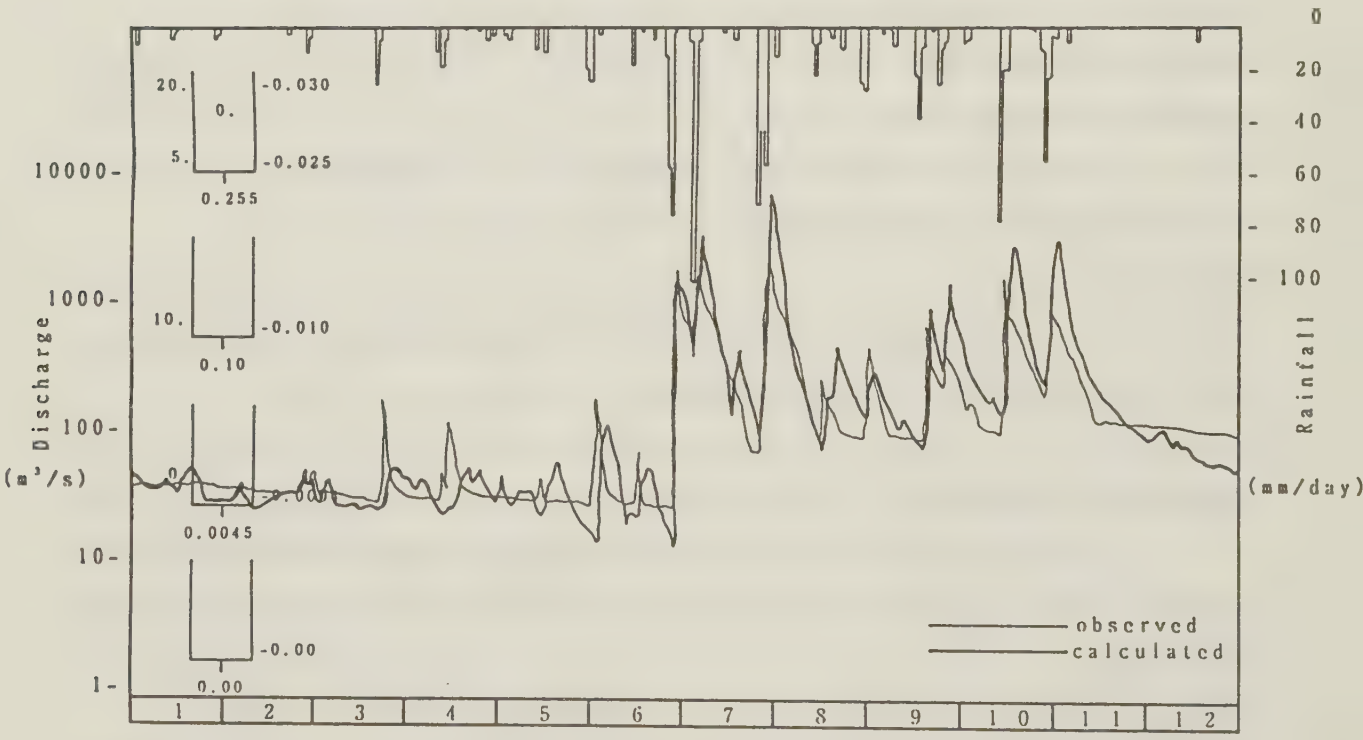

Fig. 2 Daily runoff analysis by Tank model at Bengbu

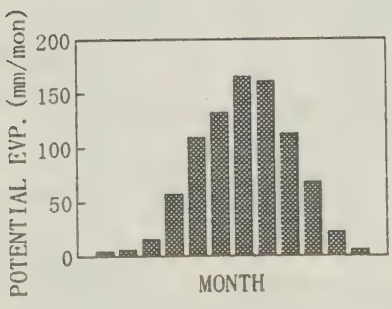

Fig. 3 Potential evapotranspiration at Bengbu

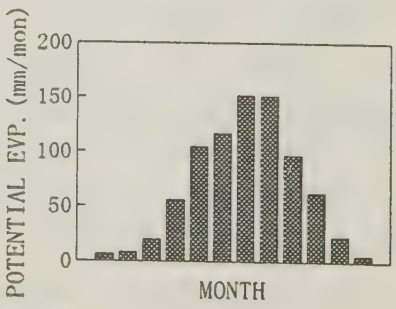

Fig. 4 Potential evapotranspiration at Huoshan

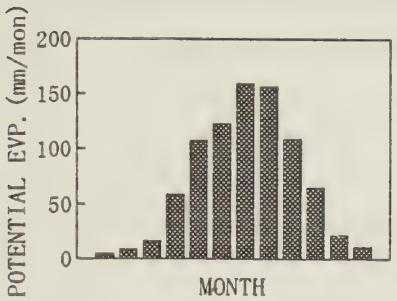

Fig. 5 Potential evapotranspiration at Xinyang

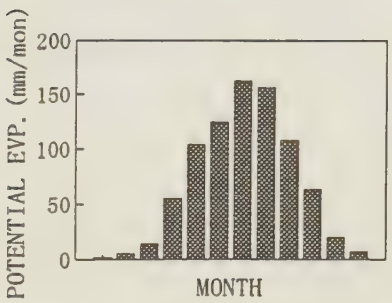

Fig. 6 Potential evapotranspiration at Zhumadian

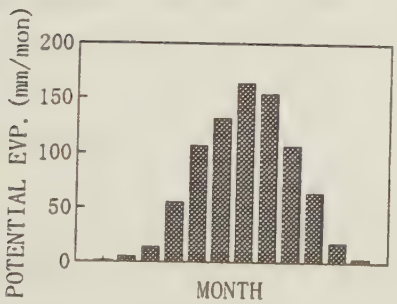

Fig. 7 Potential evapotranspiration at Boxiang

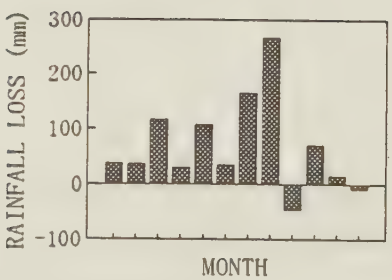

Fig. 8 Monthly rainfall loss in Bengbu

II. 数値モデルによる４次元資料同化システムの開発に関する研究

Development of the four dimensional data assimilation (4DDA) system by the use of numerical model

1. --アジアモンスーンの１カ月予報の雲のパラメータ化に対する感度実験--

--A sensitivity experiment of one-month dynamical forecast of the Asian summer monsoon to cloudiness parameterization --

気象庁　予報部
岩崎俊樹
Forecast Department, Japan Meteorological Agency
Toshiki Iwasaki

Abstract

To improve long-range numerical weather prediction (NWP) of the Asian summer monsoon, we investigate effects of cloudiness parameterization scheme on forecast performance. Clouds reduce solar radiation at the ground (Albedo effect) and then reduce surface sensible heat flux over the land. A one-month forecast experiment shows that when the cloudiness is reduced the forecast of the Asian summer monsoon is considerably enhanced. Then, horizontal moisture flux toward the Far East, which may affect activities of the Baiu front, increases due to large pressure gradient between the Eurasian continent and the Pacific Ocean.

This experiment confirms that the cloudiness parameterization has a great impact on forecast performance of the Asian summer monsoon through the land atmosphere interactions. We are planning to make intensive validation of the surface radiation with field observations and to refine parameterization schemes of cloud formation and cloud optical property. In particular, observational analyses suggest that clouds are easier to form over the land than over the ocean. Such a tendency must be included in the cloudiness parameterization scheme.

1. Objectives

The Japan Meteorological Agency (JMA) has just started one-month dynamical ensemble forecasts since March 1996, by using a T63L30 version of the global NWP model (GSM9603). In summer, forecast performance of the Asian summer monsoon is of great interest to us. The Asian summer monsoon is characterized as a large pressure gradient between heat low over the land and subtropical high over the Pacific Ocean. The south-westerlies caused by the pressure gradient transfer enormous amount of moisture toward the Far East. The weather of Japan is under strong influence of the Asian summer monsoon, especially in activities of Baiu front and subtropical high in the western North Pacific.

Figure 1 shows a one-month forecast of geographical distributions of mean-sea-level pressure (MSLP) from the initial at 12 UTC, 31 May, 1993, compared with the monthly mean objective analysis in June 1993. The forecast of heat low over the Eurasian Continent is

significantly stronger than the objective analysis, although the forecast of subtropical high over the ocean agrees well with the analysis. The overestimation of the monsoon circulation is one of the systematic errors of this model.

The Asian summer monsoon is mainly excited by both diabatic heatings of surface heat fluxes and of deep cumulus convections. Yanai et al. (1992)[1] showed that the sensible heat flux, triggering the deep cumulus convection, plays a primary role in the formation of the monsoon circulation. The sensible heat flux is heavily dependent on the ground absorption of solar radiation. Many authors have indicated that most of current general circulation models have large uncertainties associated with the absorbed solar radiation at the ground [(eg., 2)]. In the model, the cloudiness parameterization is an important control parameter of the solar radiation at the ground. Then, we make a sensitivity experiment of one month forecast of the Asian summer monsoon to the cloudiness parameterization scheme, focusing on the land atmosphere interaction.

2. Method

The numerical model used in this experiment is a global NWP model (GSM9603) at JMA. It has a truncation wave number of T63 in the horizontal and 30 levels in the vertical. Deep cumulus convections are parameterized by an Arakawa-Schubert scheme (1974)[3]. The cloudiness is diagnostically determined from relative humidity (%) as follows;

$$\text{Cloud} = \begin{cases} \left(\frac{r-r_c}{1-r_c}\right)^2 & r>r_c \\ 0 & r<r_c \end{cases}$$

where a parameter r_c is critical relative humidity of cloud formation given by a function of (p/p_s). In the experimental model, we simply take the form of

$$\text{Cloud} = \begin{cases} 0.7\left(\frac{r-r_c}{1-r_c}\right)^2 & r>r_c \\ 0 & r<r_c \end{cases}$$

to reduce cloudiness. When relative humidity remains the same to the two models, the experimental model reduces cloudiness by 30 % compared with the control. Note that the cloudiness ratio between the two models are not kept constant in the course of time integration, because relative humidity becomes different from each other.

3. Results

First, we discuss effects of the cloudiness parameterizations scheme on the cloud radiative forcing (CRF) against the ground. Figure 2 shows a geographical distribution of monthly mean difference in total cloudiness between the two forecasts. Mostly the cloud fraction is predicted less in the experimental forecast than in the control forecast, although some

exceptions are found around the western part of Asia. In the place where the cloudiness decreases, the model mostly increases short wave CRF but decreases the long wave CRF as shown in Fig. 3. The former dominates the latter so much that the major effect of reduced cloudiness is an enhancement of the ground absorption of short wave radiation as was expected.

The surface energy balance equation for long term is as follows;

$$RS - RL - LH - SH - G = 0$$

Net downward short wave radiation (RS) is almost balanced with the sum of net long wave radiation (RL), latent heat flux (LH), sensible heat flux (SH) and heat conduction (G) into deep soil. When the cloudiness decreases, the stronger solar radiation makes the ground temperature higher and increases sensible heat fluxes. Figure 4 shows that the experimental model enhances both of the sensible and latent heat fluxes around Southeast Asia compared with the control model. This is regarded as a direct effect of increased solar radiation at the ground. Over India, on the other hand, an increase in the sensible heat flux almost compensates for a decrease in the latent heat flux. In this region, the absorbed solar radiation is not significantly different between the two forecasts but the Bowen ratio is different. This may be due to an indirect effect that the modified cloudiness scheme affects the atmospheric circulation and then gives effects to precipitations and the soil moisture.

Figure 5 shows a geographical distribution of temperature difference at 850 hPa. Temperature rises are found over Siberia and Southeast Asia, roughly corresponding to portions with increasing surface heat fluxes. As a result, the experimental model enhances the depression around Southeast Asia (Fig 6). Thus, we can say that the cloudiness reduces the ground absorption of the solar radiation and suppresses the Asian summer monsoon. Figure 7 shows change in the horizontal moisture flux around monsoon Asia. The experimental model predicts horizontal moisture flux toward the Far East more than the control model. This may be closely related to the larger MSLP gradient between the Eurasian Continent and the western North Pacific.

4. Discussions

This experiment suggests that the cloudiness parameterization scheme may have considerable impacts on forecast performance of the Asian summer monsoon. It is very important to simulate the ground absorption of the short wave radiation as accurately as possible. Intensive validation of the surface radiation with field observations is planned to tune up the parameterization scheme of cloud formation and cloud optical parameters.

Recent studies have clarified that the mean cloud droplet radius over the land is smaller than that over the ocean. The smaller the mean radius is, the larger the cloud optical thickness ratio per cloud water content is[4]. In addition, smaller sizes indicate that clouds are easier to form in that place due to plenty of condensation nuclei. When relative humidity is equal, the cloud

optical thickness is considered to be much larger over the land than over the ocean. Considering this fact, parameterization schemes of cloud formation and cloud optical property must be made different between the land and the ocean.

Besides the cloud radiation, we must consider many physical processes giving effects to forecast performance of the Asian summer monsoon as well. Among them, the cumulus parameterization scheme, which is the major driving force of the general circulation in low latitudes, may have great influences on monsoon forecasts. Process studies are underway to validate and refine cumulus convection schemes.

5. References

1) M. Yanai, C. Li and Z. Song, 1992: Seasonal heating of the Tibetan Plateau and its effects on the evolution of the Asian summer monsoon. *J. Meteor. Soc. Japan*, **70**, 319-351.
2) M., A. Wide, Ohmura, H. Gilgen and E. Roeckner, 1995: Validation of general circulation model radiative fluxes using surface observations. *J. Climate*, **8**, 1309-1324.
3) A. Arakawa and W. H. Schubert, 1974: Interaction of a cumulus cloud ensemble with the large-scale environment. *J. Atmos. Sci.*, **31**, 674-701.
4) Q. Han, W. B. Rossow and A. A. Lacis, 1994: Near-global survey of effective droplet radii in liquid water clouds using ISCCP data. *J. Climate*, 7, 72-80.

6. Publications

Oral presentation at annual meeting of Meteorological Society of Japan: A sensitivity experiment of one-month dynamical forecast of the Asian summer monsoon to land-atmosphere interactions.

（要旨）

数値モデルによるアジアモンスーンの長期予報を改善するために、雲量のパラメータ化が予報精度に及ぼす影響を調べる。雲は地表面での日射を減らし（アルベド効果）、その結果陸面からの熱フラックスを減少させる。一ヶ月予報実験の結果、雲量を減らすことによってアジアモンスーンが強化されることが見出された。この時、ユーラシア大陸と太平洋との間の大きな気圧傾度のために、極東方面への水蒸気輸送量が増える。これは、梅雨前線の活動の予報に影響を与えると考えられる。

この実験で、雲量のパラメータ化は大気陸面相互作用を通じてアジアモンスーンの予報特性に大きな影響を与えることが分かった。今後、雲量や雲の光学的性質のパラメータ化について観測と比較しながら改良を重ねる必要がある。最近の観測によれば雲の形成効率は海上に比べ陸上で大きいことが示されている。このような観測事実もパラメータ化に含める必要がある。

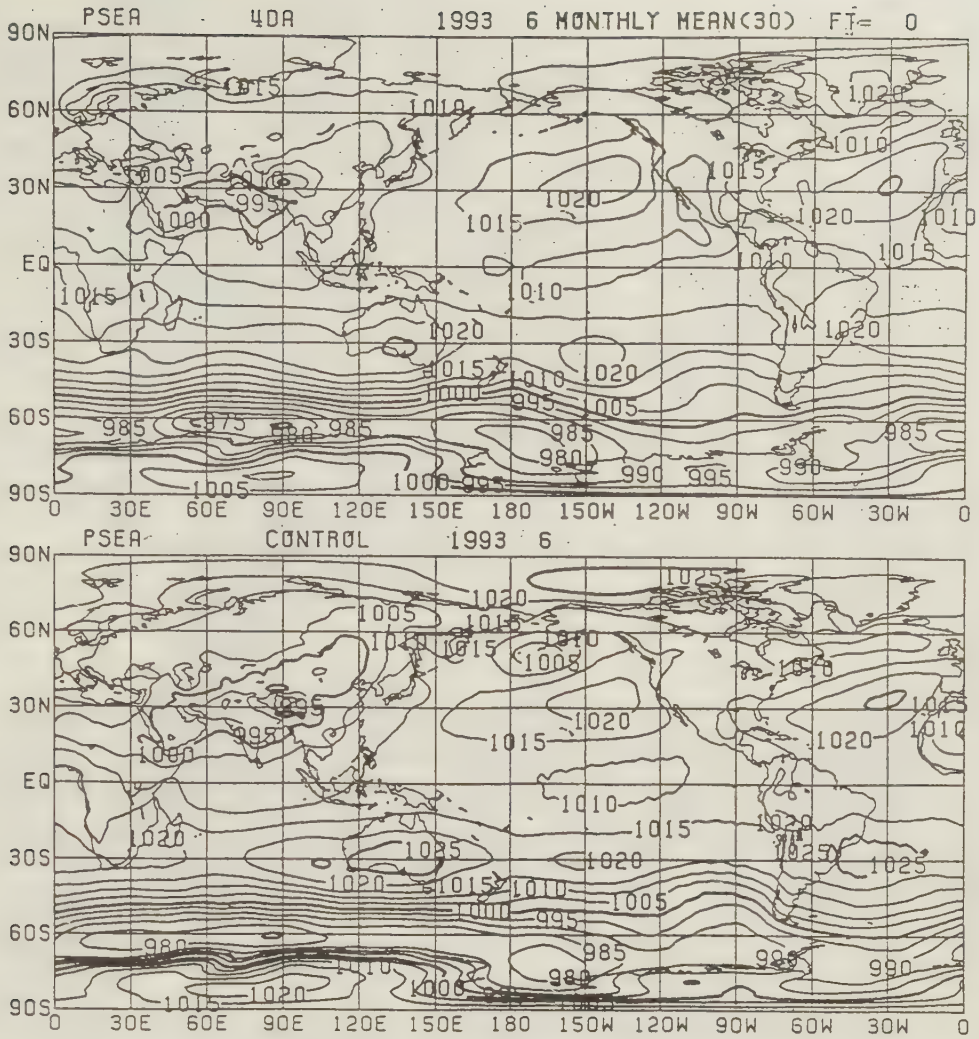

Fig. 1 Monthly averaged mean-sea-level pressure (MSLP). Upper and lower panels show objective analysis and one month forecasts from the initial of 31 May, 1993, respectively. Contour interval is 5 hPa.

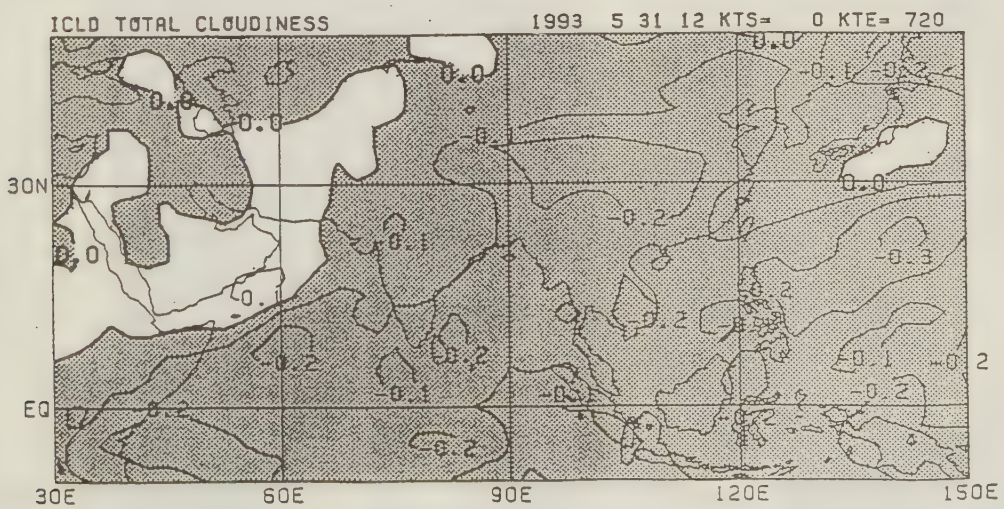

Fig. 2 Change in monthly mean cloudiness (%) due to modification of cloudiness parameterization scheme around Monsoon Asia. Areas of negative impacts are shaded.

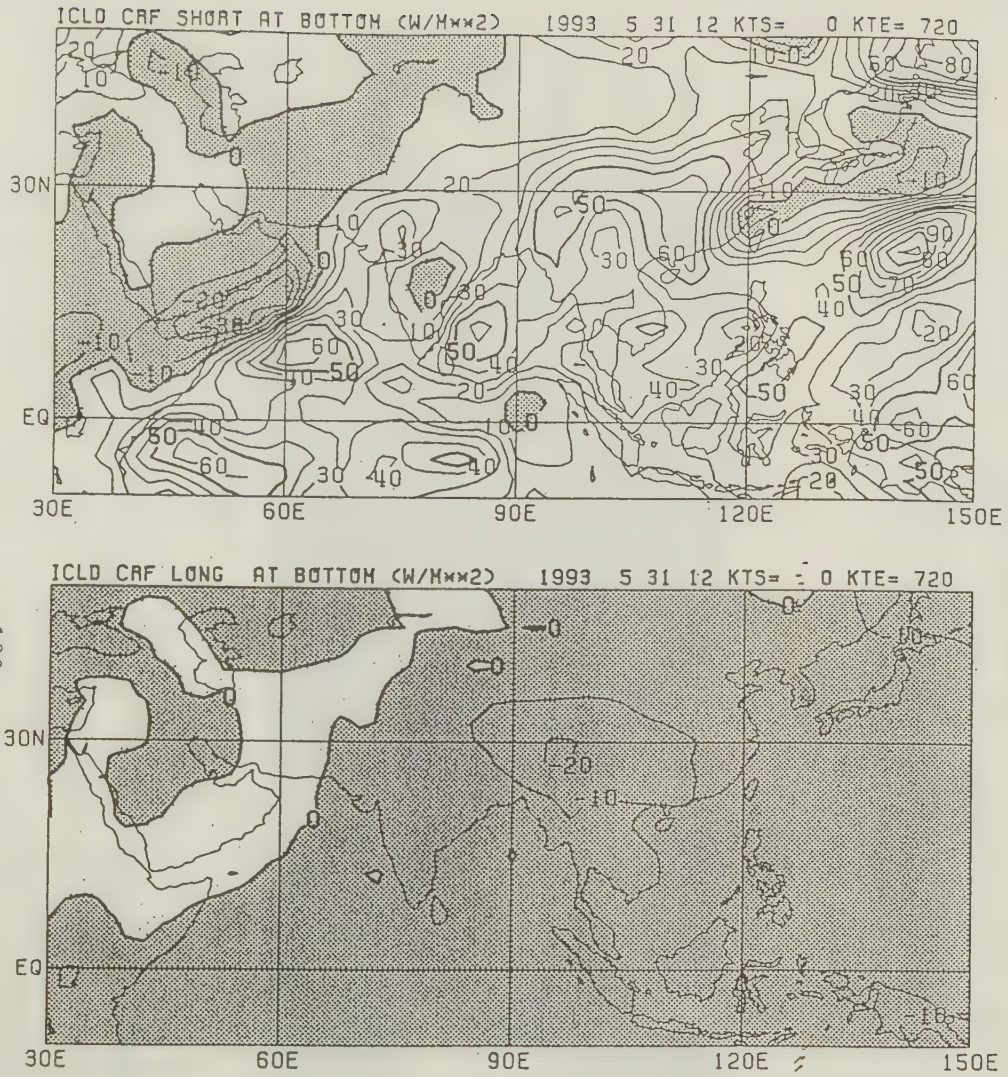

Fig. 3 Same as Fig. 2, but for short wave (upper panel) and long wave (lower panel) cloud radiative forcings against the ground with a contour interval of 10 W/m^2.

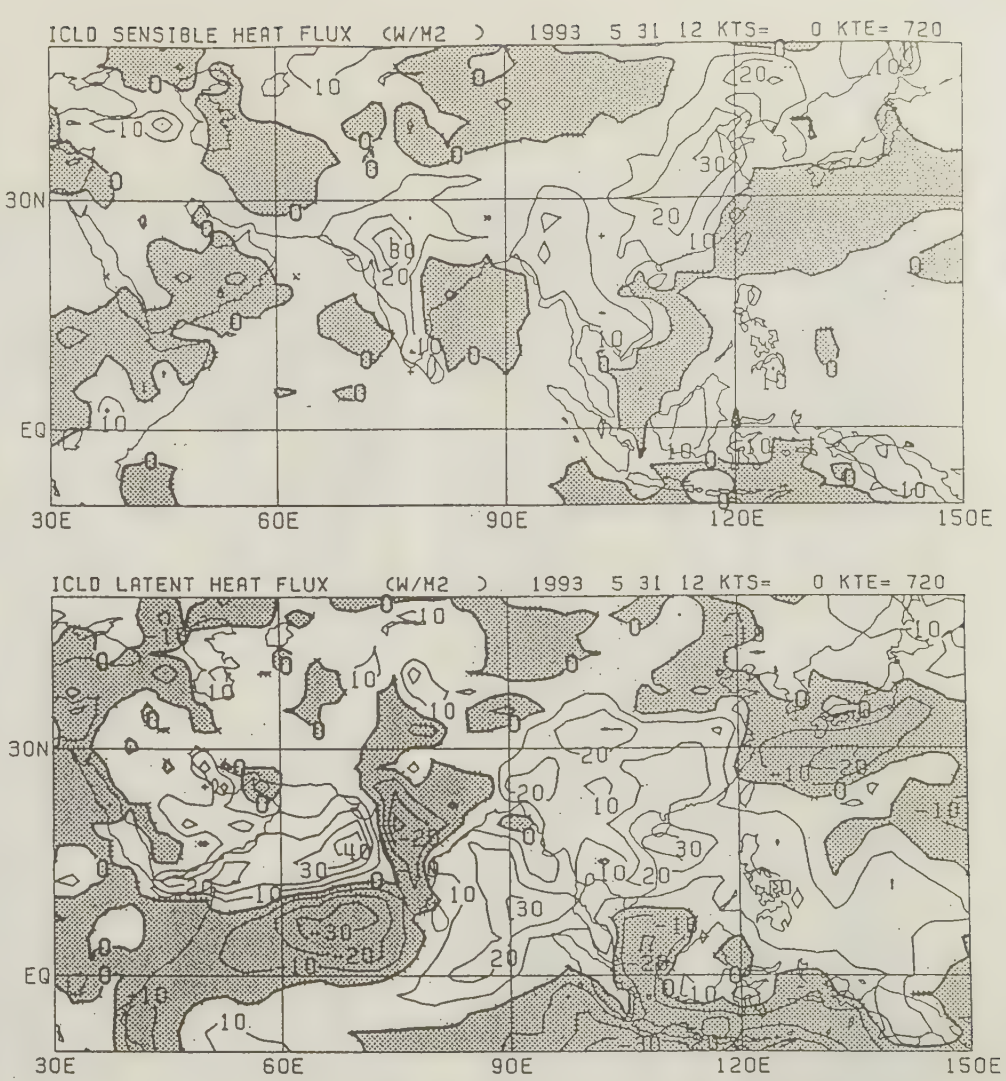

Fig. 4 Same as Fig. 2, but for sensible heat (upper panel) and latent heat (lower panel) fluxes with a contour interval of 10 W/m^2.

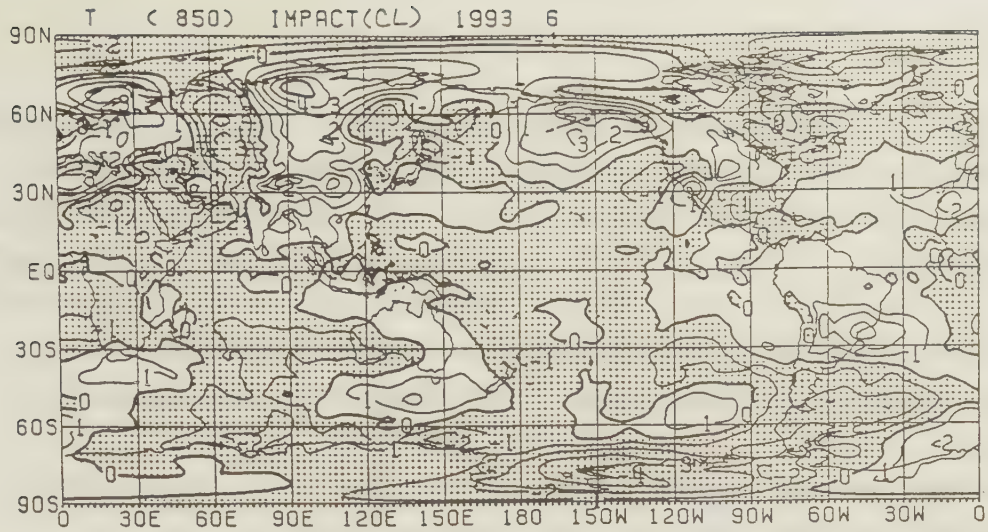

Fig. 5 Change in global distributions of monthly mean temperature at 850 hPa due to modification of cloudiness parameterization scheme. Areas of negative impacts are shaded.

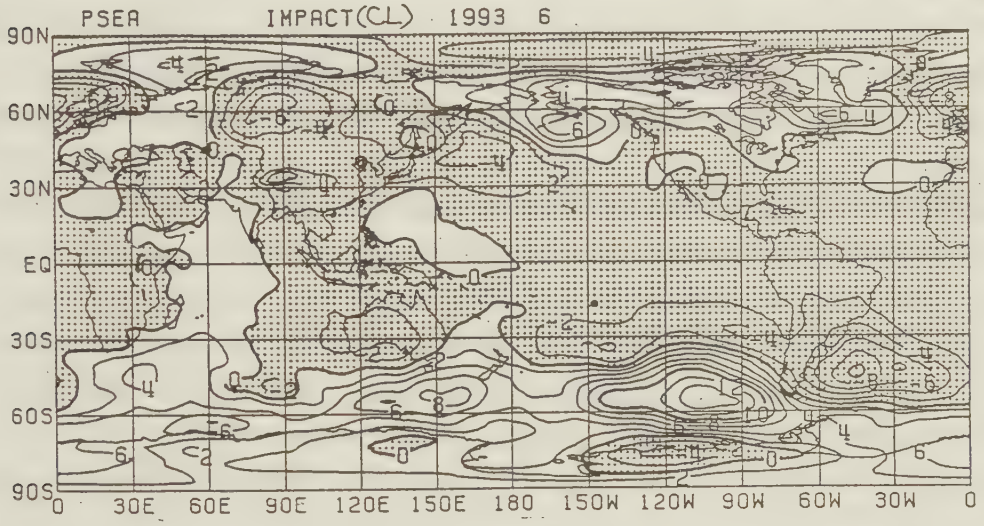

Fig. 6 Same as Fig. 5, but for MSLP with a contour interval of 5 hPa.

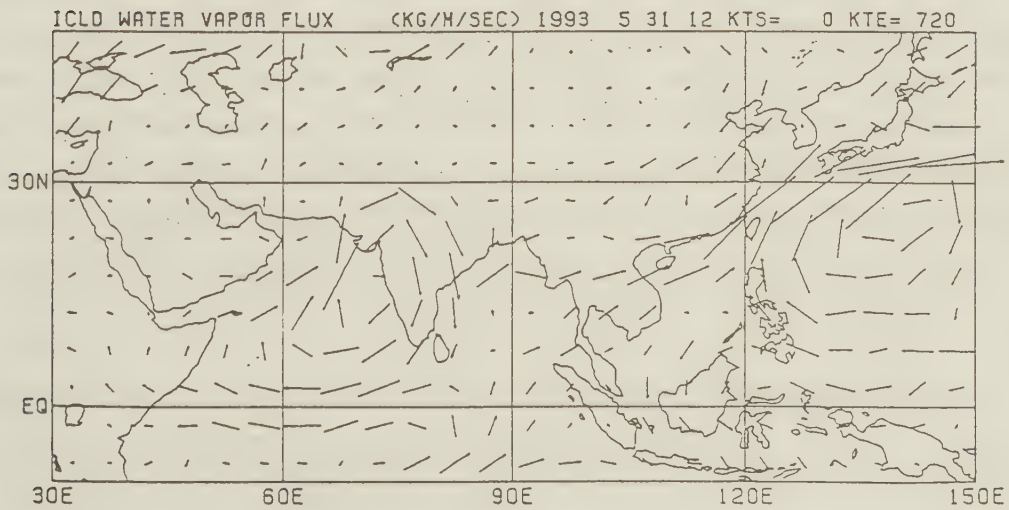

Fig. 7 Same as Fig. 2, but for horizontal moisture flux.

Fig. 1 Monthly averaged mean-sea-level pressure (MSLP). Upper and lower panels show objective analysis and one month forecasts from the initial of 31 May, 1993, respectively. Contour interval is 5 hPa.

Fig. 2 Change in monthly mean cloudiness (%) due to modification of cloudiness parameterization scheme around Monsoon Asia. Areas of negative impacts are shaded.

Fig. 3 Same as Fig. 2, but for short wave (upper panel) and long wave (lower panel) cloud radiative forcings against the ground with a contour interval of 10 W/m^2.

Fig. 4 Same as Fig. 2, but for sensible heat (upper panel) and latent heat (lower panel) fluxes with a contour interval of 10 W/m^2.

Fig. 5 Change in global distributions of monthly mean temperature at 850 hPa due to modification of cloudiness parameterization scheme. Areas of negative impacts are shaded.

Fig. 6 Same as Fig. 5, but for MSLP with a contour interval of 5 hPa.

Fig. 7 Same as Fig. 2, but for horizontal moisture flux.

II. 数値モデルによる大気・海洋・陸域間相互作用の実験研究
Experiment of the atmosphere-ocean-land interactions by the use of numerical models

2. 広域水収支モデルの開発に関する研究
Development of water balance model over the wide area

科学技術庁防災科学技術研究所
中根 和郎、幾志 新吉
National Research Institute for Earth Science and Disaster Prevention,Science and Technology Agency.
K. Nakane, S. Kishi

(Abstract) The purpose of this study is to develop the Regional Water Balance Model for assessing the variation of water resources and soil moisture over the wide area due to the fluctuation of Asian Monsoon activity. The model should predict river discharge, water contents in the soil, storage amount of water in the ground, snow deposit, snow melt and actual evapotranspiration on each area with 0.5° x 0.5° in latitude and longitude by using observed precipitation, evaporation and air-temperature. The model is made on the basis of the concepts of Tank Model. The prototype of the Regional Water Balance Model had been developed and had been applied to Chaophraya River basin(110 thousand km^2) in Thailand. The results were satisfied, though the dry season and the wet season came alternately in this region. Now, the model is going to be applied to Huaihe River basin(121 thousand km^2) in China and Ohyodo River basin(2 thousand km^2) in Japan. The model should use huge conventional observed data. However it is difficult to acquire these data over the wide area densely, especially evaporation. Therefore, it is necessary to estimate evaporation in wide area by using satellite data. Satellites could observe Brightness Temperature and Albedo, which are related with evaporation, on the land from the space globally and frequently. Evaporation relates with air-temperature strongly. The air-temperature is derived from split window data of infrared channel on NOAA AVHRR GAC data potentially. Up to this time, the new regression equation estimating the monthly mean air-temperature had been obtained. Now, generalization of the regression equation is curried out for applying to wide area.

These results in this fiscal year are summarized as follows;

(1)Data for precipitation, evaporation and discharge of dams in Huaihe River basin were acquired densely and data-set for the water balance model in

the basin from 1983 to 1989 were prepared.

(2)Method for obtaining the simplified river system on Asian Continent from DTM data-set with 5 x 5 minutes resolution were developed.

(3)New relations between coefficients of the regression equation, which derives monthly mean air-temperature using NOAA AVHRR GAC data, and latitude of target points were found. From this discovery, coefficients were obtained by using functions of latitude at target points. Coefficients derived by these functions were applied to wide area and gave reasonable estimated monthly mean air-temperature at several points.

1. Objectives

The purpose of this study is to develop the RWB Model(Regional Water Balance Model) with 0.5° x 0.5 ° resolution. The model could be used to assess the variation of water resources and soil moisture over the wide area exactly due to the fluctuation of Asian Monsoon activity. The RWB Model predicts river discharge, water contents in the soil, storage amount of water in the ground as potentially utilizable water, snow deposit, snow melt and actual evapotranspiration on each area with 0.5 ° x 0.5 ° in latitude and longitude. The model gives appropriate information for assessing hydrological regime in detail when it is compared to any general circulation models. The study had started with developing the model. Through applying to various places, the RWB Model over the Asian Continent will be developed as the final goal of this study.

2. Methods

The RWB Model is made on the basis of the concepts of Tank Model(Sugawara, 1984). The Tank Model have been applied to many river basins in the world, such as tropical humid area, snow covered area, semi-arid area, etc. As shown in Figure 1, the RWB Model is composed of four sub-models, namely, a discharge sub-model, an evaporation sub-model, a sub-model of snow-pack and snow-melt, and a precipitation sub-model. The discharge sub-model is composed of many field models and river models. The field models, which are composed of four tanks arranged vertically in series respectively, are applied to each grid areas on simply categorized fields. Field models are four types according to the categorization of fields, namely mountainous type, hilly type, diluvial type and alluvial type. River models composed of one tank are used as the river runoff model on the simplified river system. River models are also three types according to river conditions, such as mountainous type, plain type and swampy type.

These field models and river models are coupled like a tree structure. The evaporation sub-model calculates evaporation in grid area by combining conventional pan-evaporation data at several points and estimated regional evaporation from satellite data. The sub-model of snow-pack and snow-melt calculates water equivalent of snow-pack and melt on grid areas using daily precipitation and daily mean air-temperature, which has some local factors related to humidity and wind. The precipitation sub-model calculates the areal precipitation on grid areas by combining conventional rain gage data and seasonal patterns of the cloud cover, which are derived from satellite data. Up to this time, the prototype of the discharge sub-model had been developed. The sub-model had been applied to Chaophraya River basin with 110 thousand km^2 in Thailand. The results were fairly good, though the weather condition in the basin change from dry to wet alternately in annual cycle. Now, the same model are going to be applied to Huaihe River basin with 121 thousand km^2 in China and Ohyodo River basin with 2 thousand km^2

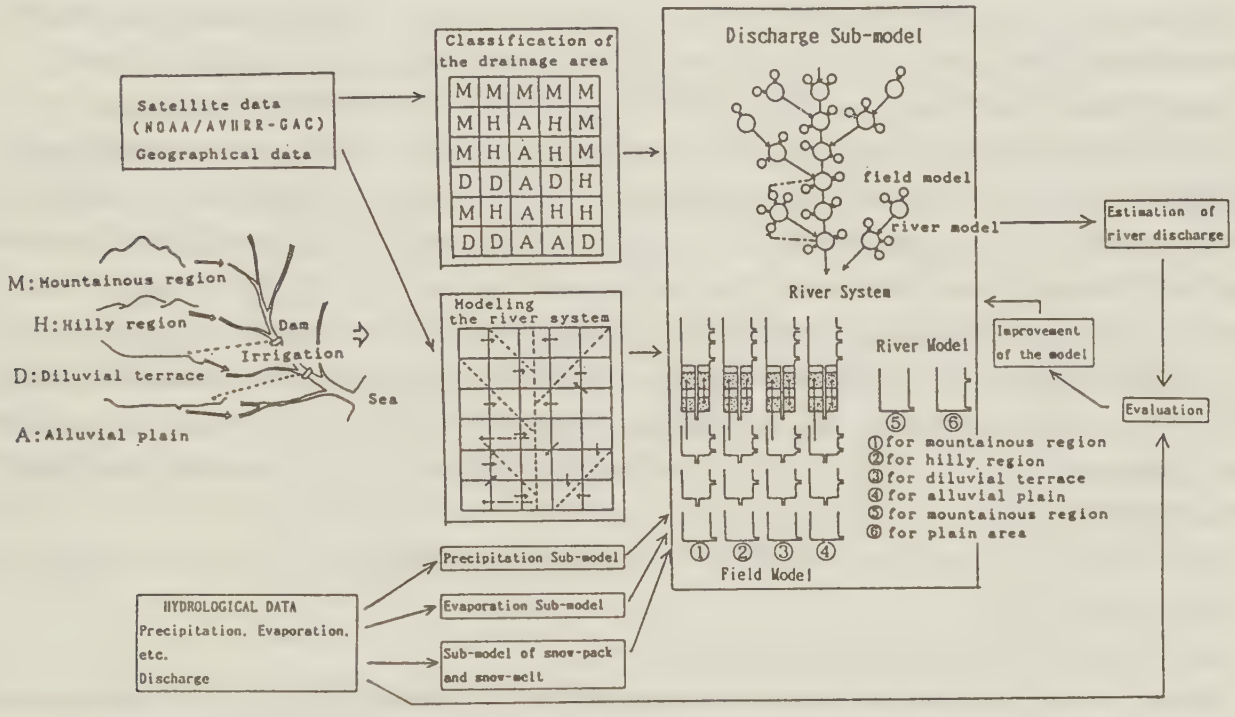

図1　広域水収支モデルの概略

Fig.1 Outline of the Regional Water Balance Model.

in Japan. Study to develop the RWB Model over Asian Continent are also curried out. In this study, making data-set of basin's conditions is important. These data-set are consist of data for simply categorized field and river system, which describe how rain-water flows into the river-mouth through the river system. It is hard to make these data-set, especially river system, because of huge data and complicated river system over the Asian Continent. In this year, the method for making these data-set were investigated.

The model should use huge conventional observed data as input data. However, it is difficult to acquire these data over the wide area densely, especially evaporation. Therefore, it is necessary to estimate evaporation in wide area by using satellite data. Because the satellite could observe Brightness Temperature and Albedo, which are related with evaporation, on the land from the space globally and frequently. Evaporation relates with air- temperature strongly(Thornthwaite, 1948). The air-temperature is potentially derived from split window data of infrared channel on NOAA AVHRR GAC data. In our institute, W-RSI(Weekly Regional Satellite Image) data covering the area from 60° N to 20° S in latitude and from 30° E to 160° E in longitude are being made from NOAA AVHRR(Advanced Very High Resolution Radiometer) GAC(Global Area Coverage) data in weekly basis(Yazaki, 1990 and Nakane, 1990). The map projection of W-RSI data is a grid coordinate system with 2 minutes equal intervals of latitude and longitude. W-RSI data unfortunately contain many cloud, which prevent to transmit information from land surface to satellite because of absorbing radiation and reflection from the land. Therefore, M-RSI(Monthly Regional Satellite Image) data are made by composing data of cloud free area on W-RSI data during a month. M-RSI data could be used for estimating M-AT(monthly mean air-temperature) successfully(Nakane, 1991). Up to now, the new regression equation described in Equation 1 had been obtained for estimating the M-AT from M-RSI data.

$$M\text{-}AT = K1 \times SR + K2 \times Tch4 + K3 \times (Tch4 - Tch5) + K0 \qquad ----(1)$$

$$SR = COS(\theta - \delta)$$

$$\delta = 0.4093 \times \sin(0.01698 \times (JDAY - 80))$$

Where, Tch4 and Tch5 are brightness temperature(unit: degree Celsius) of Channel 4(wave band: 10.5～11.5 μm) and Channel 5(wave band: 11.5～12.5 μm) on NOAA AVHRR data respectively, SR and θ are the seasonal coefficient of outer solar radiation and latitude at a target point respectively, δ is declination, JDAY is Julian Days. K0, K1, K2 and K3 are coefficients of regression equation.

The equation has four coefficients. These coefficients relate with latitude of target points, though coefficients are variable from place to place.

Because, these coefficients relate with water vapor in the atmosphere and distribution of water vapor depends on latitude. Now, the regression equations between coefficients and local latitude are investigated for applying to the Asian Continent.

3. Results

In this fiscal year, data set of the RWB Model in Huaihe River basin were made more densely. Relation between coefficients of the regression equation, which estimated M-AT from NOAA AVHRR GAC data, and latitude of target points were also investigated. These results are summarized as follows;

(1)Preparation of data-set for Huaihe River basin

Dense data for precipitation at 38 stations , discharge of river at 14 stations, discharge of 6 dams and evaporation at 15 stations in Huaihe River basin were further acquired(see Figure 2) and input data-set of the RWB Model in the basin from 1983 to 1989 were prepared. Because, rainfall data used for preliminary application of the model to the basin, which results were not good in dry years, were only located along the river.

(2)Developing the method for making data-set of simplified river system

In the development of the RWB Model over Asian Continent, data-set for simplified river system is important. However, the data-set is not only complicated for making automatically, but also too hard for human judgement. Therefore, half automatic method were developed. In this study, data-set of DTM with 5 minutes resolution and world data bank II (see Figure 3) were used for tracing ridges and valleys over the Asian Continent.

(3)Coefficients were estimated by using functions of latitude

New relations between coefficients of the regression equation, which derives M-AT by using M-RSI data, and latitude of the target point were found. From these relations, functions of latitude estimating applicable coefficients in wide area were obtained(see Figure 4). These coefficients gave reasonable estimations of M-AT(see Figure 5).

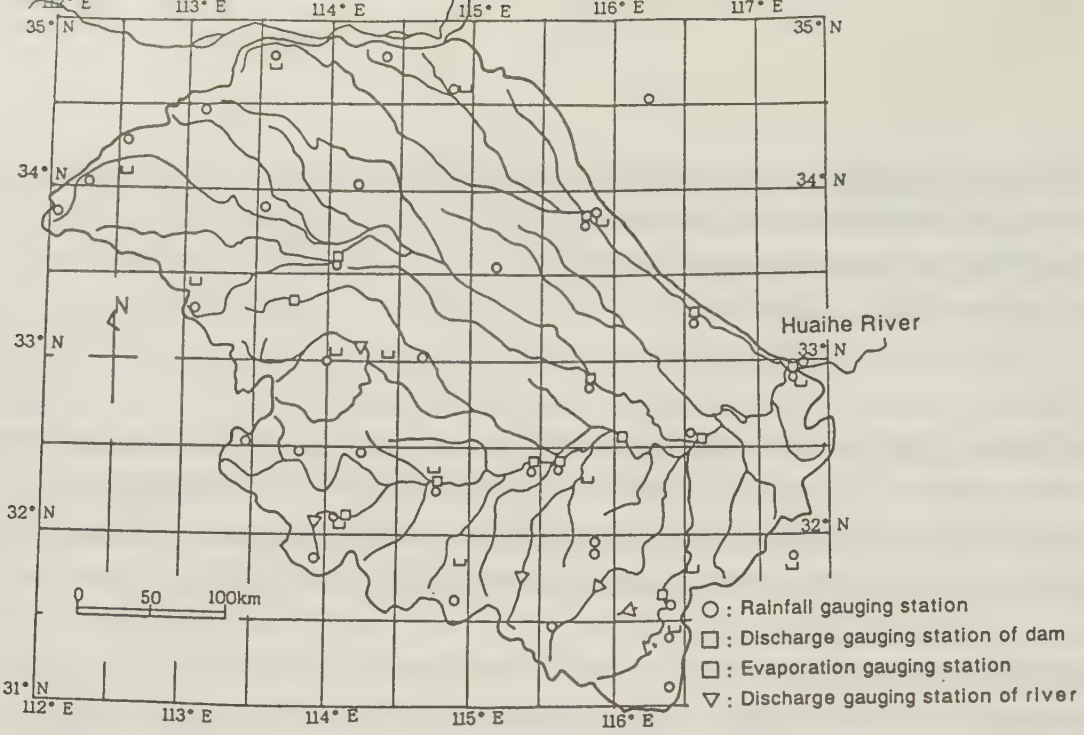

図2　淮河流域（対象流域面積:121,330km2）において、広域水収支モデルの入力データとして使用される観測所の位置

Fig.2 Location of stations used for input data of the RWB Model in Huaihe river basin.

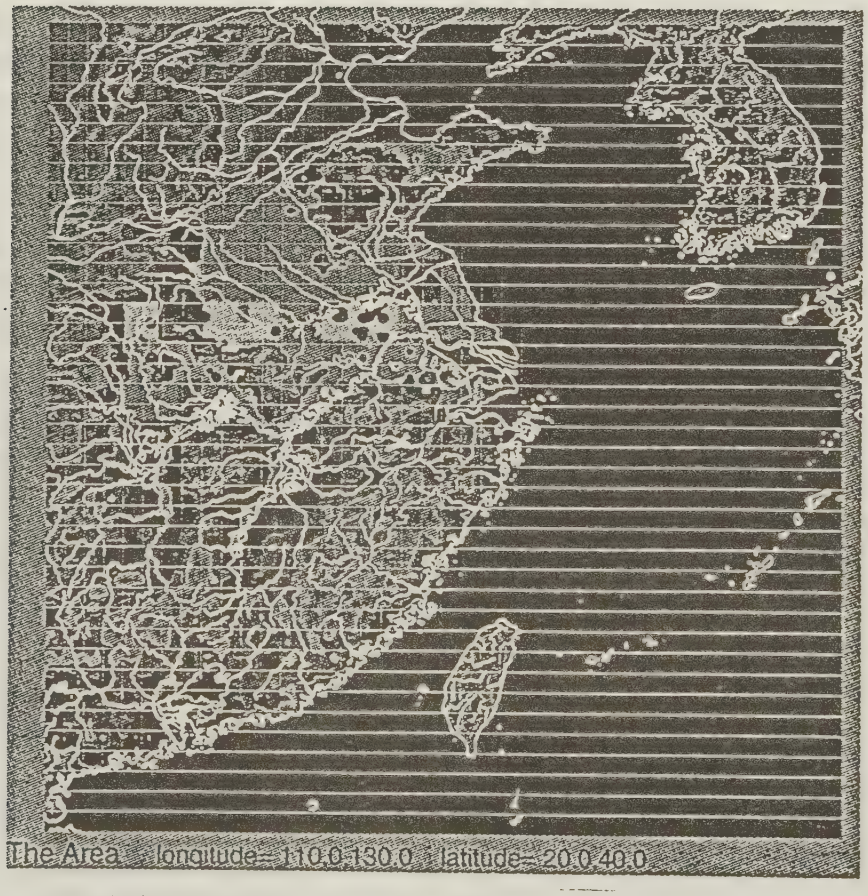

図3　アジア大陸広域水収支モデルの河川網データセット作成に用いた5分メッシュの標高データ及び世界データバンクIIの河川網の画像データ

Fig.3 Image of terrain contour map and river system using DTM data with 5 X 5 minutes resolution and the World Data Bank II respectively for making data-set of river system over Asian Continent.

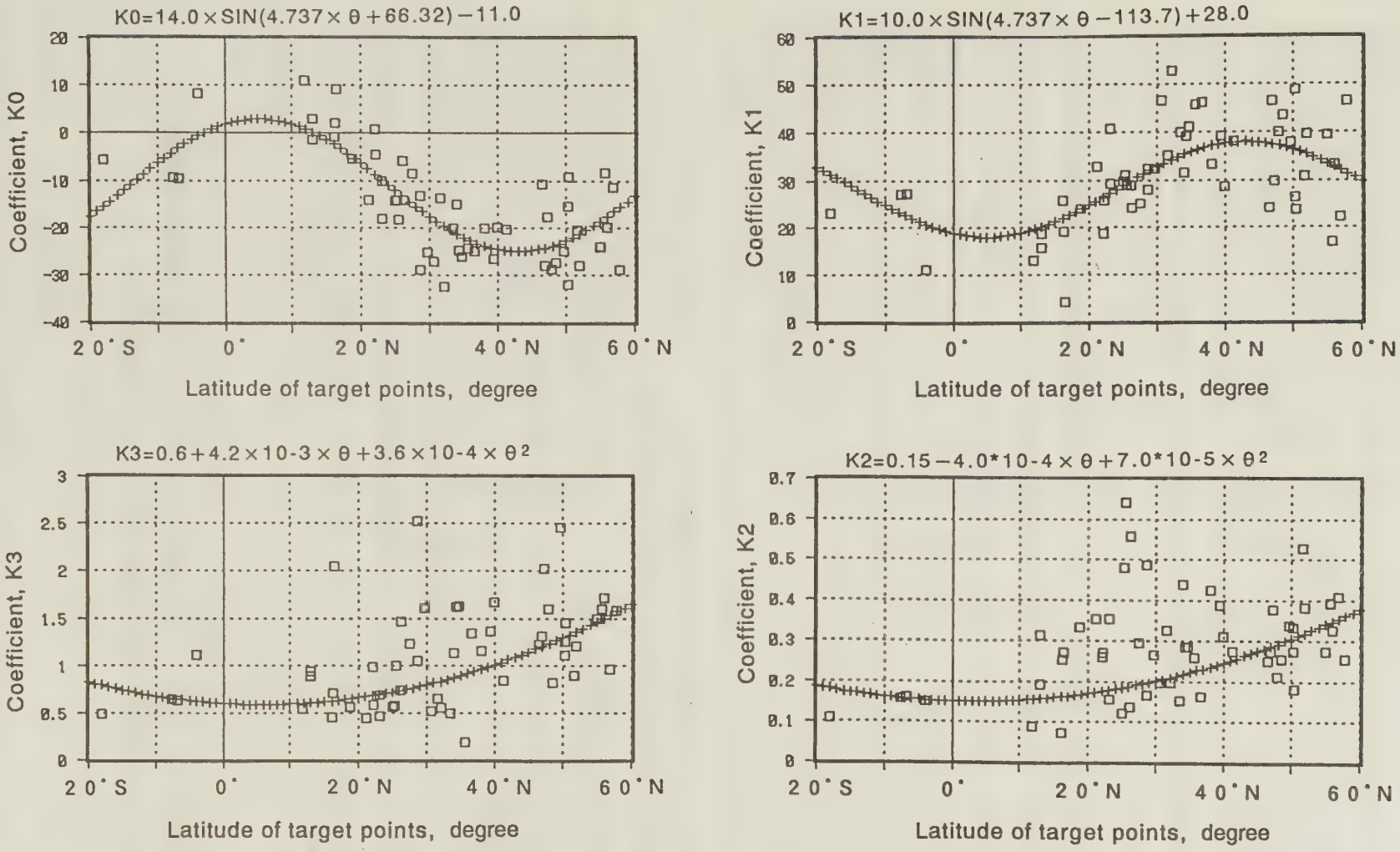

++++ : Derived function of local latitude, □ : Coefficient derived regression analysis between observed M-AT and M-RSI data at each target points

図4　月平均気温を求める回帰式の4つの定数を推定する計算式、この計算式は緯度の関数になっている。

Fig.4 Derived equations, which are functions of local latitude, for estimating coefficients(K0, K1, K2 and K3) in regression equations(Eq. 1) deriving M-AT.

(a)妥当な推定結果が得られた事例

(a) Results of appropriate estimation.

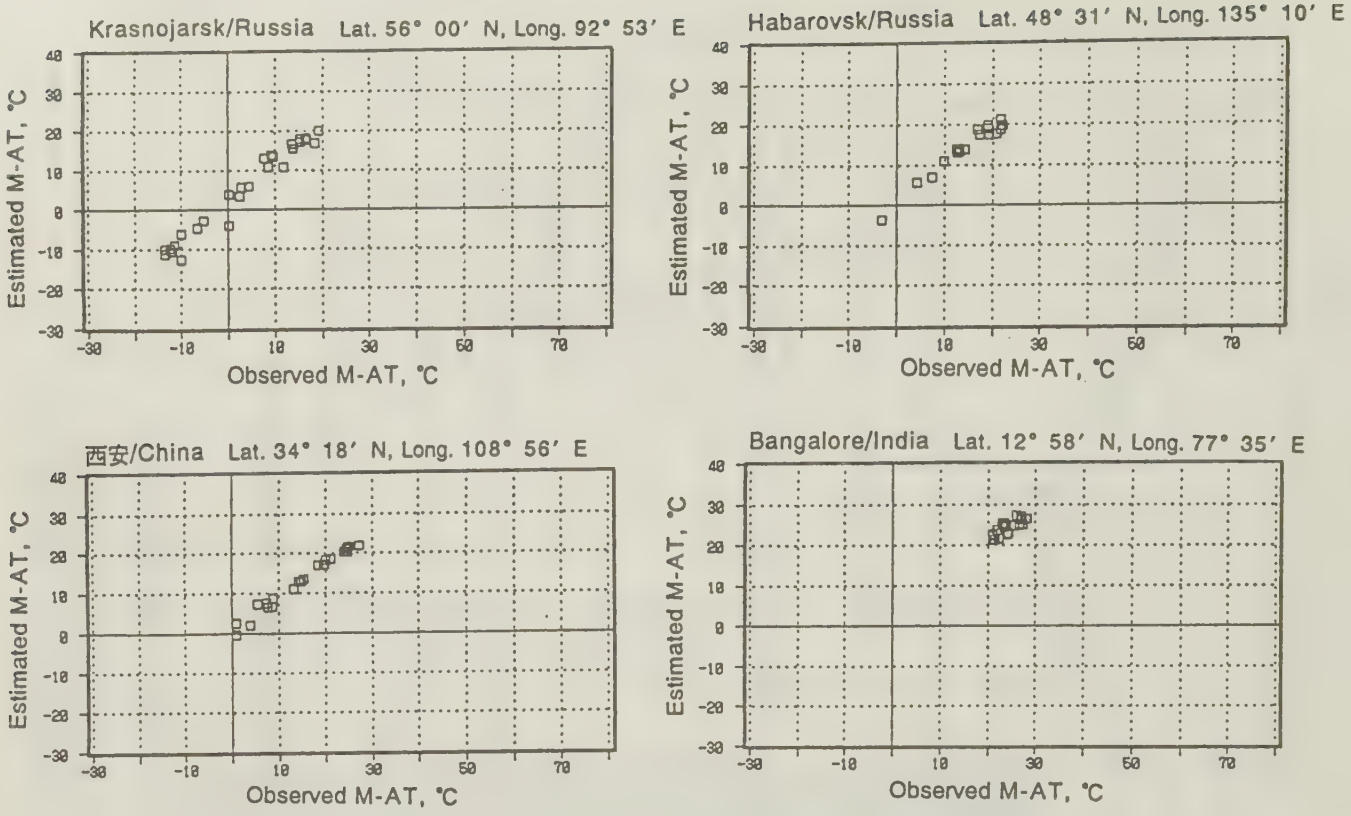

(b)推定した月平均気温に一定の誤差バイアスが現れた事例

(b) Results in which estimated M-AT had some bias of error.

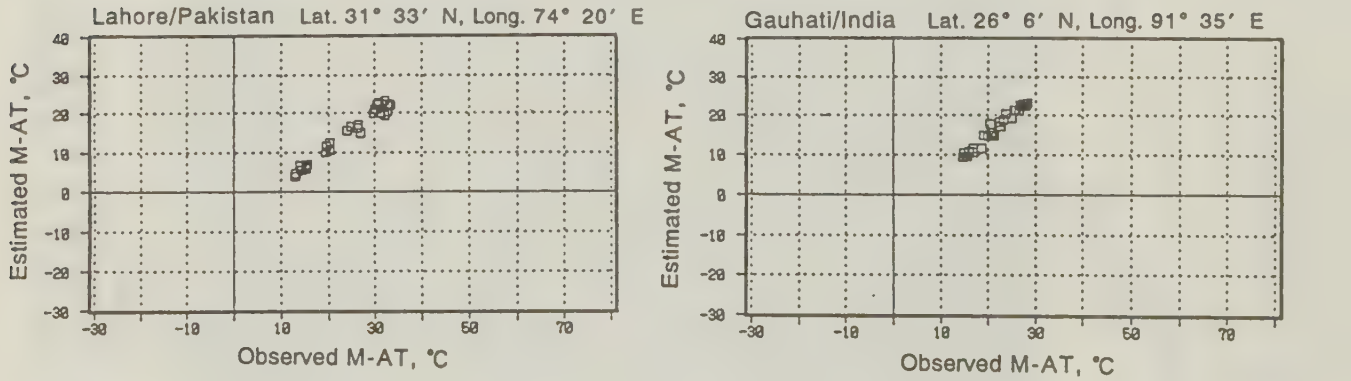

図5　緯度の関数として求めた係数を用いた月平均気温の推定

Fig.5 Estimation of M-AT(monthly mean air-temperature) by using coefficients (K0, K1, K2 and K3) derived by functions of local latitude.

4. Discussions

The RWB Model, which used same model's parameters in case of Chaophraya River basin in Thailand, had applied to Huaihe River basin from 1984 to 1988. These results could not give reasonable estimation in dry years comparing wet years. The cause was seemed that rainfall data were not representative in the basin, because these data had observed only along the river and effects of dam control were not considered. In this year, more dense data were acquired. The cause will be clear when RWB model will be applied again using dense data.

Study for making data-set of RWB model over the Asian Continent were going to be implemented. These data-set were examined to be made by using DTM data with 5 x 5 minutes resolution and world data bank II automatically. However, the quality of these data were still not good for tracing ridges and valleys automatically. Now, half automatic method were used. The method is that simplified river system and it's boundary were identified by human judgement, after drawing contour map and river system by using data-set of DTM with 5 x 5 minutes resolution and world data bank II. Then, data-set of river system were made automatically, after pointing out most upstream of the big river systems. The method is still hard to use in wide area. Therefore, it is better to wait accurate data-set of DTM and river system over the Asian Continent.

Coefficients(K0, K1, K2 and K3) in regression equations deriving M-AT relate with A-WVP(annual mean water vapor pressure) at target point. The distribution of A-WVP over the Asian Continent depend on local latitude. From these relations, equations estimating applicable coefficients in wide area were obtained as functions of latitude at target point. Coefficients derived by these equations were applied to estimate M-AT in wide area. Results were fairly good at several points. In other points, however, estimated values had some bias comparing observed one, though correlation between estimated M-AT and observed one were very high. It seems that the bias will be explained by local altitude and NDVI(normalized differential vegetation index). The problem will be investigated in the nest step of the study.

5. References

1)K. Nakane et al.; Regional Image Processing for NOAA AVHRR data Part II Composition of the wide Regional Image, Report on the 16th Remote Sensing Symposium,67-70(1990).

2)K.Nakane; Estimation of Monthly Mean Air Temperature over Asian Area

using GAC Data of NOAA AVHRR, Journal of Japan Remote Sensing Vol.13 No.1, 14-26(1993).
3)M. Sugawara et al.; Tank Model with Snow Component, Research Notes of the National Research Center for Disaster Prevention No.65, 1-293(1984).
4)C.W. Thornthwaite; An Approach Toward a Rational Classification of Climate, Geographical Review Vol.38, 55-94(1948).
6)S. Yazaki et al.; Regional Image Processing for NOAA AVHRR data Part I Geometric Correction and Map Projection, Report on the 16th Remote Sensing Symposium, 63-66(1990).

6. Publication

1)K. Nakane ; Regional Water Balance Model, Proceedings of 1995 Annual Conference, Japan Society of Hydrology and Water Resources, 130-131(1995).

7. International Cooperation

These studies are being carried out cooperatively with RSTAC/MWS(Remote Sensing Technology Application Center, Ministry of Water Resources in China) and SMRI/SMR/CMA(Satellite Meteorology Research Institute, Satellite Meteorology Center, China Meteorological Administration). In this fiscal year, we had cooperated as follows;

(1)Invitation of Chinese researcher from Feb. 28 to March 28

NIED(National Research Institute for Earth Science and Disaster Prevention) had invited a researcher from RSTAC/MWS. We cooperated to analyzing land surface conditions related to hydrological factors using MOS-1 data on Huaihe River basin and visited Ohyodo River basin for making data-set of RWB Model.

(2)Visit to RSTAC/MWS and SMRI/SMR/CMA

Nakane visited RSTAC/MWS from Feb. 3 to Feb. 12. he exchanged research ideas on analysis of the land surface conditions using satellite data and visited hydrological stations. he also installed the new software to the soil moisture apparatus. Dense data for precipitation at 20 stations , discharge of river at 9 stations, and discharge of 6 dams in Huaihe River basin from 1983 to 1991 were acquired. Some of data were acquired until 1987. In SMRI/SMR/CMA from Feb.13 to Feb. 17, he exchanged research ideas on analysis of the land surface conditions using satellite data and visited the agricultural observatory in Baoding in the west of Beijing for installing the new software to the soil moisture apparatus.

和文抄録

本研究は広域にわたるアジアモンスーン地域を対象として、降水、積雪・融雪、蒸発散、河川流出等の水文過程を的確にモデル化し、アジアモンスーンの変動が地域の水資源及び土壌水分に与える影響を0.5°×0.5°(約50km×50km)の等緯度経度の計算密度で詳しく評価できる広域水収支モデルの開発を目的としている。本研究で開発する広域水収支モデルは広域の地表を０.５度×０.５度の領域にメッシュ分割し、降水量、蒸発量、気温等から任意の地域の河川流量、水の流域貯留量（土壌水分量、地下水量など）、実蒸発散量等を計算するモデルであり、この種の広域の計算に使用されている大気大循環モデルよりも詳細に適切な広域の水資源情報を提供する。この広域水収支モデルはタンクモデルの概念を基本とし用いている。初期的な広域水収支モデルは乾期と雨期のある熱帯域に位置するタイのチャオプラヤ川流域（解析対象面積１１万ｋｍ2）に適用し、良好な予測結果を得た。現在、このモデルは中国の淮河流域（解析対象面積１２万ｋｍ2）及び日本の大淀川流域（解析対象面積２千ｋｍ2）において検証・評価を行っている。また、本研究の最終目標であるアジア大陸の広域水収支モデルを構築するため、地表状態を簡略化した河川網のデータセット作成手法の研究に着手した。この広域水収支モデルは入力データとして膨大な観測データを使用するが、これら広域のデータを密に収集するのは困難である。特に、蒸発量データは困難である。そのため、衛星データを用いた蒸発量の推定研究も行っている。蒸発量は気温と密接に関係しており、NOAA AVHRR GACデータを用いた月平均気温の新しい推定手法を開発し、その一般化手法の検討を行っている。これら研究の今年度の主な成果は以下の通りである。

(1)中国の淮河流域において、広域水収支モデルの検証・評価をより詳細に行うため、山地の降水量、蒸発量及びダム地点流量のデータを収集し、1983年から1989年の7年間の入力データセットを作成した。

(2)アジア大陸の広域水収支モデル作成において、広域の地表状態を適切に簡略化し、河川網を作成することが重要であるが、データ量が膨大なため人力作業では困難であり、また、河川網の簡略化作業が複雑なため、計算機で自動的に作成するのも困難である。そこで、半自動の作成手法を開発した。

(3)月平均気温の推定に用いた回帰式は４つの定数を持ち、それらは地域依存性を有している。この地域依存性は大気中の水蒸気量に関係しており、また、この水蒸気分布は緯度と関係していることが分かった。そこで、４つの定数を緯度の関数として求め、それらを用いて、広い地域の月平均気温を推定した。その結果、幾つかの地域で妥当な推定結果を得た。しかし、他の地域では地域ごとの定数バイアスが生じることが分かった。

III. Synthetic Study on the Atmosphere-Ocean-Land Interactions
大気・海洋・陸面間の相互作用に関する総合研究

1. Experiment of the Atmosphere-Ocean-Land Interactions by the Use of General Circulation Models
大規模モデルによる大気・海洋・陸面間の相互作用に関する実験研究

Meteorological Research institute,
Japan Meteorological Agency
A. Kitoh, K. Mabuchi and
T. Ose
気象庁気象研究所
鬼頭　昭雄、馬淵　和雄
尾瀬　智昭

(Abstract)

The impact of the anomalous sea surface temperature (SST) in the South China Sea (SCS) to the Asian summer monsoon is studied with a use of the Meteorological Research Institute atmospheric General Circulation Model (MRI AGCM). The results are summarized as follows. The SCS SST anomalies can affect (1) the onset and activity of the Asian summer monsoon, and (2) the atmospheric circulations in the northern Pacific in spring. The positive and negative SCS SST anomalies produce the different response in the summer monsoon circulations. The positive SCS SST anomalies are more influential to the circulations over the Indian Ocean, while a larger impact is found over the tropical Pacific for the negative SCS SST anomaly case.

The monsoon climatology simulated by the MRI global coupled atmosphere-ocean GCM (CGCM) is investigated. The overall monsoon region as defined by the seasonal change of wind direction and OLR agrees with the observed. However, the model failed to simulate summertime wind system in the western Pacific region. A comparison of the seasonal change of the lower and upper tropospheric zonal wind over the Indian monsoon region is also made.

1. Objectives

The monsoon is an essential part of climates in the Asian countries by contributing to establish an annual cycle in many meteorological elements. For some contries the monsoon is the climate. And the interannual variability of the Asian monsoon affects climate variations not only in Asia but also in larger parts of the globe because the Asian monsoon region is located close to the ocean with the warmest sea surface temperature and is the most vigorous heating source of the atmospheric general circulation.

The purposes of the present study are to clarify the mechanism of atmosphere-ocean-land interactions in an Asian monsoon region including the Pacific and the Indian Oceans and the Eurasian continent by performing a series of numerical experiments.

2. Methods

We use an atmospheric general circulation model (GCM) which includes interactive land surface processes (in the first phase of the program) and also an ocean-atmosphere coupled GCM (in the second phase). By a series of numerical experiments with atmospheric and/or coupled GCMs, roles of land surface conditions and sea surface temperature (SST) in establishing the monsoon and its variability will be investigated.

This year, we made a sensitivity study of the role of the South China Sea (SCS) SST on the atmosphere by the MRI atmospheric GCM. The model used for the SCS SST experiment is a 5-level version of the MRI atmospheric GCM (Tokioka, et al., 1984). The SCS is defined as the region between the equator and 20°N, enclosed with the Philippine islands and the Indochina peninsula. Two experiments are performed. One experiment with +1° SST anomalies (PEXP), the other one with -1° SST anomalies (NEXP). Each experiment consists of three integrations from February 1 to September 1. PEXP and NEXP are compared with the control with the climate SST.

We also made an analysis of a long integration of the MRI coupled atmosphere-ocean GCM (CGCM). The model has a 15-level atmosphere GCM with the top at 1 hPa and a 21-level ocean GCM. The sea-ice model is also included. The model was integrated for 70 years with flux adjustments. This is the control run of the transient CO_2 increase experiment (Tokioka et al., 1995).

3. Results

3.1 The South China Sea SST anomaly experiment

Shen and Lau (1995) showed that the SST of the SCS has the maximum spectral density at the periods of 2-3 years without any time-filter used. They also showed with a singular value decomposition (SVD) that there is a significant correlation between the summer southeast China precipitation and the SCS SST in June, July and August (JJA). The boreal winter (referred to as winter) SCS SST anomalies tend to be maintained until the following summer (not shown). If the SCS SST anomalies created in winter affect the Asian summer monsoon, the SCS SST could play an active role in producing the tropospheric biennial rhythm found in the Indian Monsoon, the East Asian Monsoon and the Pacific Ocean (Yasunari, 1991; Shen and Lau, 1995). In the above context, the effect of the SCS SST anomalies on the Asian summer monsoon is studied with use of the 5-layer MRI-GCM (Tokioka et al., 1984).

Figure 1 (a) shows the climatic 800 hPa zonal wind averaged for April and May. Figure 1 (b) and (c) are the same as Fig.1 (a) except for the PEXP and NEXP anomalies, respectively. Westerly and easterly anomalies are simulated to south of the

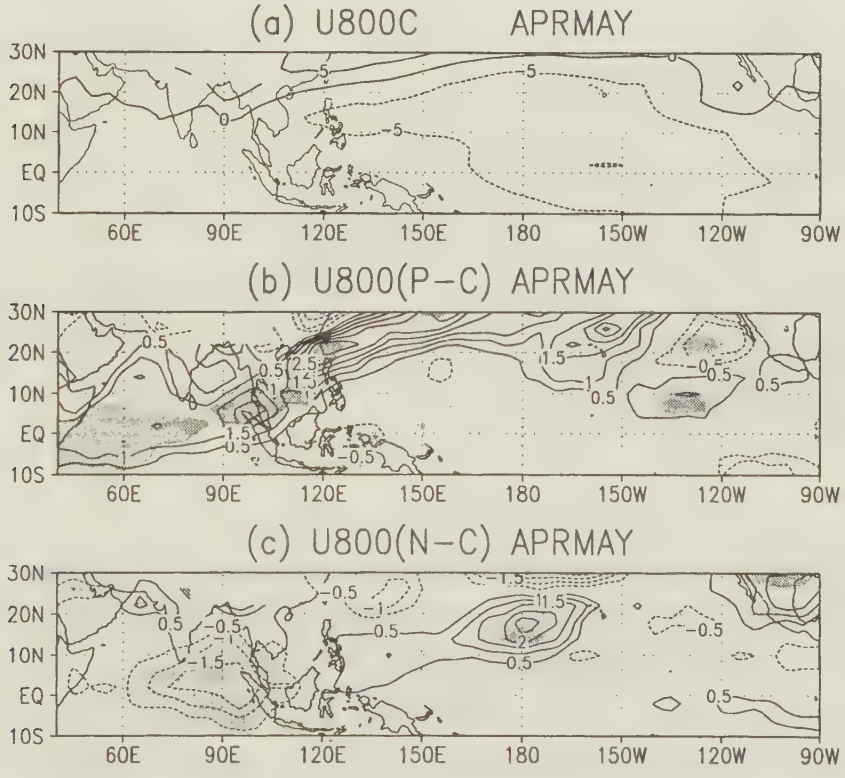

Fig. 1 Zonal wind at 800 hPa for April-May. (a) Control run. (b) Anomalies for PEXP. The 95% significant region is shaded. (c) As in (b) except for NEXP.

Bay of Bengal for PEXP and NEXP, respectively. The magnitude of the anomalies are comparable for PEXP and for NEXP. Those anomalies strongly influence the onset of the Southeast Asia monsoon. The onset occurs in the middle of May for PXEP and the middle of June for NEXP (not shown).

Figure 2 (a) (b) (c) are the same as Fig.1 (a) (b) (c) except for the average for JJA. The significant and large westerly anomalies (active Asian monsoon) are simulated over the Indian Ocean for PEXP. For NEXP, only small and negative anomalies are found in a part of the Indian Ocean. The anomalies in the equatorial Pacific contrast with those in the Indian Ocean. The westerly anomalies are significant over the equatorial Pacific for NEXP. Those magnitudes are three times as large as those of the easterlies for PEXP.

The impact of the SCS SST anomalies to the mid- and high latitudes atmosphere appears in April and May. The positive 500 hPa geopotential height anomalies are found widely over the northern Pacific in April for NEXP (Fig.3a). The similar but negative anomalies are produced in May for PEXP (not shown). The above results are confirmed from the observational data (Fig.3b; not shown for PEXP).

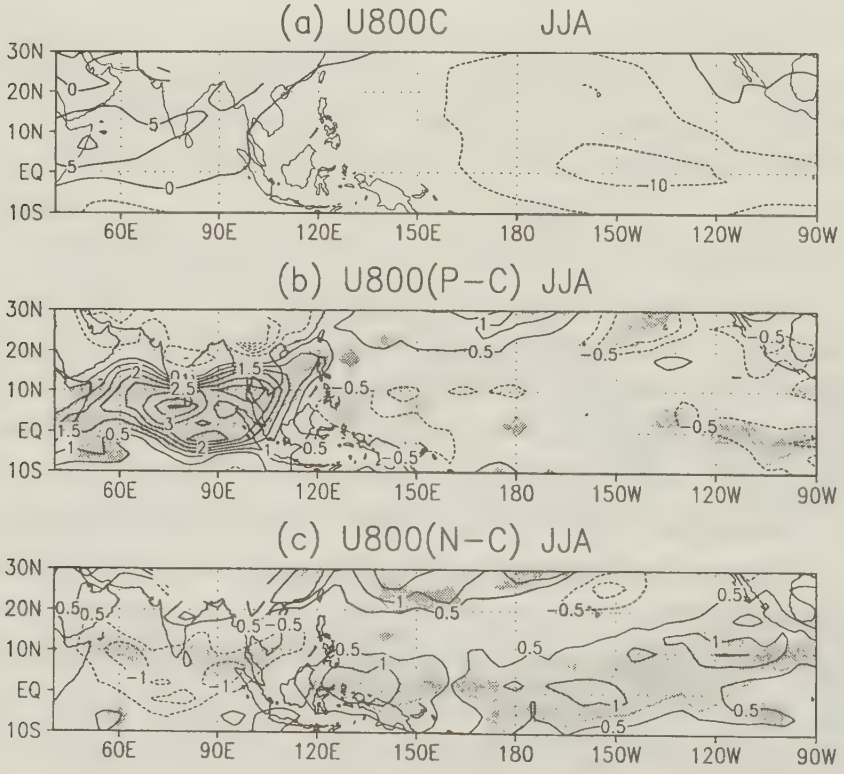

Fig. 2 Zonal wind at 800 hPa for June-July-August. (a) Control run. (b) Anomalies for PEXP. The 95% significant region is shaded. (c) As in (b) except for NEXP.

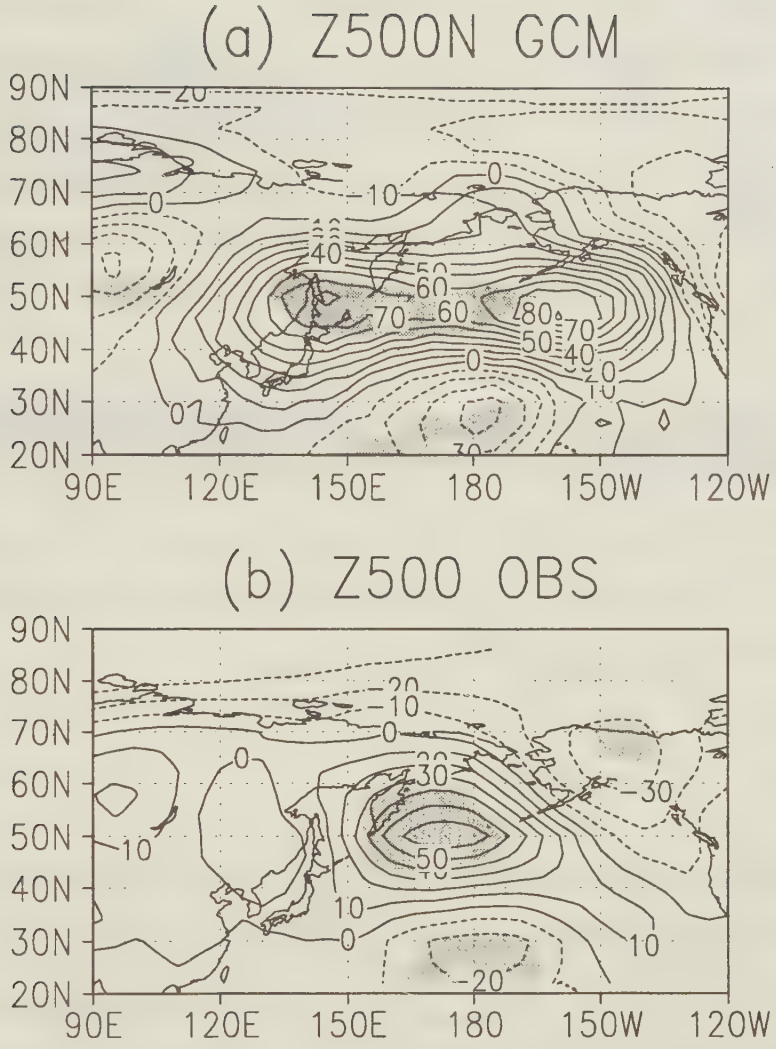

Fig. 3 (a) Geopotential height anomalies at 500 hPa in April for NEXP. The 95% significant region is shaded.
(b) Observed composite anomalies corresponding to the negative SCS SST anomalies.

3.2 Monsoon in the MRI coupled GCM

First, we define the monsoon region simulated by the MRI CGCM. Figure 4 shows the simulated monsoon region by two methods. Large dots are the monsoon region followed by Murakami and Matsumoto (1994) where the summertime OLR is less than 240 W m^{-2} and the seasonal change of monthly mean OLR is greater than 60 W m^{-2}. Compared to the observed (Fig. 1 of Murakami and Matsumoto, 1994), the monsoon area extends northward of 20°N in the model. This corresponds to the northward shift bias of the subtropical anticyclone. The hatched area is where the monthly mean wind direction between January and July shifts more than 120° at 850 hPa. This broadly agrees with the observation (see Fig. 3 of Kitoh and Tokioka, 1987). One of differences is that the South China Sea is not classified as the monsoon region in the model. This is because the summertime 850 hPa winds flow along the Tibetan plateau from the Indian Ocean to China and the westerlies do not penetrate into this region.

Figure 5 shows the seasonal change of zonal winds at 850 hPa and 200 hPa averaged over 40°-110° E, 0° N-20° N. The magnitude of both the lower and upper troposhperic zonal wind in the Indian monsoon region is well simulated by the CGCM. As for the seasonal march, the model is slightly ahead of the observed one. Corresponding to this, the snow cover over the Tibetan plateau also disappears earlier in spring than the observed (not shown).

4. Discussions

The atmospheric GCM experiment showed that the SCS SST affects the Asian summer monsoon circulations not only over the regions near the SCS but also over the Indian Ocean and the tropical Pacific, especially in JJA. The SCS SST anomalies are mainly created by the strength of the winter cold surge from the Eurasian Continent. According to the results, the high SCS SST created by the warm winter, can bring the early onset of an active Asian monsoon in the following summer. Some interesting questions to solve are left. One is the contrast of the lower zonal wind response over the Indian Ocean and the Pacific Ocean for the PEXP and NEXP. It may be related to the nonlinear response of the precipitation to the SST anomalies over the SCS in summer. The second is why the extra-tropical circulation anomalies appear in April and May.

The coupled model showed some discrepancy in reproducing the monsoon in the western Pacific region. However, the broad-scale features of the Asian monsoon are well reproduced. We plan to investigate the relationship among the monsoon, model El Niño and the land surface conditions over the Eurasia continent.

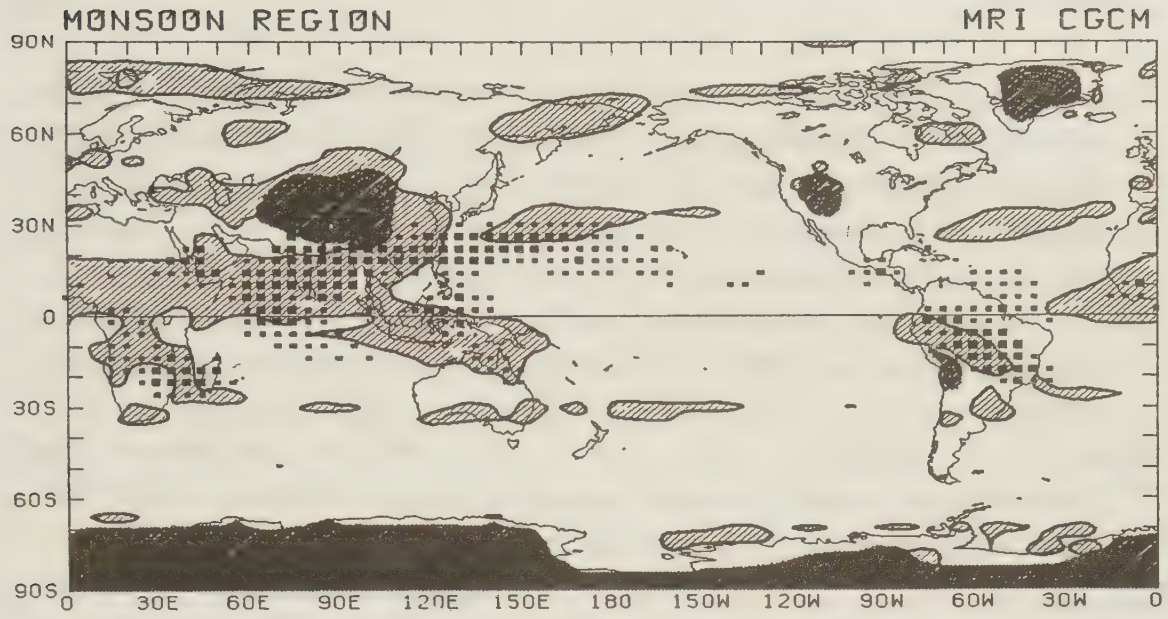

Fig. 4 Monsoon region in the MRI CGCM.

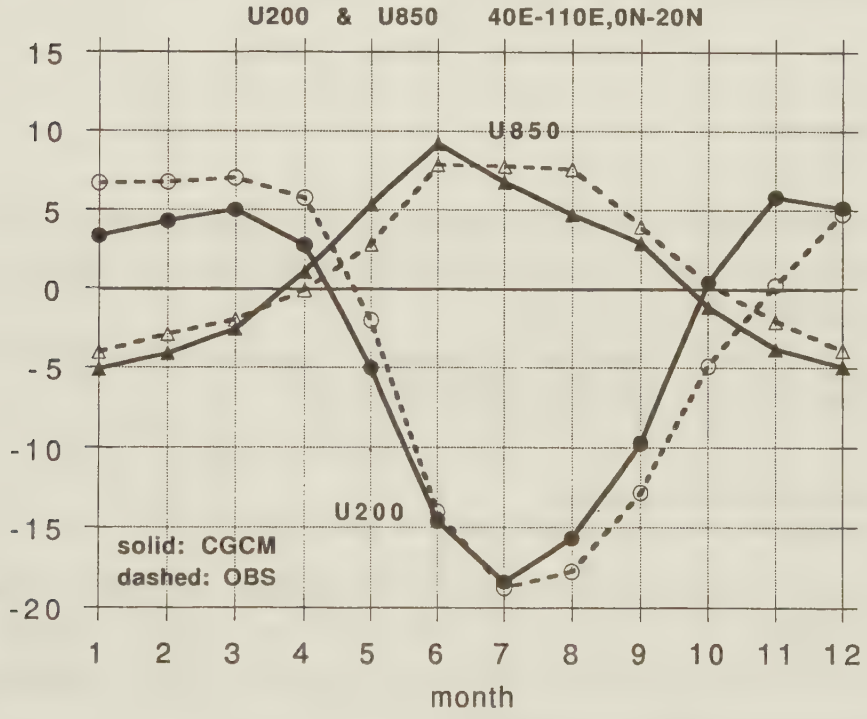

Fig. 5 Zonal wind at 850 hPa and 200 hPa averaged for 40°E -110°E, 0°N-20°N.
Solid: MRI CGCM. Dashed: Observation.

5. References

Kitoh, A. and T. Tokioka, 1987: A simulation of the tropospheric general circulation with the MRI atmospheric general circulation model. Part III: The Asian summer monsoon. *J. Meteor. Soc. Japan*, **65**, 167-187.

Murakami, T. and J. Matsumoto, 1994: Summer monsoon over the Asian Continent and western North Pacific. *J. Meteor. Soc. Japan*, **72**, 719-745.

Shen, S. and K.-M. Lau, 1995: Biennial oscillation associated with the east Asian summer monsoon and tropical sea surface temperature. *J. Meteor. Soc. Japan*, **73**, 105-123.

Tokioka, T., K. Yamazaki, I. Yagai and A. Kitoh, 1984: A description of the Meteorological Research Institute atmospheric general circulation model (The MRI-GCM-I). Tech. rep. of the MRI. No.13. 249pp.

Tokioka, T., A. Noda, A. Kitoh, Y. Nikaidou, S. Nakagawa, T. Motoi and S. Yukimoto, 1995: A transient CO_2 experiment with the MRI CGCM -Quick report-. *J. Meteor. Soc. Japan*, **73**, 817-826.

Yasunari, T., 1991; The monsoon year - A new concept of the climate year in the tropics. *Bull. Amer. Meteor. Soc.*, **72**, 1331-1338.

6. Publications

Kitoh, A., 1995: Observation and simulation of the relationship between the global sea surface temperature variability and the 500 hPa height in the northern summer. *J. Meteor. Soc. Japan*, **73**, 247-253.

Kitoh, A., A. Noda, Y. Nikaidou, T. Ose and T. Tokioka, 1995: AMIP simulation of the MRI GCM. *Pap. Met. Geophys.*, **45**, 121-148.

7. International Cooperation

One researcher, Mr. Song Yukuan, of the Chinese Academy of Meteorological Sciences (CAMS) was invited to the MRI for 32 days from 1 October 1995 to 1 November 1995 to carry out an SST anomaly experiment with the MRI GCM. The model output was provided to the CAMS.

One researcher, Dr. Akio Kitoh, of Japan Meteorological Research Institute (MRI) was invited to Beijing and Guangzhou for 16 days from 13 June 1995 to 28 June 1995 to attend the workshop and discuss research results.

要旨

中国国家気象局気象科学研究院から招聘した研究員とともに、南シナ海の海面水温偏差がアジアモンスーンに与える影響を調べる数値実験を行った。その結果、南シナ海の海面水温偏差は、（1）夏のアジアモンスーンの開始時期と活動度、（2）春の北太平洋の大気循環に影響を与える、ことが示された。南シナ海の海面水温が正偏差の場合と負偏差の場合では、熱帯域の大気応答に地域性が見られる。正偏差の場合はインド洋で、負偏差の場合は熱帯太平洋で大きな応答が見られた。

気象研究所全球大気海洋結合モデルでのモンスーン循環について解析した。モンスーン域の面的な再現はほぼなされているが、季節推移が観測より若干早いことが分かった。

III. Synthetic study of the monsoon circulations
大気、海洋、陸面間の相互作用に関する総合研究

2. Analysis of the energy balance of monsoon
モンスーンのエネルギー収支に関する解析研究

Meteorological Research Institute (MRI)
Japan Meteorological Agency
Tomoaki Ose
気象庁気象研究所
尾瀬　智昭

(Abstract)

The air column heat budget of a General Circulation Model is obtained in association with the Asian summer monsoon. The characteristics of the heat budget over several regions in the Eurasian Continent are studied. The cause for the climatic temperature increase is considered from the heat budget.

The large increase of sensible heating contributes to the temperature increase over Tibet in summer. The air downward motion is important for the summer hot air over the arid region. The Siberia air temperature increases due to the condensation heating especially in mid-summer. The temperature over the ocean near Japan increases by the horizontal advection and the condensation heating in summer. The small temperature increase over the Indochina is due to the condensation heating. The diabatic heating is well balanced with the cooling due to the upward motion over the Indian Ocean.

1. Objectives

Asian monsoon is formed basically by the solar heat difference between land and ocean. In order to understand the mechanism of the Asian monsoon activities including its onset, it is one way to analyze the spatial and temporal variabilities of the energy budget associated with the Asian monsoon.

We have studied Earth Radiation Budget (ERB) at the top of the atmosphere in the Asian monsoon system. ERB at the top of the atmosphere is distributed into the other regions through the ground and ocean heat budget and through the atmospheric heat budget. It is important to know how ERB is distributed in the Asian monsoon system. As the first step, the atmospheric heat budget of the Asian summer monsoon simulated with the 5-layer Meteorological Research Institute Atmospheric General Circulation Model (MRI-AGCM;1: Tokioka et al., 1984) is studied with that purpose.

2. Methods

The GCM is integrated with three different initial conditions from February 1 to September 1. The data is interpolated from the GCM coordinate to every 100hPa pressure surface. Then, the three integrations are averaged to obtain the time series data for the GCM climate. The heat budget is analyzed twice a day (00Z and 12Z).

The heat budget comprises the net increase of temperature, horizontal advection, vertical advection plus adiabatic compression, and diabatic heating. The diabatic heating is separated to condensation heating, sensible heating from the ground, net radiative heating. These terms are obtained from the GCM output once an hour. All heat budget terms are averaged vertically with mass weight in the whole air column.

3. Results

Fig.1(a),(b), and (c) show the increase of the mass weighted average air temperature during February and March, April and May, June and July, respectively. The air temperature increase from spring to summer is apparently large over the Eurasian Continent as compared with oceanic regions in the tropics.

The air column heat budget for several regions is shown next.

a. Tibet region (30°-42°N,70°-100°E)

Tibet already becomes warm during early spring. But the large increase of the temperature is found in April and May. Fig.2 (a) shows the heat budget of the air column over Tibet from February to September. Each month is represented with three about 10 day periods. DT(C) is the net temperature increase, -UDT(C); the temperature increase due to horizontal advection, -WDT(C); vertical advection plus adiabatic heating, RESID(C); diabatic heating.

DT(C) is positive during almost all periods from March to July. The change of RESID(C) is roughly balanced with the change of -WDT(C). -UDT(C) is constantly negative due to the advection of relatively cold air.

Fig.2(b) shows the contents of the diabatic heating rate Q1(C) over Tibet. Q1(C) corresponds to RESID(C) except for the difference in the data time sequences and the analysis error. LTOTP(C) is the condensation heating rate, FSS(C); the sensible heating rate from ground, NETR(C); the radiative heating rate. LTOTP(C) contributes to positive DT(C) through the season. -WDT(C) and FSS(C) also contribute to positive DT(C) in spring and summer, respectively.

b. Arid region (30°-50°N,50°-70°E, land only)

Fig.3 is the same as Fig.2 except for the arid region. The arid region air becomes warm during June and July. -WDT(C) increases from May to July. The downward motion warms the arid region air together with RESID(C). The cool air advection from the west balances to those terms. The increase of Q1(C) is due to the large increase of FSS(C). FSS(C) is comparable with -WDT(C) in summer. LTOTP(C) becomes small in summer.

c. Siberia region (50°-90°N,90°-160°E, land only)

Fig.4 is for Siberia region. The temperature increase DT(C) is positive from March to August. Large DT(C) is found in June and July. The negative RESID(C) is roughly balanced with the warm air advection from the west due to -UDT(C) in spring. LTOTP(C) increases gradually from March and drastically in June and July. LTOTP(C) apparently contributes to positive DT(C) in summer. FSS(C) is relatively small almost all months.

d. Ocean near Japan region (30°-50°N,130°-160°E, ocean only)

Fig.5 is for near Japan region. Positive DT(C) is found from April to July. The diabatic heating and the cool air advection from the continent are cancelled in spring to large extent. LTOTP(C) is relatively maintained through the season as compared with FSS(C). -UDT(C) becomes positive

and is comparable to LTOTP(C) in summer. -UDT(C) contributes to DT(C) in summer.

e. Indochina region (10°-26°N,90°-120°E, land only)

Fig.6 is for Indochina region. Indochina region starts to get warm from early spring. The magnitude of DT(C) is very small. RESID(C) is well balanced with -WDT(C). LTOTP(C) is dominant in Q1(C). FSS(C) and -UDT(C) are relatively small.

f. Indian Ocean region (6°-14°N,70°-100°E)

Fig.7 is for Indian Ocean region. DT(C) is very small. RESID(C) is well balanced with -WDT(C). Q1(C) is controlled by LTOTP(C). FSS(C) and -UDT(C) are negligible.

4. Discussions

The model results will be compared with the observational study. For example over Tibet, the heat budget seems to be rather different from the observational results (2: Yanai, et al., 1992). The condensatiion heating is large even in spring. The comparison will contribute to the improvement of the model.

5. References

1) Tokioka, T., K. Yamazaki, I. Yagai and A. Kitoh, 1984; A description of the Meteorological Research Institute atmospheric general circulation model (The MRI-GCM-I). *Tech. rep. of the MRI.* No.13. 249pp.

2) Yanai, M., C. Li, and Z. Song, 1992: Seasonal heating of the Tibetan Plateau and its effects on the evolution of the Asian summer monsoon. *J. Meteor. Soc. Japan*, **70**, 319-351.

6. Publications

Oral presentation

speaker : Tomoaki Ose

Title : The MRI-GCM response to the regional snowmass anomalies

Prints : Abstracts for the Japanese Meteorological Society Spring Meeting in 1995 (in Japanese)

7. International Cooperation

None

要旨

アジアモンスーンに関連して、大気大循環モデル大気の熱収支を調べた。大陸のいくつかの地域での熱収支の特徴から、春から夏にかけての気候的な気温上昇の原因を考察した。

チベットでの春から夏にかけての気温の上昇には、凝結熱とともに、この期間、大きく増加している顕熱が寄与している。大陸西部の乾燥域では、夏期に昇温が大きく、これには、春から増加する顕熱とともに、夏期の下降流の強まりが寄与している。シベリアでは、他の地域に比べて、夏期に昇温が大きく、これには凝結熱の急激な増加が対応している。日本付近の海域では、凝結熱とともに、夏期は水平移流が寄与する。インドシナでは、凝結熱によると想像される気温の上昇が見られるが、わずかである。インド洋では、非断熱加熱と上昇流による冷却がよく釣り合っていて、気温の変化はほとんどない。

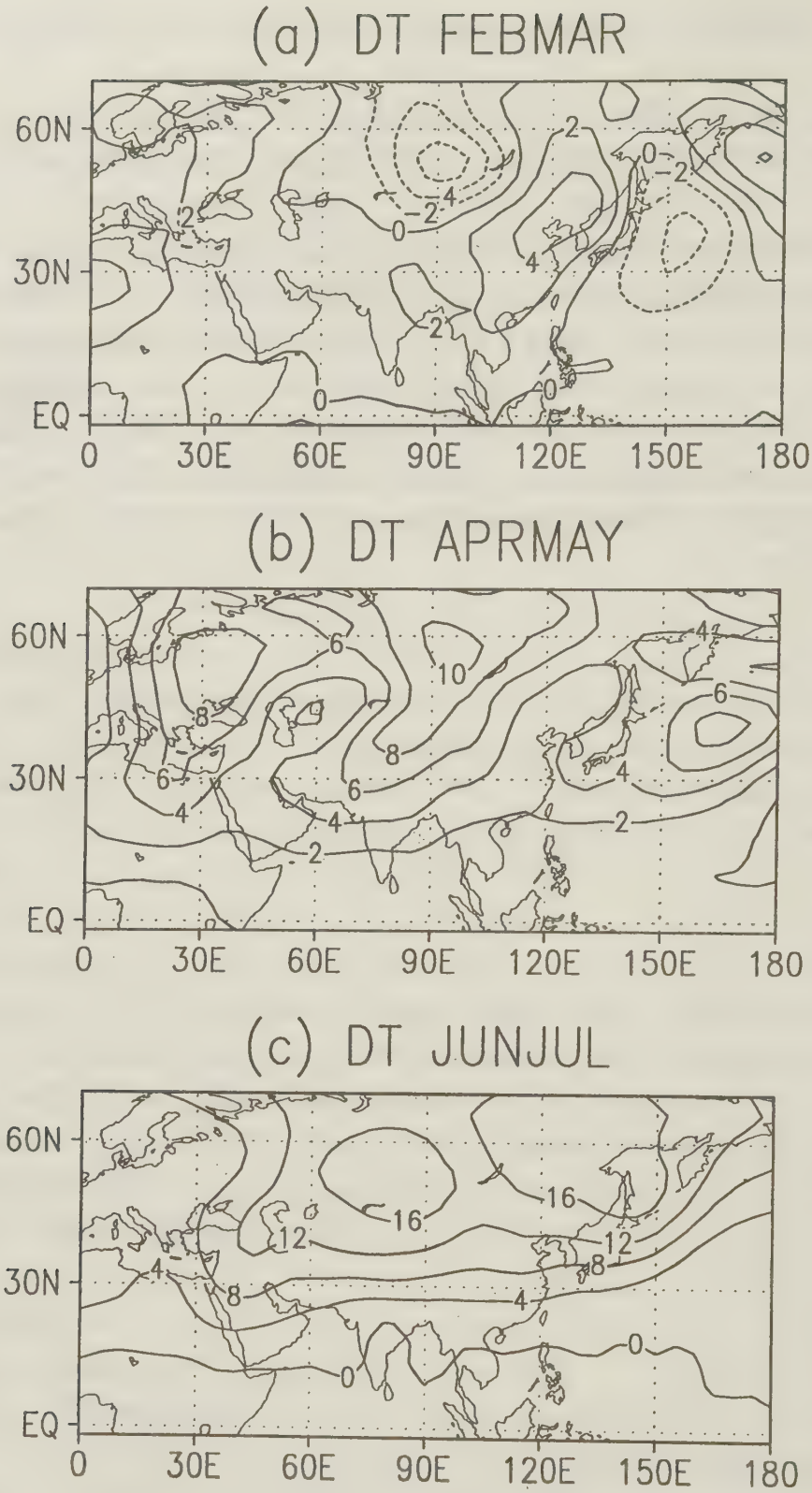

Fig.1 The temperature increase during (a) February and March, (b) April and May, (c) June and July. Unit is K.

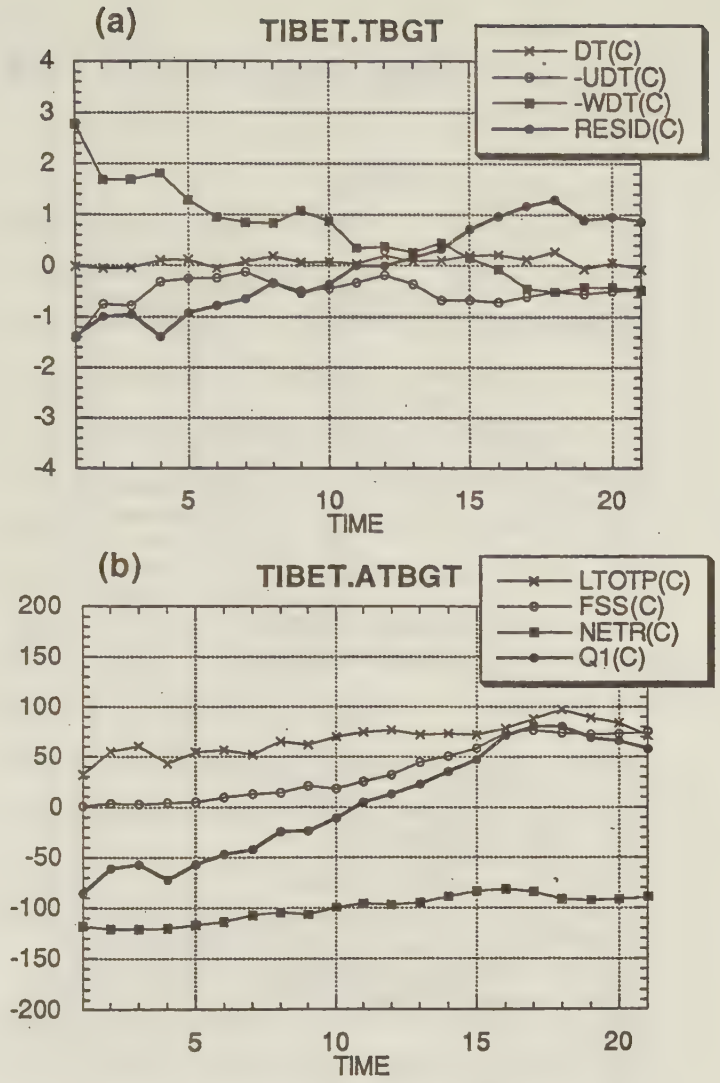

Fig.2 (a) The air column heat budget over Tibet. Unit is K/day. Time is from February through August. Each month is represented with three units. (b) The content of the diabatic heating. Unit is W/m^2. Time representation is the same as (a).

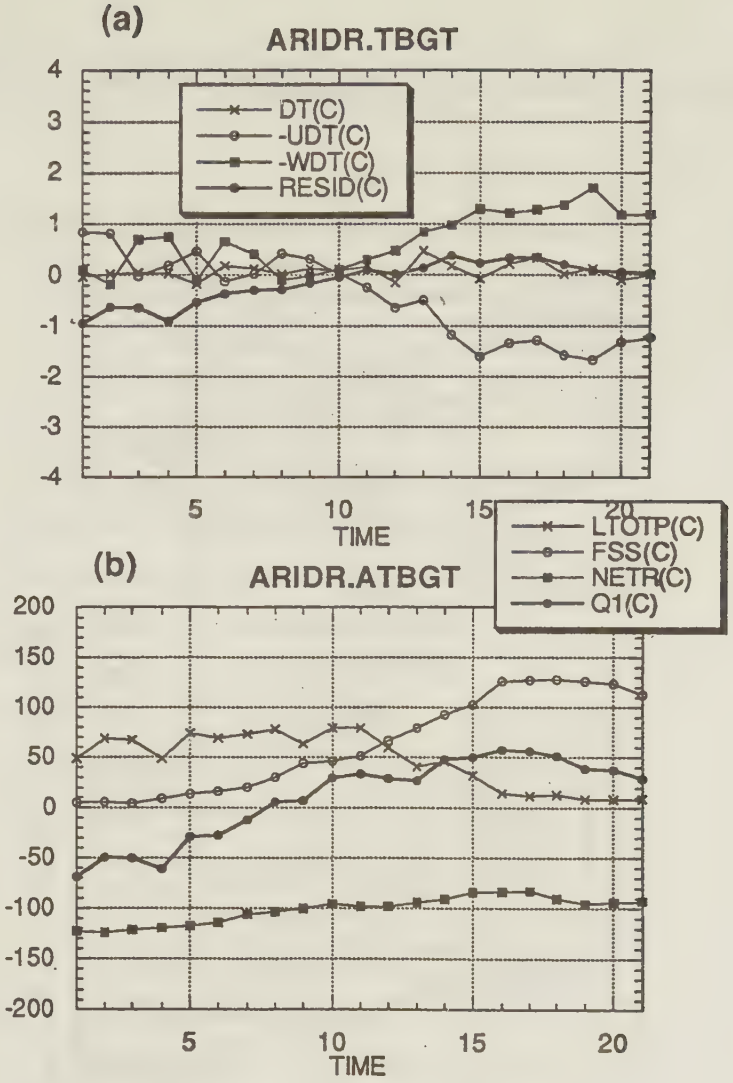

Fig.3 The same as Fig.2 except for the arid region.

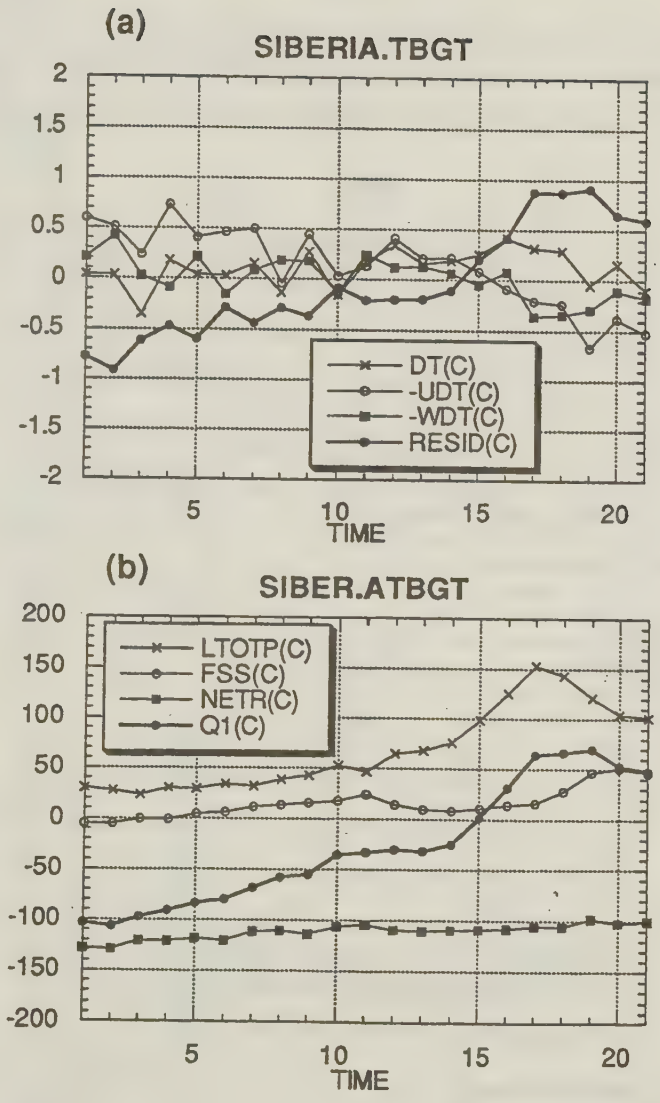

Fig.4 The same as Fig.2 except for the Siberia.

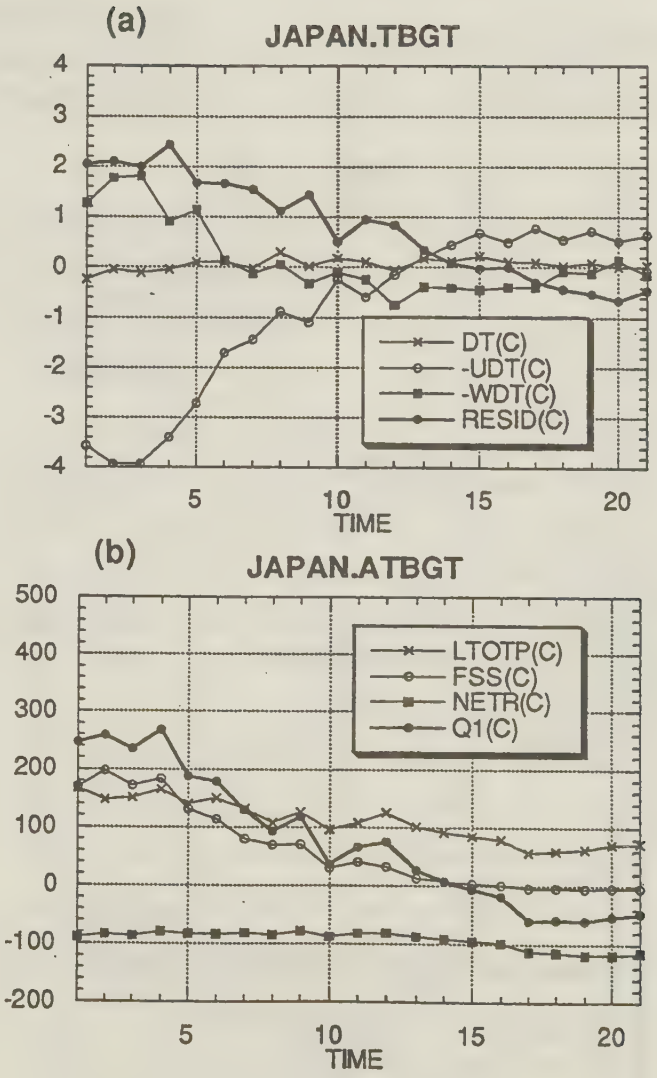

Fig.5 The same as Fig.2 except for the ocean near Japan.

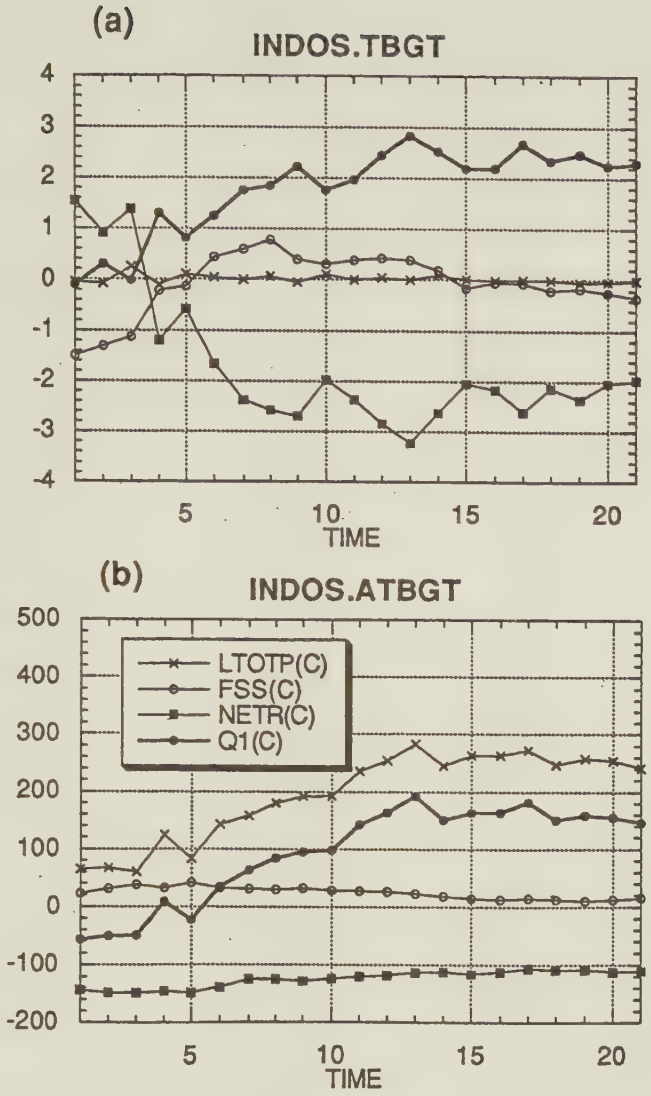

Fig.6 The same as Fig.2 except for the Indochina.

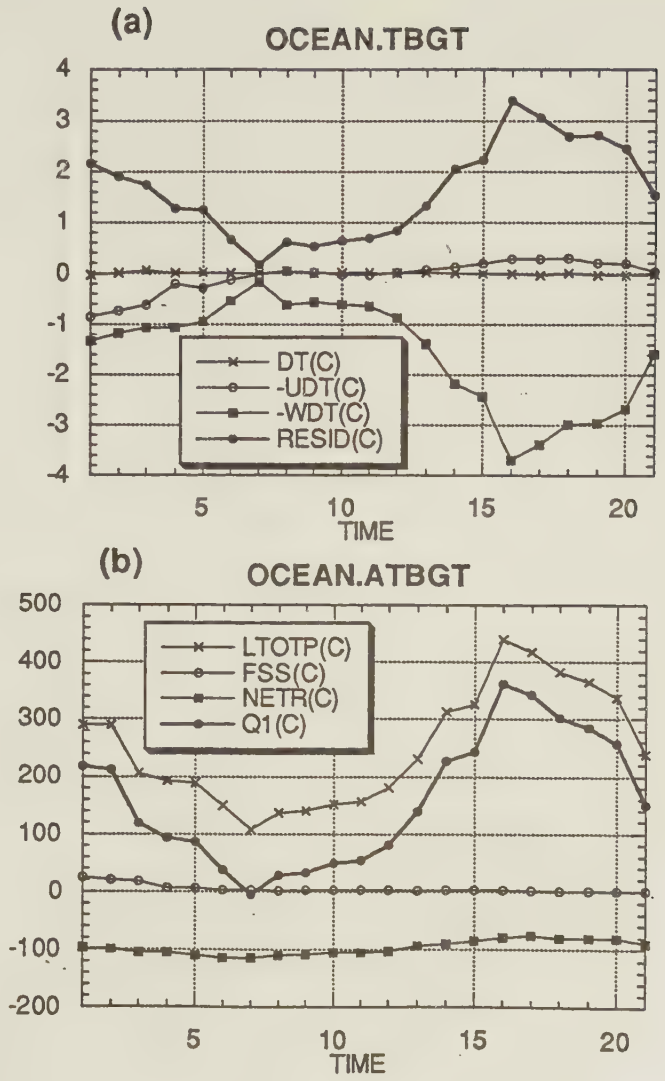

Fig.7 The same as Fig.2 except for the Indian Ocean.

Ⅲ. 大気・海洋・陸面間の相互作用に関する解析的研究
Ⅲ. Synhtetic study on the atmosphere-ocean-land interactions

3.モンスーン循環系の総合的解析
3. Synthetic study of the monsoon circulaions

気象庁
予報部
長期予報課
藤川典久、多田一正
N. Fujikawa, K. Tada
Long-range Forecast Division
Forecast Department
Japan Meteorological Agency

(**Abstract**) In the summer of 1994, the record high temperature and the significantly small amount of precipitation took place over the most parts of Japan during July and August. To investigate the cause of the prominent observation data and their relation to the asian monsoon circulation, heat budget analysis and vorticity analysis were made in the large scale. The activity of asian monsoon in this year was also analyzed by the deviation from normal in outgoing longwave radiation (OLR) data.

The wind analysis at 500hPa along the longitude showed the northward movement of strong westerly wind around Japan, which started half a month earlier than normal. Such a change was also analyzed in Indian region . After that the Tibetan high extended remarkably towards the northeast side and the subtropical high extended to Japan. The barotropic high around Japan was formed as a result of an influence of both highs. The record high temperature was caused by the subsidence of the air in this barotropic high and the supply of sensible heat from the ground surface.

At that time the convective activity around Phillipine islands was stronger than normal and gave some influence on the maintenance of the high over Japan, though for a short time. It appears that the maintenance of the barotropic high and the weak rainy front brought the small amount of precipitation to Japan.

Asian monsoon in 1994 was more active compared with the normal and caused the stronger meridional circulation around India than normal and the northward movement of the strong westerly wind accompanied with the cloud.

1. **Objectives**

The asian monsoon circulation shows the variation on the time scales from several ten days to several years and has a sifnificant influence on the climate in Japan and the world through the global atmospheric circulation. The purposes of this study are to clarify long-term variations of the monsoon circulation and to assess the influence on the climate in Japan and the world by the observational data analysis.

2. **Methods**

The data of July was mainly used in this paper as a representative of the summer (June, July, August). The global objective analysis data in Japan Meteorological Agency were also used in the grid point (2.5° x 2.5°) and the normal values are defined as the mean from 1988 to 1993 except for OLR. The cross-section of vorticity and temperature were produced along the latitude or longitude to investigate the atmospheric characteristics. The latitudinal variation of the strong westerly wind is calculated by the five-day running mean. The deviation from normal in outgoing longwave radiation was calculated in terms of the monthly mean for July.

3. **Results**

Figure 1 represents the negative vorticity over Japan from ground to upper tropospher, which indicates barotropic structure. The lower troposphere over Japan is covered with the positive vorticity in the normal, which indicates a relation of the rainy front.

Figure 2 shows that the temperature of the air mass over Japan has the vertical profile of positive deviation from normal. The temperature near the ground surface is about 3 degrees higher than normal. This value almost corresponds to the analysis of the observations in the summer of 1994.

Figure 3 indicates the northward movement of strong westerly wind. This event appeared in the late June and about half a month earlier compared with the appearrance in the middle July in the normal.

Figure 4 shows that the active convection area, where OLR anomaly is negative, moved northward compared with the normal and to the northwestern part of India and Pakistan. The negative anomaly around phillipines islands is also remarkable.

4. **Discussions**

According to monthly mean geopotential heights at 500hPa and 100hPa (not shown), the extension of Tibetan high into Japan is remarkable during the summer of 1994, and subtropical high extended into Japan from the early July. As a rerult, the characteristics of the high around Japan became barotropic as shown in Figs. 1 and 2. This year the asian monsoon was very active according to OLR anomalies in figure 4. The situation of these highs seems to associate with the activity of asian monsoon.

The high temperature observation and the small precipitation amount took place at meteorological stations under the large scale condition described above. The heat budget was calculated to investigate the cause of this high temperature. The effect of horizontal and vertical advection, cumulus convection, radiation, latent and sensible heat flux from the ground surafce were estimated in the thermodynamic equation using the physical quantities of JMA global spectral model (Sugi, et al, 1990). The result shows that the higher temprature of observations was caused by the subsidence in the high and sensible heat supply from the ground. Particularly, heating rate of the latter is three degrees and equal to the deviation from normal in observations. The significantly small amount of precipitation results from the maintenance of high and the inactive rainy front around Japan.

The convective activity of July around Phillipine islands was the strongest in 1978 to 1994, but it gave only a small impact on the maintenance of the high around Japan, judging from the result of wave activity flux (Plumb, 1985). The mechanism of the maintenance of highs is a very exciting problem, but it remains unresolved with the relation of asian monsoon activity.

5. **References**

Plumb, R.A. : On the three dimensional propagation of stationary waves, JAS 42 217-229 (1985)

Sugi, M., K. Kuma, K. Tada, K. Tamiya, N. hasegawa, T. Iwasaki, S. Yamada, and T. Kitade : Description and performance of the JMA Operational Global Spectral Model (JMA- GSM88), Geophys. Magazine, 43, 105-130 (1990)

6. **Pubilications**

Fujikawa, N., K.Kurihara, S.Sakai : Low rainfall and high temperatures, Technical report of the Japan Meteorological Agency, 1996, 117-136.

7. **International cooperation**

none

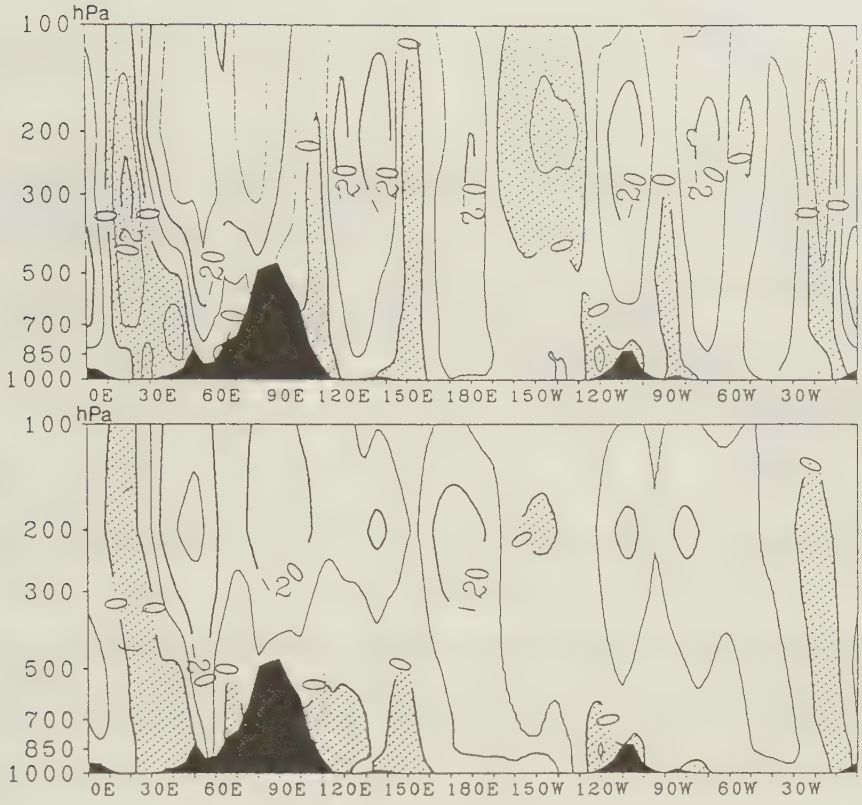

Figure.1 Longitude-pressure cross-section of monthly mean vorticity at 35N. Contours are drawn by every 1x10-5/sec. Positive vorticity is shaded and corresponds to the low. Top and bottom figures are that of 1994 and normal respectively.

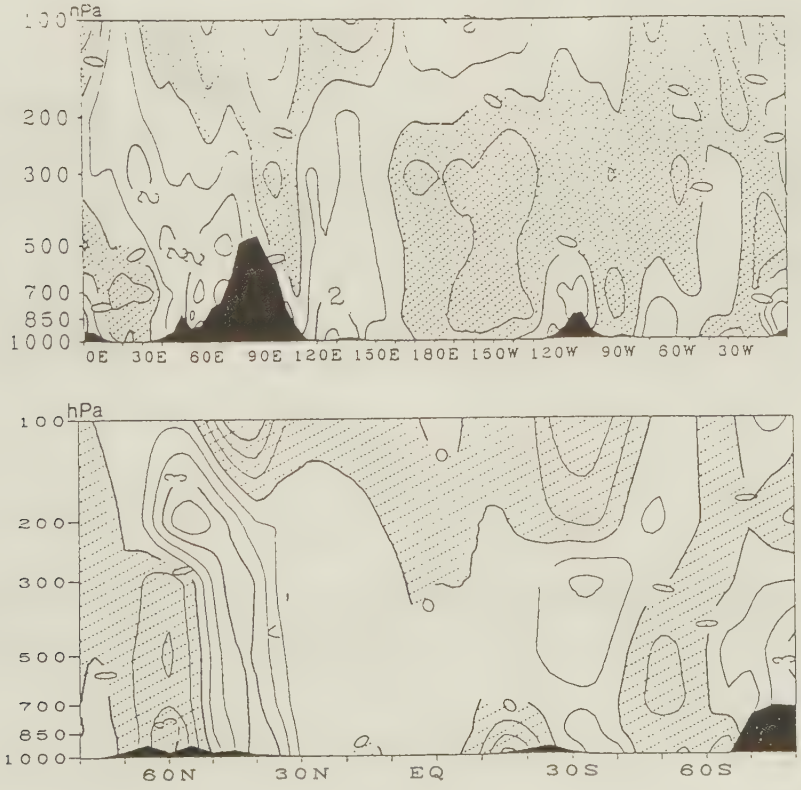

Fig.2 Cross section of monthly mean temperature deviation from normal. Contours are drawn by every one degree. Shaded areas show the negative deviation. Top and bottom figures show the cross section along at 35N and 130E, respectively.

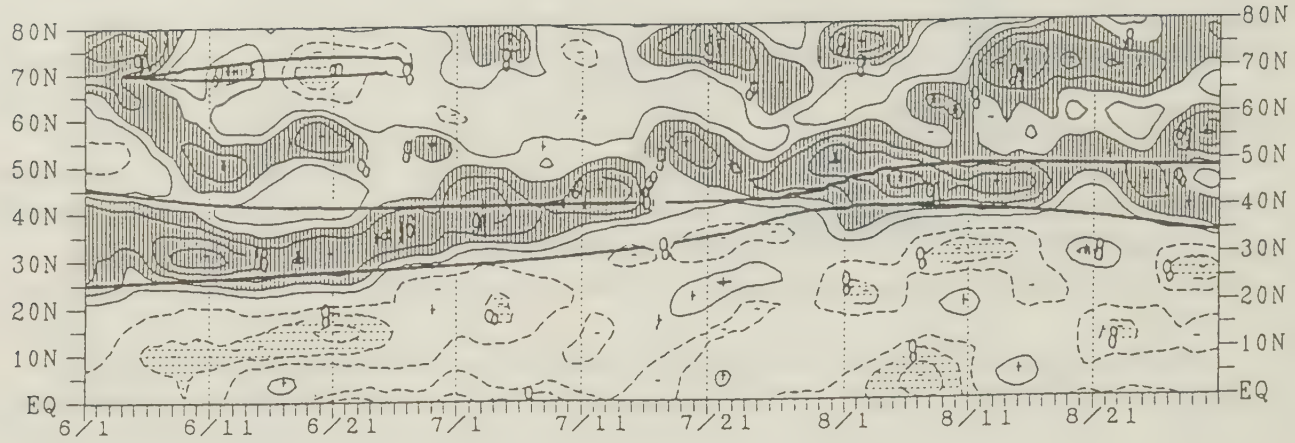

Fig.3 Westerly wind averaged from 130E to 140E at 500hpa. Ordinate and abscissa show the latitude and the date from 1 June to 31 August, respectively. Thick solid line indicates the normal westerly wind more than 8m/s and drawn by every 4m/s. Thin solid broken lines represent the westerly and easterly winds drawn by every 4m/s in 1994. Shades area shows the westerly wind more than 8m/s in 1994.

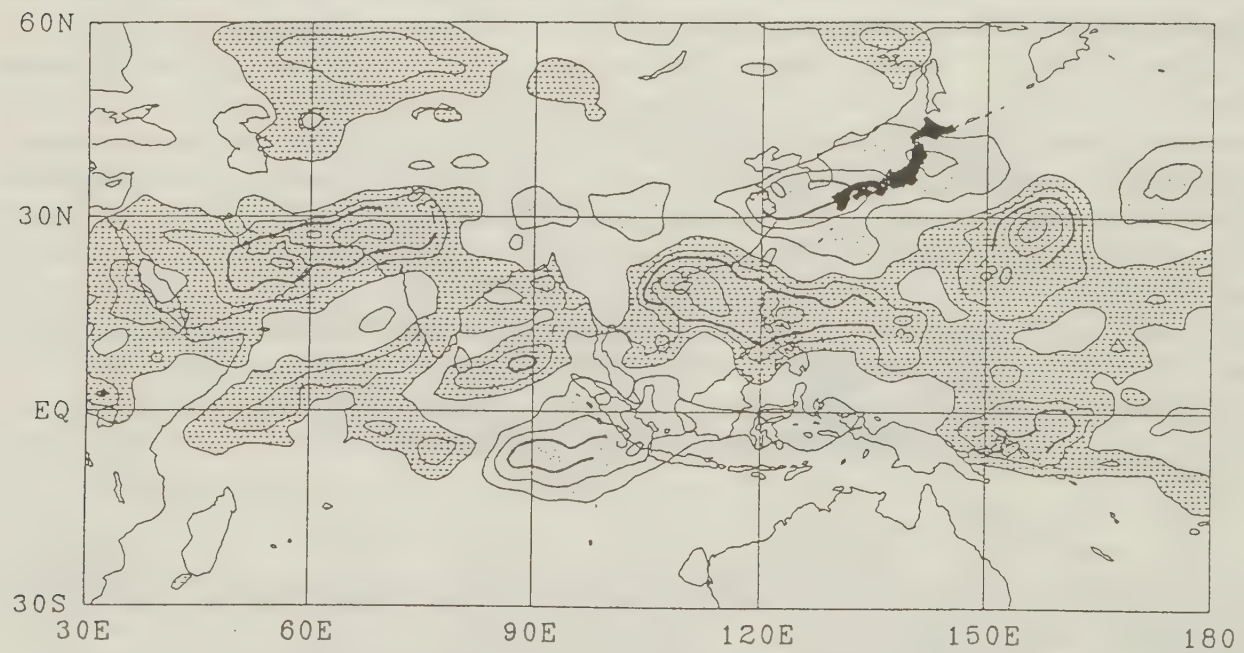

Fig.4 The deviation of monthly mean OLR in July 1994 from normal. The normal is defined as the mean of July from 1979 to 1990. The negative area shaded and contours are drawn by every 10w/m2.

アブストラクト

平成６年の夏は、記録的な高温・少雨が日本の広い範囲に長期間持続するという特徴があった。この特徴の解析とアジアモンスーンとの関連を調べるために、大規模場の熱収支解析と渦度解析を行った。また、この年のアジアモンスーンの活動を外向き長波放射（ＯＬＲ）の平年偏差を用いて解析した。

平成６年の夏は、チベット高気圧の北東方向への張り出しと亜熱帯高気圧の影響を受け、日本付近はバロトロッピク的な高気圧の圏内にあった。記録的な高温は、この高気圧圏内での下降流による昇温と地表面からの顕熱の輸送から生じたことが分かった。この高気圧の持続は、日本付近において梅雨明けに対応する偏西風の北偏が平年に比べ半月以上も早く見られた後に始まった。強風域の北偏はアジア領域でも顕著に見られた。この高気圧の持続は、短期間ではあるが平年に比べ活発なフィリピン付近の対流活動の影響を受けた。少雨は、この高気圧に覆われ続けたこと、梅雨前線の活動が弱かったために記録的なものとなった。

夏のアジアモンスーンの活動は平年に比べ活発であった。インド付近の子午面循環は平年より強く、モンスーンによる雲域は平年より北まで進入し、偏西風の北偏を示していた。

観測・解析研究ディレクトリー

Directory of Observation/Analysis Data Set

1. Directory Entry Title .
GMS IR Histogram

2. Directory Entry Start and Stop Date
Start Date : 1995-01-01
Stop Date : 1995-12-31

3. Sensor Name
VISSR

4. Source Name
GMS

5. Investigator, Technical Contact, and Author
(1) Investigator
Last name : Yamazaki
First name : Nobuo
Email : nyamazak@mri-jma.go.jp
Phone : +81-298-53-8668
Address : MRI, 1-1 Nagamine, Tsukuba, Ibaraki 305, Japan
(2) Technical Contact
Last name : Ohno
First name : Tomoo
Email :
Phone :
Address : Meteorological Satellite Center, Tokyo, Japan
(3) Author
Last name :
First name :
Email :
Phone :
Address :

6. Data Center
(1) Data Center Name : M R I >Meteorological Research Institute
(2) Dataset ID :
(3) Data Center Contact
Last Name :
First Name :
Email :
Phone :
Address :

7. Originating Center

8. Campaign or Project
J E X A M >Japanese Experiment on Asian Monsoon

9. Storage Medium

130 CCT's 13 G Bytes

10. Parameter Measured

Earth Radiative Process > IR equivalent black body temperature

11. Discipline Keywords

Earth Science > Atmosphere

12. Coverage

Minimum Latitude: 50S
Maximum Latitude: 50N
Minimum Longitude: 80E
Minimum Longitude: 160W

13. Location Keywords

Western Pacific

14. General Keywords

15. Revision Date

16. Science Review Date

17. Future Review Date

18. References

19. Summary

Available on the basis of cooperative research

1. Directory Entry Title :
GMS water vaper channel Histogram

2. Directory Entry Start and Stop Date
Start Date : 1995-01-01
Stop Date : 1995-12-31

3. Sensor Name
VISSR

4. Source Name
GMS

5. Investigator, Technical Contact, and Author
(1) Investigator
Last name : Yamazaki
First name : Nobuo
Email : nyamazak@mri-jma.go.jp
Phone : +81-298-53-8668
Address : MRI, 1-1 Nagamine, Tsukuba, Ibaraki 305, Japan
(2) Technical Contact
Last name : Ohno
First name : Tomoo
Email :
Phone :
Address : Meteorological Satellite Center, Tokyo, Japan
(3) Author
Last name :
First name :
Email :
Phone :
Address :

6. Data Center
(1) Data Center Name : M R I >Meteorological Research Institute
(2) Dataset ID :
(3) Data Center Contact
Last Name :
First Name :
Email :
Phone :
Address :

7. Originating Center

8. Campaign or Project
J E X A M >Japanese Experiment on Asian Monsoon

9. Storage Medium

130 CCT's 13 G Bytes

10. Parameter Measured

Earth Radiative Process > water vapor channel equivalent black body temperatur

11. Discipline Keywords

Earth Science > Atmosphere

12. Coverage

Minimum Latitude: 50S
Maximum Latitude: 50N
Minimum Longitude: 80E
Minimum Longitude: 160W

13. Location Keywords

Western Pacific

14. General Keywords

15. Revision Date

16. Science Review Date

17. Future Review Date

18. References

19. Summary

Available on the basis of cooperative research

1.Directory Entry Title

XBT observation between the South China Sea and the Persian Gulf

2.Directory Entry Start and Stop Date

Start Date:07 Oct. 1990

Stop Date:

3.Sensor Name

XBT>Expendable bathythermograph

4.Source Name

Kashimasan Maru

5.Investigator,Technical Contact, and Author

(1)Investigator

(Last Name) (First Name) (Middle Name)

Name : Mikawa Tetsuya

Email : ocean@umi.hq.kishou.go.jp

Phone : +81-3-3212-8341 Ext.5135

Address : Oceanographical Division
Marine Department, Japan Meteorological Agency
1-3-4, Otemachi, Chiyoda-ku, Tokyo, 100
JAPAN

(2)Technical Contact

Name : Yoshida Takashi

Email : ocean@umi.hq.kishou.go.jp

Phone : +81-3-3212-8341 Ext.5129

Address : Oceanographical Division
Marine Department, Japan Meteorological Agency
1-3-4, Otemachi, Chiyoda-ku, Tokyo, 100
JAPAN

6.Data Center

(1)Data Center Name: Global Subsurface Data Center

(2)Dataset ID :

(3)Data Center Contact

(Last Name) (First Name) (Middle Name)

Name : Marie-Claire Fabri

Email : mcfabri@ifremer.fr

Phone : +33-98-22-42-00

Address : IFREMER Brest-SISMER
PB 70
29280 Plouzane
FRANCE

7.Originating Center

8.Campaign or Project

Campaign : TOGA>Tropical Oceans and Global Atmosphere

Campaign : WOCE>World Ocean Circulation Experiment

9.Storage Medium

magnetic disks

10.Parameter Measured

Ocean Dynamics>Temperature

11.Discipline Keywords Earth Science>Ocean
12.Coverage Minimum Latitude : 5N Maximum Latitude : 23N Minimum Longitude : 60E Maximum Longitude : 121E
13.Location Keywords Indian Ocean
14.General Keywords
15.Revision Date
16.Science Review Date
17.Future Review Date
18.References
19.Summary Japan Meteorological Agency is operating a voluntary ship for XBT observations at South China Sea, the Strait of Malacca to Sri Lanka, to the Persian Gulf. The ship, Kashimasan Maru, is a crude oil tanker. About 12 sections per year and 4 casts a day are observed.

1. Directory Entry Title : JEXAM drifting buoy data in teh tropical Indian Ocean

2. Directory Entry Start and Stop Date
Start date : Feb. 2, 1990
Stop date :

3. Sensor Name : Surface drifter with SST sensor

4. Source Name : ARGOS

5. Investigator, Technical Contact and Author
(1) Investigator
Last Name : Michida
First Name: Yutaka
Email : ymichida@osman.jhd.go.jp (internet)
Phone : +81-3-3541-4387 FAX : +81-3-3545-2885
Address : 5-3-1 Tsukiji, Chuo-ku, Tokyo 104 Japan
(2) Technical Contact
Last Name : Michida
First Name: Yutaka
Email : ymichida@osman.jhd.go.jp (internet)
Phone : +81-3-3541-4387 FAX : +81-3-3545-2885
Address : 5-3-1 Tsukiji, Chuo-ku, Tokyo 104 Japan
(3) Author
Last Name : Michida
First Name: Yutaka
Email : ymichida@osman.jhd.go.jp (internet)
Phone : +81-3-3541-4387 FAX : +81-3-3545-2885
Address : 5-3-1 Tsukiji, Chuo-ku, Tokyo 104 Japan

6. Data Center
(1) Data Center Name : Japan Oceanographic Data Center
(2) Data Set ID :
(3) Data Center Contact
Last Name : Tatsuno
First Name: Tadao
Email : jodc@osman.jhd.go.jp (internet)
Phone : +81-3-3541-4295 FAX : +81-3-3545-2885
Address : 5-3-1 Tsukiji, Chuo-ku, Tokyo 104 Japan

7. Originating Center

8. Campaign or Project
Project : Japanese Experiment on Asian Monsoon (JEXAM)

9. Storage Medium : Magnetic Tape, 5.5 Mbyte

10. Parameter Measured : Locations of drifters, SST

11. Discipline Keywords
Earth science > Tropical Indian Ocean > Oceanic currents

12. Coverage
Minimum latitude : 33 S
Maximum latitude : 24 N
Minimum longitude : 38E
Maximum longitude : 135E

13. Location Keywords
Indian Ocean > Tropical Region

14. General Keywords
Surface currents > Heat Transport

15. Revision Date
March 31, 1996

16. Science Review Date

17. Future Review Date

18. References
Hydrographic Department of Japan, Surface Currents and Upper Oecan Thermal Structure in the Indian Ocean(small atlas), 1994.

Michida, Y. and H. Yoritaka, Survivability of the surface drifters deployed by Hydrographic Department of Japan for the period from 1988 to 1993, *J. Japan Soc. Mar. Surv. Tech.* 7(2), 21-28, 1995.

Michida, Y. and H. Yoritaka, Surface currents in the area of the Indo-Pacific throughflow and in the tropical Indian Ocean observed with surface drifters, *J. Geophys. Res.* 101, 12475-12482, 1996.

1. Directory Entry Title Snow cover and permafrost data
2. Directory Entry Start and Stop Date Start : July, 1993 Stop :
3. Sensor Name Snow weight meter and frozen ground depth meter
4. Source Name
5. Investigator, Technical Contact, and Author Takeshi Sato E-mail : tsato@shinjo.bosai.go.jp Phone : +81-233-22-7550 Fax : +81-233-23-3353 Address : Tokamachi, Shinjo, Yamagata 996, Japan
6. Data Center National Research Institute for Earth Science and Disaster Prevention (NIED), Shinjo Branch of Snow and Ice Studies
7. Originating Center
8. Campaign or Project Japanese Experiment of Asian Monsoon (JEXAM)
9. Storage Medium FDD
10. Parameter Measured Snow weight, frozen ground depth, ground temperature
11. Discipline Keywords Earth science, cryosphere
12. Coverage Lhasa : 29° 40´ N, 91° 08´ E Rikeze : 29° 15´ N, 88° 53´ E Nagqu : 31° 29´ N, 92° 04´ E
13. Location Keywords Tibetan Plateau
14. General Keywords
15. Revision Date
16. Science Review Date
17. Future Review Date
18. Reference
19. Summary In preparation

1. Directory Entry Title
   Surface Meteorological data of AWS

2. Dirtectry Entry Start and Stop Date
   Start Date: 6 July 1993
   Stop Date:

3. Sensor Name
   wind vane, anemometer, thermometer, hygrometer, rain gauge, barometer, soil moisture gauge, pyranometer, radiometer

4. Source Name
   AWS > Automatic Weather Station

5. Investigator, Technical Contact, and Author
   (1) Investigator
   Last Name: Shigenori
   First name: Haginoya
   E-mail: shaginoy@mri-jma.go.jp
   Phone: +81-298-53-8706
   Adress: M.R.I., 1-1 Nagamine, Tsukuba, Ibaraki 305, Japan
   (2) Technical Contact
   Last Name:
   First name:
   E-mail:
   Phone:
   Adress:
   (3) Author
   Last Name:
   First name:
   E-mail:
   Phone:
   Adress:

6. Data Center
   (1) Data Center Name: MRI > Meteorological Research Institute
   (2) Dataset ID:
   (3) Data Center Contact
   Last Name
   First name:
   E-mail:
   Phone:
   Adress:

7. Originating Center

8. Campaign or Project
   JEXAM > Japanese Experiment of Asian Monsoon

9. Storage Medium
   FDD, 3.5" MO disk

10. Parameter Measured wind direction, wind speed, air temperature, relative humidity, precipitation, air pressure, soil temperature, soil water content, global solar radiation, reflective solar radiation, net radiatioon.
11. Discipline Keywords Earth Science > Atmosphere
12. Coverage Lhasa: 29° 40'N, 91° 08'E Rikeze: 29° 15'N, 88° 53'E Nagqu: 31° 29'N, 92° 04'E Lingzi: 29° 34'N, 94° 28'E
13. Location keywords Tibetan Plateau
14. General Keywords
15. Revision Date
16. Science Review Date
17. Future Review Date
18. References
19. Summary This data set is in preparation.

1. Directory Entry Title
   Sea Surface Meteorological data of AWS

2. Dirtectry Entry Start and Stop Date
   Start Date: 23 Ocober 1991
   Stop Date: 7 Ocober 1995

3. Sensor Name
   wind vane, anemometer, thermometer, hygrometer, rain gauge, barometer, pyranometer, radiometer

4. Source Name
   AWS > Automatic Weather Station

5. Investigator, Technical Contact, and Author
   (1) Investigator
      Last Name: Shigenori
      First name: Haginoya
      E-mail: shaginoy@mri-jma.go.jp
      Phone: +81-298-53-8706
      Adress: M.R.I., 1-1 Nagamine, Tsukuba, Ibaraki 305, Japan
   (2) Technical Contact
      Last Name:
      First name:
      E-mail:
      Phone:
      Adress:
   (3) Author
      Last Name:
      First name:
      E-mail:
      Phone:
      Adress:

6. Data Center
   (1) Data Center Name: MRI > Meteorological Research Institute
   (2) Dataset ID:
   (3) Data Center Contact
      Last Name
      First name:
      E-mail:
      Phone:
      Adress:

7. Originating Center

8. Campaign or Project
   JEXAM > Japanese Experiment of Asian Monsoon

9. Storage Medium
   FDD, 3.5" MO disk

10. Parameter Measured wind direction, wind speed, air temperature, relative humidity, precipitation, air pressure, sea surface temperature, global solar radiation, long wave radiatioon.
11. Discipline Keywords Earth Science > Atmosphere
12. Coverage Minimun Latitude:36S Maximum Latitude: 36N Minimun Longitude: 18E Maximum Longitude: 140E
13. Location keywords Indian Ocean
14. General Keywords
15. Revision Date
16. Science Review Date
17. Future Review Date
18. References
19. Summary This data set is in preparation.

1. Directory Entry Title: Lower Atmosphere Observation by Wind Profiling Radar
2. Directory Entry Start and Stop Date Start Date: Feb. 24, 1994, Stop Date: March 31, 1996
3. Sensor Name: Boundary Layer Radar & RASS
4. Source Name: Clear air turbulence and Acoustic wave
5. Investigator, Technical Contact, and Author Name : Yoshihisa Masuda, E-mail: masuda@crl.go.jp. Phone: +81-98-895-2045 Address:829-3,Daigusukubaru, Aza-kuba, Nakakgusukuson, Nakagami-gun, Okinawa 901-24, Japa
6. Data Center (1) Name: CRL(Communications Research Laboratory) (2) Contact: Name :Yoshihisa Masuda, E-mail: masuda@crl.go.jp. Phone: +81-98-895-2045 Address:829-3,Daigusukubaru, Aza-kuba, Nakakgusukuson, Nakagami-gun, Okinawa 901-24, Japa
7. Originating Center:
8. Campaign or Project: JEXAM(Japanese Experiment on Asia Monsoon)
9. Storage Medium: DOS formatted 5 inch MO disk
10. Parameter Measured: Wind velocity
11.Discipline Keywords: Atmospheric remote sensing with radio- and acoustic waves
12. Coverage
13. Location Keywords: Subtropical region
14. General Keywords: Asia monsoon
15. Revision Date:
16. Science Review Date:
17. Future Review Date:
18. References

19. Summary

Our data-set is the Doppler spectra measured with a boundary layer radar(BLR).

The target of the BLR is the clear air turbulence. The BLR can measure the tropospheric wind profiles composed with three-dimensional wind vectors, and the intensity of the turbulence up to about 3 km from 300 m over ground.

全般の問い合せ先

〒１００　東京都千代田区霞ケ関２－２－１

科学技術庁研究開発局海洋地球課

Inquiries to:

Ocean and Earth Division,
Research and Development Bureau,
Science and Technology Agency,
2-2-1, Kasumigaseki, Chiyoda-ku, Tokyo 100
Japan